

DISSERTATION

LOW-TEMPERATURE OXIDIZING PLASMA SURFACE MODIFICATION AND
COMPOSITE POLYMER THIN-FILM FABRICATION TECHNIQUES FOR TAILORING
THE COMPOSITION AND BEHAVIOR OF POLYMER SURFACES

Submitted by

Brendan D. Tompkins

Department of Chemistry

In partial fulfillment of the requirements

For the Degree of Doctor of Philosophy

Colorado State University

Fort Collins, Colorado

Summer 2014

Doctoral Committee:

Advisor: Ellen R. Fisher

Charles S. Henry
Travis S. Bailey
Grzegorz Szamel
Susan P. James

Copyright by Brendan D. Tompkins 2014

All Rights Reserved

ABSTRACT

LOW-TEMPERATURE OXIDIZING PLASMA SURFACE MODIFICATION AND COMPOSITE POLYMER THIN-FILM FABRICATION TECHNIQUES FOR TAILORING THE COMPOSITION AND BEHAVIOR OF POLYMER SURFACES

This dissertation examines methods for modifying the composition and behavior of polymer material surfaces. This is accomplished using (1) low-temperature low-density oxidizing plasmas to etch and implant new functionality on polymers, and (2) plasma enhanced chemical vapor deposition (PECVD) techniques to fabricate composite polymer materials. Emphases are placed on the structure of modified polymer surfaces, the evolution of polymer surfaces after treatment, and the species responsible for modifying polymers during plasma processing.

H₂O vapor plasma modification of high-density polyethylene (HDPE), low-density polyethylene (LDPE), polypropylene (PP), polystyrene (PS), polycarbonate (PC), and 75A polyurethane (PU) was examined to further our understanding of polymer surface reorganization leading to hydrophobic recovery. Water contact angles (wCA) measurements showed that PP and PS were the most susceptible to hydrophobic recovery, while PC and HDPE were the most stable. X-ray photoelectron spectroscopy (XPS) revealed a significant quantity of polar functional groups on the surface of all treated polymer samples. Shifts in the C_{1s} binding energies (BE) with sample age were measured on PP and PS, revealing that surface reorganization was responsible for hydrophobic recovery on these materials. Differential scanning calorimetry (DSC) was used to rule out the intrinsic thermal properties as the cause of

reorganization and hydrophobic recovery on HDPE, LDPE, and PP. The different contributions that polymer cross-linking and chain scission mechanisms make to polymer aging effects are considered.

The H₂O plasma treatment technique was extended to the modification of 0.2 μm and 3.0 μm track-etched polycarbonate (PC-TE) and track-etched polyethylene terephthalate (PET-TE) membranes with the goal of permanently increasing the hydrophilicity of the membrane surfaces. Contact angle measurements on freshly treated and aged samples confirmed the wettability of the membrane surfaces was significantly improved by plasma treatment. XPS and SEM analyses revealed increased oxygen incorporation onto the surface of the membranes, without any damage to the surface or pore structure. Contact angle measurements on a membrane treated in a stacked assembly suggest the plasma effectively modified the entire pore cross section. Plasma treatment also increased water flux through the membranes, with results from plasma modified membranes matching those from commercially available hydrophilic membranes (treated with wetting agent). Mechanisms for the observed modification are discussed in terms of OH and O radicals implanting oxygen functionality into the polymers.

Oxidizing plasma systems (O₂, CO₂, H₂O vapor, and formic acid vapor) were used to modify track-etched polycarbonate membranes and explore the mechanisms and species responsible for etching polycarbonate during plasma processing. Etch rates were measured using scanning electron microscopy; modified polycarbonate surfaces were further characterized using x-ray photoelectron spectroscopy and water contact angles. Etch rates and surface characterization results were combined with optical emission spectroscopy data used to identify gas-phase species and their relative densities. Although the oxide functionalities implanted by each plasma system were similar, the H₂O vapor and formic acid vapor plasmas yielded the

lowest contact angles after treatment. The CO₂, H₂O vapor, and formic acid vapor plasma-modified surfaces were, however, found to be similarly stable one month after treatment.

Overall, etch rate correlated directly to the relative gas-phase density of atomic oxygen and, to a lesser extent, hydroxyl radicals.

PECVD of acetic acid vapor (CH₃COOH) was used to deposit films on PC-TE and silicon wafer substrates. The CH₃COOH films were characterized using XPS, wCA, and SEM. This modification technique resulted in continuous deposition and self-limiting deposition of a-C_xO_yH_z films on Si wafers and PC-TE, respectively. The self-limiting deposition on PC-TE revealed that resulting films have minimal impact on 3D PC structures. This technique would allow for more precise fabrication of patterned or nano-textured PC.

PECVD is used to synthesize hydrocarbon/fluorocarbon thin films with compositional gradients by continuously changing the ratio of gases in a C₃F₈/H₂ plasma. The films are characterized using variable angle spectroscopic ellipsometry (VASE), Fourier transform infrared spectroscopy (FTIR), XPS, wCA, and SEM. These methods revealed that shifting spectroscopic signals can be used to characterize organization in the deposited film. Using these methods, along with gas-phase diagnostics, film chemistry and the underlying deposition mechanisms are elucidated, leading to a model that accurately predicts film thickness.

DEDICATION

I dedicate this work to my grandfather, the chemist I never knew, and to my father, for giving the subject a sense of glamor.

TABLE OF CONTENTS

ABSTRACT.....	ii
DEDICATION.....	v
TABLE OF CONTENTS.....	vi
LIST OF TABLES.....	xii
LIST OF FIGURES.....	xiii
CHAPTER 1. Introduction.....	1
1.1. Polymers: A Case for Surface Modification.....	1
1.2. Plasmas for Polymer Processing.....	3
1.2.1. Low-density low-temperature plasmas.....	3
1.2.2. Early history of plasma surface modification of polymers.....	4
1.2.3. Modern plasma techniques for polymer surface modification.....	5
1.2.4. Plasma modification of porous polymer membrane materials.....	6
1.3. Overview of Research.....	8
REFERENCES.....	11
CHAPTER 2. Experimental Methods.....	14
2.1. Reactor Design and Plasma Processing Methods.....	14
2.1.1. General reactor design.....	14
2.1.2. Plasma surface modification of polymer substrates.....	16
2.1.3. Plasma surface modification of polymer membranes.....	16
2.1.4. Plasma etching of polymer membranes.....	17
2.1.5. PECVD of thin films using organic acid precursors.....	20

2.1.6. PECVD of homogeneous and gradient hydrocarbon/fluorocarbon films	20
2.2. Materials and Surface Analysis Equipment and Methods	21
2.2.1. X-ray photoelectron spectroscopy	21
2.2.2. H ₂ O contact angle goniometry	22
2.2.3. Variable angle spectroscopic ellipsometry	23
2.2.4. Scanning electron microscopy	24
2.2.5. Fourier transform infrared spectroscopy	25
2.2.6. Differential scanning calorimetry	25
2.2.7. Pure H ₂ O flux measurements	26
2.3. Gas-phase Diagnostic Equipment and Methods	26
REFERENCES	32
 CHAPTER 3. Hydrophobic Recovery Behavior of Various Polymers Following H ₂ O Plasma	
Processing	34
3.1. Introduction	34
3.2. Results	39
3.2.1. Hydrophobic recovery on polyolefins	39
3.2.2. Hydrophobic recovery on aromatic polymers	49
3.3. Discussion	63
3.3.1. Hydrophobic recovery on polyolefins	63
3.3.2. Hydrophobic recovery on polystyrene	66
3.3.3. Hydrophobic recovery on polycarbonate	67
3.3.4. Hydrophobic recovery on polyurethane 75A	68
3.4. Summary	69

REFERENCES	70
CHAPTER 4. H ₂ O Plasma Modification of Track-etched Polymer Membranes for Increased Wettability and Improved Performance.....	75
4.1. Introduction.....	75
4.2. Results.....	79
4.2.1. Efficacy of plasma modification.....	79
4.2.2. Surface morphology and pore size.....	83
4.2.3. Wettability and the effect of aging on treated membranes	88
4.2.4. Composition of membranes via XPS analysis	88
4.2.5. Stacked membranes	94
4.2.6. Gas-phase diagnostics.....	96
4.2.7. Performance assessment: pure water flux.....	98
4.3. Discussion.....	100
4.3.1. Effectiveness and permanence of polar surface functionality	100
4.3.2. Mechanism for surface modification	102
4.3.3. Modification of pore surfaces	105
4.3.4. Membrane performance	107
4.4. Summary	109
REFERENCES	110
CHAPTER 5. Etching and Post-treatment Surface Stability of Track-etched Polycarbonate Membranes by Plasma Processing Using Various Related Oxidizing Plasma Systems	114
5.1. Introduction.....	114
5.2. Results.....	117

5.2.1. Plasma etching of PC-TE and etch rate measurements	117
5.2.2. Etched PC-TE surface analysis	120
5.2.3. Actinometric optical emission spectroscopy	128
5.3. Discussion	132
5.3.1. Gas-phase processes leading to PC etching	132
5.3.2. Implications of etching on PC surface modification and stability	136
5.3.3. PC-TE morphology with oxidizing plasma treatment	139
5.4. Summary	140
REFERENCES	143
 CHAPTER 6. Acetic Acid Plasma Polymer Coatings on Polycarbonate for Improved Coating Integrity and Structure Retention in Optical and Biomedical Applications	
6.1. Introduction	147
6.2. Results and Discussion	149
6.2.1. CH ₃ COOH PECVD films on PC-TE	149
6.2.2. CH ₃ COOH PECVD films on silicon	158
6.2.3. CH ₃ COOH plasma diagnostics	160
6.3. Summary	162
REFERENCES	164
 CHAPTER 7. Plasma Synthesis of Hydrocarbon/Fluorocarbon Thin Films with Compositional Gradients	
7.1. Introduction	167
7.2. Results	171
7.2.1. Analysis of homogeneous films from a static C ₃ F ₈ /H ₂ PECVD system	171

7.2.2. Dynamic C ₃ F ₈ /H ₂ PECVD system.....	181
7.3. Discussion	191
7.3.1. Variable film composition from a single PECVD system	191
7.3.2. Depositing film composition is independent of underlying film	195
7.3.3. Composition of sub-surface layers remain fixed	196
7.4. Summary	199
REFERENCES	201
CHAPTER 8. Summary of Research and Perspectives	204
8.1. Research Summary	204
8.2. Future Directions	206
REFERENCES	211
APPENDIX A. Programming and Control Interface for Automation of Data Collection and External Control of Mass Flow Controllers.....	212
A.1. National Instruments DAQ to MKS 247D Hardware Interface.....	212
A.2. LabVIEW® Mass Flow Controller Data Acquisition and Control Program.....	213
A.3. System Test Results	228
REFERENCES	236
APPENDIX B. An Investigation of the Mechanisms and Film Structure that Control Hydrophilic/Oleophobic Behavior on Coatings and Materials with Switchable Affinity	237
B.1. Statement of Motivation and Previous Research	238
B.2. Novel Research and Proposed Techniques	239
B.2.1. Fabrication of OPB/HPL films.....	243
B.2.2. OPB/HPL film characterization and study of switchable affinity.....	252

B.2.3. Preparation of SOPB/SHPL materials and pilot separation experiments	254
B.3. Summary and Research Perspectives	258
REFERENCES	259
LIST OF ABBREVIATIONS.....	262

LIST OF TABLES

2.1.	Select manufacturer specifications for track-etched membranes.....	18
3.1.	wCA and composition of aged H ₂ O plasma modified aliphatic polymers	42
3.2.	C _{1s} moiety distribution of aged H ₂ O plasma modified aliphatic polymers.....	45
3.3.	C _{1s} moiety binding energies of aged H ₂ O plasma modified polypropylene	50
3.4.	wCA and composition of aged H ₂ O plasma modified aromatic polymers	53
3.5.	C _{1s} moiety binding energies of aged H ₂ O plasma modified polystyrene	56
3.6.	C _{1s} moiety distribution of aged H ₂ O plasma modified aromatic polymers	58
4.1.	Pore size measurements of untreated and treated PC-TE and PET-TE	86
4.2.	wCA and compositional data from aged H ₂ O plasma modified 0.2 μm PC-TE	89
4.3.	wCA and compositional data from aged H ₂ O plasma modified 3.0 μm PET-TE	90
5.1.	wCA and compositional data of PC-TE oxidized using various plasma systems	122
5.2.	C _{1s} moiety distribution of PC-TE oxidized using various plasma systems	125
6.1.	wCA and compositional data from CH ₃ COOH plasma modified substrates	150
6.2.	C _{1s} moiety distribution of CH ₃ COOH plasma modified substrates	151
7.1.	C _{1s} moiety distribution of homogeneous HC/FC films.....	179
B.1.	Proposed starting materials for the synthesis of various mono and di-alkynes	247

LIST OF FIGURES

2.1.	General design for inductively coupled glass barrel style plasma reactor.....	15
2.2.	Membrane sample holders for plasma surface modification	19
2.3.	Dead end ultrafiltration system for testing track-etched membrane performance.....	27
2.4.	Reactor design for TR-OES on membranes and oxidizing plasma systems.....	29
2.5.	Reactor design for TR-OES on C ₃ F ₈ /H ₂ dynamic plasma system.....	31
3.1.	DSC results from untreated HDPE, LDPE, and PP samples	40
3.2.	wCA and O/C results from modified HDPE, LDPE, and PP	41
3.3.	High resolution C _{1s} XPS spectra untreated, freshly treated, and aged HDPE	46
3.4.	High resolution C _{1s} XPS spectra untreated, freshly treated, and aged LDPE.....	48
3.5.	High resolution C _{1s} XPS spectra untreated, freshly treated, and aged PP	51
3.6.	wCA and O/C results from modified PS, PC, and PU.....	52
3.7.	High resolution C _{1s} XPS spectra untreated, freshly treated, and aged PS	59
3.8.	High resolution C _{1s} XPS spectra untreated, freshly treated, and aged PC.....	60
3.9.	High resolution C _{1s} XPS spectra untreated, freshly treated, and aged PU.....	62
4.1.	wCA on PC-TE and PET-TE membranes acquired in “movie-mode”	80
4.2.	wCA on PC-TE and PET-TE as a function of pressure, <i>P</i> , and time	82
4.3.	SEM images of untreated and treated PC-TE and PET-TE.....	84
4.4.	SEM images of PC-TE and PET-TE treated using extreme conditions	87
4.5.	High resolution C _{1s} spectra from untreated and treated PC-TE and PET-TE.....	92
4.6.	wCA data from upstream side of stacked PC-TE membranes.....	95
4.7.	TR-OES H ₂ O plasmas emission with and without a membrane.....	97

4.8.	Pure water flux through untreated and treated PC-TE and PET-TE.....	99
4.9.	Hydroxyl radical modification of PC and PET.....	103
4.10.	Ring opening and functionalization of PC by oxygen radicals.....	104
5.1.	SEM images of untreated and O ₂ plasma treated PC-TE	118
5.2.	SEM images of PC-TE modified using CO ₂ , H ₂ O, and HCOOH plasmas.....	121
5.3.	High resolution C _{1s} spectra from O ₂ , CO ₂ , and HCOOH plasma treated PC-TE.....	124
5.4.	wCA as a function PC-TE sample age after CO ₂ and HCOOH plasma treatment	127
5.5.	OES spectra from O ₂ , CO ₂ , H ₂ O, and HCOOH plasmas.....	129
5.6.	Stacked OH* and O* regions from O ₂ , CO ₂ , H ₂ O, and HCOOH OES spectra.....	130
5.7.	Relative OH* and O* densities compared to measured etch rates on PC-TE	131
6.1.	High resolution C _{1s} XPS spectra of CH ₃ COOH plasma modified samples.....	152
6.2.	wCA measurements on PC-TE samples coated using CH ₃ COOH PECVD.....	153
6.3.	SEM images of untreated and CH ₃ COOH plasma modified PC-TE.....	155
6.4.	Upstream and downstream mean pore radius measurements on PC-TE	156
6.5.	CH ₃ COOH plasma polymer film thickness on Si wafers	158
6.6.	OES spectrum from CH ₃ COOH plasma.....	160
7.1.	Transmission FTIR spectra from homogeneous HC/FC films	172
7.2.	Elemental composition, wCA, and F/C ratio from homogeneous HC/FC films	174
7.3.	High resolution XPS C _{1s} spectra of homogeneous HC/FC films	177
7.4.	Stacked high resolution XPS C _{1s} spectra of homogeneous HC/FC films.....	180
7.5.	TR-OES of plasma emission from multiple cycles of a HC/FC deposition program.....	182
7.6.	wCA measurements on homogeneous and gradient HC/FC films	183
7.7.	Transmission FTIR spectra from gradient HC/FC films	185

7.8.	Deposition rate of homogeneous HC/FC films from various C ₃ F ₈ /H ₂ mixtures	186
7.9.	Deposition rate per % C ₃ F ₈ as a function of % C ₃ F ₈	188
7.10.	SEM image of the cross section of a gradient HC/FC film	189
7.11.	CF ₂ frequency, CF ₂ C _{1s} BE, and permittivity for homogeneous HC/FC films.....	190
8.1.	wCA on PC-TE with various CH ₃ COOH/H ₂ O plasma treatments.....	208
8.2.	wCA on PC-TE with various CO ₂ /H ₂ plasma treatments.....	210
A.1.	LabView® “MKS 247D Control v8.vi” front panel, upper left quadrant	214
A.2.	LabView® “MKS 247D Control v8.vi” front panel, upper right quadrant	215
A.3.	LabView® “MKS 247D Control v8.vi” front panel, lower left quadrant	216
A.4.	LabView® “MKS 247D Control v8.vi” front panel, lower right quadrant	217
A.5.	LabView® “MKS 247D Control v8.vi” Frame 0, clear history instructions	219
A.6.	LabView® “MKS 247D Control v8.vi” Frame 1, logarithmic case.....	220
A.7.	LabView® “MKS 247D Control v8.vi” Frame 1, constant case.....	221
A.8.	LabView® “MKS 247D Control v8.vi” Frame 1, none case	222
A.9.	LabView® “MKS 247D Control v8.vi” Frame 1, linear case	223
A.10.	LabView® “MKS 247D Control v8.vi” Frame 1, array concatenation.....	225
A.11.	LabView® “MKS 247D Control v8.vi” Frame 2, timed loop and I/O.....	226
A.12.	LabView® “MKS 247D Control v8.vi” Frame 2, I/O output instructions.....	227
A.13.	LabView® “MKS 247D Control v8.vi” Frame 2, read output array.....	229
A.14.	LabView® “MKS 247D Control v8.vi” Frame 2, loop control	230
A.15.	LabView® “MKS 247D Control v8.vi” Frame 3, close contact instructions	231
A.16.	LabView® “MKS 247D Control v8.vi” Frame 4, save file instructions.....	232
A.17.	MFC Channel 1 flow rate control results.....	234

A.18.	MFC Channel 2 flow rate control results.....	235
B.1.	Diffusion and rearrangement mechanisms for switchable affinity	240
B.2.	Predicted contact angle as a function of thickness and cross-link density	242
B.3.	Scheme for the incorporation of azide surface functionality	244
B.4.	Scheme for the synthesis of partially fluorinated mono- and dialkynes.....	246
B.5.	Scheme for Azide/alkyne "Click" chemistry	248
B.6.	Pulse modulation for controlled cross-linking in plasma polymerized films	251
B.7.	Desired behavior of liquids on substrates with reentrant features	256
B.8.	Apparatus for oil-in-water separation experiments.....	257

CHAPTER 1

INTRODUCTION

This chapter contains general information pertinent to the research described in this dissertation. A case is made for the importance of and need for the surface modification of polymer materials. Low-density low-temperature inductively coupled radio frequency (rf) plasmas, the primary technique used in this research, and concepts relating to their use for polymer surface modification are explained. Earlier work on the plasma modification of polymer membranes within the Fisher Research Group is also reviewed. The chapter finishes with an overview of the research presented in the remainder of this dissertation.

1.1. Polymers: A Case for Surface Modification

Hydrocarbon-based organic polymers are ubiquitous in modern society and find uses in many important industries, including automotive,^{1,2} biomedical,^{3,4} environmental,⁵ and laboratory applications.⁶ Polymers consist of repeating units where molecular size becomes so large that the bulk properties become unique compared to the monomers and oligomers from which they are built. For example, polyethylene (PE), a very simple olefinic-type polymer, consists of ethyl units connected end to end or in a variety of branched configurations to make a long hydrocarbon chains or networks composed of CH₂ units. Although the repeat units in PE are built from ethylene, the bulk properties of PE, such as rigidity, durability, and chemical inertness, bear very little resemblance to ethylene or ethane. The behavior that results from these large chains or networks of monomer units is also responsible for the surface properties of the polymer material. This can lead to a paradox. The structure and composition that gives a

polymer the most desirable bulk properties often yields a surface that is incompatible with the intended application. Among the most common issues related to surface properties are adhesive failure and delamination resulting from interface incompatibility,^{1, 7-9} wetting and fouling issues due to undesirable surface tension or surface functionality,¹⁰⁻¹⁵ and surface instability causing the polymer surface to denature or degrade.² Each of these problems can be addressed by surface modification.

Many processes have been developed to alter polymer surface while the bulk properties remain unchanged. Exposing a polymer to an intense ultra-violet (UV) light source is known to alter its surface.^{16, 17} When the polymer absorbs photons of sufficient energy, excitations occur that break bonds, induce rearrangements, and facilitate other chemical reactions. This technique works best when the incident wavelength is well matched to the molar absorptivity of the polymer. Under these circumstances photons do not penetrate far into the polymer and the treatment is confined to the surface according to the Beer-Lambert law. Regardless, photons do penetrate into the polymer surface, and confinement of the treatment remains a problem with photo-induced surface modification of polymers. Moreover, surfaces modified by light irradiation are unstable, making them subject to hydrophobic recovery.¹⁸ Another technique, known as flame treatment, exposes a polymer surface to a carefully controlled flame fed by fuel, oxidizer, and other reactive gases.¹⁹ Similar to UV-irradiation, flame treatments break bonds, induce rearrangement, and alter the functional groups on the surface of a polymer material. Although flame treatments are effective for modifying some polymers, such as polypropylene¹⁹ and polyethylene,²⁰ the thermal energy in the flame makes it difficult to confine the treatment to the absolute surface of the polymer. This can have significant effects on bulk polymer

properties. Although all of these techniques have their merits, the remainder of this dissertation focuses exclusively on plasma processes techniques for surface modification of polymers.

1.2. Plasmas for Polymer Processing

1.2.1. Low-density low-temperature plasmas. Plasma is the term given to a quasi-neutral partially ionized substance consisting of a variety of species, including neutrals, radicals, ions, ground state species, excited state species, electrons, and photons.²¹ Plasmas comprise a large portion of the known universe as the high-density medium of stars and the low-density medium of solar winds are both examples of naturally occurring plasmas. Low-pressure (i.e. $\ll 1$ Torr) low-temperature (gas temperatures $< \sim 10^3$ K) plasmas, routinely created for the purpose of material surface modification in laboratory and industrial settings, are the subject of this dissertation and the work described herein. Plasmas have been the subject of intense research for many decades owing to the ability of reactive plasma species to participate in energy intensive surface reactions while limiting the transfer of energy to a bulk material. Plasma processing has an advantage over the surface modification techniques discussed in Section 1.1. for these reasons.

Low-temperature low-density radio frequency (rf) plasmas alter the surface of a material in a number of ways, include, etching, surface modification, and deposition.²¹ Etching refers to the removal of material from a surface, often performed to change the dimensions of surface features or otherwise pattern a material; surface modification is the process of implanting new chemical functionality on a surface; and deposition involves the fabrication of a film composed of some new material on the original surface. This diversity results from the large set of parameters that define any plasma system. Chief among these parameters are applied rf power

(P), pressure, time, gas-phase composition, feed gas flow rate, substrate temperature (T_s), and proximity of the substrate to the plasma discharge.

The etching, modification, and deposition processes in plasmas are not mutually exclusive, and a process designed to accomplish one task can result in one or both of the other processes as well. For example, microchip manufacturers routinely use electrically biased, high P , capacitively-coupled CF_4 plasmas to etch features into silicon wafers.²² Although these etching processes are very efficient, the resulting wafer is coated with a thin amorphous film composed of fluorocarbon material. The extent to which plasma variables exacerbate or minimize undesired processing outcomes is critically important to designing materials modification strategies. This is especially true with polymers. Plasmas capable of implanting some desired functionality often etch a polymer surface.^{23, 24} Likewise, a plasma system effective for etching a polymer materials may leave behind residues that completely change the surface functionality.²⁵ There is even a recent example of plasma system intended to improve adhesion by implanting appropriate functionality on a polymer that also etches the polymer surface while depositing a thin-film.¹ These entwined phenomena make plasma surface modification a complicated, versatile, and powerful technique. Considerations such as these motivate much of the work reported in this dissertation, and will be a theme throughout this work.

1.2.2. Early history of plasma surface modification of polymers. The plasma surface modification of polymers has a long history. Research accounts that discuss surface modification of polymers using plasmas were first published in the 1960s. These investigations largely evolved from the use of flame treatments to activate otherwise inert polymer surfaces.²⁶ In 1964, Mantell and Ormand²⁷ investigated the use of oxygen plasma jet from a corona discharge to alter the hardness, adhesion, and wettability of a variety of polymer surfaces. Low-

temperature, low-density rf plasmas, similar to those described in this dissertation, were first investigated as a method for improving the adhesion between polymer surfaces in 1966 by Hansen and Schonhorn.^{28, 29} They reasoned that plasmas would activate the surface with minimal impact on the bulk or surface properties. Their work highlights the ability of plasma surface modification to tailor one specific aspect of a surface while leaving other surface and bulk properties unchanged. These early works foreshadowed polymer surface modification research continuing to this day.

1.2.3. Modern plasma techniques for polymer surface modification. Since the 1960s, virtually continuous attention has been given to the plasma surface modification of polymers by the plasma science community. The continued development and enhancement of these processes has led to nearly as many plasma modification techniques as there are applications for such techniques.^{30, 31} These methods can be grouped into three broad categories. Non-depositing plasmas that implant new surface functionality are commonly used to modify polymer surfaces. This is accomplished by using a gas that can be incorporated (either directly or via fragments created in the plasma) into a surface as new functional groups, but does not continue to react with the surface to form a film. Common precursors include O₂, N₂, NH₃, H₂, and mixtures of these gases. As mentioned in Section 1.2.1., it is difficult to prevent non-depositing plasmas from etching the material to be modified. The dual role of such plasmas will be the subject of Chapter 5.

Inert gas plasmas, such as Ar and He, are often used to modify polymer surfaces; though, strictly speaking, the inert gas is not incorporated onto the surface. Inert gas plasmas cause reactive sites on polymer surfaces and these sites are then able to react with other gases or atmosphere to form stable functional groups. When the surface is exposed to a polymerizable

species, the radical sites can propagate to form polymer chains using a mechanism closely related to radical polymerization.³² Polymerization proceeds for the lifetime of the radical site, so long as enough monomer is available. When polymerization slows down or stops the process can be repeated, making it possible to grow films that are quite thick.

Plasma enhanced chemical vapor deposition (PECVD) or plasma polymerization is another important method for modifying polymer surfaces. PECVD is carried out by feeding a deposition precursor gas, directly into a plasma discharge. A film begins to form and grows for the duration of the treatment. The deposition mechanism depends largely on the precursor gas used. Otherwise stable gases, such as simple alkanes and perfluoroalkanes, are fragmented in the plasma discharge, and these reactive fragments attach to the surface forming an interconnected, often amorphous, layer of new material. Certain reactive precursors, such as allyl alcohol, allyl amine, and acrylic acid, react with radical sites on the polymer surface, growing a polymer film via a mechanism akin to radical polymerization.

1.2.4. Plasma modification of porous polymer membrane materials. The Fisher Research Group has a rich history with plasma surface modification of porous polymer membrane materials. Early investigations examined the modification of asymmetric polysulfone membranes (PSf) using H₂O vapor plasmas.³³ Plasma treatment conditions were optimized to improve the wettability of the outer surface and internal pore structure of the membrane. The plasma treatments rendered the PSf completely wettable and the treatment was found to persist for months to years.³⁴ Separate experiments using the imaging of radicals interacting with surfaces technique (IRIS) were performed and found that OH radical have a 56% probability of reacting with the PSf surface.³⁵ From this, it was reasoned that the OH radicals were primarily responsible for implanting polar functionality and effecting a hydrophilic surface treatment.

Indeed, the NH_3/O_2 plasma system, also known for generating large quantities of OH radicals, was found to be similarly effective.¹³

The earlier study,³³ investigating H_2O vapor plasma treatments on PSf, was later expanded to include polyethersulfone (PES) and PE membranes.³⁴ Treatments on PES were similarly effective and the induced wettability was equally as persistent. Treated PE membrane surfaces were, however, less stable. Initially, a drop of water placed on the freshly-treated PE membrane surface was quickly absorbed by the material, revealing similar wettability to the freshly-treated or aged PSf and PES. After aging for 9 months, however, the side of the membrane that faced the plasma glow demonstrated 45% recovery and the side of the membrane facing away from the plasma glow demonstrated complete recovery of the untreated wCA. This hydrophobic recovery was attributed to structural rearrangements of the polymer chains on the PE surface. It is unclear if this rearrangement was exacerbated by the H_2O plasma treatment or if the tendency towards rearrangement is an intrinsic property of the PE material.

Further studies¹³ were carried out on PES membranes using nitrogen containing plasmas (e.g. N_2 , NH_3 , Ar/NH_3 , and O_2/NH_3) to both increase the wettability of the membrane surfaces and to implant nitrogen containing functionalities. Interestingly, treatments using 100% N_2 or NH_3 were not very effective for increasing wettability on the PES surface and any treatment imparted to the membrane was unstable. PES with persistently wettable surfaces was only achieved when O_2 was mixed with the NH_3 gas feed. PES treated using 5:3 NH_3/O_2 mixtures were also found to have the most nitrogen functionality incorporated onto the surface. Moreover, the 5:3 NH_3/O_2 plasma treatments, increased pure water flux through the PES membranes, decreased protein adsorption and improved flux recovery with cleaning.

1.3. Overview of Research

This dissertation presents research on the modification of polymer materials using oxidizing plasmas and the fabrication of composite polymer materials using PECVD techniques. An emphasis is placed on understanding the mechanisms contributing to surface modification or the organization of the thin film deposited at the plasma-polymer interface. The relationship between these mechanisms and aging phenomena that take place on plasma modified surfaces are also considered. Chapter 2 presents the materials, reagents, plasma modification procedures, surface analysis methods, and plasma diagnostic techniques used to conduct the research presented in subsequent chapters.

Research on the plasma modification of non-porous polymers to understand their aging and hydrophobic recovery behavior is presented in Chapter 3. Water contact angles (wCA) and x-ray photoelectron spectroscopy (XPS) measurements are used to characterize H₂O plasma modified samples. Differential scanning calorimetry (DSC) is used to rule out intrinsic thermal properties as the primary cause of hydrophobic recovery. Instead, shifts in the C_{1s} binding energies (BE) with sample age coincide with the most extreme cases of hydrophobic recovery. Results show that stability is derived from plasma induced cross-linking or a similar processes.

Chapter 4 builds on the work presented in Chapter 3 by investigating the H₂O plasma modification of track-etched polycarbonate (PC-TE) and track-etched polyethylene terephthalate (PET-TE) membranes to permanently increasing their hydrophilicity. XPS and wCA measurements show that the implantation of new oxygen functionality increases membrane wettability. Further experiments reveal that the treatment is effective throughout the pore cross-section, improving the membrane performance. The results of XPS analysis and time-resolved

optical emission spectroscopy (TR-OES) are used to develop reaction mechanisms responsible for implanting oxygen functionality and inducing polymer chain scission.

Chapter 5 further explores oxidizing plasmas systems by comparing the H₂O plasma with three other systems, O₂, CO₂, and formic acid vapor (HCOOH). These plasmas were used to modify PC-TE to determine the treatment effectiveness and to explore the mechanisms and species responsible for etching PC. Pore radii are measured and etching rates are calculated using scanning electron microscopy (SEM) images of treated PC-TE. These results are compared with relative gas-phase density of atomic oxygen and hydroxyl radicals, measured using optical emission spectroscopy (OES), and show that atomic oxygen and, to a lesser extent, hydroxyl radicals are responsible for etching PC-TE. This work validates and expands upon the mechanisms described in Chapter 4.

The work in Chapter 6 describes the development of a new PECVD method for fabrication of composite structures on PC surfaces. Surface analysis methods are used to characterize $a\text{-C}_x\text{O}_y\text{H}_z$ deposited on PC-TE and Si wafer substrates using an acetic acid vapor (CH₃COOH) plasma. Pore radii measured from SEM images reveal that the $a\text{-C}_x\text{O}_y\text{H}_z$ film deposition on PC-TE is self-limiting. These preliminary results show this PECVD system allows more precise fabrication of patterned or nano-textured PC. Potential use of this PECVD system for optical and biomedical applications is also discussed.

Chapter 7 further explores the use of PECVD to fabricate composite polymer structures. Gradient hydrocarbon/fluorocarbon thin films are prepared on Si wafers by continuously changing the ratio of gases in a C₃F₈/H₂ plasma. The resulting films are characterized using a variety of bulk spectroscopic and surface analysis techniques. Notably, a detailed analysis of XPS and Fourier transform infrared spectroscopy (FTIR) peak positions furthers our

understanding of the internal film structure. Along with gas-phase diagnostics, the underlying deposition mechanisms are elucidated, leading to a model that accurately predicts film thickness.

Chapter 8 summarizes the collective work described in this dissertation. The specific impact of this work and the global themes addressed in each chapter are considered.

Perspectives and future research directions arising from this work are also considered. Two appendices are included at the end to provide additional details not described within the body of this dissertation. Appendix A describes the instrument control program and interface designed to manipulate the mass flow controller (MFC) set points in real time for the fabrication of the arbitrary film structures described in Chapter 7. Appendix B is an adapted version of a research proposal that describes the fabrication of novel oleophobic/hydrophilic coatings.

REFERENCES

1. Hall, C.; Murphy, P.; Griesser, H., Etching and deposition mechanism of an alcohol plasma on polycarbonate and poly(methyl methacrylate): an adhesion promotion mechanism for plasma deposited a:SiO_xC_yH_z Coating. *Plasma Processes Polym.* **2012**, *9*, (9), 855-865.
2. Hall, C. J.; Murphy, P. J.; Griesser, H. J., Direct imaging of mechanical and chemical gradients across the thickness of graded organosilicone microwave PECVD coatings. *ACS Appl. Mater. Interfaces* **2014**, *6*, (2), 1279-1287.
3. Intranuovo, F.; Howard, D.; White, L. J.; Johal, R. K.; Ghaemmaghami, A. M.; Favia, P.; Howdle, S. M.; Shakesheff, K. M.; Alexander, M. R., Uniform cell colonization of porous 3-D scaffolds achieved using radial control of surface chemistry. *Acta Biomater.* **2011**, *7*, (9), 3336-3344.
4. De Bartolo, L.; Morelli, S.; Bader, A.; Drioli, E., Evaluation of cell behaviour related to physico-chemical properties of polymeric membranes to be used in bioartificial organs. *Biomaterials* **2002**, *23*, (12), 2485-2497.
5. Howarter, J. A.; Youngblood, J. P., Amphiphile grafted membranes for the separation of oil-in-water dispersions. *J. Colloid Interface Sci.* **2009**, *329*, (1), 127-132.
6. Baytekin, H. T.; Wirth, T.; Gross, T.; Treu, D.; Sahre, M.; Theisen, J.; Schmidt, M.; Unger, W. E. S., Determination of wettability of surface-modified hot-embossed polycarbonate wafers used in microfluidic device fabrication via XPS and ToF-SIMS. *Surf. Interface Anal.* **2008**, *40*, (3-4), 358-363.
7. Gururaj, T.; Subasri, R.; Raju, K. R. C. S.; Padmanabham, G.; Raju, K., Effect of plasma pretreatment on adhesion and mechanical properties of UV-curable coatings on plastics. *Appl. Surf. Sci.* **2011**, *257*, (9), 4360-4364.
8. Hofrichter, A.; Bulkin, P.; Drevillon, B., An interfacial study of a hydrogenated carbon interlayer for adhesion enhancement of plasma deposited silica thin films on polycarbonate. *J. Adhes. Sci. Technol.* **2002**, *16*, (4), 395-407.
9. Muir, B.; Thissen, H.; Simon, G.; Murphy, P.; Griesser, H., Factors affecting the adhesion of microwave plasma deposited siloxane films on polycarbonate. *Thin Solid Films* **2006**, *500*, (1-2), 34-40.
10. Xu, W. D.; Chellam, S., Initial stages of bacterial fouling during dead-end microfiltration. *Environ. Sci. Technol.* **2005**, *39*, (17), 6470-6476.
11. Zhang, M. M.; Li, C.; Benjamin, M. M.; Chang, Y. J., Fouling and natural organic matter removal in adsorben/membrane systems for drinking water treatment. *Environ. Sci. Technol.* **2003**, *37*, (8), 1663-1669.

12. Qu, F.; Liang, H.; Zhou, J.; Nan, J.; Shao, S.; Zhang, J.; Li, G., Ultrafiltration membrane fouling caused by extracellular organic matter (EOM) from *Microcystis aeruginosa*: Effects of membrane pore size and surface hydrophobicity. *J. Membr. Sci.* **2014**, 449, (0), 58-66.
13. Kull, K. R.; Steen, M. L.; Fisher, E. R., Surface modification with nitrogen-containing plasmas to produce hydrophilic, low-fouling membranes. *J. Membr. Sci.* **2005**, 246, (2), 203-215.
14. Tompkins, B. D.; Dennison, J. M.; Fisher, E. R., H₂O plasma modification of track-etched polymer membranes for increased wettability and improved performance. *J. Membr. Sci.* **2013**, 428, 576-588.
15. Shi, X.; Field, R.; Hankins, N., Review of fouling by mixed feeds in membrane filtration applied to water purification. *Desalin. Water Treat.* **2011**, 35, (1-3), 68-81.
16. He, D.; Susanto, H.; Ulbricht, M., Photo-irradiation for preparation, modification and stimulation of polymeric membranes. *Prog. Polym. Sci.* **2009**, 34, (1), 62-98.
17. Lippert, T., Interaction of photons with polymers: from surface modification to ablation. *Plasma Processes Polym.* **2005**, 2, (7), 525-546.
18. Truica-Marasescu, F.; Jedrzejowski, P.; Wertheimer, M. R., Hydrophobic recovery of vacuum ultraviolet irradiated polyolefin surfaces. *Plasma Processes Polym.* **2004**, 1, (2), 153-163.
19. Alexander, C. S.; Branch, M. C.; Strobel, M.; Ulsh, M.; Sullivan, N.; Vian, T., Application of ribbon burners to the flame treatment of polypropylene films. *Prog. Energy Combust. Sci.* **2008**, 34, (6), 696-713.
20. Song, J.; Gunst, U.; Arlinghaus, H. F.; Vancso, G. J., Flame treatment of low-density polyethylene: Surface chemistry across the length scales. *Appl. Surf. Sci.* **2007**, 253, (24), 9489-9499.
21. Grill, A., *Cold Plasma Matierls Fabrication: From Fundamentals to Applications*. IEEE Press: Piscataway, NJ, 1994.
22. Standaert, T.; Hedlund, C.; Joseph, E. A.; Oehrlein, G. S.; Dalton, T. J., Role of fluorocarbon film formation in the etching of silicon, silicon dioxide, silicon nitride, and amorphous hydrogenated silicon carbide. *J. Vac. Sci. Technol., A* **2004**, 22, (1), 53-60.
23. Larsson, A.; Dérand, H., Stability of polycarbonate and polystyrene surfaces after hydrophilization with high intensity oxygen RF plasma. *J. Colloid Interface Sci.* **2002**, 246, (1), 214-221.
24. Occhiello, E.; Morra, M.; Cinquina, P.; Garbassi, F., Hydrophobic recovery of oxygen-plasma-treated polystyrene. *Polymer* **1992**, 33, (14), 3007-3015.

25. Spohr, R.; Sharma, G.; Forsberg, P.; Karlsson, M.; Hallén, A., Stroke asymmetry of tilted superhydrophobic ion track textures. *Langmuir* **2010**, 26, (9), 6790-6796.
26. Allan, A. J. G., The spreading of liquids on polyethylene film. The effect of preprinting treatments. *Journal of Polymer Science* **1959**, 38, (134), 297-306.
27. Mantell, R. M.; Ormand, W. L., Activation of plastic surfaces in a plasmajet. *Ind. Ena. Chem. Prod. Res. Dev.* **1964**, 3, (4), 300-303.
28. Hansen, R. H.; Schonhorn, H., A new technique for preparing low surface energy polymers for adhesive bonding. *J. Polym. Sci., Part B: Polym. Lett.* **1966**, 4, (3), 203-209.
29. Schonhorn, H.; Hansen, R. H., Surface treatment of polymers for adhesive bonding. *J. Appl. Polym. Sci.* **1967**, 11, (8), 1461-1474.
30. Grace, J. M.; Gerenser, L. J., Plasma treatment of polymers. *J. Dispersion Sci. Technol.* **2003**, 24, (3-4), 305-341.
31. Kravets, L. I.; Dmitriev, S. N.; Gil'man, A. B., Modification of properties of polymer membranes by low-temperature plasma treatment. *High Energ. Chem.* **2009**, 43, (3), 181-188.
32. Gupta, B.; Hilborn, J. G.; Bisson, I.; Frey, P., Plasma-induced graft polymerization of acrylic acid onto poly(ethylene terephthalate) films. *J. Appl. Polym. Sci.* **2001**, 81, (12), 2993-3001.
33. Steen, M. L.; Hymas, L.; Havey, E. D.; Capps, N. E.; Castner, D. G.; Fisher, E. R., Low temperature plasma treatment of asymmetric polysulfone membranes for permanent hydrophilic surface modification. *J. Membr. Sci.* **2001**, 188, (1), 97-114.
34. Steen, M. L.; Jordan, A. C.; Fisher, E. R., Hydrophilic modification of polymeric membranes by low temperature H₂O plasma treatment. *J. Membr. Sci.* **2002**, 204, (1-2), 341-357.
35. Steen, M. L.; Butoi, C. I.; Fisher, E. R., Identification of gas-phase reactive species and chemical mechanisms occurring at plasma-polymer surface interfaces. *Langmuir* **2001**, 17, (26), 8156-8166.

CHAPTER 2

EXPERIMENTAL METHODS

This chapter contains information regarding the materials, methods, and techniques used in performing the research reported in this dissertation. Much of this chapter is adapted from the publications that arose from data presented in Chapters 4, 5, and 7 are based on; those text and figures are reproduced here with permission from their respective publishers. This chapter is organized into sections based on the following topics: reactor design and plasma processing procedures (2.1.), material and surface analysis equipment and techniques (2.2.), and gas-phase diagnostic techniques (2.3.).

2.1. Reactor Design and Plasma Processing Methods

2.1.1. General reactor design. In general, all plasma enhanced chemical vapor deposition (PECVD) and plasma surface modifications were performed using an inductively coupled glass barrel style rf plasma reactor described previously,¹ Figure 2.1. The reactors were constructed using borosilicate glass tubing (50 mm, i.d.) and were 34-57 cm in length, depending on experimental requirements. The 8-9 turn induction coil was made from 5 AWG nickel plated copper wire and powered by a 13.56 MHz rf power generator (RFX 600; Advanced Energy Industries Inc., Fort Collins, CO). Vacuum was achieved using a two-stage rotary vane pump and Baratron® capacitance manometers (MKS Instruments Inc., Andover, MA) were used to monitor the reactor pressure (<10 mTorr base pressure). Gas-phase precursors (e.g. O₂) and high vapor pressure liquid precursors (e.g. C₃F₈) were introduced into the reactor using mass flow controllers (MFC) (MKS Instruments Inc., Andover, MA). Liquid-phase precursors (e.g. H₂O)

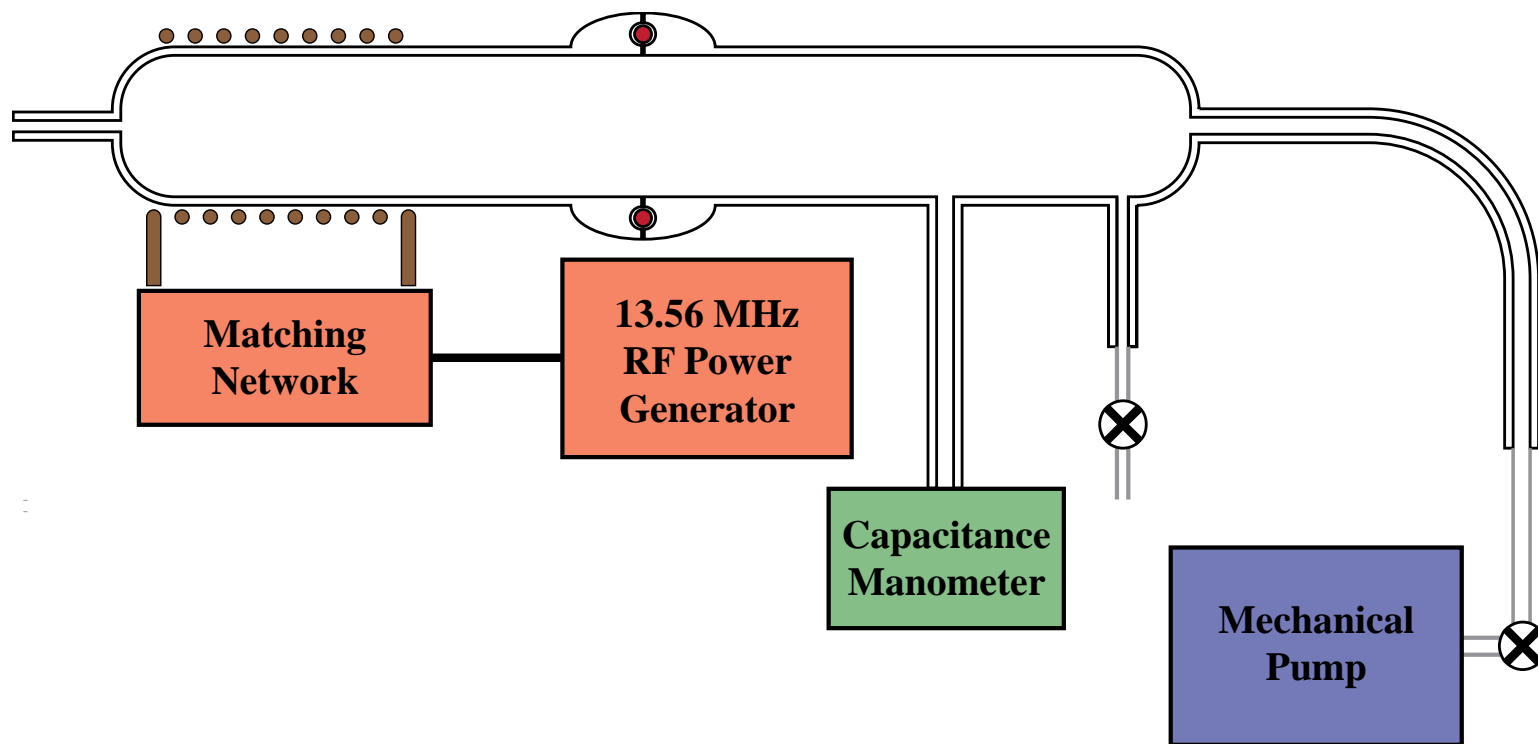


Figure 2.1. General design for 13.56 MHz inductively coupled borosilicate glass barrel style plasma reactor.

were placed into a borosilicate round bottom side arm flasks, degassed using three freeze-pump-thaw cycles, and were introduced into the reactor via a needle metering valve. The reactor was typically purged with precursor gas for ≥ 5 min before and after plasma ignition to minimize contamination prior to ignition and to quench the reactive sites known to form during plasma processing.

2.1.2. Plasma surface modification of polymer substrates. Polymer substrates, including high-density polyethylene (HDPE), low-density polyethylene (LDPE), polypropylene (PP), polystyrene (PS), polycarbonate (PC), 75A polyurethane (PU) (0.060 in. sheet stock; United States Plastic Corporation, Lima, OH), and polycarbonate (Lexan® 9034V; Sabic Innovative Plastics, Pittsfield, MA) were chosen to encompass a wide variety of functionalities, structural characteristics and material properties. Cuttings of each polymer (~1x2 cm) were first cleaned by agitating in ethanol (absolute, reagent grade; Mallinckrodt Baker) for 60 s followed by rinsing with ultra-pure H₂O [reverse osmosis (RO) purified, ≥ 18 M Ω] for 60 s to remove residues from manufacturing and environmental contamination. The washed polymer substrates were then stored in a vacuum desiccator for 24 h prior to treatment or analysis. The prepared polymer substrates were placed on a glass slide at the desired position within the plasma reactor and plasma modification was performed using H₂O vapor (RO purified, ≥ 18 M Ω) as feed gas. The conditions used [applied rf power (P) = 25 W, 50 mTorr, 9 cm downstream substrate position, and 2 min treatment time] were based on previous studies²⁻⁴ and are hereafter referred to as “standard treatment conditions.” Treated and control samples were stored in cleaned PS Petri dishes under ambient laboratory conditions and protected from light prior to analysis.

2.1.3. Plasma surface modification of polymer membranes. The procedures used for the plasma surface modification of polymer membranes were similar to those used for the plasma

surface modification of solid polymer substrates. The track-etched polycarbonate (PC-TE) and track etched polyethylene terephthalate (PET-TE) membranes (Sterlitech Corporation, Kent, WA) and select manufacturer specifications are listed in Table 2.1. Circular samples were cut using an arch punch and mounted in one of two different sample holders developed for these experiments, Figure 2.2. The holder shown in Figure 2.2.a. (1.5 in. diameter) was initially developed because the parts used to fabricate the holders used in previous studies²⁻⁸ were no longer available and because the all glass design was desirable for use in experiments that might be sensitive to potential products etched from the holder during processing (e.g. gas-phase diagnostics). The second holder, shown in Figure 2.2.b. (1.375 in. diameter), was developed later because of issues with reproducing working copies of the first membrane holder. That holder is similar to the one original reported² except that it clamps the sample between a glass ring and the glass body of the holder, thereby holding the sample flat. The holder was placed in the reactor such that the mounted membrane was at the desired position and plasma modification was carried out using H₂O vapor (RO purified, ≥ 18 M Ω) as feed gas. In addition to the standard treatment conditions, other treatment parameters studied include: $P = 25$ -100 W, 50-350 mTorr, and treatment times of 0.5-40 min.

2.1.4. Plasma etching of polymer membranes. The procedures used for the plasma etching of polymer membranes (0.2 μ m PC-TE) were similar to those used for plasma surface modification of polymer membranes studies. Precursors used for etching studies include CO₂ (industrial grade; General Air), O₂ (medical grade; Airgas), H₂O (RO purified, ≥ 18 M Ω), and formic acid (HCOOH, High Purity, 98.0-100%; Sigma-Aldrich). The gas phase precursors were used as received and the liquid phase precursors were degassed using three freeze-pump-thaw cycles prior to use. The separate sides of the PC-TE membranes used in these experiments had

Table 2.1. Track-etched membranes and manufacturer specifications.

Membrane	Manufacturer Reported Pore Size (μm)	Pore Density (cm^{-2})	Thickness (μm)
PET-TE	0.2	3×10^8	10
	3	2×10^8	9
PC-TE (hydrophobic)	0.2	3×10^8	10
	3	2×10^8	9
PC-TE (hydrophilic) ^a	0.2	3×10^8	10

^aThese membranes were PVP-coated and thus had been chemically altered to make them hydrophilic and were used only for performance tests as a comparison to our plasma-treated hydrophilic membranes.

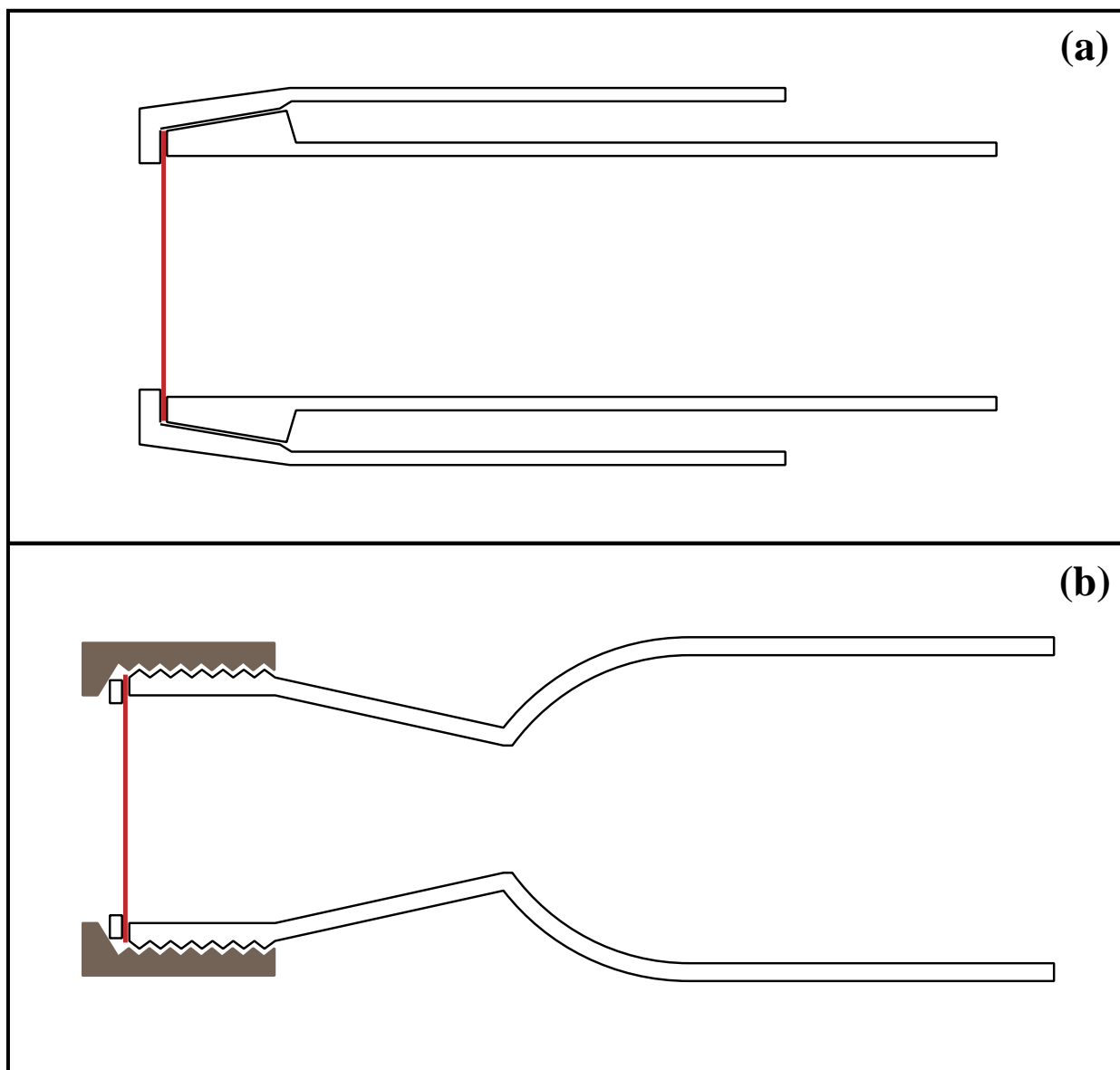


Figure 2.2. Membrane samples holders used to hold membranes perpendicular to the flow of gases during plasma surface modification. Design (a) was constructed entirely from borosilicate glass, and design (b) was made from the threaded half of a Rodaviss® joint.

radically different morphologies following long treatments times (>10 min for all plasma systems); therefore, only the side designated as *Side B* was used for etching experiments because the pore boundaries remained well-defined following treatment. The membrane holder shown in Figure 2.2.b was used to mount the PC-TE for all etching experiments. As the primary goal of the PC-TE etching study was to establish the etching rate of PC-TE, samples were exposed to the plasma for different times (2-40 min). All other treatment parameters conformed to the standard treatment conditions discussed in section 2.1.2.

2.1.5. PECVD of thin films using organic acid precursors. PC-TE (0.2 μm) and Si wafer substrates ([100], p-type; Wacker-Chemtronic GmbH) were coated with thin hydrocarbon-like films using PECVD. The Si wafer substrates were cleaned using an O_2 plasma ($P = 200 \text{ W}$, 100 mTorr O_2 , 10 minutes) to remove residual carbon immediately prior to use (confirmed by XPS). Extra pure acetic acid (CH_3COOH , 99.8-100.5%; Sigma-Aldrich) was degassed using three freeze-pump-thaw cycles. The procedures used for the deposition of CH_3COOH thin films onto polymer membranes were similar to those used for studies of plasma surface modification and plasma etching of polymer membranes. Wafer cleaning and CH_3COOH thin film depositions were performed in the same plasma reactor, described in section 2.1.1. All samples were modified using standard treatment conditions, unless otherwise stated.

2.1.6. PECVD of homogeneous and gradient hydrocarbon/fluorocarbon films. Homogeneous hydrocarbon/fluorocarbon films were deposited by PECVD using static gas mixtures and gradient films with hydrocarbon and fluorocarbon regions were deposited by PECVD using dynamic gas mixtures. The film precursor gases were C_3F_8 (99.96%; Airgas) and H_2 (99.9%; Airgas), and were used as received. Films were deposited on Si wafer substrates ([100], p-type; Wacker-Chemtronic GmbH), used as received, or on pressed KBr pellets [Fourier

transform infrared spectroscopy (FTIR) grade, Sigma-Aldrich]. All PECVD was carried out in the plasma reactor described in section 2.1.1., Figure 2.1. As an additional precaution, ceramic sleeves were inserted into the reactor to prevent etching and re-deposition of SiO_x material from the borosilicate glass reactor walls, in accordance with previous work.⁹ The goal of this study was to control film deposition in real time to prepare gradient films, films with compositions that vary continuously with respect to depth. To this end, an additional control system was designed using Labview™ v8.5 to monitor and adjust the mass flow controller set points (see Appendix A). This allowed C₃F₈ and H₂ to be adjusted in real time based on a preset deposition program. Although the control program permits a wide variety of possible feed gas profiles, only two profiles were used to prepare films for these experiments: a constant ratio (static system) and changing ratio based a linear function (dynamic system). To avoid wall effects known to influence plasma chemistry and deposition rate measurements, the walls of the reactor were “seasoned” before introducing substrates by operating the plasma reactor under the same deposition condition for a given set of substrates. Substrates were placed on a glass slide and positioned 9 cm downstream from the end of the coil region. All film depositions were carried out at $P = 50$ W with a total feed gas flow rate of 5 standard cubic centimeters per second (sccm) (C₃F₈ flow + H₂ flow) resulting in a typical reactor pressure of ~100 mTorr. All film samples were stored under ambient laboratory conditions.

2.2. Material and Surface Analysis Equipment and Methods

2.2.1. X-ray photoelectron spectroscopy. X-ray photoelectron spectroscopy (XPS) analysis was performed using a PHI 5800 ESCA system (Physical Electronics, Eden Prairie, MN) operating with a monochromatic Al K α source (350 W) and a hemispherical electron

analyzer. Low energy electron flood gun (~5 eV electron energy) and argon ion neutralizers were used to compensate for surface charging, as necessary. Initially, a spectrum was collected using survey mode (50-1100 eV, 187.85 eV pass energy, 1.600 eV/step, 20 ms/step, 45° take-off angle) to determine the approximate composition of each sample surface. High resolution spectra (23.5 eV pass energy, 0.100 eV/step, 100 ms/step, 45° take-off angle) were then collected in triplicate, from different sample spots, for all elements present at concentrations $\geq 1\%$. Initial data analysis was performed using MultiPak v6.1A (Physical Electronics, Eden Prairie, MN). All high resolution spectra were smoothed, indexed based on an aliphatic carbon binding energy of 285.0 eV, and atomic concentrations were calculated. Additional deconvolution was performed using the XPSPeak v4.1 software to determine the relative contribution of binding environments to high resolution peaks of interest. Generally, high resolution C_{1s} spectra from polymer samples (i.e. polymer membranes, solid polymer substrates) were fit using a combination of binding environments, including hydrocarbon (C-C/C-H), ether/alcohol (C-O), carbonyl (C=O), acid/ester (O-C=O), and carbonate (O=C(-O)₂).¹⁰ The high resolution C_{1s} spectra of homogeneous hydrocarbon and fluorocarbon film samples were fit using additional binding environments to account for fluorine incorporation, including C-CF, CF-C, CF-CF, CF₂, and CF₃, based on previous work¹¹⁻¹³ and other literature sources.¹⁴ All reported mean relative % binding environment contributions and elemental compositions were calculated from the triplicate measurements and error reported was one standard deviation of that mean.

2.2.2. H₂O contact angle goniometry. All H₂O contact angle (wCA) measurements were made using a DSA 10 contact angle goniometer (Krüss GmbH, Hamburg, Germany) to quantify the wetting behavior on native, cleaned, or modified solid surfaces. The typical dose volume for a wCA measurement was 2 μ L of ultra-pure H₂O (RO purified, ≥ 18 M Ω). Two types of contract

angle goniometer experiments were performed: static mode (still images) and movie mode (time-resolved images). Static wCA measurements were performed by manually capturing a still image immediately after dosing the surface. Movie mode wCA measurements were performed using the software controlled trigger lines to start acquisition and images were collected at 2.5 frames per second. For wCA measurements made on freshly plasma treated samples, images were collected as quickly as possible (20-60 min) following surface modification. All still images and movies were then analyzed using the Drop Shape Analysis software provided with the instrument. The fitting algorithm used to extract the wCA from each image, circle or tangent-1 fitting, was chosen based on the guidelines outlined in the instrument manual.¹⁵ Generally, the circle fitting method was used to fit hydrophilic surfaces (e.g. oxidized polymer surfaces) and the tangent-1 method was used to fit hydrophobic surfaces (e.g. fluorocarbon films). In cases where a range of wettabilities were measured, a single method was chosen for consistency. The wCA values reported in this dissertation are the mean of all measurements taken from a given sample or set of conditions and the error is one standard deviation of that mean.

2.2.3. Variable angle spectroscopic ellipsometry. Variable angle spectroscopic ellipsometry (VASE) measurements were made using the M-2000 VASE Ellipsometer (J.A. Woollam Co., Lincoln, NE). Film samples prepared for VASE measurements were deposited on Si wafer pieces ([100], p-type; Wacker-Chemtronic GmbH) and measurements were performed at angles of 55, 65, and 75° using a wavelength range of 300-1700 nm (20 nm increments). The results were typically fit using some variation of the Cauchy dispersion model to extract optical parameters including film thickness. Model optimization was performed until the mean square error was minimized. Deposition rate measurements were made using either a time point

(Chapter 7) or by measuring the film thickness from multiple time points and performing linear regression to calculate the deposition rate (Chapter 6). Deposition rates were always calculated from thickness measurements made on a minimum of three separate samples and error is one standard deviation.

2.2.4. Scanning electron microscopy. Scanning electron microscopy (SEM) images were obtained with a JSM 6500F (JEOL, Ltd., Japan) scanning electron microscope equipped with a field emission source. Flexible samples (e.g. polymer membranes) were prepared by mounting a small cutting on an aluminum sample stub with conductive carbon tape (3M) and sputter coated with ≤ 10 nm of Au to mitigate charging. Cross-sections of thin films on solid substrates were prepared by freeze fracturing the solid substrate using liquid nitrogen. The cleaved sample was then clamped axially such that the exposed cross section could be sputter coated with 5 nm of Au. All images were collected with an accelerating voltage of 5-15 kV to optimize contrast. Select SEM images were analyzed further using Adobe Photoshop® CS5.5 wherein the ruler tool was used to measure the size of sample features against the image scale bar. Pore diameters reported are the mean of measurements made on a minimum of 12 pores per image from 2 separate images taken of a given sample.

SEM was used extensively to measure the pore sizes of PC-TE and PET-TE samples (see Chapters 4, 5, and 6). Pore size measurements were made manually using the ruler tool in Photoshop® CS5.5. Because we were interested in the extent of change from etching or deposition, only isolated pores with a regular circular or elliptical shape were measured; pores whose boundaries were overlapping or irregularly shaped were not included in the measurement. For experiments to measure the rate of change of pore radius, the average pore radius was calculated for each image from the measured pore diameters. The procedure was repeated for at

least 3 separate images for each sample/treatment time as well as the untreated PC-TE (117 ± 1 nm) and the pore radius rate of change was determined by calculating the slope of the radius-plasma exposure time x-y data using a weighted linear regression. The two sides of the PC-TE membranes used in these studies had radically different morphologies following long treatment times (>10 min for all plasma systems); only the pore boundaries on *Side B* remained well-defined following treatment. Therefore, the PC-TE membrane was oriented with *Side B* facing upstream to measure the upstream etch rate and with *Side B* facing downstream to measure the downstream etch rate. Although PC-TE has a very narrow pore size distribution, this is still the largest contributor to error before and after plasma processing. Given our strict criteria in choosing the pores to measure, the error reported here cannot be used as an absolute measure of pore size distribution.

2.2.5. Fourier transform infrared spectroscopy. Films prepared for FTIR analysis were deposited on freshly pressed KBr pellets (FTIR Grade; Sigma-Aldrich) made using a pellet die (#3619; Carver, Wabash, IN) at 18000 pounds of pressure. All KBr pellets were stored in a desiccator prior to deposition and analysis. FTIR spectra were collected in transmission mode using a Nicolet 6700 FTIR (Thermo Fisher Scientific, Madison, WI). Spectra were compiled from 256 scans with an 8 cm^{-1} resolution. Spectra used to identify peak positions were collected in triplicate from different regions on select samples and at a higher resolution (4 cm^{-1}). Baseline correction, blank sample subtraction and atmospheric signal suppression were performed on each spectrum using Omnic v8.2.

2.2.6. Differential scanning calorimetry. The thermal properties of HDPE, LDPE and PP sample substrates were measured using differential scanning calorimetry (DSC) using the DSC 2920 (TA Instruments, New Castle, DE). Samples were crimped into hermetically sealed

aluminum sample pans, cooled below -100 °C and heated past melting for two full heating cycles at a rate of 10 °C/min. Cooling was aided by a liquid nitrogen cooling system. Analysis of the DSC results was performed using the TA Universal Analysis v4.2E software, provided with the instrument.

2.2.7. Pure H₂O flux measurements. Water flux experiments were performed on membranes using the Amicon® 8010 stirred cell, from Millipore, Figure 2.3. Membranes were pre-compacted with ultra-pure water under 15 psi of nitrogen pressure for 15 min. The pressure was immediately reduced to 5 psi and flux was determined gravimetrically by collecting effluent for 1 min every 30 min for 180 min. Given that concentration polarization is of little concern when measuring pure water flux, the cell was not stirred during the measurements. The reported flux results are the mean of 5 separate measurements and the error is one standard deviation of that mean.

2.3. Gas-phase Diagnostic Equipment and Methods

Optical emission spectroscopy (OES) experiments were performed using the AvaSpec 3648 (Avantes, Broomfield, CO) equipped with four spectral channels, giving the spectrometer a total spectral range of 187-1016 nm and a ~0.05 nm resolution. OES was always performed in irradiance mode using a modified reactor that included a fused silica window to maximize the transmission of UV wavelengths. A small amount of Ar ($\leq 10\%$ by partial pressure) was added to the feed for actinometry unless otherwise noted. The configuration of this equipment was altered based on experimental requirements.

Time-resolved optical emission spectroscopy (TR-OES) was performed to measure the relative gas-phase density of radical species with and without a 0.2 μm PC-TE membrane

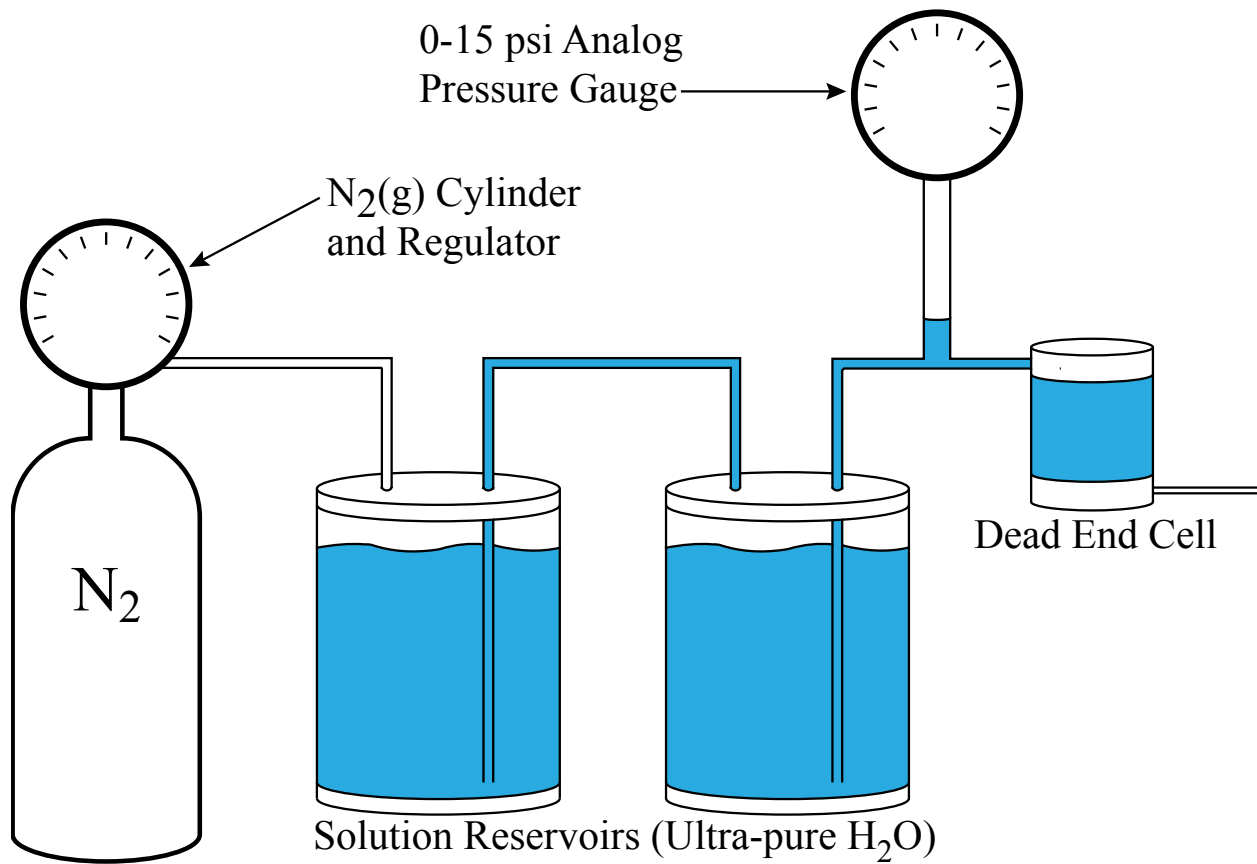


Figure 2.3. Schematic of dead end style ultrafiltration cell for testing water flux performance of track-etch membranes.

installed in the plasma reactor (Chapter 4). To better characterize the plasma at the position where membranes are modified, the fused silica collection port was located 9 cm downstream from the end of the coil region of the plasma reactor and oriented perpendicular to the long axis of the reactor, Figure 2.4. Because of low plasma glow intensity at lower P , only the higher P systems could be examined in this experiment. The conditions tested were thus $P = 100$ W and 100 mTorr reactor pressure. In this configuration, three types of experiments were run for the H₂O vapor plasmas: (1) no membrane; (2) with a membrane and the OES collection port placed immediately upstream of the membrane; and (3) with a membrane and the collection port placed immediately downstream of the membrane. Spectra were collected over the entire spectral range in a time-resolved fashion at 0.2 Hz with integration times of 1000-5000 ms depending on the intensity of the plasma. Time-resolved data were analyzed to examine the relative gas phase densities of selected species as a typical sample treatment proceeded. Relative gas phase densities were extracted from OES data by normalizing key spectral lines from species of interest [O*(777.11 nm), H α (656.22 nm), OH* (308.87 nm), and CO* (519.67 nm)] to an Ar emission line (750.31 nm) and normalizing those results against the most intense data point measured in a given experiment.

Discrete emission spectra were collected to identify excited state species present in O₂, CO₂, H₂O, and HCOOH plasma systems and to measure the relative gas-phase density of key radical species (Chapter 5). Plasma emission was collected by placing the fiber optic probe from the spectrometer against the fused silica window oriented perpendicular to the long axis of the reactor, positioned 9 cm downstream from the end of the induction coil region, Figure 2.4. The actinometer was added to the reactor feed from a differentially pumped region (500 mTorr Ar) via a needle metering valve to yield 5 mTorr of partial pressure, measured before the addition of

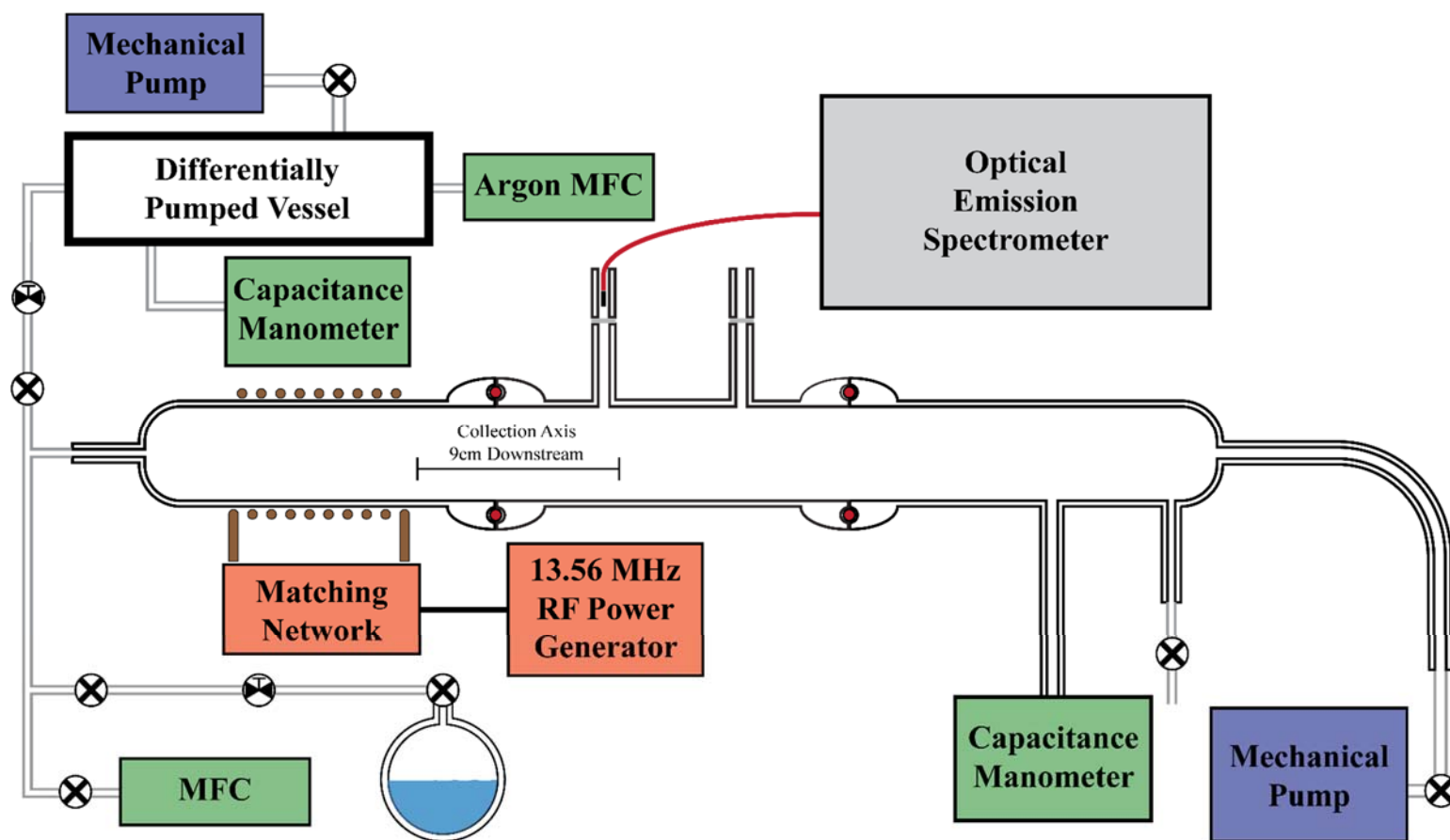


Figure 2.4. Reactor design used for TR-OES on track-etched membranes and oxidizing plasma systems. The fused silica window is oriented perpendicular to the long axis of the reactor and the system is equipped with a differentially pumped region to aid in the addition of Ar for actinometry.

other feed gases. After setting the feed gas pressure, the reactor pressure was allowed to equilibrate for 20-30 min prior to igniting the plasma and the plasma was allowed to equilibrate for >30 min (50 mTorr, $P = 25$ W) prior to data collection. The entire experiment was restaged three separate times, collecting spectra in triplicate from each trial to determine errors associated with reproducibly establishing gas ratios. The ratio of O* (844.63 nm) and OH* (309.03 nm) emission line intensities to Ar* emission line intensity (750.31 nm) were calculated to characterize the relative gas-phase density of each radical species. The reported relative gas phase densities are the calculated mean from these experiments and error is one standard deviation.

TR-OES was also used to determine the relative density of excited state gas phase species in the dynamic C₃F₈/H₂ PECVD system (Chapter 7). In this experiment, the fused silica window was oriented co-axially to the reactor so that plasma emission could be sampled from the entire length of the plasma glow, Figure 2.5. A deposition program was used to change the feed gas composition during TR-OES collection. The actinometer gas was introduced into the reactor along with the feed gas using a separate controller box and MFC. The complete emission spectrum was collected every 5 s by averaging 30 spectra using a 150 ms integration time. Emission line intensities from species of interest [CF₂* (251.7 nm), CF* (202.5 nm), H α (656.2 nm), CH* (431.0 nm), CHF* (578.5 nm)] were normalized against the Ar* emission line (750.3 nm). The normalized emission intensities were plotted as a function of time to investigate changes in gas phase density with changing feed gas composition.

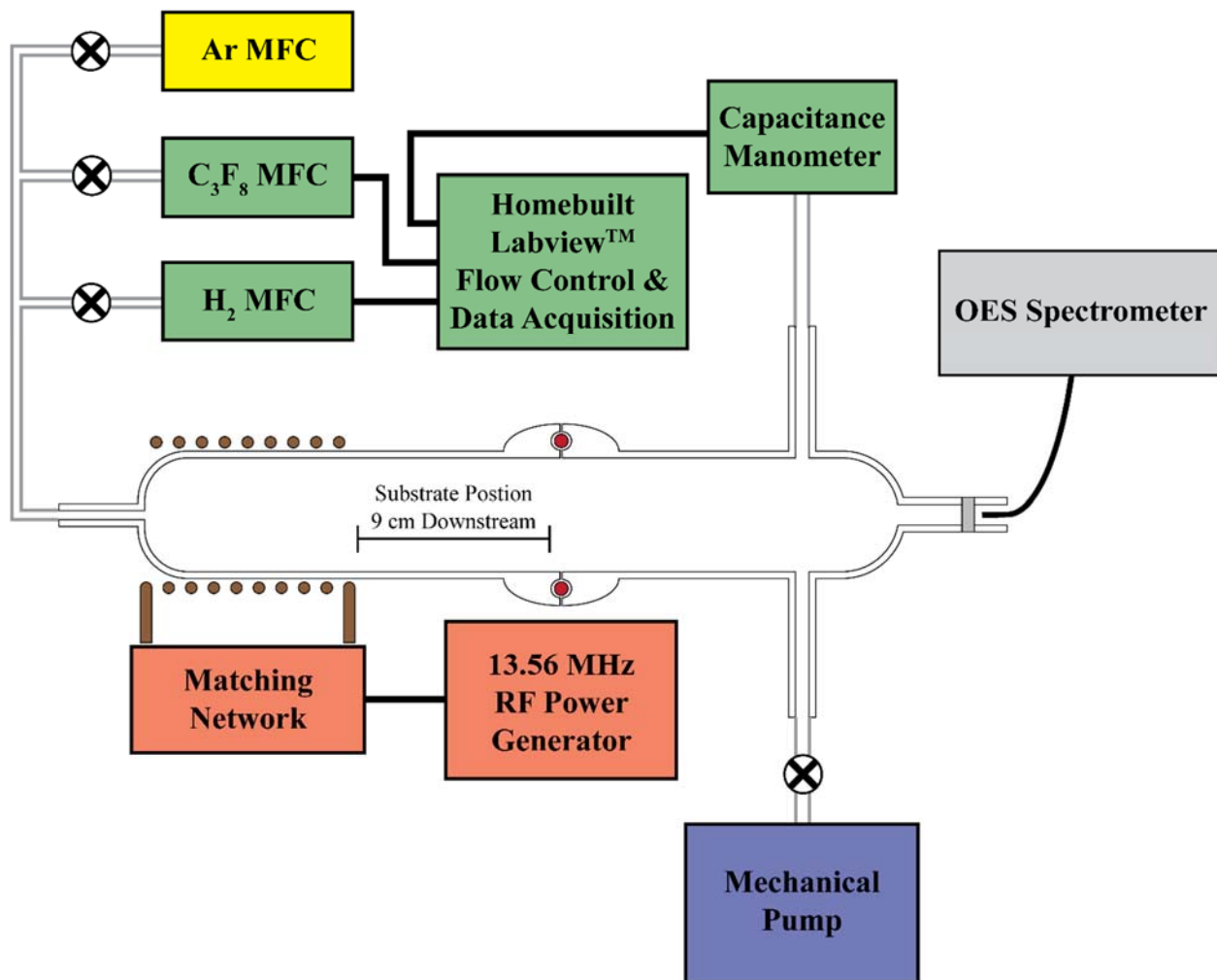


Figure 2.5. Reactor design used for TR-OES on the C₃F₈/H₂ dynamic plasma system. The fused silica window is oriented co-axially to allow sampling of emission from the entire length of the reactor.

REFERENCES

1. Bogart, K. H. A.; Dalleska, N. F.; Bogart, G. R.; Fisher, E. R., Plasma enhanced chemical vapor deposition of SiO₂ using novel alkoxy silane precursors. *J. Vac. Sci. Technol., A* **1995**, 13, (2), 476-480.
2. Steen, M. L.; Hymas, L.; Havey, E. D.; Capps, N. E.; Castner, D. G.; Fisher, E. R., Low temperature plasma treatment of asymmetric polysulfone membranes for permanent hydrophilic surface modification. *J. Membr. Sci.* **2001**, 188, (1), 97-114.
3. Steen, M. L.; Jordan, A. C.; Fisher, E. R., Hydrophilic modification of polymeric membranes by low temperature H₂O plasma treatment. *J. Membr. Sci.* **2002**, 204, (1-2), 341-357.
4. Steen, M. L.; Butoi, C. I.; Fisher, E. R., Identification of gas-phase reactive species and chemical mechanisms occurring at plasma-polymer surface interfaces. *Langmuir* **2001**, 17, (26), 8156-8166.
5. Wavhal, D. S.; Fisher, E. R., Hydrophilic modification of polyethersulfone membranes by low temperature plasma-induced graft polymerization. *J. Membr. Sci.* **2002**, 209, (1), 255-269.
6. Wavhal, D. S.; Fisher, E. R., Modification of porous poly(ether sulfone) membranes by low-temperature CO₂-plasma treatment. *J. Polym. Sci., Part B: Polym. Phys.* **2002**, 40, (21), 2473-2488.
7. Kull, K. R.; Steen, M. L.; Fisher, E. R., Surface modification with nitrogen-containing plasmas to produce hydrophilic, low-fouling membranes. *J. Membr. Sci.* **2005**, 246, (2), 203-215.
8. Wavhal, D. S.; Fisher, E. R., Modification of polysulfone ultrafiltration membranes by CO₂ plasma treatment. *Desalination* **2005**, 172, (2), 189-205.
9. Mackie, N. M.; Dalleska, N. F.; Castner, D. G.; Fisher, E. R., Comparison of pulsed and continuous-wave deposition of thin films from saturated fluorocarbon/H-2 inductively coupled rf plasmas. *Chem. Mater.* **1997**, 9, (1), 349-362.
10. Vickerman, J. C., *Surface Analysis: The Principal Techniques*. John Wiley & Sons, Ltd.: West Sussex, U.K., 1997.
11. Cuddy, M. F.; Fisher, E. R., Contributions of CF and CF₂ species to fluorocarbon film composition and properties for C_xF_y plasma-enhanced chemical vapor deposition. *ACS Appl. Mater. Interfaces* **2012**, 4, (3), 1733-1741.
12. Liu, D. P.; Cuddy, M. F.; Fisher, E. R., Comparison of CH, C₃, CHF, and CF₂ surface reactivities during plasma-enhanced chemical vapor deposition of fluorocarbon films. *ACS Appl. Mater. Interfaces* **2009**, 1, (4), 934-943.

13. Martin, I. T.; Malkov, G. S.; Butoi, C. I.; Fisher, E. R., Comparison of pulsed and downstream deposition of fluorocarbon materials from C₃F₈ and c-C₄F₈ plasmas. *J. Vac. Sci. Technol., A* **2004**, 22, (2), 227-235.
14. Sandrin, L.; Silverstein, M. S.; Sacher, E., Fluorine incorporation in plasma-polymerized octofluorocyclobutane, hexafluoropropylene and trifluoroethylene. *Polymer* **2001**, 42, (8), 3761-3769.
15. Krüss GMBH, *Krüß DSA Drop Shape Analysis Manual*. Krüss GMBH: Hamburg, Germany, 1997.

CHAPTER 3

HYDROPHOBIC RECOVERY BEHAVIOR OF VARIOUS POLYMERS FOLLOWING H₂O PLASMA PROCESSING

This chapter is based on unpublished work performed to further our understanding of hydrophobic recovery processes on different polymer surfaces. The polymers used in these experiments were chosen based on their diverse composition and properties, as well as their ubiquitous use as engineering materials. Cleaned control, freshly treated, and aged polymer samples were tested using various materials analysis methods to characterize their respective hydrophobic recovery behaviors. The experiments and results reported here were first reported as part of the author's preliminary orals report. All reported data were, however, reexamined at the time that this chapter was written, several years after the original report. This is highlighted by the XPS results included here, the interpretation of which relies on concepts and data analysis techniques developed after this original work and reported in later chapters of this dissertation. Thus, this chapter provides an account of early work that provided insight and direction to the more recent projects reported in this dissertation. Funding for this research was provided by the National Science Foundation (CHE-0911248).

3.1. Introduction

Polymers find uses in many important modern industries, including automotive,^{1,2} biomedical,^{3,4} environmental,⁵ and laboratory applications.⁶ However, because the properties of the polymer surface, including surface tension and surface functionality, are often incompatible with the intended application, the utility of polymers can be problematic. Among the most

common issues are adhesive failure and delamination due to interface incompatibility,^{1, 7-9} wetting and fouling issues resulting from undesirable surface tension or surface functionality,¹⁰⁻¹⁵ and surface instability causing the polymer surface to denature or degrade.² Each of these issues can be mitigated by surface modification. Processes developed to alter polymer surfaces include exposure to ultraviolet radiation,^{16, 17} flame treatment,¹⁸ and plasma surface modification.^{19, 20} Indeed, the plasma surface modification of polymers has a long history²¹⁻²³ and has, perhaps, attracted the most attention to date. This arises in part from the many plasma techniques and chemistries available, and the ability to limit the modification only to the outermost layer of a polymer material.¹⁹ Many of these polymer surface modifications lack permanence and are unstable. The tendency for polymer surfaces to revert back to their untreated states is known as aging or hydrophobic recovery.²⁰

Researchers have forwarded several postulated theories on processes contributing to aging effects and hydrophobic recovery of plasma modified polymer surfaces. As outlined by Truica-Marasescu et al.¹⁷ and others,²⁴ these include (1) adsorption of non-polar contaminants to the surface; (2) long-range reorganization, including the diffusion of oligomers and additives to the surface;²⁵ (3) short-range reorganization, including the reorientation of the polymer to present a lower energy surface;²⁵ and (4) the diffusion of low molecular weight oxidized material (LMWOM) beneath the polymer surface. Overall, a reduction in surface energy provides the driving force for each of these aging processes. The adsorption of non-polar contaminants happens when environmental contaminants from any number of sources adsorb onto the surface of the treated polymer. This is an unavoidable consequence of exposing the treated surface to laboratory air or any other uncontrolled environment. Long-range reorganization occurs when short polymer oligomers and additives, ubiquitous byproducts of the polymer synthesis, diffuse

from the bulk to the surface of the polymer, thereby decreasing the surface energy. Short-range reorganization takes place when native or implanted functional groups are capable of reorienting in such a way to reduce the surface energy. Finally, the formation of LMWOM can result during the surface modification of the polymer. Plasma modification, for example, is responsible for implanting oxide functionalities on the surface as well as breaking bonds in the polymer causing polymer chain scission. These processes lead to formation of oxidized polymer oligomers that can more easily diffuse through the polymer structure. The mobility of these fragments allows the oxide functionalities to migrate below the surface of the polymer, thereby minimizing the surface energy. Overall, researchers have made strides toward understanding the aging process on polymer surfaces leading to a model that accurately predicts the rate and extent of hydrophobic recovery.²⁶ Despite the strength of such models, however, researchers have not agreed on the technique or conditions that yield the most desirable surface modification outcome. Or rather, the literature demonstrates there is no single best strategy, and the surface modification technique, polymer, and application must be considered collectively.

Preventing polymer surface aging is of the great interest with porous polymer membranes, which are ubiquitous in biomedical applications,²⁷ gas separations,^{28, 29} and the purifications of liquids such as water and dairy products.^{15, 29-32} As with many polymer materials, engineering functional membranes can be problematic. The surface properties of polymers that yield the strongest membranes with a desirable pore size and geometry are often incompatible with the desired application. For example, an ideal membrane for the reverse osmosis (RO) desalination of water would have a hydrophilic surface, allowing the highest water flux with the least applied pressure.²⁹ Such materials are, however, either incompatible with aqueous environments or structurally weak. Engineers are forced to compromise and use

hydrophobic polymers such as polysulfone (PSf) or polyethersulfone (PES). The direct result is that the energy costs of water purification increase. Indeed, surface modification techniques are critical to improving the performance of membranes in such applications. Many of the polymer surface modification techniques mentioned above have been investigated to solve these problems. Plasma surface modification is uniquely suited to modifying the surface of porous structures, and the recent review by Kravets et al.³³ outlines the significant research efforts on this topic. The reactive species generated in the plasma can negotiate the tortuous path into the membrane structure whereas the relatively low temperature and low density conditions limit damage to the bulk material. Nevertheless, the polymer surfaces are still subject to aging and hydrophobic recovery.

The Fisher Research Group has a long history of membrane modification using oxidizing inductively coupled radio frequency (rf) plasmas. This research has demonstrated that H₂O plasmas can be used to impart hydrophilic functionality on the surface of asymmetric PSf membranes, materials often used for RO water filtration applications.³⁴ The goal was to achieve a membrane with increased wettability for the purpose of decreasing protein fouling while maintaining or improving selectivity. The study found that the optimal conditions for PSf surface modification consisted of a 2 min treatment time, applied rf power (P) = 25 W, and 50 mTorr H₂O vapor with the sample oriented perpendicular to the gas flow 9 cm downstream from the coil region. Indeed, these conditions rendered PSf completely wettable. Subsequent studies³⁵ found that treated surfaces are remarkably stable, showing that the surface was still wettable after 18 months of aging. The stability and performance of H₂O plasma modified PSf was the impetus for an expanded study³⁵ that extended the H₂O plasma system to a variety of other porous polymer membrane systems, including PES and polyethylene (PE). Each polymer

membrane was initially rendered completely wettable following H₂O plasma treatment. In contrast to the persistent wettability on PSf and PES, PE exhibited significant hydrophobic recovery. One hypothesis that explains this is that the structural and thermal properties of PE make it more susceptible to aging compared to PSf or PES. Indeed, Jokinen et al.³⁶ demonstrated that a range of solid polymers exposed to O₂ or N₂ plasmas will exhibit a range of different aging behaviors. However, a similar comprehensive study examining H₂O plasma surface modification has yet to be published.

The goals of this research are to investigate treatment effectiveness of H₂O plasmas and the aging of plasma-modified polymer surfaces using a variety of solid polymer substrates, ultimately guiding future research on the plasma modification of porous polymer membranes. A wide range of polymers, encompassing different compositions, structures, and physical properties, are used in this research, including high-density polyethylene (HDPE), low-density polyethylene (LDPE), polypropylene (PP), polystyrene (PS), polycarbonate (PC), and 75A polyurethane (PU). Cleaned samples are treated using a home-built inductively coupled rf plasma reactor using H₂O vapor as the feed gas and the standard treatment conditions developed previously.^{34, 35, 37} Cleaned control, freshly treated, and aged samples are analyzed using a range of surface and materials analysis techniques, including XPS, H₂O contact angles (wCA), and differential scanning calorimetry (DSC). Hydrophobic recovery results, measured using wCA, are compared to the surface composition, measured using XPS, to characterize treatment effectiveness and surface stability of each polymer over the one month aging period. These results are used to further develop our understanding of how plasma surface modification influences the surface and near surface polymer structure leading to hydrophobic recovery.

Select DSC measurements are also used to ascertain the influence of thermal properties, such as melting temperature (T_m) and glass transition temperatures (T_g), on hydrophobic recovery.

3.2. Results

3.2.1. Hydrophobic recovery on polyolefins. DSC was performed on untreated HDPE, LDPE, and PP to verify their thermal properties and to confirm their identity, given their non-descript appearance. In each case, the thermal properties of the HDPE, LDPE, and PP samples are consistent with typical properties of these polymers, Figure 3.1.³⁸ The T_m of HDPE, LDPE, and PP are 140.5, 116.7, and 161.7 °C, respectively. The T_g of PP, identified during the second heating cycle, occurs at -9.1 °C. Careful inspection of the HDPE and LDPE traces does not reveal a measurable T_g , which typically occurs below -100 °C. DSC was not attempted on H₂O plasma treated polymer samples because the volume of the modified surface layer is insignificant with respect to the total volume of the bulk sample. Furthermore, modifying a subsample of a sufficiently small size for DSC would further influence the results of the measurement compared to the larger sample sizes required for wCA or XPS measurements.

The results from wCA measurements on HDPE, LDPE, and PP are shown in Figure 3.2. (left column) and listed in Table 3.1. The wCAs measured on cleaned control samples are all $\geq 100^\circ$, consistent with typical wCA measurements on polyolefin surfaces. H₂O plasma modification using standard treatment conditions results in a marked change in wettability on each polyolefin. For example, the wCA on HDPE decreases to $18 \pm 3^\circ$ upon treatment, which amounts to a decrease in wCA of 82% compared to the fresh untreated control sample. Indeed, HDPE demonstrates the most significant change in wettability among purely aliphatic polymers. By comparison, the wCAs of LDPE and PP decrease by only 50 and 32%, respectively. Over the

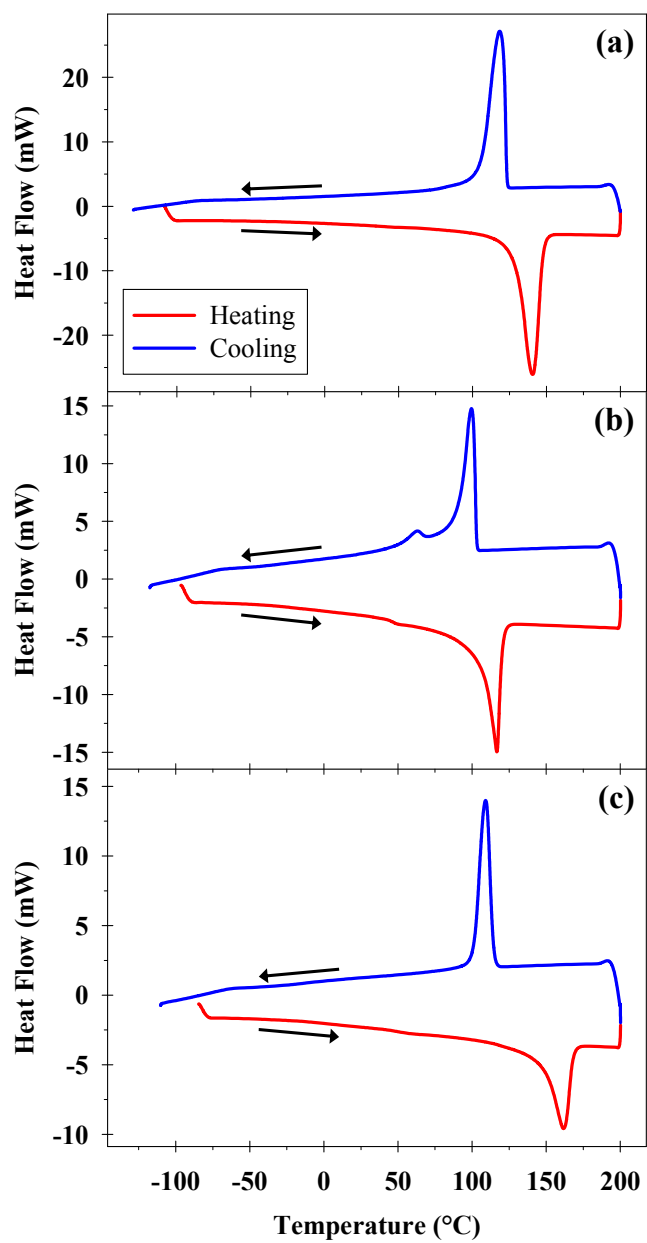


Figure 3.1. DSC results from untreated (a) HDPE, (b) LDPE, and (c) PP. Samples were first cooled (not shown) and then subjected to one full heating (red) and cooling cycle (blue).

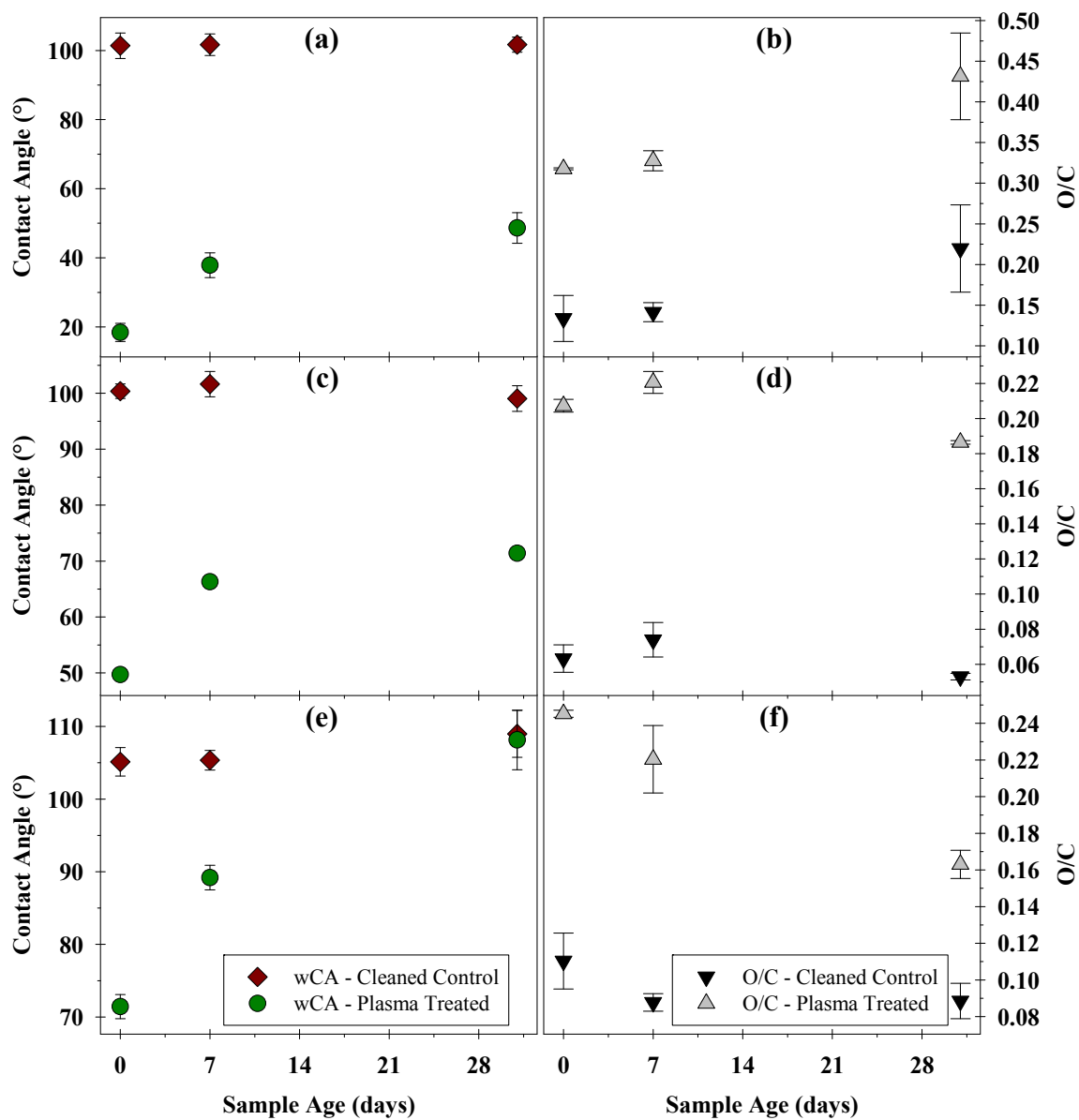


Figure 3.2. wCA (left) and O/C (right) results as a function of sample age after H₂O plasma surface modification from (a-b) HDPE, (c-d) LDPE, and (e-f) PP. Cleaned control samples were subjected to the same cleaning regimen and aging conditions as the treated samples.

TABLE 3.1. wCA and elemental composition of untreated, freshly-treated, and aged H₂O plasma modified HDPE, LDPE, and PP.

Sample	Age	wCA (°)	Elemental Composition (%) ^a			
			Carbon	Oxygen	Silicon	O/C
Polyethylene (High Density)	Untreated ^b	101 ± 4	82.1 ± 3.2	10.9 ± 1.9	6.9 ± 1.3	0.134 ± 0.028
	Fresh	18 ± 3	73.1 ± 0.1	23.2 ± 0.1	3.6 ± 0.1	0.318 ± 0.001
	1 Week	38 ± 4	72.0 ± 0.7	23.6 ± 0.7	4.4 ± 0.2	0.328 ± 0.012
	1 Month	49 ± 4	65.0 ± 3.4	27.9 ± 2.1	7.1 ± 1.3	0.431 ± 0.053
Polyethylene (Low Density)	Untreated ^b	100 ± 1	90.4 ± 0.9	5.7 ± 0.7	3.9 ± 0.3	0.063 ± 0.008
	Fresh	50 ± 1	82.8 ± 0.2	17.2 ± 0.2	--	0.207 ± 0.004
	1 Week	66 ± 1	80.3 ± 0.6	17.7 ± 0.4	2.0 ± 0.2	0.221 ± 0.006
	1 Month	71 ± 1	84.3 ± 0.1	15.7 ± 0.1	--	0.186 ± 0.001
Polypropylene	Untreated ^{b,c}	105 ± 2	85.7 ± 1.8	9.4 ± 1.1	2.7 ± 0.3	0.110 ± 0.015
	Fresh	71 ± 2	79.0 ± 0.3	19.4 ± 0.1	1.7 ± 0.2	0.245 ± 0.002
	1 Week	89 ± 2	80.8 ± 1.2	17.8 ± 1.3	1.4 ± 0.5	0.220 ± 0.018
	1 Month	108 ± 4	86.0 ± 0.6	14.0 ± 0.6	--	0.163 ± 0.008

^aReported error is one standard deviation. ^bThe reported untreated sample is the fresh cleaned control analysis, performed in conjunction with the freshly-treated sample time point. ^cApproximately 2% nitrogen was also detected in this sample.

one month aging study, each polyolefin undergoes significant hydrophobic recovery, consistent with previous studies³⁵ on porous polymer membranes composed of similar materials. Here, we find that HDPE is the least susceptible to hydrophobic recovery. The wCA on HDPE samples aged for 1 month increase to $49 \pm 4^\circ$, corresponding to a 36% recovery compared to freshly treated HDPE. By contrast, PP is the most susceptible to hydrophobic recovery. After one month of aging, the wCA is indistinguishable from that measured on untreated control samples.

The XPS elemental composition results for HDPE, LDPE, and PP surfaces are listed in Table 3.1., and the calculated O/C results are shown in Figure 3.2. (right column). The O/C of cleaned control HDPE, LDPE, and PP surfaces each reveal the presence of significant oxygen. This could result from natural oxidation of the polymer surface or from adsorption of oxide-containing contaminants after cleaning. However, the presence of silicon on many of these samples suggests that (1) silicone based release agents were used during manufacturing and that these release agents persisted despite cleaning, or (2) silicon containing additives are incorporated into the polymer and these additives were unaffected by cleaning. Upon treatment, the O/C increases for each polymer sample, consistent with the oxidizing nature of the H₂O plasma treatment and the observed decreases in wCA. Despite the hydrophobic recovery observed on each polymer, however, XPS measurements do not reveal a corresponding pattern of decreasing O/C. Indeed, PP is the only material where the O/C on the plasma treated samples evolves with age relative to the untreated control samples.

High resolution C_{1s} spectra from untreated, freshly treated, and aged HDPE samples were further analyzed to ascertain the distribution of oxidized carbon (CO_x) binding environments with H₂O plasma modification. Deconstruction of the high resolution C_{1s} spectra from HDPE was performed using XPSPeak v4.1. All spectra were fit with a Shirley baseline, the full width

at half maximum (FWHM) was constrained to ≤ 1.8 eV, and the component peak shapes were assumed to be 95:5 Gaussian:Lorentzian. Model C_{1s} spectra were generated based on the following binding environments: aliphatic hydrocarbon (C-C/C-H at 285.0 eV), ether/alcohol (C-O at 286.4 eV), carbonyl (C=O at 287.9 eV), and acid/ester (O-C=O at 289.5 eV). The peak positions were constrained by fixing the binding energy (BE) of each CO_x peak relative to the C-C/C-H peak. The raw spectrum, modeled spectrum, and spectral components from each sample were shifted so that the BE of the C-C/C-H component was 285.0 eV. The deconstruction results from HDPE, LDPE, and PP are listed in Table 3.2. The untreated HDPE sample comprises mostly C-C/C-H with trace amounts of the CO_x binding environments, including C-O, C=O, and O-C=O functional groups, Figure 3.3.a. These CO_x binding environments only account for $5.5 \pm 1.3\%$ of the total C_{1s} peak area, meaning that the oxygen bound to carbon only accounts for $47 \pm 6\%$ of the total oxygen concentration on the sample surface. This result suggests that the oxygen indeed originates from the three possible sources of contamination mentioned above: oxidation of the polymer surface, adsorption of oxidized carbon contaminants, and persistent silicone based release agents. Upon treatment, the area of each CO_x binding environment increases, consistent with oxidation of the polymer surface during treatment, Figure 3.3.b. Considering a similar analysis of the oxygen binding environment distributions for the treated sample, the CO_x environments account for $22 \pm 0.3\%$ of the total C_{1s} peak area on the freshly treated HDPE sample, corresponding to $91 \pm 1\%$ of the oxygen concentration on the sample surface. The high resolution C_{1s} spectra from the one week and one month aged HDPE samples suggest that these CO_x binding environments are stable, Figures 3.3.c. and 3.3.d. Indeed, the areas of these binding environments change very little as the treated HDPE ages, Table 3.2. However, CO_x only accounts for 80 ± 8 and $72 \pm 6\%$ of the total oxygen on the one week and one month HDPE

Table 3.2. C_{1s} moiety distribution of untreated, freshly-treated, and aged H₂O plasma modified HDPE, LDPE, and PP.

Sample	Age	C _{1s} Relative Contribution (%) ^a			
		Aliphatic	C-O	C=O	O-C=O
Polyethylene (High Density)	Untreated ^b	94.5 ± 1.3	3.1 ± 0.8	1.9 ± 0.5	0.4 ± 0.1 ^c
	Fresh	78.1 ± 0.3	11.4 ± 0.5	4.3 ± 0.3	6.2 ± 0.2
	1 Week	80.1 ± 2.6	10.1 ± 1.4	5.0 ± 0.4	4.8 ± 1.2
	1 Month	77.8 ± 0.3	11.6 ± 0.1	5.2 ± 0.3	5.5 ± 0.1
Polyethylene (Low Density)	Untreated ^b	97.8 ± 0.8	1.8 ± 0.4	0.4 ± 0.4	--
	Fresh	80.0 ± 0.6	10.5 ± 0.6	4.1 ± 0.1	5.3 ± 0.1
	1 Week	81.6 ± 0.3	9.2 ± 0.5	5.4 ± 0.6	3.9 ± 0.2
	1 Month	82.3 ± 0.3	8.3 ± 0.1	5.4 ± 0.1	4.0 ± 0.3
Polypropylene	Untreated ^b	91.4 ± 2.2	4.8 ± 1.6	3.4 ± 0.6	0.5 ± 0.1
	Fresh	79.2 ± 1.2	11.1 ± 1.2	4.9 ± 0.4	4.9 ± 0.4
	1 Week	80.7 ± 0.3	11.0 ± 0.6	3.1 ± 0.7	5.2 ± 0.4
	1 Month	85.0 ± 0.3	9.3 ± 0.2	1.0 ± 0.3	4.7 ± 0.2

^aReported error is one standard deviation. ^bThe reported untreated sample is the fresh cleaned control analysis, performed in conjunction with the freshly-treated sample timepoint. ^cReported error is three standard deviations.

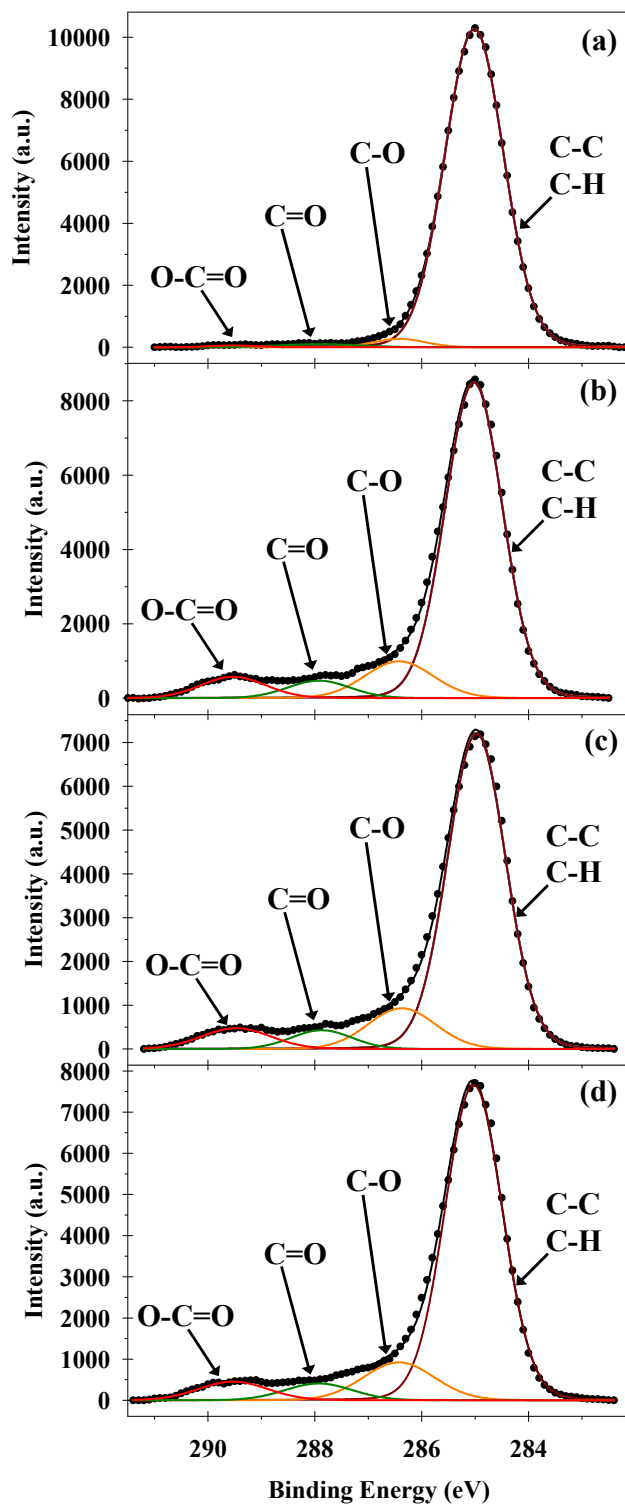


Figure 3.3. High resolution C_{1s} XPS spectra from (a) cleaned control and (b) freshly treated HDPE, as well as treated HDPE aged for (c) 1 week and (d) 1 month. H_2O plasma surface modifications of HDPE were performed using standard treatment conditions.

samples, respectively. These decreases in surface oxygen coincide with an increase in the surface silicon concentration and suggest that the surface is unstable. As the greatest change in surface composition is most pronounced between the fresh and one week time points, this likely explains the significant hydrophobic recovery observed over this period.

Spectra of cleaned control, freshly treated, and aged LDPE samples fit using the same procedure reveal similar trends following H₂O plasma modification. Representative spectra are shown in Figure 3.4. and results from their deconstruction are listed in Table 3.2. The distribution of CO_x binding environments is similar to that on HDPE, Figure 3.4.a. The lower oxygen concentration on LDPE is reflected in the magnitude of the CO_x binding environments, representing only $35 \pm 10\%$ of the total oxygen concentration on the sample surface. Surface modification of LDPE leads to a similar distribution of CO_x binding environments compared to HDPE, Figure 3.4.b. The peak areas of the CO_x binding environments on freshly treated LDPE account for $117 \pm 2\%$ of the oxygen concentration on the sample surface. This high percentage is consistent with the absence of silicon in these samples. The high resolution C_{1s} spectra for plasma treated LDPE samples aged for one week and one month, Figures 3.4.c. and 3.4.d., do not change appreciably and the CO_x binding environments continue to represent the majority of the oxygen detected on the sample surface.

Spectra from PP samples were fit using a slightly different procedure compared to the other polyolefins. Initial attempts to fit the PP samples revealed that changes in the CO_x peak areas were inconsistent as the samples aged. As this is likely an artifact resulting from the CO_x components shifting to lower BEs as the samples aged, we developed a procedure to substantiate these shifts by calculating the total amount of oxygen represented in the C_{1s} CO_x peak area on freshly treated PP ($104 \pm 5\%$). Assuming that oxygen loss pathways were unlikely to involve

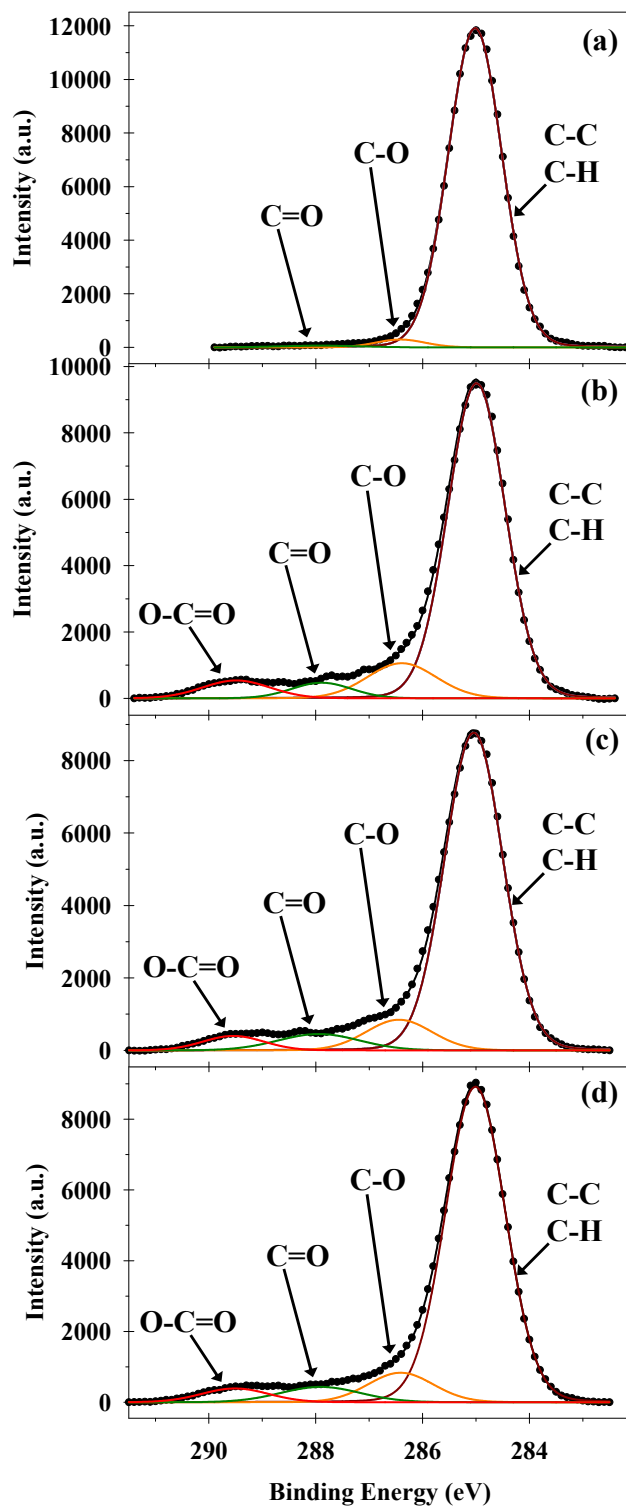


Figure 3.4. High resolution C_{1s} XPS spectra from (a) cleaned control and (b) freshly treated LDPE, as well as treated LDPE aged for (c) 1 week and (d) 1 month. H_2O plasma surface modifications of LDPE were performed using standard treatment conditions.

conversion to some persistent inorganic oxide, the proportion of oxygen represented by CO_x in the C_{1s} spectrum should remain constant. This assumption is supported by the silicon concentration measured on the treated PP sample surface, which is slightly above the limit of detection and disappears completely as the PP ages. The result of this fitting technique shows that the areas of the CO_x peaks evolved in a fashion similar to HDPE and LDPE while yielding favorable χ^2 values, Table 3.3. Cleaned control PP is very similar to HDPE and LDPE, consisting primarily of C-C/C-H with small amounts of C-O, C=O, and O-C=O functionalities, Table 3.2. and Figure 3.5.a. H₂O plasma treatment also resulted in similar increases in each of the CO_x binding environments, Figure 3.5.b., and their contributions stay relatively constant during aging, Figures 3.5.c. and 3.5.d.

The shift in CO_x BEs is an interesting phenomenon and provides insight into processes occurring at the surface of PP during aging. The BEs of each CO_x moiety on freshly treated PP are identical to those of HDPE and LDPE. As the PP surface ages, however, these BEs shift to lower energy. The magnitude of a given shift appears to coincide with the degree of oxidation of that CO_x moiety. For example, the BE of the O-C=O group after one month is 0.8 eV lower when compared to the freshly treated PP sample. Shifts in BE such as these result from changes in the local chemical environment of a functional group (see Chapter 7)³⁹ and are discussed further in Section 3.3.

3.2.1. Hydrophobic recovery on aromatic polymers. Results from wCA measurements on PS, PC, and PU are shown in Figure 3.6. (left column) and listed in Table 3.4. The wCAs measured on cleaned control PS, PC, and PU are $93 \pm 4^\circ$, $88 \pm 4^\circ$, and $108 \pm 1^\circ$, respectively. The increased variance in these measurements results from more diverse functionality in these polymers, compared to the polyolefin series. H₂O plasma modification using standard treatment

Table 3.3. C_{1s} moiety binding energies of freshly-treated and aged H₂O plasma modified PP.

Age	Fitting Error (mean χ^2) ^a	Polypropylene C_{1s} Moiety Binding Energy (eV)			
		Aliphatic	C-O	C=O	O-C=O
Fresh	2.2583 ± 0.5899	285.00	286.40	287.90	289.50
1 Week	0.8034 ± 0.5321	285.00	286.30	287.70	289.20
1 Month	1.3716 ± 0.3563	285.00	286.25	287.60	288.70

^aReported error is one standard deviation.

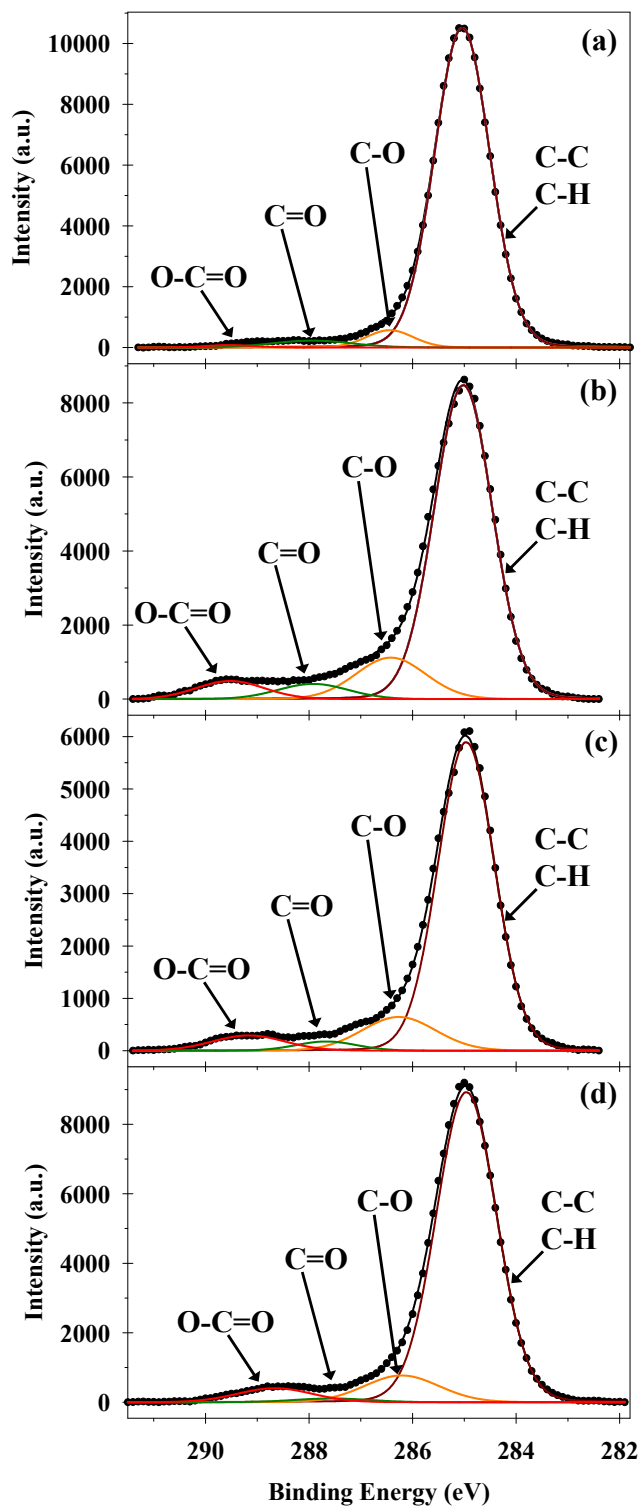


Figure 3.5. High resolution C_{1s} XPS spectra from (a) cleaned control and (b) freshly treated PP, as well as treated PP aged for (c) 1 week and (d) 1 month. H_2O plasma surface modifications of PP were performed using standard treatment conditions.

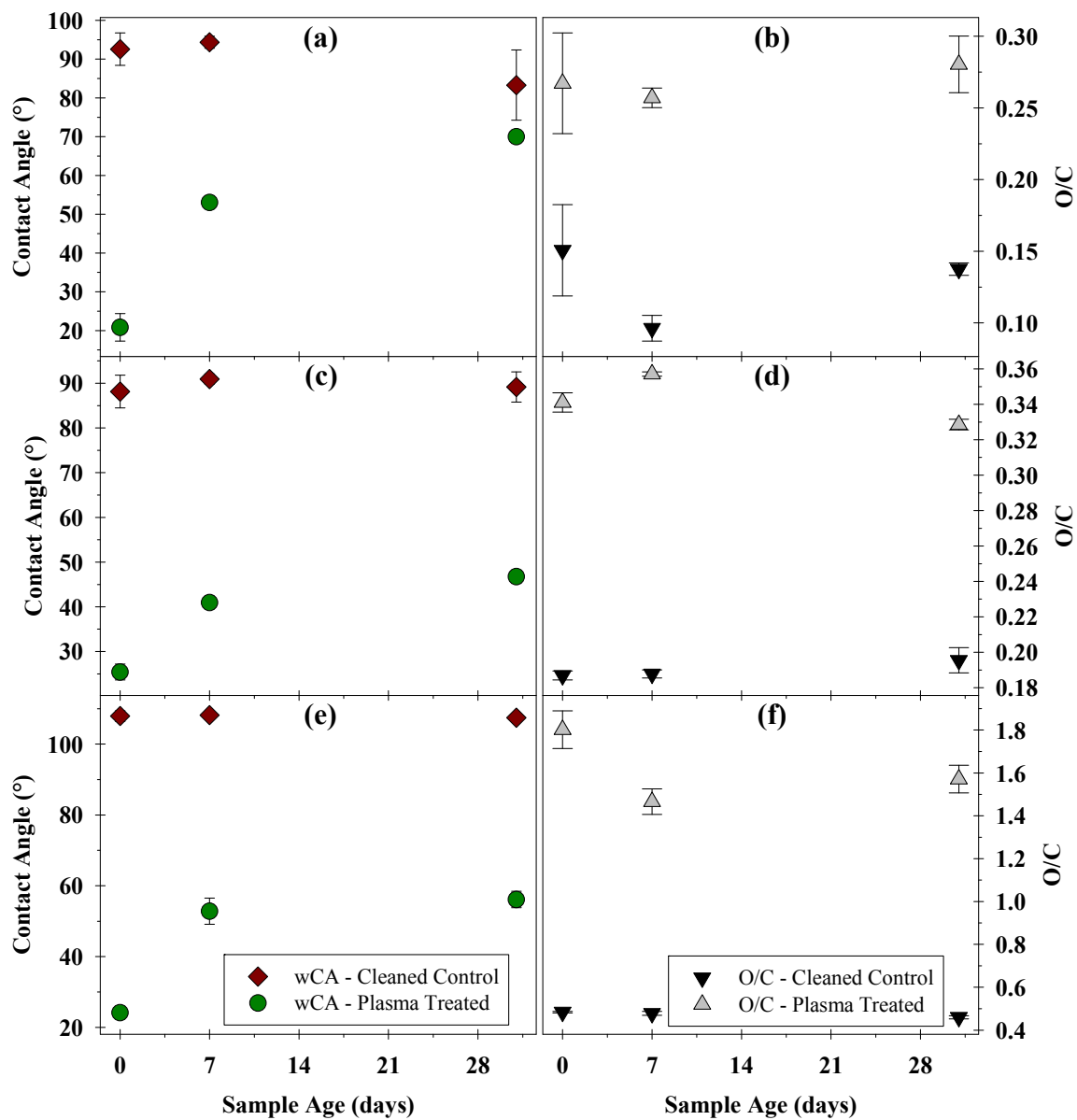


Figure 3.6. wCA (left) and O/C (right) results as a function of sample age after H₂O plasma surface modification from (a-b) PS, (c-d) PC, and (e-f) PU. Cleaned control samples were subjected to the same cleaning regimen and aging conditions as the treated samples.

Table 3.4. wCA and elemental composition of untreated, freshly-treated, and aged H₂O plasma modified PS, PC, and PU.

Sample	Age	wCA (°)	Elemental Composition (%) ^a			
			Carbon	Oxygen	Silicon	O/C
Polystyrene	Untreated ^{b,c}	93 ± 4	81.4 ± 3.2	12.2 ± 2.1	4.4 ± 0.3	0.151 ± 0.032
	Fresh	21 ± 4	79.0 ± 2.2	21.0 ± 2.2	--	0.267 ± 0.035
	1 Week	53 ± 2	79.6 ± 0.4	20.4 ± 0.4	--	0.257 ± 0.007
	1 Month	70 ± 1	77.5 ± 1.4	21.7 ± 1.1	--	0.280 ± 0.020
Polycarbonate	Untreated ^b	88 ± 4	84.3 ± 0.2	15.7 ± 0.2	--	0.187 ± 0.003
	Fresh	25 ± 2	74.6 ± 0.3	25.4 ± 0.3	--	0.341 ± 0.005
	1 Week	41 ± 1	73.7 ± 0.1	26.3 ± 0.1	--	0.357 ± 0.001
	1 Month	47 ± 1	75.3 ± 0.2	24.7 ± 0.2	--	0.329 ± 0.003
Polyurethane	Untreated ^b	108 ± 1	51.3 ± 0.7	24.9 ± 0.2	23.8 ± 0.9	0.484 ± 0.004
	Fresh	24 ± 2	28.1 ± 0.9	50.6 ± 0.8	21.4 ± 0.2	1.802 ± 0.088
	1 Week	53 ± 4	31.7 ± 1.0	46.4 ± 0.5	21.9 ± 0.5	1.466 ± 0.060
	1 Month	56 ± 2	29.8 ± 1.0	46.8 ± 0.4	23.4 ± 0.7	1.571 ± 0.064

^aReported error is one standard deviation. ^bThe reported untreated sample is the fresh control analysis, performed in conjunction with the freshly-treated sample timepoint. ^cApproximately 2% nitrogen was also detected in this sample.

conditions results in a marked change in wettability for each polymer material. Coincidentally, the wCA measurements on each treated polymer are the same within error, ranging from $21 \pm 4^\circ$ to $25 \pm 2^\circ$ on PS and PC, respectively. During aging, each of these polymers undergoes significant hydrophobic recovery, consistent with previous studies of PS, PC, and PU modification.^{25, 36, 40-45} Here, we find that PC is the least susceptible to hydrophobic recovery, yielding similar performance to HDPE. The wCA on PC samples aged for 1 month increases to $47 \pm 1^\circ$, corresponding to a 34% recovery compared to freshly treated PC. PU has similar aging behavior, exhibiting a 38% recovery; as discussed in Section 3.3.4., however, this similarity may be misleading. By contrast, PS is the most susceptible to hydrophobic recovery. After one month of aging, the wCA begins to approach that measured on untreated control samples, corresponding to a 69% recovery compared to the untreated sample.

XPS was used to measure the elemental composition of PS, PC, and PU surfaces, Table 3.4., and the calculated O/C results are shown in Figure 3.6. (right column). The O/C of the cleaned control PS, PC, and PU surfaces each reveal the presence of significant oxygen. The sources of oxygen on untreated PS are likely the same as those discussed above for the untreated polyolefin polymers, although PC and PU also contain native oxygen functionality. Upon treatment, the O/C increases for each polymer sample, consistent with the oxidizing nature of the H₂O plasma treatment and the observed decreases in wCA. Despite the hydrophobic recovery observed on each polymer, however, XPS measurements do not reveal a corresponding pattern of decreasing O/C. Interestingly, although PU should also contain nitrogen as a result of the urethane linkages in the polymer backbone, no nitrogen is detected in any of the untreated or H₂O plasma treated samples. This could be because the urethane linkages in PU 75A are buried

beyond the sampling depth of XPS or the concentration of urethane is below the limit of detection on XPS.

High resolution C_{1s} XPS spectra from untreated, freshly treated, and aged PS samples were fit using a similar procedure to that used for PP but with a slightly different set of binding environments. Each PS spectrum was fit using a mixed Shirley/linear baseline to compensate for higher background levels arising from the influence of the conjugated π system on the higher energy end of the spectrum. A linear contribution with a slope value of 2.3 gave the most reasonable peak shapes and was used to fit all control and H₂O plasma treated spectra. The presence of conjugated π systems due to aromatic functionality also resulted in significant signal from π - π^* shake-up satellites. The BE and FWHM of the π - π^* satellite was somewhat variable, but were typically ~291.5 eV and ~2.3 eV, respectively. The reduced carbon was fit assuming contributions from aliphatic carbon (C-C/C-H, 285.0 eV) and allylic carbon (C=C/C=C-H, 284.5 eV) to account for the presence of aromatic functionality on the polymer backbone. The BE of the C=C/C=C-H binding environment was not constrained. Similar to the analysis of PP, initial attempts to fit the PS sample spectra revealed that the peak areas were changing erratically as the samples aged. In this case, the ratio of C-C/C-H and C=C/C=C-H peak areas appeared to be changing. It is unlikely that stable aromatic functionality would continue to spontaneously convert to aliphatic functionality to the extent suggested by this change. Again this was compensated for by allowing the CO_x components to shift to lower BEs for aged samples. Unlike in our analysis of PP, however, the positions of the CO_x binding environments were adjusted to optimize the shape of the C_{1s} region where the C-C/C-H and C=C/C=C-H binding environments are located. The resulting PS fitting χ^2 values are generally favorable and are listed in Table 3.5.

Table 3.5. C_{1s} moiety binding energies of freshly-treated and aged H₂O plasma modified PS.

Age	Fitting Error (mean χ^2) ^a	Polystyrene C _{1s} Moiety Binding Energy (eV)				
		Aromatic	Aliphatic	C-O	C=O	O-C=O
Fresh	1.0234 ± 0.3497	284.50	285.00	286.40	287.85	289.35
1 Week	1.3770 ± 0.2080	284.50	285.00	286.30	287.65	289.05
1 Month	1.4732 ± 0.3913	284.50	285.00	286.25	287.60	288.90

^aReported error is one standard deviation.

Results from fitting the PS C_{1s} spectra are listed in Table 3.6. and representative spectra are shown in Figure 3.7. Untreated PS comprises primarily C=C/C=C-H and C-C/C-H functionalities, Figure 3.7.a., and the ratio of these two peak areas is 4.6, somewhat higher than the expected ratio of 3. Comparing the C=C/C=C-H area to C-C/C-H and CO_x peaks yields a ratio of 3.6. This would suggest that the native surface oxidation exists on the aliphatic backbone of PS, consistent with the stability of aromatic functionality that comprises the rest of the polymer. The area of each CO_x binding environment increases upon plasma treatment, Figure 3.5.b., and continue to increase slightly as the samples age, Figures 3.7.c. and 3.7.d. This is largely at the expense of the C=C/C=C-H binding environment, suggesting that the aromatic functionality affected by plasma treatment continues to oxidize as the surface ages. Moreover, each CO_x binding environment shifts to lower BE as the surface ages, Table 3.6. Notably, these shifts are very similar to those observed on aged PP surfaces, the only other polymer found to undergo significant hydrophobic recovery.

Spectra from untreated, freshly treated, and aged PC samples were fit using a similar procedure to that used for PS, with some exceptions. Despite the presence of aromatic functionality in bisphenol A-based PC, the carbon peak was fit with one component representing both allylic and aliphatic carbon functionalities. Spectra from H₂O plasma treated PC were fit using only a Shirley baseline to be as consistent as possible because there was no practical method for determining the appropriate linear contribution for a mixed baseline. Representative spectra are shown in Figure 3.8. and results from their deconvolution are listed in Table 3.5. Untreated PC is composed of C-C/C-H/C=C, C-O, and O=C(-O)₂ functionalities in proportions consistent with bisphenol A PC, Figure 3.8.a., similar to that reported previously.¹⁴ Following plasma treatment, the surface of the freshly treated sample is generally more oxidized, resulting

Table 3.6. C_{1s} moiety distribution of untreated, freshly-treated, and aged H₂O plasma modified PS, PC, and PU.

Sample	Age	C _{1s} Relative Contribution (%) ^a						
		C-Si	Aromatic	Aliphatic	C-O	C=O	O-C=O	O=C(-O) ₂
Polystyrene ^c	Untreated ^b	--	78.1 ± 5.4	17.1 ± 3.4	3.1 ± 1.0	1.5 ± 0.8	0.2 ± 0.2	--
	Fresh	--	54.5 ± 0.5	27.4 ± 0.5	9.3 ± 0.3	3.4 ± 0.8	5.4 ± 0.5	--
	1 Week	--	53.6 ± 0.5	27.0 ± 0.3	11.0 ± 0.7	2.3 ± 0.2	6.3 ± 0.2	--
	1 Month	--	52.1 ± 0.2	26.2 ± 0.1	11.3 ± 1.1	3.2 ± 0.8	7.2 ± 0.2	--
Polycarbonate ^c	Untreated ^b	--	80.3 ± 0.1 ^d		13.8 ± 0.4	--	--	5.9 ± 0.3
	Fresh	--	65.2 ± 1.1 ^d		21.5 ± 1.1	3.6 ± 0.7	4.8 ± 0.4	4.9 ± 0.1
	1 Week	--	66.5 ± 0.7 ^d		20.9 ± 0.5	4.1 ± 0.8	3.7 ± 0.3	4.8 ± 0.1
	1 Month	--	67.1 ± 0.6 ^d		21.0 ± 0.7	3.5 ± 0.2	3.6 ± 0.5	4.7 ± 0.5
Polyurethane	Untreated ^b	--	--	96.7 ± 0.5	3.3 ± 0.5	--	--	--
	Fresh	9.7 ± 0.5	--	54.4 ± 0.2	19.4 ± 1.2	--	16.6 ± 0.8	--
	1 Week	2.2 ± 0.6	--	63.1 ± 0.3	23.2 ± 0.1	--	11.6 ± 0.3	--
	1 Month	--	--	68.1 ± 1.5	22.3 ± 1.3	--	9.6 ± 0.2	--

^aReported error is one standard deviation. ^bThe reported untreated sample is the fresh control analysis, performed in conjunction with the freshly-treated sample time point. ^cSamples had significant contributions from π - π^* transition. This area was ignored for relative contribution calculations. ^dAliphatic and aromatic C-C/C-H regions were fit as one peak to improve fitting reproducibility and minimize error.

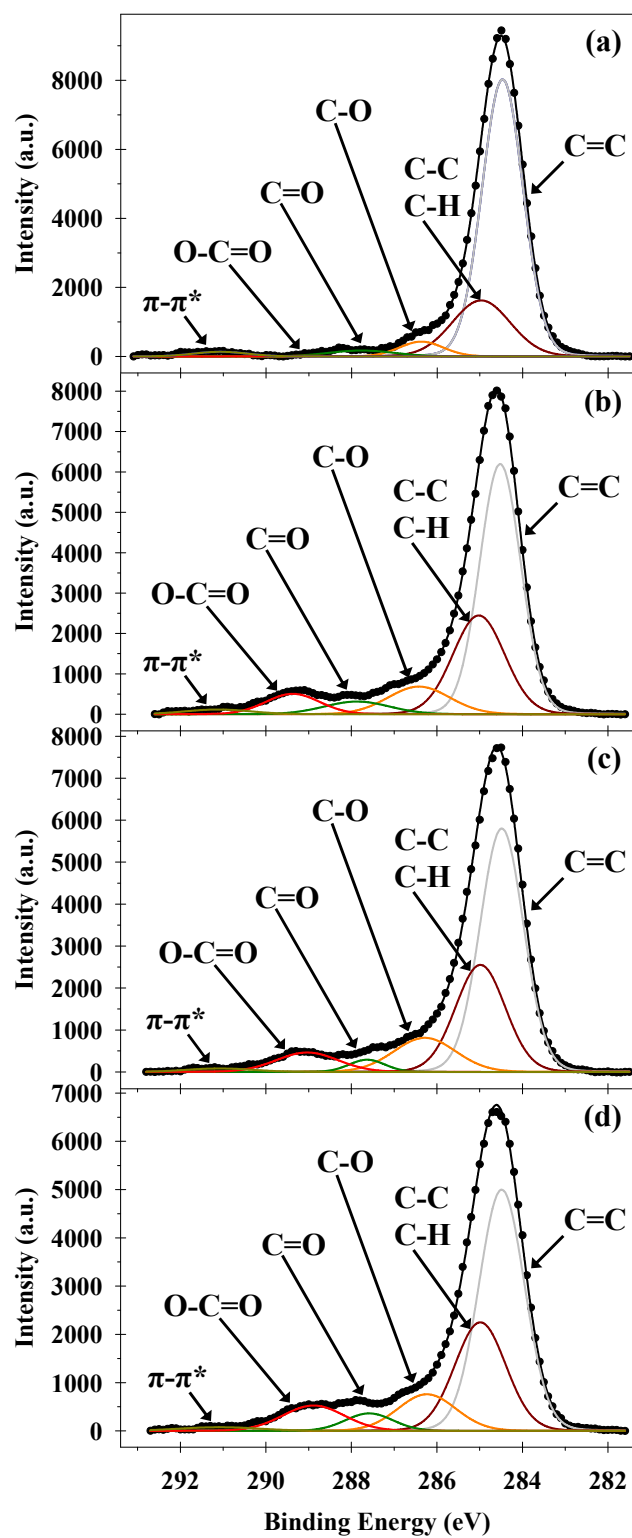


Figure 3.7. High resolution C_{1s} XPS spectra from (a) cleaned control and (b) freshly treated PS, as well as treated PS aged for (c) 1 week and (d) 1 month. H_2O plasma surface modifications of PS were performed using standard treatment conditions.

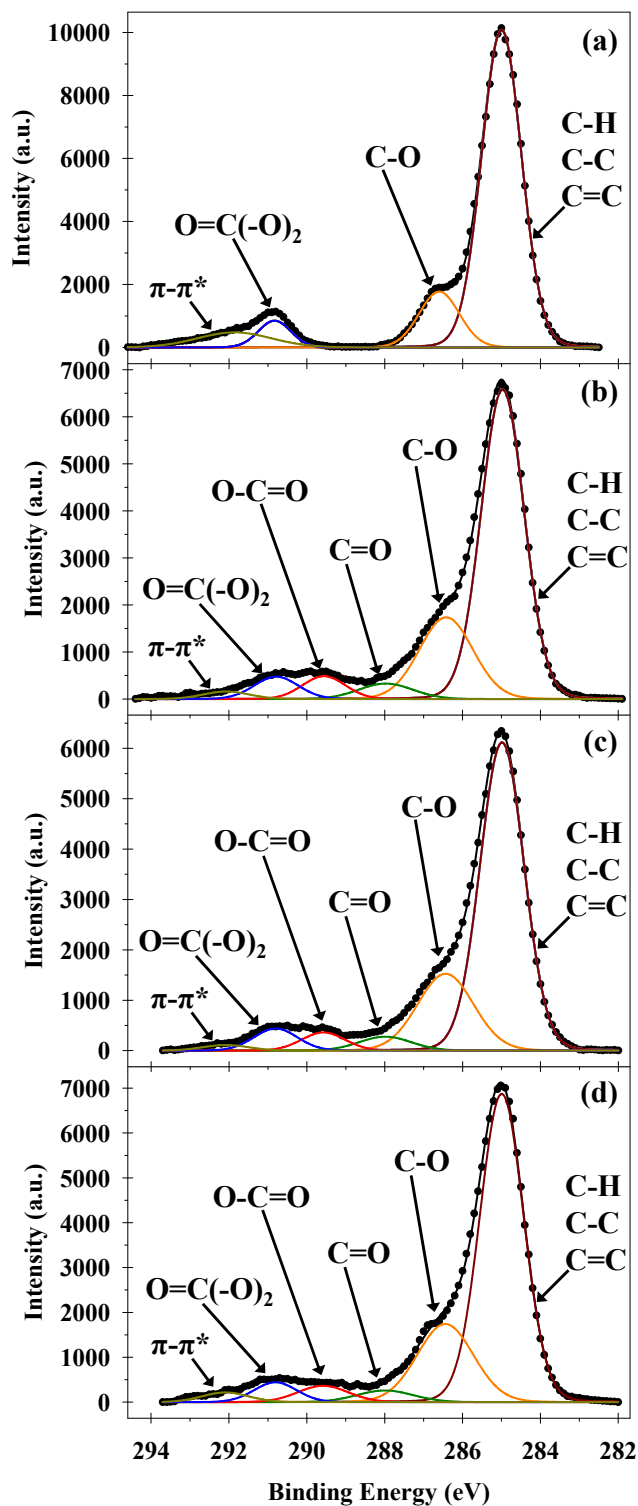


Figure 3.8. High resolution C_{1s} XPS spectra from (a) cleaned control and (b) freshly treated PC, as well as treated PC aged for (c) 1 week and (d) 1 month. H_2O plasma surface modifications of PC were performed using standard treatment conditions.

in significantly more C-O along with the introduction of C=O and O-C=O functional groups, Figure 3.8.b. This oxidation occurs at the expense of the C-C/C-H/C=C and O=C(-O)₂ binding environments, consistent with other reports.⁴⁶ Samples aged for one month show very little change in the distribution of CO_x binding environments, Figures 3.8.c. and 3.8.d., and there are no BE shifts observed.

Spectra from untreated, freshly treated, and aged PU samples were fit using a similar procedure to that used for HDPE and LDPE. The analysis of PU samples used in this study, however, was influenced by the significant concentration of silicon detected on the sample surface. The spectrum of cleaned untreated PU sample comprises mostly C-C/C-H with some slight oxidation in the form of C-O, Figure 3.9.a. It is likely that this spectrum is not that of the PU but that of additives or contaminants, such as hydrocarbon- or silicone-based release agents. Following H₂O plasma treatment, the C_{1s} spectrum displays a dramatic increase in the contributions from C-O and O-C=O and a low BE peak appears, consistent with C-Si functionality, Figure 3.9.b. Interestingly, the shape of the overall spectrum and the ratio of the C-O and O-C=O peaks are more consistent with a polyester material than with PU.¹⁴ It is also likely that the PU sample contains silica, a material often added to commercial polymer formulations intended to improve abrasion resistance. An alternative hypothesis is that the PU contains significant quantities of a siloxane based polymer such as polydimethylsiloxane (PDMS) or contains siloxane based cross-linking agents. The spectrum from freshly H₂O plasma treated PU is, however, inconsistent with previous reports on O₂ plasma oxidized PDMS.⁴⁷ The areas of the C-O and O-C=O binding environments were stable as the treated PU surface aged over one month, Figures 3.9.c and 3.9.d. The only notable change was the loss of the lower

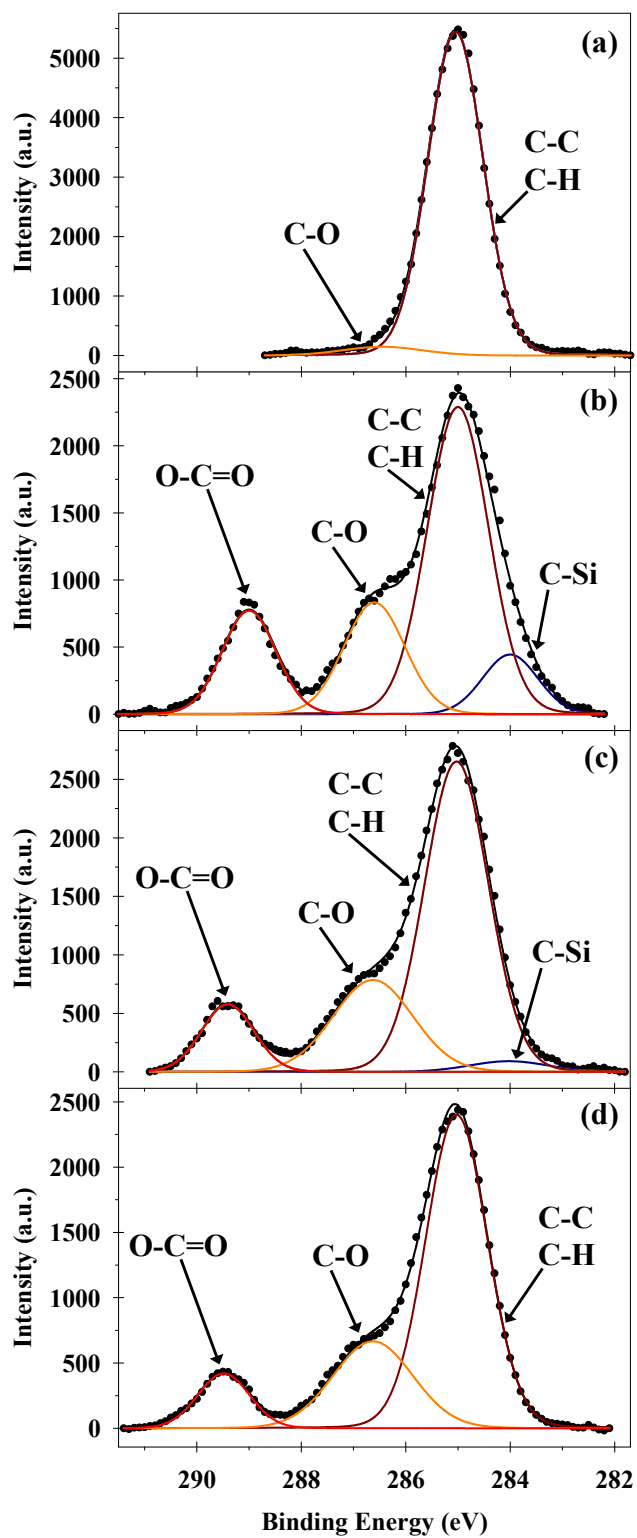


Figure 3.9. High resolution C_{1s} XPS spectra from (a) cleaned control and (b) freshly treated PU, as well as treated PU aged for (c) 1 week and (d) 1 month. H_2O plasma surface modifications of PU were performed using standard treatment conditions.

energy shoulder on the C-C/C-H peak attributed to Si-C functionality. After one month of aging the Si-C peak was no longer detectable.

3.3. Discussion

Past work in the Fisher Research Group examined aging effects on certain polymer membranes, including PSf, PES, and PE, following treatment using H₂O vapor plasma.³⁵ That work demonstrated that some polymer membranes exhibited hydrophobic recovery (e.g. PE) and others did not (e.g. PSf and PES). This study seeks to further investigate these phenomena by undertaking a more comprehensive study of H₂O plasma treatments on different classes of polymer materials, namely polyolefins, polymers with aromatic functionality, and polyurethanes.

3.3.1. Hydrophobic recovery on polyolefins. We find that the extent of hydrophobic recovery from most recovery to least recovery is PP>LDPE>HDPE. In each case, the loss of oxygen on the surface could not fully explain the observed recovery behavior. One possible hypothesis to explain hydrophobic recovery on polyolefins is that the thermal properties dictate surface reorganization. If the amount of energy required to reorganize the polymer chains near the surface was sufficiently small, the rate that polar surface functionalities are subsumed would increase. Under those circumstances, low T_m and T_g at the polymer surface would correlate with the tendency of a surface to undergo hydrophobic recovery. This simple relationship, however, does not take into account the observation that PP has the highest T_m and T_g and is simultaneously the most prone to hydrophobic recovery.

The fact that PE exhibits very little hydrophobic recovery and PP exhibits complete hydrophobic recovery suggests that these surfaces respond to plasma modification differently. A similar trend was observed by Jokinen et al.,³⁶ who showed that PP is more susceptible to

hydrophobic recovery after O₂ plasma modification and attributed it to the formation of LMWOM during plasma treatment that subsequently reorganizes with aging. Likewise, Guimond and Wertheimer⁴⁸ used air and N₂ atmospheric pressure glow discharges to modify the surface of LDPE and PP, and also observed significant formation of LMWOM on PP. Again, LMWOM formation correlated with the extent of hydrophobic recovery during aging. Behnisch et al.⁴⁹ compared oxygen plasma treatments on PE and PP surfaces and found that ultrasonic cleaning immediately after plasma treatment produced a much higher wCA on PP. They cited the work of Garbassi and coworkers,⁵⁰ explaining that PP is prone to chain scission during plasma treatment, whereas PE is more likely to crosslink. Chain scission at the PP surface further lowers the energy barrier for reorganization. Polar functionalities are buried and a nonpolar surface is presented, decreasing surface energy and wettability. Cross-linking on PE, however, prevents hydrophobic recovery by creating an interconnected network of polymer chains on the surface. This anchors polar functionalities at or near the surface and increases the energy required to reorganize the polymer.

The observation that O/C remains unchanged after the surface reorganizes can be explained by noting that the diffusion distance of LMWOM fragments is less than the sampling depth of the XPS measurement. This is corroborated by the work of Truica-Marasescu et al.,¹⁷ who used ToF-SIMS to examine LDPE and PP surfaces modified in NH₃ using VUV light and noted that polar groups migrated below the surface but remained within the sampling depth of XPS (~10 nm). Although elemental composition data cannot be used to follow surface reorganization, high resolution XPS peak fitting does give us insight into this process. The work presented in Chapter 7³⁹ correlates shifts in C_{1s} CF_x BEs with changes in the local chemical environment. As the local concentration of fluorine decreased, the BEs of individual

contributions decreased because of the lower electron withdrawing power on the carbon center. It is likely something similar is occurring with the polymers examined in this study. As polar functionalities are subsumed by the polymer surface, the oxygen atoms are further influenced by nearby carbon atoms. The additional electron density from these interactions decreases the withdrawing power of the oxygen and, concomitantly, decreases the C_{1s} BE of the CO_x functional group.

Comparing HDPE and LDPE, wCA results show H_2O plasma treatments are more effective at creating hydrophilic surfaces with HDPE samples. Silicon residues, detected using XPS before and after treatment, may be contributing to this improved performance as they can be converted to either an intermediate oxidation state of silicon (Si_xO_y) or to SiO_2 during treatment.⁵¹ H_2O plasma treatments of silicon wafers showed those surfaces are populated with SiOH functional groups, yielding low wCAs.⁵¹ Although some of the silicon on our polymer surfaces is lost during H_2O plasma treatment, the silicon that remains is likely oxidized to SiO_2 which contributes to the low wCA we observe on freshly-treated HDPE.

The extent of hydrophobic recovery on HDPE and LDPE reveals that the HDPE surface is more stable. This is surprising as XPS measurements reveal changes in oxygen and silicon distribution with treatment and aging on HDPE. A significant portion of the oxygen on the untreated HDPE exists in the form of inorganic oxide likely bound to the silicon contamination. The H_2O plasma removes a significant amount of this silicon, leaving the majority of the oxygen in the form of CO_x . As the treated samples age, the distribution of organic oxide to inorganic oxide reverts, coinciding with the amount of silicon measured by XPS. These results suggest that the silicon contamination was not just on the surface of the HDPE sample only and is likely diffusing from the bulk of the HDPE sample. Although one possible source of silicon is silicone

oils applied as release agents during HDPE manufacturing, these would be expected to exacerbate hydrophobic recovery. Additional experiments are required to learn the identity of these contaminants and their impact on HDPE surface aging.

3.3.2. Hydrophobic recovery on polystyrene. The PS material exhibits significant aging behavior, resulting in the second most hydrophobic recovery of the materials included in this study. To our knowledge, there are no published accounts of H₂O vapor plasma modifications on PS. Garbassi and coworkers^{25, 43} examined the aging of polystyrene after O₂ plasma surface modification using a number of different techniques. They found that all samples were subject to significant hydrophobic recovery, regardless of *P*, polymer molecular weight (MW), or storage temperature. They demonstrated that increased storage temperature during aging exacerbates hydrophobic recovery and that low MW PS is more susceptible to hydrophobic recovery.²⁵ They attributed this to short and long range rearrangements driven by surface thermodynamics. From this, it would seem reasonable to assume that increasing the energy required to rearrange the polymer structure would reduce the extent of hydrophobic recovery. However, Larrieu, et al.⁴¹ compared O₂ plasma modification of atactic (less crystalline) and isotactic (more crystalline) polystyrene, finding that both were equally susceptible to hydrophobic recovery immediately after treatment.

The notable hydrophobic recovery on PP has been attributed to surface rearrangement exacerbated by chain scission, and it seems reasonable to assume that the same mechanisms are responsible for aging effects on the PS surface. Garbassi and coworkers²⁵ quantified surface cross-linking by gravimetric analysis of the insoluble fraction of plasma treated PS and showed that low *P* does not induce cross-linking and leads to increased hydrophobic recovery. This is especially true for low MW PS, ostensibly because low MW PS is the most susceptible to

diffusion based hydrophobic recovery. Although gravimetric analysis experiments revealed that high P could induce cross-linking on the PS surface, interestingly, this did not prevent hydrophobic recovery even at decreased storage temperatures. Short range rearrangement of implanted polar functional groups is likely responsible for this and causes hydrophobic recovery, regardless of cross-linking or storage temperature. This is further supported by the work of two other research groups. Murakami, et al.⁴⁴ found that PS samples cross-linked prior to O₂ plasma treatment were susceptible to additional hydrophobic recovery even when attempts were made to wash away the LMWOM thought to contribute to diffusion-based rearrangements. It was only when samples were stored in H₂O that hydrophobic recovery was prevented. Larsson and Derand⁴² found that high P (500 W) O₂ plasma and a correspondingly high self-bias voltage (600 V) somewhat reduced hydrophobic recovery, although the induced surface roughness accompanying the higher P treatment may also be responsible for this observation.

3.3.3. Hydrophobic recovery on polycarbonate. The results of H₂O plasma modification and subsequent aging behavior of solid bisphenol A PC (Lexan®) is similar to that of track-etched PC membranes, described in Chapters 4¹⁴ and 5. As discussed in more detail in those chapters, PC is rendered wettable by the H₂O plasma modification and this treatment is persistent with PC showing a manageable amount of hydrophobic recovery. Here, our discussion will be limited to the H₂O plasma modification of PC in comparison to the other polymer materials.

The properties and structure of PC are very different from those of polyolefins. Like PP and PS, plasma modification of PC is believed to result in a significant amount of chain scission and comparatively little cross-linking. Hofrichter et al.⁵² compared O₂ plasma treatments on high-purity spin coated PC substrates and commercially available Lexan®. They found plasma treatments induced chain scission on the spin coated PC and that impurities in the surface of the

Lexan® samples used for that study facilitated cross-linking. Muir et al.⁵³ examined O₂ plasma modification on optical grade Lexan® and noted the formation of LMWOM, even with short treatment times (>10 s). They attribute this to chain scission at the aromatic and carbonate groups in the PC backbone. The LMWOM formed as a result of chains scission was easily washed away, confirming the role of LMWOM in the stability of modified PC surfaces.

It appears the only reason that PC surfaces are as stable as they are compared to PP and PS is the high T_m and T_g of PC. In this respect PC is more easily compared to the sulfone based polymers PSf and PES, studied previously.^{13, 34, 35} Each of these polymers contain aromatic functionality within their polymer backbone and can be described as having high thermal stability. For example, published T_g and T_m values for PC are 150 and 157 °C, respectively.³⁸ Gonzalez et al.⁵⁴ showed that O₂ plasma was responsible for aromatic ring opening on PSf and PES materials. Taken to their fullest extent, such mechanisms will lead to chain scission, as discussed in Section 4.3.2. Collectively these studies suggest that oxidation to the point of chain scission occurs on PSf and PES. Although it is unclear from the literature if cross-linking confers additional stability to PSf and PES, it is reasonable to assume that the thermal stability assists in preventing aging effects and hydrophobic recovery and that thermal stability assists in stabilizing the non-cross-linked H₂O plasma modified PC surface.

3.3.4. Hydrophobic recovery on polyurethane 75A. Our analysis of H₂O plasma modified PU 75A samples highlights the pitfalls of attempting plasma modification of uncharacterized composite materials. XPS results reveal the absence of nitrogen and the presence of significant quantities of silicon on the untreated PU samples; the treated PU samples give similar results. The high resolution C_{1s} XPS spectra from untreated and treated PU samples are inconsistent with PU materials. These results show that the PU 75A material is a composite material and our XPS

results likely represent silicon containing components in the PU 75A formulation. Plasma modification studies on composite materials are certainly important, however, additional experiments will be needed to fully understand the H₂O plasma modification outcome and subsequent aging behavior of this material. For example, experiments are needed to identify the components of the PU 75A formulation and the independent effect of H₂O plasma modification on each component.

3.4. Summary

The research described in this chapter furthers our understanding of H₂O plasma modifications on a variety of polymer surfaces. Each treated polyolefin sample is rendered wettable due to the implantation of CO_x functional groups, and exhibits some degree of hydrophobic recovery when aged. The treated HDPE surface is the most stable owing to plasma-induced cross-linking, whereas the treated PP surface is the least stable as a result of chain scission leading to significant surface rearrangement. H₂O plasma modification outcomes on the two polymers containing aromatic functionality are quite different from one another. Modified PC surfaces are rendered wettable and show excellent stability with age. Although chain scission is the dominant process on PC, thermal stability limits hydrophobic recovery. PS is initially rendered wettable, but the aged PS samples exhibit behavior similar to that of PP. Shifts in the XPS C_{1s} CO_x moiety BEs of both PS and PP are consistent with polar functionalities being subsumed by the polymer surface as samples age. These results show that H₂O plasma modifications are broadly applicable and give improved wettability a range of polymers. During aging, however, the H₂O plasma modified polymers exhibit similar aging behavior similar to that of O₂ plasma modified polymers described in the literature.

REFERENCES

1. Hall, C.; Murphy, P.; Griesser, H., Etching and deposition mechanism of an alcohol plasma on polycarbonate and poly(methyl methacrylate): an adhesion promotion mechanism for plasma deposited a:SiO_xC_yH_z Coating. *Plasma Processes Polym.* **2012**, *9*, (9), 855-865.
2. Hall, C. J.; Murphy, P. J.; Griesser, H. J., Direct imaging of mechanical and chemical gradients across the thickness of graded organosilicone microwave PECVD coatings. *ACS Appl. Mater. Interfaces* **2014**, *6*, (2), 1279-1287.
3. Intranuovo, F.; Howard, D.; White, L. J.; Johal, R. K.; Ghaemmaghami, A. M.; Favia, P.; Howdle, S. M.; Shakesheff, K. M.; Alexander, M. R., Uniform cell colonization of porous 3-D scaffolds achieved using radial control of surface chemistry. *Acta Biomater.* **2011**, *7*, (9), 3336-3344.
4. De Bartolo, L.; Morelli, S.; Bader, A.; Drioli, E., Evaluation of cell behaviour related to physico-chemical properties of polymeric membranes to be used in bioartificial organs. *Biomaterials* **2002**, *23*, (12), 2485-2497.
5. Howarter, J. A.; Youngblood, J. P., Amphiphile grafted membranes for the separation of oil-in-water dispersions. *J. Colloid Interface Sci.* **2009**, *329*, (1), 127-132.
6. Baytekin, H. T.; Wirth, T.; Gross, T.; Treu, D.; Sahre, M.; Theisen, J.; Schmidt, M.; Unger, W. E. S., Determination of wettability of surface-modified hot-embossed polycarbonate wafers used in microfluidic device fabrication via XPS and ToF-SIMS. *Surf. Interface Anal.* **2008**, *40*, (3-4), 358-363.
7. Gururaj, T.; Subasri, R.; Raju, K. R. C. S.; Padmanabham, G.; Raju, K., Effect of plasma pretreatment on adhesion and mechanical properties of UV-curable coatings on plastics. *Appl. Surf. Sci.* **2011**, *257*, (9), 4360-4364.
8. Hofrichter, A.; Bulkin, P.; Drevillon, B., An interfacial study of a hydrogenated carbon interlayer for adhesion enhancement of plasma deposited silica thin films on polycarbonate. *J. Adhes. Sci. Technol.* **2002**, *16*, (4), 395-407.
9. Muir, B.; Thissen, H.; Simon, G.; Murphy, P.; Griesser, H., Factors affecting the adhesion of microwave plasma deposited siloxane films on polycarbonate. *Thin Solid Films* **2006**, *500*, (1-2), 34-40.
10. Xu, W. D.; Chellam, S., Initial stages of bacterial fouling during dead-end microfiltration. *Environ. Sci. Technol.* **2005**, *39*, (17), 6470-6476.
11. Zhang, M. M.; Li, C.; Benjamin, M. M.; Chang, Y. J., Fouling and natural organic matter removal in adsorben/membrane systems for drinking water treatment. *Environ. Sci. Technol.* **2003**, *37*, (8), 1663-1669.

12. Qu, F.; Liang, H.; Zhou, J.; Nan, J.; Shao, S.; Zhang, J.; Li, G., Ultrafiltration membrane fouling caused by extracellular organic matter (EOM) from *Microcystis aeruginosa*: Effects of membrane pore size and surface hydrophobicity. *J. Membr. Sci.* **2014**, 449, (0), 58-66.
13. Kull, K. R.; Steen, M. L.; Fisher, E. R., Surface modification with nitrogen-containing plasmas to produce hydrophilic, low-fouling membranes. *J. Membr. Sci.* **2005**, 246, (2), 203-215.
14. Tompkins, B. D.; Dennison, J. M.; Fisher, E. R., H₂O plasma modification of track-etched polymer membranes for increased wettability and improved performance. *J. Membr. Sci.* **2013**, 428, 576-588.
15. Shi, X.; Field, R.; Hankins, N., Review of fouling by mixed feeds in membrane filtration applied to water purification. *Desalin. Water Treat.* **2011**, 35, (1-3), 68-81.
16. O'Connell, C.; Sherlock, R.; Ball, M. D.; Aszalós-Kiss, B.; Prendergast, U.; Glynn, T. J., Investigation of the hydrophobic recovery of various polymeric biomaterials after 172 nm UV treatment using contact angle, surface free energy and XPS measurements. *Appl. Surf. Sci.* **2009**, 255, (8), 4405-4413.
17. Truica-Marasescu, F.; Jedrzejowski, P.; Wertheimer, M. R., Hydrophobic recovery of vacuum ultraviolet irradiated polyolefin surfaces. *Plasma Processes Polym.* **2004**, 1, (2), 153-163.
18. Song, J.; Gunst, U.; Arlinghaus, H. F.; Vancso, G. J., Flame treatment of low-density polyethylene: Surface chemistry across the length scales. *Appl. Surf. Sci.* **2007**, 253, (24), 9489-9499.
19. Grill, A., *Cold Plasma Matierls Fabrication: From Fundamentals to Applications*. IEEE Press: Piscataway, NJ, 1994.
20. Grace, J. M.; Gerenser, L. J., Plasma treatment of polymers. *J. Dispersion Sci. Technol.* **2003**, 24, (3-4), 305-341.
21. Hansen, R. H.; Schonhorn, H., A new technique for preparing low surface energy polymers for adhesive bonding. *J. Polym. Sci., Part B: Polym. Lett.* **1966**, 4, (3), 203-209.
22. Mantell, R. M.; Ormand, W. L., Activation of plastic surfaces in a plasmajet. *Ind. Ena. Chem. Prod. Res. Dev.* **1964**, 3, (4), 300-303.
23. Schonhorn, H.; Hansen, R. H., Surface treatment of polymers for adhesive bonding. *J. Appl. Polym. Sci.* **1967**, 11, (8), 1461-1474.
24. Pascual, M.; Balart, R.; Sánchez, L.; Fenollar, O.; Calvo, O., Study of the aging process of corona discharge plasma effects on low density polyethylene film surface. *J. Mater. Sci.* **2008**, 43, (14), 4901-4909.

25. Occhiello, E.; Morra, M.; Cinquina, P.; Garbassi, F., Hydrophobic recovery of oxygen-plasma-treated polystyrene. *Polymer* **1992**, 33, (14), 3007-3015.
26. Mortazavi, M.; Nosonovsky, M., A model for diffusion-driven hydrophobic recovery in plasma treated polymers. *Appl. Surf. Sci.* **2012**, 258, (18), 6876-6883.
27. Lee, L. J., Polymer nanoengineering for biomedical applications. *Ann. Biomed. Eng.* **2006**, 34, (1), 75-88.
28. Robeson, L. M., Polymer membranes for gas separation. *Curr. Opin. Solid State Mater. Sci.* **1999**, 4, (6), 549-552.
29. Koros, W. J.; Fleming, G. K.; Jordan, S. M.; Kim, T. H.; Hoehn, H. H., Polymeric membrane materials for solution-diffusion based permeation separations. *Prog. Polym. Sci.* **1988**, 13, (4), 339-401.
30. Sagle, A. C.; Van Wagner, E. M.; Ju, H.; McCloskey, B. D.; Freeman, B. D.; Sharma, M. M., PEG-coated reverse osmosis membranes: Desalination properties and fouling resistance. *J. Membr. Sci.* **2009**, 340, (1-2), 92-108.
31. Hausmann, A.; Sanciuolo, P.; Vasiljevic, T.; Weeks, M.; Schroën, K.; Gray, S.; Duke, M., Fouling of dairy components on hydrophobic polytetrafluoroethylene (PTFE) membranes for membrane distillation. *J. Membr. Sci.* **2013**, 442, (0), 149-159.
32. Hassan, A. N.; Anand, S.; Avadhanula, M., Microscopic observation of multispecies biofilm of various structures on whey concentration membranes. *J. Dairy Sci.* **2010**, 93, (6), 2321-2329.
33. Kravets, L. I.; Dmitriev, S. N.; Gil'man, A. B., Modification of properties of polymer membranes by low-temperature plasma treatment. *High Energ. Chem.* **2009**, 43, (3), 181-188.
34. Steen, M. L.; Hymas, L.; Havey, E. D.; Capps, N. E.; Castner, D. G.; Fisher, E. R., Low temperature plasma treatment of asymmetric polysulfone membranes for permanent hydrophilic surface modification. *J. Membr. Sci.* **2001**, 188, (1), 97-114.
35. Steen, M. L.; Jordan, A. C.; Fisher, E. R., Hydrophilic modification of polymeric membranes by low temperature H₂O plasma treatment. *J. Membr. Sci.* **2002**, 204, (1-2), 341-357.
36. Jokinen, V.; Suvanto, P.; Franssila, S., Oxygen and nitrogen plasma hydrophilization and hydrophobic recovery of polymers. *Biomicrofluidics* **2012**, 6, (1), 016501-10.
37. Steen, M. L.; Butoi, C. I.; Fisher, E. R., Identification of gas-phase reactive species and chemical mechanisms occurring at plasma-polymer surface interfaces. *Langmuir* **2001**, 17, (26), 8156-8166.

38. Mark, J. E., *Polymer Data Handbook*. Oxford University Press, Inc.: New York, NY, 1999.
39. Tompkins, B. D.; Fisher, E. R., Plasma synthesis of hydrocarbon/fluorocarbon thin films with compositional gradients. *Plasma Processes Polym.* **2013**, 10, (9), 779-791.
40. Kosobrodova, E.; Kondyurin, A.; McKenzie, D. R.; Bilek, M. M. M., Kinetics of post-treatment structural transformations of nitrogen plasma ion immersion implanted polystyrene. *Nucl. Instrum. Methods Phys. Res., Sect. B* **2013**, 304, (0), 57-66.
41. Larrieu, J.; Held, B.; Martinez, H.; Tison, Y., Ageing of atactic and isotactic polystyrene thin films treated by oxygen DC pulsed plasma. *Surf. Coat. Technol.* **2005**, 200, (7), 2310-2316.
42. Larsson, A.; Dérand, H., Stability of polycarbonate and polystyrene surfaces after hydrophilization with high intensity oxygen RF plasma. *J. Colloid Interface Sci.* **2002**, 246, (1), 214-221.
43. Morra, M.; Occhiello, E.; Garbassi, F., Hydrophobic recovery and misting behavior of plasma treated PS and PC surfaces. *Angew. Makromol. Chem.* **1991**, 189, (1), 125-136.
44. Murakami, T.; Kuroda, S.-i.; Osawa, Z., Dynamics of polymeric solid surfaces treated by oxygen plasma: plasma-induced increases in surface molecular mobility of polystyrene. *J. Colloid Interface Sci.* **1998**, 200, (1), 192-194.
45. Sanchis, M. R.; Calvo, O.; Fenollar, O.; Garcia, D.; Balart, R., Characterization of the surface changes and the aging effects of low-pressure nitrogen plasma treatment in a polyurethane film. *Polym. Test.* **2008**, 27, (1), 75-83.
46. Greenwood, O. D.; Hopkins, J.; Badyal, J. P. S., Non-isothermal O₂ plasma treatment of phenyl-containing polymers. *Macromolecules* **1997**, 30, (4), 1091-1098.
47. Larson, B. J.; Gillmor, S. D.; Braun, J. M.; Cruz-Barba, L. E.; Savage, D. E.; Denes, F. S.; Lagally, M. G., Long-term reduction in poly(dimethylsiloxane) surface hydrophobicity via cold-plasma treatments. *Langmuir* **2013**, 29, (42), 12990-12996.
48. Guimond, S.; Wertheimer, M. R., Surface degradation and hydrophobic recovery of polyolefins treated by air corona and nitrogen atmospheric pressure glow discharge. *J. Appl. Polym. Sci.* **2004**, 94, (3), 1291-1303.
49. Behnisch, J.; Holländer, A.; Zimmermann, H., Factors influencing the hydrophobic recovery of oxygen-plasma-treated polyethylene. *Surf. Coat. Technol.* **1993**, 59, (1-3), 356-358.
50. Morra, M.; Occhiello, E.; Gila, L.; Garbassi, F., Surface dynamics vs. adhesion in oxygen plasma treated polyolefins. *J. Adhes.* **1990**, 33, (1-2), 77-88.

51. Trevino, K. J.; Shearer, J. C.; Tompkins, B. D.; Fisher, E. R., Comparing isoelectric point and surface composition of plasma modified native and deposited SiO₂ films using contact angle titrations and x-ray photoelectron spectroscopy. *Plasma Processes Polym.* **2011**, 8, (10), 951-964.
52. Hofrichter, A.; Bulkin, P.; Dré villon, B., Plasma treatment of polycarbonate for improved adhesion. *J. Vac. Sci. Technol., A* **2002**, 20, (1), 245-250.
53. Muir, B. W.; McArthur, S. L.; Thissen, H.; Simon, G. P.; Griesser, H. J.; Castner, D. G., Effects of oxygen plasma treatment on the surface of bisphenol A polycarbonate: a study using SIMS, principal component analysis, ellipsometry, XPS and AFM nanoindentation. *Surf. Interface Anal.* **2006**, 38, (8), 1186-1197.
54. Gonzalez, E., II; Barankin, M. D.; Guschl, P. C.; Hicks, R. F., Ring opening of aromatic polymers by remote atmospheric-pressure plasma. *IEEE Trans. Plasma Sci.* **2009**, 37, (6), 823-831.

CHAPTER 4

H₂O PLASMA MODIFICATION OF TRACK-ETCHED POLYMER MEMBRANES FOR INCREASED WETTABILITY AND IMPROVED PERFORMANCE

This chapter is based on work published under the same title in the *Journal of Membrane Science*, written by Brendan D. Tompkins, Jordan M. Dennison, and Ellen R. Fisher.¹ The text, figures, and tables from this publication are reproduced here with permission from Elsevier B. V. (License Number 3361550031904, April 3rd, 2014). This chapter describes work in which an inductively-coupled H₂O vapor plasma was used to modify the surface of 0.2 μm and 3.0 μm polycarbonate and polyethylene terephthalate track-etched membranes with the goal of permanently increasing the hydrophilicity of the membrane surfaces. Surface analysis techniques were used to understand how the plasma modified membrane surface evolved with age and plasma diagnostics were used to elucidate the mechanisms by which plasma surface modification took place. Funding for this research was provided by the National Science Foundation (CHE-0911248).

4.1. Introduction

Microfiltration membranes enjoy widespread use in many applications including protein separations, cell culture work, and water treatment.²⁻⁶ Within this extensive group of materials, microporous track-etched polycarbonate (PC-TE) and polyethylene terephthalate (PET-TE) membranes are highly valued for their robustness and consistent pore geometry. Use of these membranes in aqueous environments, however, is complicated because of their relatively low surface energy and correspondingly low wettability.^{7, 8} Initial wetting of membrane surfaces and

pore cross-section can be facilitated by applying wetting agents such as polyvinylpyrrolidone (PVP) to the membrane after fabrication. Although wetting agents like PVP initially decrease the surface energy and improve wettability, they can be washed away, leading to unstable performance and possible filtrate contamination. Removal of wetting agents can also increase susceptibility to fouling, which remains a key issue facing membrane separation technologies.⁸⁻¹⁰

To address the need to create more hydrophilic polymeric membranes, researchers have explored several modification strategies in addition to the application of wetting agents, including copolymerization with hydrophilic polymers, blending polymers with hydrophilic additives, and blending polymers with other materials.^{6, 7, 11-14} In general, the hydrophilic surface forms from the way the polar material organizes during fabrication or annealing. Although these modification strategies have often been effective, some remaining issues include the persistent problem of fouling and inefficient control over bulk polymer properties, pore geometry, and membrane surface morphology. Furthermore, these techniques are of limited applicability because they occur during initial fabrication steps using a phase inversion or solvent casting process; thus, additional modification could be needed if the desired surface properties were not achieved during membrane formation. More importantly, the surface modification of membranes prepared using other fabrication techniques (e.g. track etching processes) requires a different approach.

One alternative treatment is plasma surface modification, which continues to be a popular and reliable technique for polymer surface modification. Plasma based techniques are desirable because they tend to be inexpensive, environmentally friendly, and can be used to permanently modify the membrane surface without changing the bulk properties of the polymer. Two different approaches to plasma modification of membrane surfaces have been extensively

explored: surface modification through treatment and functionalization of the existing polymer surface and surface modification through deposition of a thin film with a different functionality than the underlying polymeric membrane. The former process is the more desirable for membrane modification because implanting polar functional groups onto the surface of the membrane allows for increased wettability while still maintaining the original pore size and geometry.¹⁵⁻¹⁷

Numerous studies have explored the modification of polymeric materials, including membranes, with oxidizing/non-depositing plasma systems. For example, O₂ plasmas have been widely used to modify the surface of polymers, including polycarbonate (PC) and polyethylene terephthalate (PET),¹⁸⁻²⁶ albeit with limited success in creating hydrophilic surfaces. This is because O₂ plasmas effectively etch PC-TE and PET-TE pore structures, which can create desirable pore structures, but also results in the formation of low molecular weight oxidized material (LMWOM).²³ Given that LMWOM is easily removed by washing, the desired polar surface functional groups are not permanent, resulting in serious hydrophobic recovery. For example, Muir et al. reported on the modification of bisphenol A PC films modified with O₂ in a rf glow discharge plasma chamber to investigate the extent to which the polymer is degraded with modification.²³ They found that extremely short treatment times, on the order of seconds, were sufficient to form a significant oxidized layer. When their treatment times were increased beyond 2 s, however, they were able to wash the oxide layer away with ethanol and the surface O/C ratio was nearly identical to the untreated substrate. This was attributed to new polar functionality being incorporated into loosely bound LMWOM that formed during the treatment. Baytekin et al. reported similar results from their study on O₂ plasma modification of PC for use in microfluidic devices.¹⁸ They found that much of the new C-O/C=O functionality was

removed after rinsing with water. Despite this loss of polar functionality and subsequent hydrophobic recovery, the H₂O contact angle (wCA) of rinsed substrates was still far below that of untreated PC. This lack of robust surface modification has not been limited to solid substrates. Li et al. found that PC-TE membranes etched using O₂ plasma required PVP treatment to facilitate wetting prior to AC impedance transport measurements.²² These reports suggest that an oxidizing environment is not enough to affect a robust polar surface treatment. Thus, alternative plasma chemistries are required to afford a more permanent hydrophilic surface treatment for polymer substrates.

Past work in our laboratories focused on the use of H₂O vapor plasma systems to impart polar functionality to polyethersulfone (PES), polysulfone (PSf) and polyethylene (PE) membranes to improve hydrophilicity.^{16, 17} The treated asymmetric PES and PSf membranes were extremely stable when stored under laboratory conditions, with effectively no hydrophobic recovery, even after 2 years of aging. Additional studies of PSf treated using NH₃/O₂ plasmas gave similar results.¹⁵ In contrast, these treatments were not, however, successful at modifying symmetric PE membranes to the same extent, as they showed significant hydrophobic recovery after only a few days.¹⁷ Despite this behavior, no samples recovered completely, suggesting that there is some degree of permanence to the plasma modification methods. It was unclear, however, whether chemical structure (i.e. the aromatic and sulfonate functionalities found in PES and PSf as compared to the hydrocarbon functionality of PE), physical structure (i.e. pore structure and symmetry), or some unknown factor could be responsible for the efficacy of the treatments for each material.

The present work focuses on the efficacy of H₂O vapor plasma modification of the two most common track-etched membrane materials, PC-TE and PET-TE. Although PC and PET

have physical properties closer to those of PSf and PES compared to PE, there are notable differences in the chemical structure of the materials used here compared to the previously studied polymers. For example, although both PC and PET have aromatic functionalities like PSf and PES, neither contain sulfur linkages. Furthermore, the process used to create the pores in PC-TE and PET-TE results in non-interconnected pores that are nearly symmetrical, unlike the pore networks of PSf, PES, and PE membranes. Here, membranes were treated in a home-built inductively coupled rf plasma reactor, described in Section 2.1., using H₂O vapor plasmas. Several characterization techniques were used to analyze treated membranes, including static wCA measurements for surface wettability, x-ray photoelectron spectroscopy (XPS) for surface elemental composition and functionality, scanning electron microscopy (SEM) for surface morphology and pore size, and H₂O flux measurements tested the impact of plasma treatment on membrane performance. To more fully understand the overall plasma chemistry, time resolved-optical emission spectroscopy (TR-OES) was employed to track relative gas phase densities of plasma species during membrane treatment.

4.2. Results

4.2.1. Efficacy of plasma modification. Our previous studies investigated H₂O plasma treatment of PSf and PES membranes and found that plasmas produced at applied rf power (P) = 25 W, 50 mTorr reactor pressure (H₂O), 2 min treatment time, and 9 cm downstream membrane placement yielded the best improvement in wettability for those materials.^{16, 17} Here, we consider these as “standard treatment conditions” as they were used for the majority of the studies reported here. Figure 4.1. shows wCA data as a function of the age of the drop on the surface (movie mode) for untreated and treated (standard treatment conditions) PC-TE and

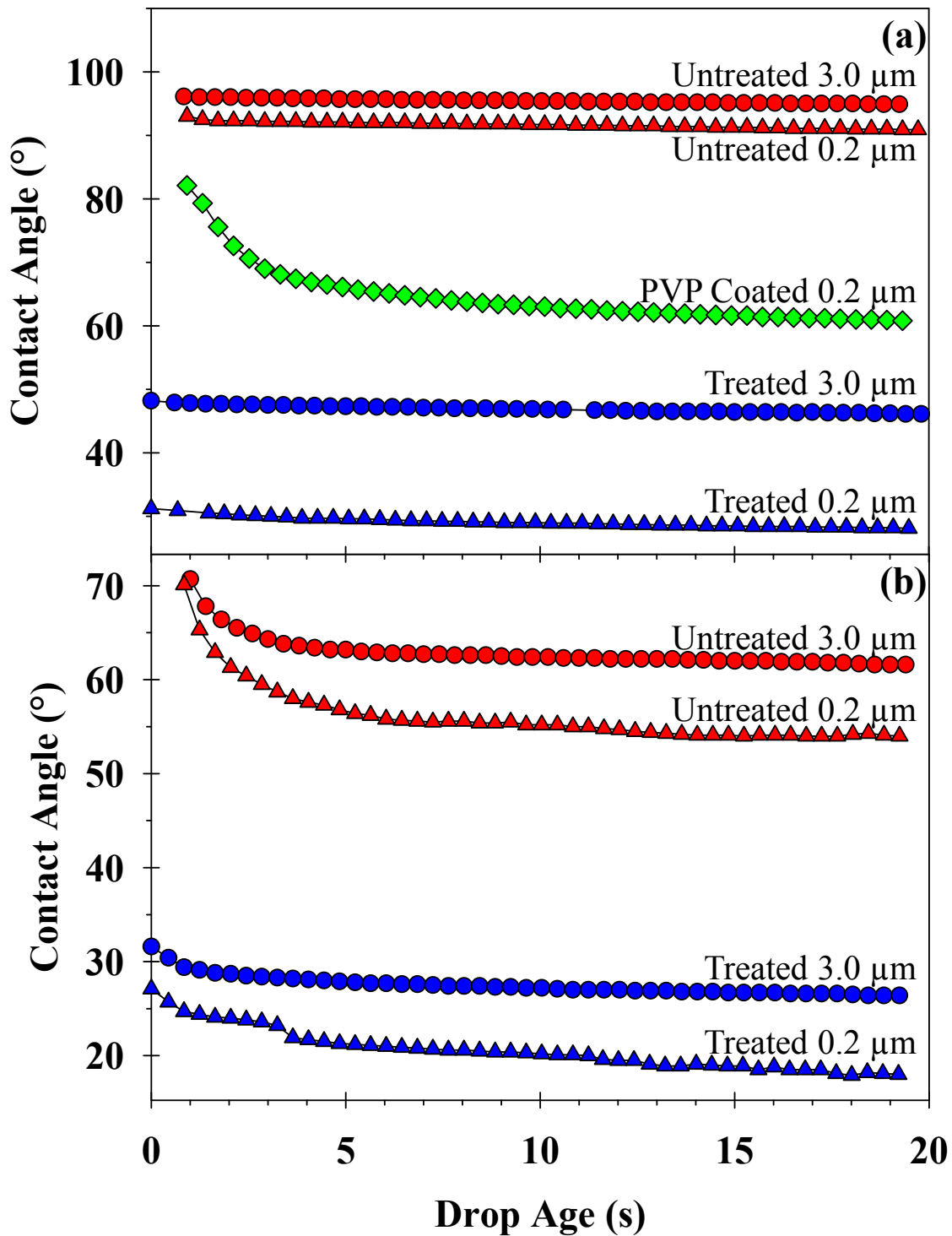


Figure 4.1. wCA data acquired in “movie-mode” on (a) PC-TE and (b) PET-TE membranes. Treated membranes were modified using standard treatment conditions ($P = 25$ W, 50 mTorr reactor pressure, 2 min, and 9 cm downstream from the coil).

PET-TE membranes with two different pore sizes (0.2 and 3.0 μm) as well as hydrophilic PVP coated 0.2 μm PC-TE. Note for the untreated PC-TE membranes, Figure 4.1.a., the wCA measured does not change appreciably with changing pore size as the drop is aged through 20 s. Minor variations in wCA (over the 20 s collection time) are likely the result of differences in pore density for the 0.2 and 3.0 μm membranes. The relatively high wCAs ($>90^\circ$) indicate the untreated PC-TE membranes are very hydrophobic, consistent with an unmodified PC surface. The treated PC-TE membranes show a large decrease in wCA to 28° and 46° , for the upstream side of 0.2 and 3.0 μm membranes, respectively, indicating the H_2O plasma treatment effectively produces a much more hydrophilic membrane. Indeed, at the 20 s collection time, the wCA of treated PC-TE is even lower than that of hydrophilic PVP coated 0.2 μm PC-TE (61°). Likewise, the treated PET-TE membranes show much lower wCAs than their untreated counterparts, Figure 4.1.b. The wCAs for both the 0.2 and 3.0 μm PET-TE membranes decrease to 18° and 26° , respectively, upon treatment (20 s collection time).

Although the above results demonstrate our standard treatment conditions are reasonably effective at modifying both the PC-TE and PET-TE membranes, we also investigated the plasma parameter space in more detail to potentially optimize our treatments for these materials. Figure 4.2. shows wCA results for the upstream side of 0.2 μm PC-TE and 3.0 μm PET-TE membranes modified using the standard treatment conditions and the effect of reactor pressure, P , and treatment time on wettability. For comparison, measurements made on untreated 0.2 μm PC-TE and 3.0 μm PET-TE yield wCAs of $97 \pm 3^\circ$ and $54 \pm 9^\circ$, respectively. As shown in Figure 4.2.a., the reactor pressure (50-300 mTorr) has very little effect on wettability. Indeed, PC-TE membranes treated at 50 mTorr, attain a wCA of $38 \pm 2^\circ$, a 61% decrease from untreated, and PET-TE membranes attain a wCA of $27 \pm 4^\circ$, a 50% decrease compared to untreated PET-TE.

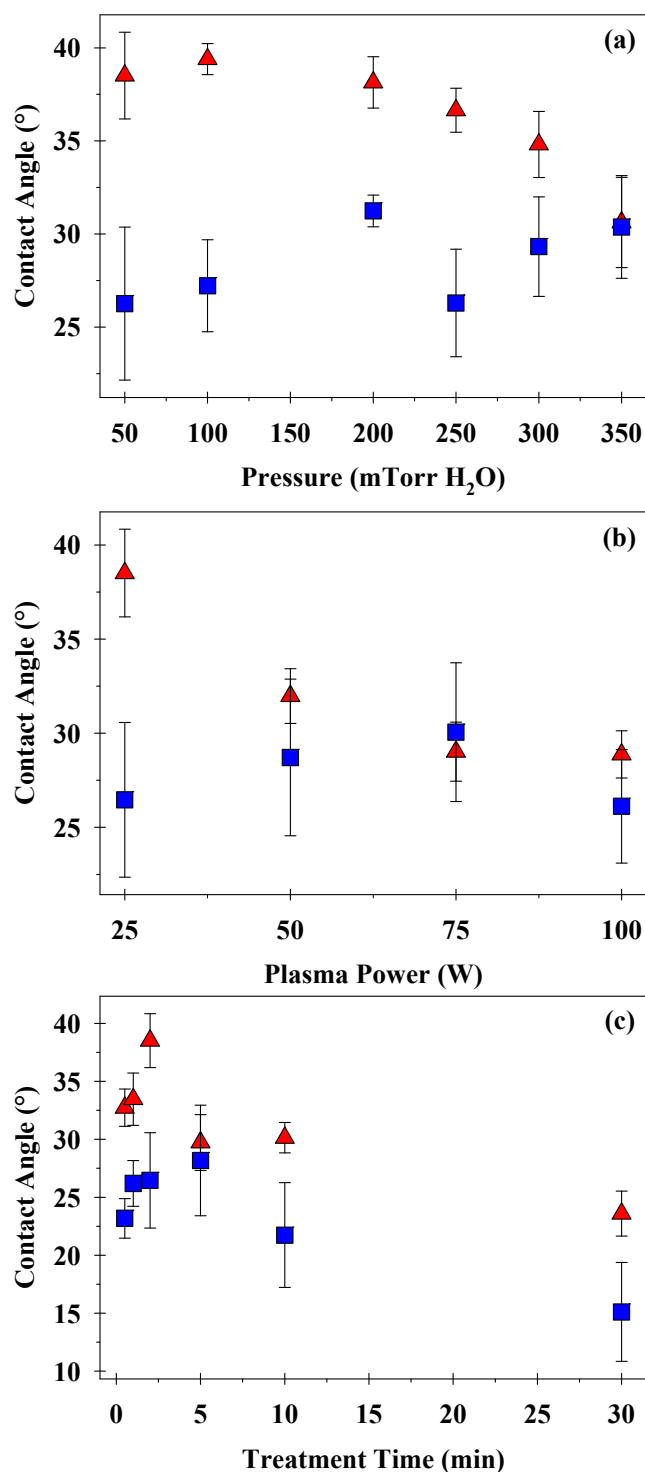


Figure 4.2. Dependence of wCA of 0.2 μm PC-TE (red triangles) and 3 μm PET-TE (blue squares) membranes on various plasma parameters: (a) reactor pressure from 50-350 mTorr; (b) applied rf power from 25-100 W; and (c) treatment time from 0.5-30 min. Other plasma parameters were held constant at the standard treatment conditions (25 W, 50 mTorr H₂O pressure, and 2 min treatment time), for each set of experiments.

As the treatment pressure is increased, there is a small improvement in wettability on PC-TE membranes. The PET-TE is even less responsive to changes in treatment pressure, however, with no additional improvement in wettability observed at higher pressures.

Figure 4.2.b. shows wCAs for membranes treated in H₂O plasmas with $P = 25$ -100 W. The wettability of PC-TE increases with P , where the lowest wCA ($29 \pm 1^\circ$) is observed for samples treated at $P = 100$ W. Note that this decrease in wCA may be the result of changing surface morphology, which is discussed further in Section 4.2.2. Interestingly, the PET-TE does not show any change in wettability with increased P , as wCAs of $27 \pm 3^\circ$ and $26 \pm 1^\circ$ were measured for samples treated at $P = 25$ W and $P = 100$ W, respectively. Figure 4.2.c. shows wCAs for PC-TE and PET-TE membranes over a range of treatment times (0.5-30 min). In contrast to the results for P and pressure dependence studies, both materials show similar changes in wettability as treatment time is increased. The wCA of PC-TE is $33 \pm 2^\circ$ when treated for 0.5 min, increases to $38 \pm 2^\circ$ at 2 min, and steadily decreases to $23 \pm 2^\circ$ when samples are treated as long as 30 min. The wettability of PET-TE has a similar dependence on treatment time.

4.2.2. Surface morphology and pore size. Notably, previous work in our laboratory and others have shown that plasma surface modification can damage the surface by altering the morphology (e.g. formation of surface structures, cracking or pitting) or by altering the pore geometry (e.g. increasing pore size, collapsing the pore structure).^{21, 22, 27} Thus, examining the morphology of both treated and untreated membranes is critical in determining the true effects of the plasma modification. Figure 4.3. shows SEM images of untreated 0.2 μm PC-TE and 3.0 μm PET-TE membranes and the same materials modified using standard treatment conditions. The outer surfaces of the untreated membranes are generally smooth and the pore sizes agree well

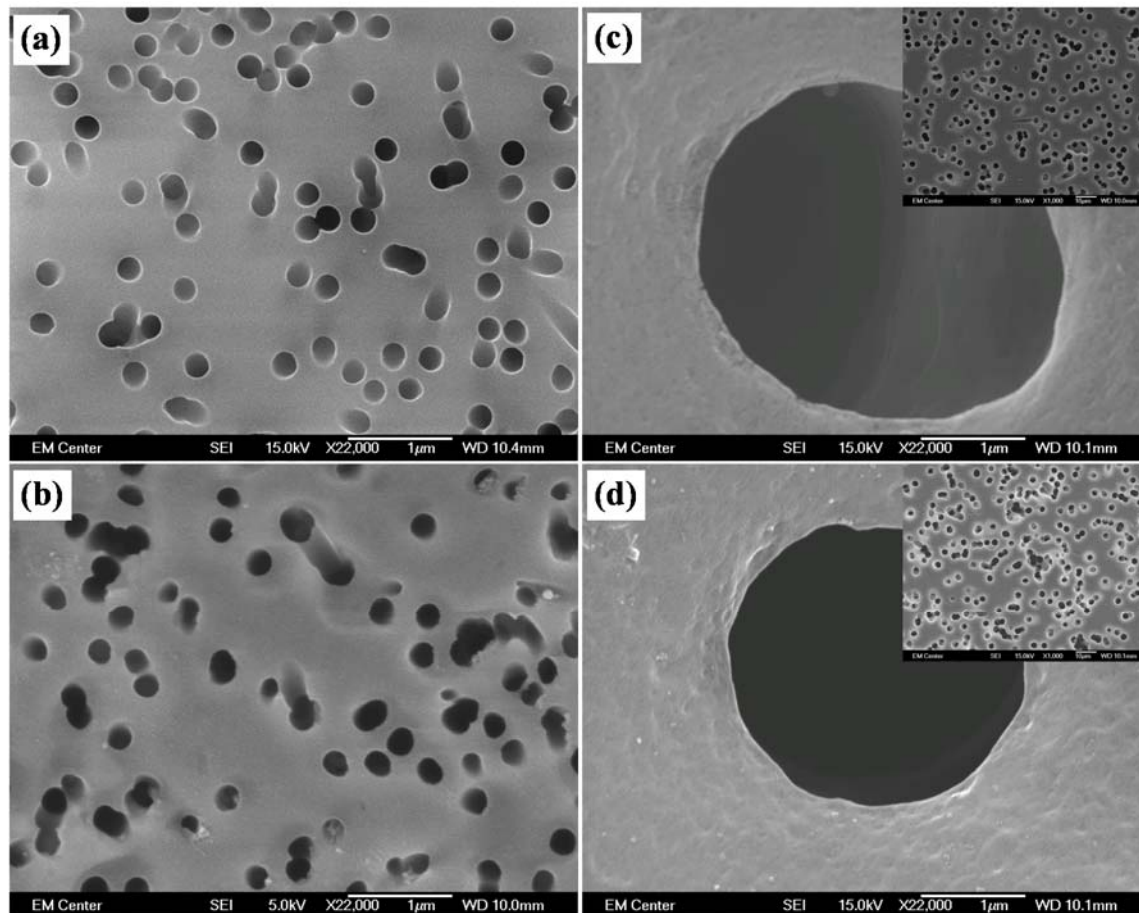


Figure 4.3. SEM images of (a) untreated 0.2 μm PC-TE; (b) treated 0.2 μm PC-TE; (c) untreated 3.0 μm PET-TE; and (d) treated 3.0 μm PET-TE membranes. Membranes were treated using standard conditions (see caption of Figure 4.1.). The insets in panels (c) and (d) show lower magnification images of the membrane surfaces.

with manufacturer specifications, Figures 4.3.a. and 4.3.c. Images of treated PC-TE and PET-TE are almost indistinguishable from the untreated sample and show little change to the surface morphology and no change in pore dimensions, Figure 4.3.b. and 4.3.d. Indeed, pore diameters at the surface of treated PC-TE and PET-TE were 0.23 ± 0.03 and 3.08 ± 0.19 μm , respectively, identical to those measured on untreated membranes within experimental error, Table 4.1.

It is also useful to examine the effects of plasma parameters on surface morphology given the results of our wCA studies (Figure 4.2.), as changes in wettability can be a result of both chemical and morphological changes in a material's surface. Although our H_2O plasma has little impact on the membrane structure when mild treatment conditions are used, changing plasma parameters can result in significant changes to pore dimensions. Figure 4.4. shows representative SEM images of PC-TE and PET-TE membranes treated at the upper end of our parameter space for reactor pressure, P , and treatment time. Corresponding pore measurements are listed in Table 4.1. As with samples treated under standard conditions, increasing the reactor pressure to 350 mTorr does not change the outcome of plasma treatment for either PC-TE or PET-TE membranes. In contrast, elevated P and longer treatment times appear to alter PC-TE and PET-TE surface structures. Specifically, the pore diameter of 0.2 μm PC-TE membranes treated at $P = 100$ W increases slightly to 0.27 ± 0.03 μm , Figure 4.4.a. The expansion of pores becomes more pronounced as treatment time is extended to 30 min, Figure 4.4.c., where an 87% increase in pore diameter (0.43 ± 0.04 μm) is observed in addition to a visible texturing of the surface between the pores. We observe only a slight increase in pore size for PET-TE membranes with increasing P and longer treatment times; however, the larger pores of the 3.0 μm PET-TE make it difficult to evaluate the significance of changes in the pore size.

Table 4.1. Pore size measurements of untreated and treated PC-TE and PET-TE.

Membrane	Pressure (mTorr)	<i>P</i> (W)	Treatment Time (min)	Pore Size (μm)^a
PC-TE	--	--	--	0.23 ± 0.01^b
	50	25	2	0.23 ± 0.03
	350	25	2	0.24 ± 0.02
	50	100	2	0.27 ± 0.03
	50	25	30	0.43 ± 0.04
PET-TE	--	--	--	2.96 ± 0.31^b
	50	25	2	3.08 ± 0.19
	350	25	2	2.99 ± 0.44
	50	100	2	2.83 ± 0.34
	50	25	30	3.16 ± 0.51

^aPore diameters reported are the mean of measurements made on a minimum of 12 pores per image from 2 separate images taken of a given sample.

^bThese samples were untreated membranes, prepared for SEM using the same protocol as the other samples, but were otherwise unmodified.

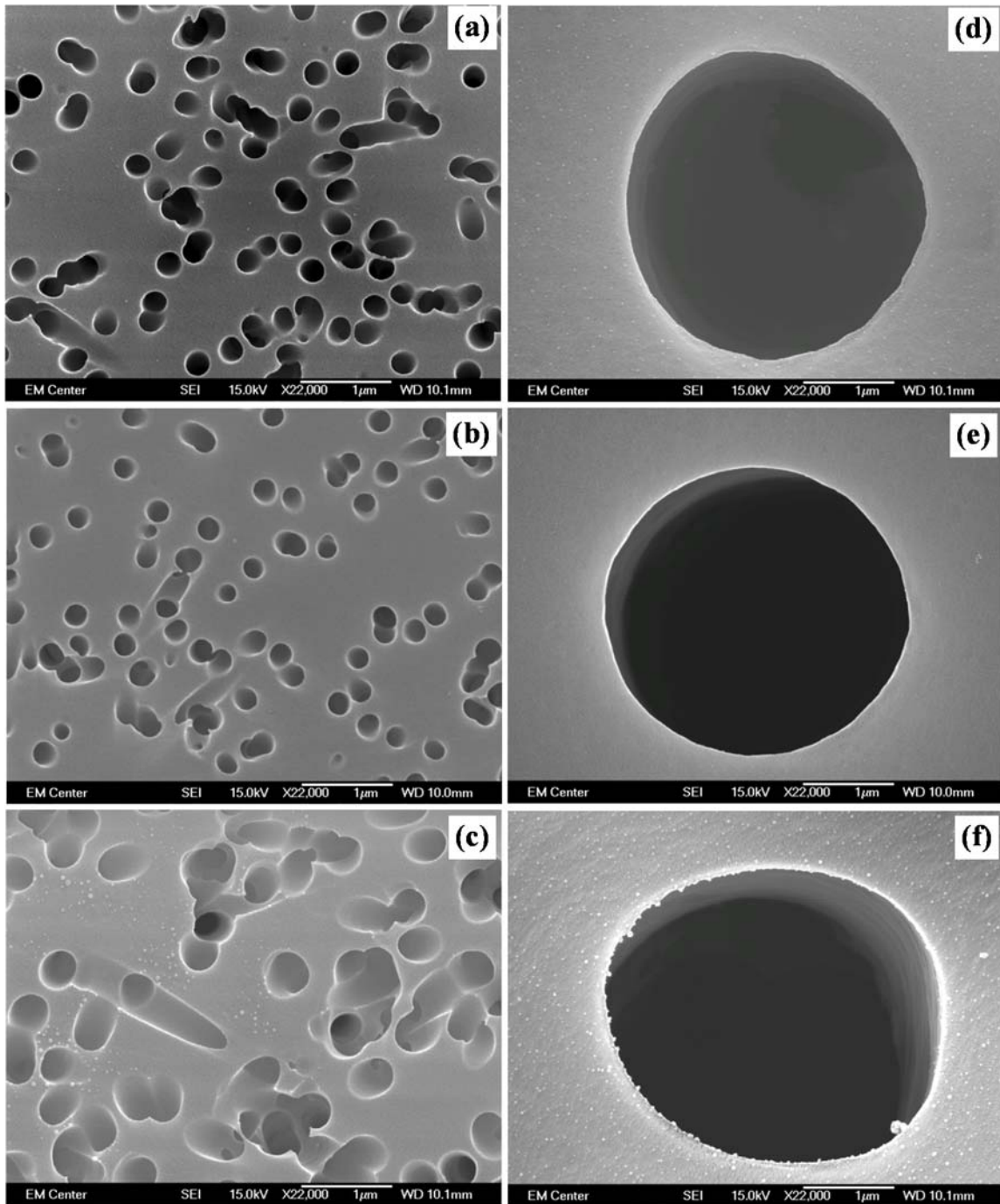


Figure 4.4. SEM images of (a)-(c) 0.2 μm PC-TE and (d)-(f) 3 μm PET-TE treated to determine the effect of plasma treatment parameters on surface morphology. Images in (a) and (d) are membranes treated using $P = 100$ W (50 mTorr, 2 min); (b) and (e) are membranes treated using 350 mTorr reactor pressure (25 W, 2 min); (c) and (f) are membranes treated for 30 min (25 W, 50 mTorr).

Nonetheless, similar to PC-TE, the surface becomes rougher with the formation of distinct 3-dimensional structures, Figures 4.4.b. and 4.4.f.

4.2.3. Wettability and the effect of aging on treated membranes. In previous studies we showed that wettability can vary significantly with time after treatment, and this can be used as a diagnostic tool to evaluate the viability of a plasma treatment.^{15, 17} Here, we examined the effects of aging on H₂O plasma treated 0.2 μm PC-TE modified under standard treatment conditions. wCA measurements were taken within 20 min of treatment for freshly treated samples and after a designated period of time for aging studies. As noted above, the wCA of the upstream side of PC-TE membranes decreases from $97 \pm 3^\circ$ to $38 \pm 2^\circ$ upon H₂O plasma treatment, Table 4.2. Samples exhibit a slight hydrophobic recovery as they age, with the wCA of the upstream side increasing to $55 \pm 1^\circ$ after 1 month, a 17% recovery. Notably, both sides experience comparable wCA changes from the treatment and aging, although the upstream side is slightly more hydrophobic than the downstream side after 1 month. Similar data for PET-TE membranes are listed in Table 4.3. For these materials, the wCA decreases from $59 \pm 9^\circ$ to $27 \pm 4^\circ$ on both sides of the membrane upon treatment. Interestingly, the wCA for the PET-TE membranes does not change appreciably over the 1 month aging period.

4.2.4. Composition of membranes via XPS analysis. For both materials, the significant decrease in the wCA can be largely explained by changes in the surface composition of the membranes resulting from plasma exposure. Indeed, XPS measurements of the surface atomic composition show a significant increase in the oxygen content in freshly treated membranes, Tables 4.2. and 4.3. The O/C of unmodified PC-TE is 0.171, comparable to bisphenol A PC (predicted O/C = 0.188). The difference between the measured and theoretical oxygen to carbon ratio (O/C) is likely the result of adventitious carbon on the membranes. H₂O plasma treatment

Table 4.2. XPS surface composition of untreated, freshly treated and aged 0.2 μm PC-TE.^a

Age	Orientation	CA (°)	Atomic Concentration (%)			High Resolution C _{1s} Moieties (%)				
			Carbon	Oxygen	O/C	C-C/C-H	C-O	C=O	O=C-O	O=C(-O) ₂
Untreated	--	97 ± 3	85.0 ± 0.4	14.6 ± 0.1	0.171 ± 0.001	75.6 ± 1.1	16.9 ± 0.9	--	--	7.6 ± 0.2
Fresh	Upstream	38 ± 2	74.3 ± 1.8	25.7 ± 1.8	0.347 ± 0.033	66.7 ± 1.2	20.4 ± 0.8	3.9 ± 0.4	5.6 ± 0.3	3.4 ± 0.3
	Downstream	35 ± 3	73.9 ± 0.8	26.1 ± 0.8	0.354 ± 0.014	64.0 ± 1.4	21.1 ± 0.6	5.6 ± 0.4	6.7 ± 0.4	2.6 ± 0.1
1 Week	Upstream	47 ± 3	75.3 ± 0.1	24.7 ± 0.1	0.328 ± 0.002	68.0 ± 0.7	20.1 ± 0.9	4.0 ± 0.1	4.5 ± 0.1	3.3 ± 0.2
	Downstream	43 ± 2	74.4 ± 0.1	25.6 ± 0.1	0.343 ± 0.001	67.1 ± 1.7	18.7 ± 2.3	6.6 ± 0.7	4.6 ± 0.1	3.1 ± 0.2 ^b
1 Month	Upstream	55 ± 1	75.9 ± 0.3	24.1 ± 0.3	0.318 ± 0.005	67.3 ± 0.6	20.9 ± 0.4	4.0 ± 0.2	4.6 ± 0.1	3.2 ± 0.1
	Downstream	48 ± 2	77.5 ± 0.7	22.5 ± 0.7	0.290 ± 0.012	69.0 ± 1.3	20.5 ± 0.6	3.3 ± 0.6	4.0 ± 0.2	3.2 ± 0.1

^aUnless otherwise indicated, reported error represents one standard deviation of the mean. ^bReported error is three standard deviations.

Table 4.3. XPS surface composition of untreated, freshly treated and aged 3.0 μm PET-TE.^a

Age	Orientation	CA (°)	Atomic Concentration (%)			High Resolution C _{1s} Moieties (%)				
			Carbon	Oxygen	O/C	C-C/C-H	C-O	C=O	O=C-O	O=C(-O) ₂
Untreated	--	54 ± 9	73.1 ± 0.4	26.9 ± 0.4	0.369 ± 0.008	68.6 ± 0.1	16.9 ± 0.3	--	14.7 ± 0.3	--
Fresh	Upstream	27 ± 4	58.8 ± 0.3	37.4 ± 0.3	0.636 ± 0.008	45.3 ± 0.3	24.2 ± 0.1	7.2 ± 0.3	22.6 ± 0.2	0.7 ± 0.2
	Downstream	25 ± 4	59.3 ± 0.1	37.0 ± 0.2	0.623 ± 0.004	45.8 ± 0.1	24.3 ± 0.3	7.4 ± 0.4	22.0 ± 0.2 ^b	2.6 ± 0.1
1 Week	Upstream	27 ± 6	61.5 ± 0.3	34.9 ± 0.7	0.568 ± 0.017	52.9 ± 1.1	19.0 ± 0.3	10.7 ± 1.2	17.2 ± 0.3	3.3 ± 0.2
	Downstream	27 ± 5	63.9 ± 1.6	33.2 ± 1.3	0.520 ± 0.032	54.5 ± 3.8	20.7 ± 3.0	7.2 ± 1.2	17.4 ± 2.4	3.1 ± 0.3
1 Month	Upstream	25 ± 5	59.4 ± 0.2 ^b	36.4 ± 0.1	0.613 ± 0.002	48.2 ± 0.2	23.2 ± 0.3	7.8 ± 0.3	20.3 ± 0.4	3.2 ± 0.2
	Downstream	25 ± 6	61.6 ± 0.1	35.1 ± 0.1	0.570 ± 0.003	49.7 ± 0.4	24.9 ± 0.8	4.8 ± 0.7	20.3 ± 0.5	3.2 ± 0.1

^aUnless otherwise indicated, reported error represents one standard deviation of the mean. ^bReported error is three standard deviations.

of PC-TE results in a significant increase in O/C. The O/C measured on the upstream side of fresh treated samples increases by 103% to 0.347, Table 4.2. Upon aging, the O/C recovers slightly, decreasing to 0.318 after 1 month. The O/C ratios for both upstream and downstream sides of PC-TE are similar at all times and are consistent with changes in wCA over the aging period, suggesting that the changes in elemental composition (i.e. increasing surface polarity) are responsible. XPS composition measurements on the PET-TE membranes reveal $O/C = 0.369 \pm 0.008$ for untreated membranes, increasing to 0.636 ± 0.008 upon treatment. This is consistent with the decrease in wCA, with the upstream side having a slightly higher O/C compared to the downstream side. Upon aging, the O/C ratio stays relatively constant, although there are some fluctuations between the 1 week and 1 month measurements. Overall, surface oxygen incorporation via plasma treatment explains why the treated PC-TE and PET-TE membranes exhibit improved wettability.

Further analysis of the high resolution C_{1s} spectra from our membranes reveals in detail how oxygen is incorporated into the membrane surface, Figure 4.5., Tables 4.2. and 4.3. Optimized C_{1s} spectral fits were calculated based on the following binding environments: hydrocarbon (C-C/C-H at 285.0 eV), ether/alcohol (C-O at 286.4 eV), carbonyl (C=O at 287.9 eV), acid/ester (O-C=O at 289.6 eV), and carbonate (O=C(-O)₂ at 290.8 eV); the full width at half maximum (FWHM) was constrained to ≤ 1.8 eV; and the peak shape was assumed to be 95:5 Gaussian:Lorentzian. All spectra were fit with a Shirley baseline, except for untreated PC-TE, which required a mixed Shirley/linear baseline. Small shake up satellites were observed in the C_{1s} spectra of some samples from the $\pi \rightarrow \pi^*$ transition (expected for a material containing aromatic functionality); however, this peak area was ignored for the purposes of calculating %

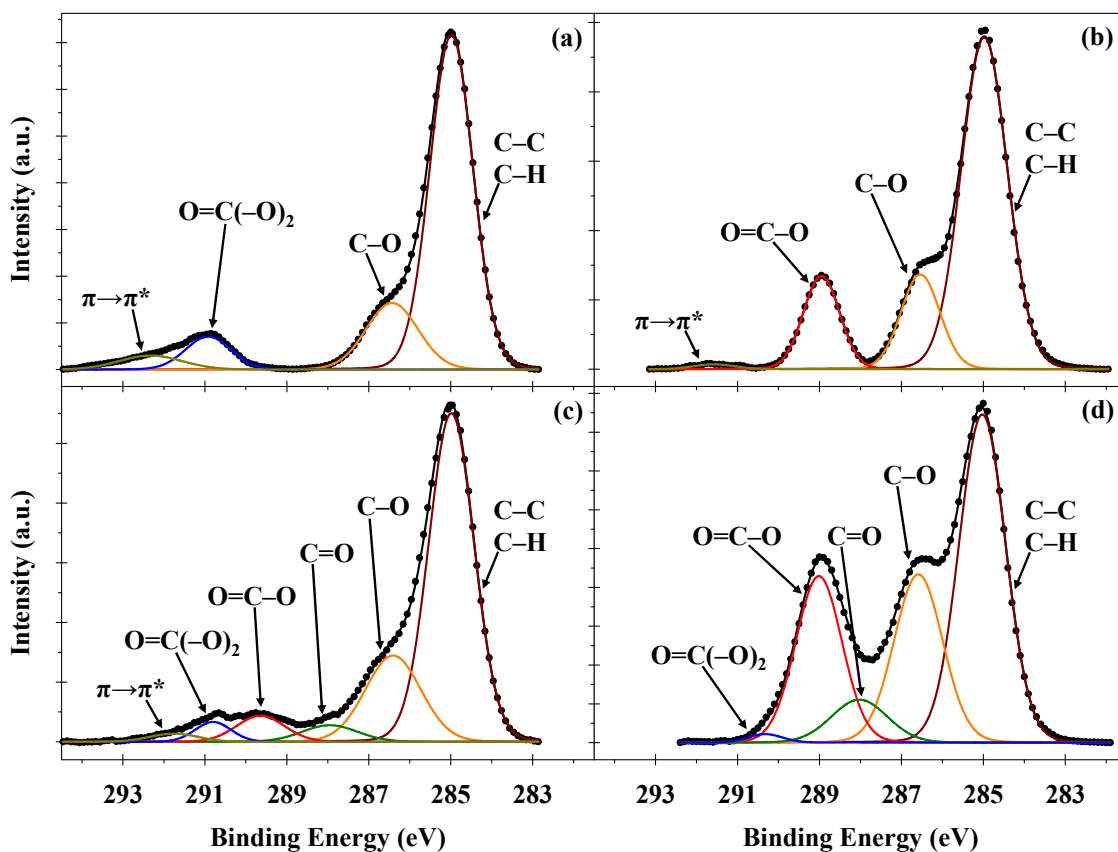


Figure 4.5. High resolution XPS C_{1s} spectra for (a) untreated 0.2 μm PC-TE, (b) untreated 3 μm PET-TE, (c) freshly treated 0.2 μm PC-TE, and (d) freshly treated 3 μm PET-TE. Treated membranes were modified using standard treatment conditions ($P = 25$ W, 50 mTorr, 2 min, and 9 cm downstream).

binding environment contributions. Fits to high resolution O_{1s} spectra, not shown here, support the results from the C_{1s} spectra.

The C_{1s} spectrum of untreated PC-TE is consistent with expected results for PC, Figure 4.5.a. The C-O fraction is slightly elevated from the theoretical value, most likely from atmospheric contamination or slight surface oxidation during membrane fabrication. Upon treatment, all carbon oxidation states are observed including the carbonyl and ester/acid functionalities, Figure 4.5.c. Notably, there is a significant decrease in the contribution of carbonate in the freshly treated surface. We believe this is a result of polymer chain scission around the carbonate functional group during plasma treatment, which would result in conversion (reduction) to ester/acid functionality or complete loss of the carbonate functionality by conversion to volatile products (i.e. CO_2). There is little difference in the C_{1s} binding environment of PC-TE samples as they age through one month, and no significant differences are observed between the upstream and downstream sides, Table 4.2.

A similar analysis of the XPS high resolution C_{1s} spectra from PET-TE samples reveals a slightly different mechanism for oxygen incorporation. Figure 4.5.b. shows the high resolution C_{1s} spectrum of untreated PET-TE fit with three carbon binding environments (C-C/C-H; C-O; and O=C-O) expected for PET materials. Upon treatment, there is a large decrease in the hydrocarbon peak and significant increases in all carbon-oxygen binding environments, Table 4.3. Treated samples show a large peak consistent with the formation of carbonyl functionality and a trace of the carbonate binding environment Figure 4.5.d. The formation of carbonyl groups could be the result of chain scission at the C-O bond of the ester groups in the polymer chain, but is more likely the result of incorporation of oxygen from the plasma at other points in the polymer chain given that the contribution of both carbonyl and acid/ester functionalities

increase with treatment, Table 4.3. Similarly, formation of carbonate likely results from further oxidation of the ester groups. As the samples age, the only change observed is in the trace carbonate. Consistent with wCA measurements, there is very little difference between the upstream and downstream sides of the membrane throughout the aging period.

4.2.5. Stacked membranes. As in our previous studies,^{16, 17} we explored the effectiveness of the plasma in treating the entire pore structure, including pore walls. Here, we examined how treating multiple membranes simultaneously affects the wettability of each membrane within the stack. Stacks of 3, 4, 5, 10, and 15 PC-TE membranes (0.2 μm pore size) were mounted in the same tubular borosilicate glass holder used for the treatment of single membranes, Figure 2.2.a. Each membrane stack was modified using standard treatment conditions and fresh wCAs were measured on the upstream side of each membrane in the stack immediately after treatment. Some treatment effectiveness will be observed on all surfaces in the gaps between membranes in the stack if the active plasma species responsible for the treatment are able to reach that layer. Conversely, if no change in wettability is observed, then it is assumed that the plasma could not negotiate through the pore structure before reacting. Figure 4.6. shows the wCA of the upstream side of each membrane in stacks of 0.2 μm PC-TE membranes as a function of placement within the stack. Regardless of the number of membranes in the stack, the first two membranes display wCAs of 35-38°. The third and fourth membranes in all of the stacks also display relatively low wCAs of ~40-50°. The fifth membrane in a stack of 5 also shows a similar wCA of ~50°, but larger stacks of 10 or 15 membranes show little improvement in wettability over untreated membranes for layers 5-8 or 5-13, respectively, where the wCA is typically ~90°. The last two membranes in stacks of 10 or 15 membranes display significantly decreases in wCA, falling back to ~55° for the last membrane in the stack. The low wCA of the bottom layers in the stacks

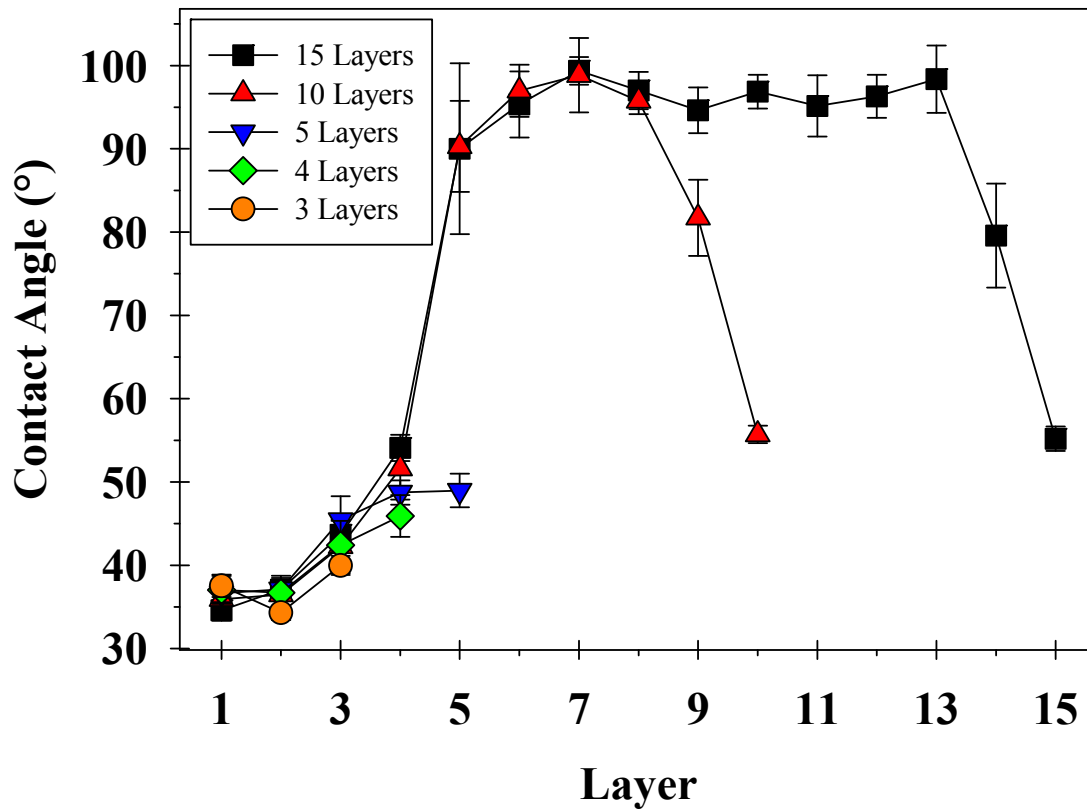


Figure 4.6. wCA data for upstream side of stacked 0.2 μm PC-TE membranes as a function of placement in the stack (e.g. “3” refers to the upstream side of the third membrane in the stack). Contact angles were measured on the upstream side of each membrane in stacks of 3, 4, 5, 10, and 15 layers using standard treatment conditions ($P = 25$ W, 50 mTorr, 2 min, and 9 cm downstream).

demonstrates that the plasma treats the membranes primarily from the upstream side, but also from the downstream side. Regardless, the furthest downstream side of the membrane stack is in contact with active gas species. More importantly, the changes observed through several layers of membranes demonstrates the plasma penetrates the pore structure of the membrane to treat the upstream side of the membrane directly below it in the stack. These results also clearly show there is a limit to the depth to which plasma species are able to penetrate through a porous material such as those used here. Based on the results presented in Figure 4.6., the maximum penetration depth for this system and standard conditions is ~40-50 μm .

4.2.6. Gas-phase diagnostics. TR-OES demonstrates how the relative densities of key gas phase species evolve during the H_2O plasma treatment of membranes. Three types of experiments were run: (1) no membrane; (2) with a membrane and the OES collection port placed immediately upstream of the membrane; and (3) with a membrane and the collection port placed immediately downstream of the membrane. These experiments could not be performed at standard treatment conditions for practical reasons. A reactor pressure of 100 mTorr was used to allow for Ar actinometry and $P = 100 \text{ W}$ was used so that a more intense plasma glow could be obtained on the downstream side of the membrane, making OES on the downstream side possible. The TR-OES spectra were analyzed to examine the relative gas phase densities of selected species as the sample treatment proceeded, Figure 4.7. Relative gas phase densities were extracted from the individual OES spectra by normalizing key spectral lines from species of interest [$\text{O}^*(777.11 \text{ nm})$, $\text{H}\alpha$ (656.22 nm), OH^* (308.87 nm), and CO^* (519.67 nm)] to an Ar emission line (750.31 nm) and normalizing those results against the most intense data point measured in a given time resolved experiment.

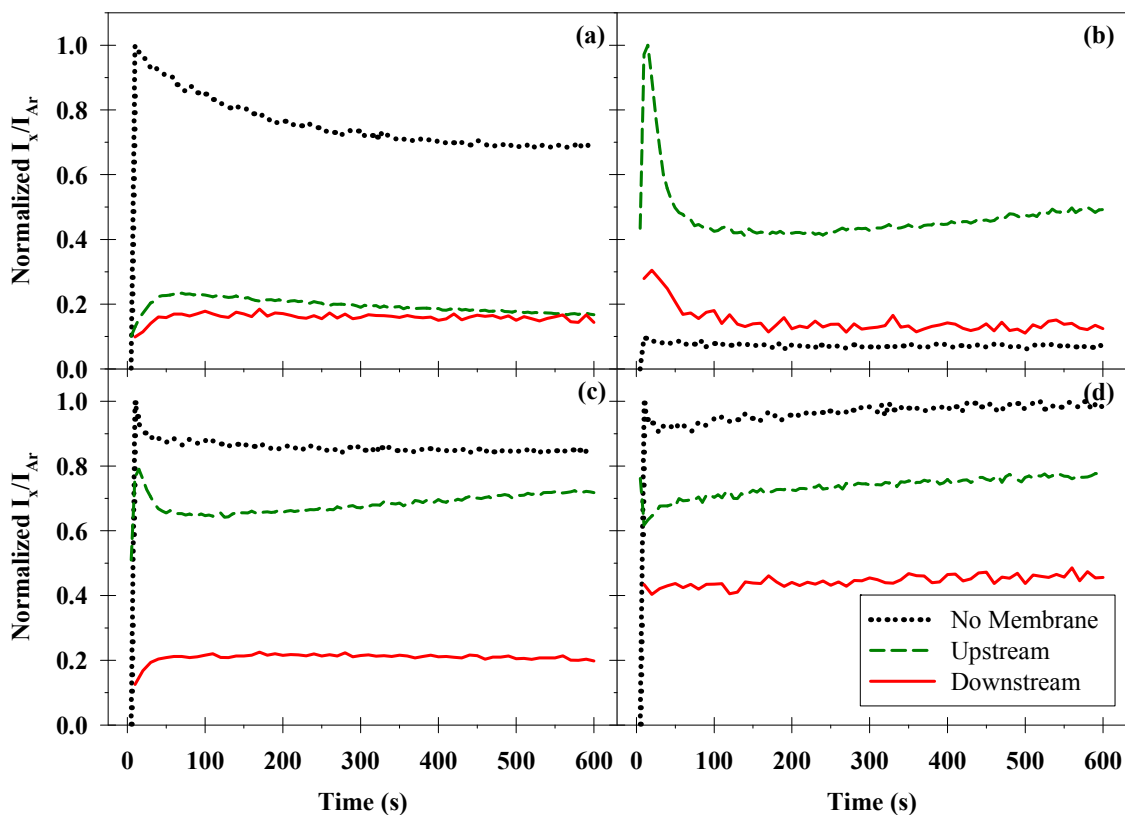


Figure 4.7. Time-resolved actinometric OES data for H₂O plasmas without a membrane (dotted line) as well as taken in H₂O plasmas with a 0.2 μm PC-TE membrane placed 9 cm downstream of the plasma region, both upstream (dashed line) and downstream (solid line) of the membrane. Data shown are for emission from (a) O*, (b) CO*, (c) Hα, and (d) OH*.

Without a membrane in the reactor, O* quickly reaches an initial maximum that slowly decreases until reaching a plateau at 300 s, Figure 4.7.a., whereas H α and OH* reach a constant level within the first 30 s after igniting the plasma, Figures 4.7.c. and 4.7.d. Similar results are observed for all three species on both the upstream and downstream sides of the membrane, albeit at lower intensities. For O*, the signal intensities on the upstream and downstream sides are significantly lower with the membrane in the reactor, but are quite similar to each other over the entire treatment time. Although the intensities of OH* and H α are ~20-30% lower on the upstream side of the membrane (relative to data with no membrane in the reactor), the intensity drops by 60-80% on the downstream side. Figure 4.7.b. shows emission signals from CO* as a function of treatment time. The presence of signal arising from CO* indicates formation of carbon-containing gas-phase species, most likely from etching of the membrane; thus, changes in the gas phase density of CO* can be used to infer how etch rates change during membrane processing. With no membrane in the reactor, the CO* signal is effectively buried in the noise of the spectrum. Notably, signals from CO* emission are measured on both sides of the membrane, with the signal from the upstream side on the membrane peaking very quickly and then falling to a relatively constant level after 100 s. Although at a much lower intensity, similar behavior is seen on the downstream side. Similar experiments were performed under standard treatment conditions without the use of actinometry, with OES collection only on the upstream side of a PC-TE membrane. Although direct comparisons of the gas phase densities between the two experiments are impossible, similar trends in O*, H α , CO*, and OH* signal intensity were observed.

4.2.7. Performance assessment: pure water flux. To determine if plasma treatment negatively affected the internal pore structure, water flux experiments were performed on

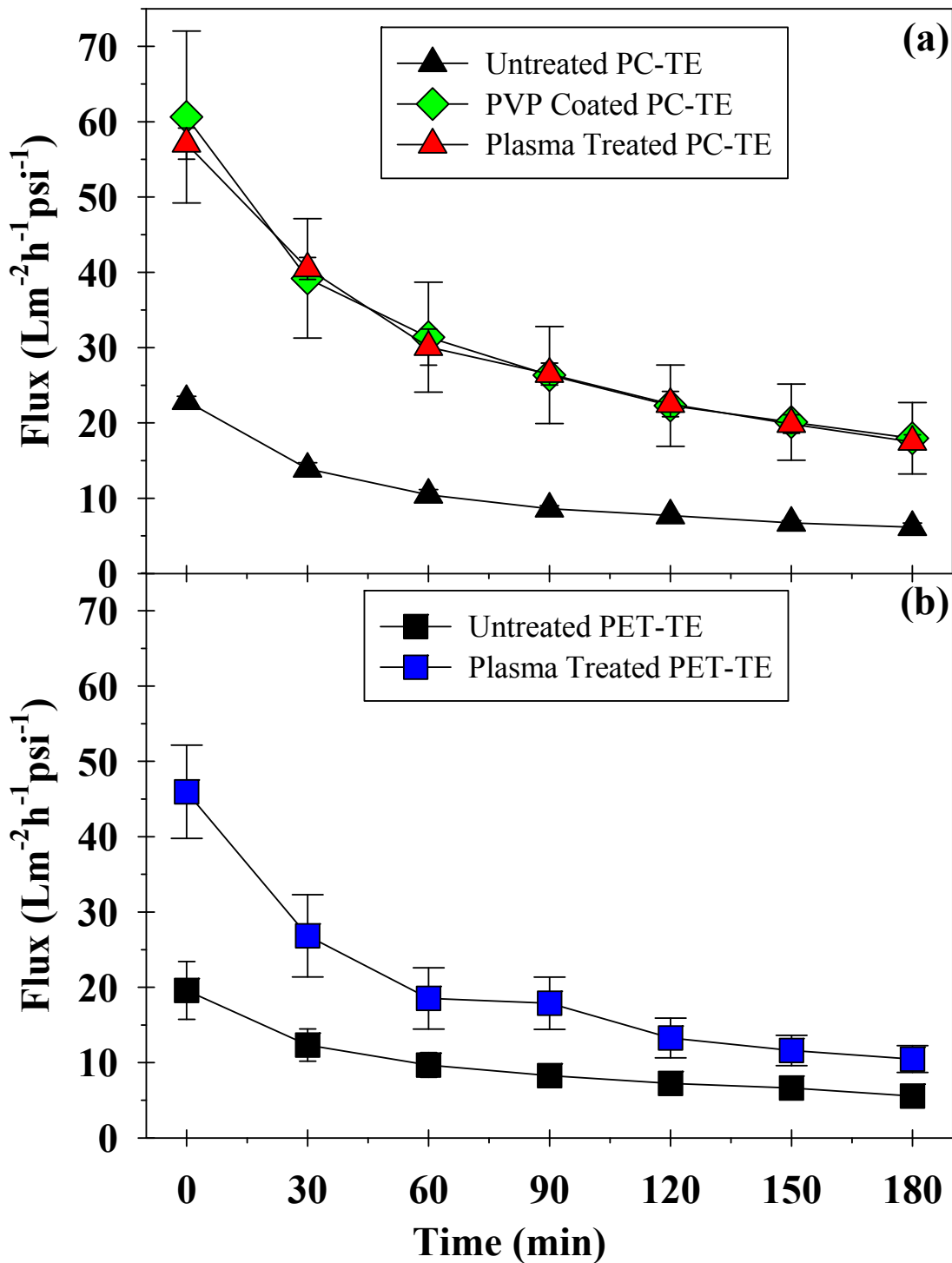


Figure 4.8. Pure water flux through (a) PC-TE and (b) PET-TE treated and untreated 0.2 μm PC-TE membranes. Membranes were treated using the standard treatment conditions ($P = 25$ W, 50 mTorr, 2 min, and 9 cm downstream). Also shown in (a) are results for 0.2 μm PVP-coated PC-TE membranes.

untreated and treated 0.2 μm PC-TE and PET-TE membranes. With all of the membranes, the flux is initially high and then stabilizes at longer times, Figure 4.8., reflecting expansion and settling by the membrane throughout the flux experiment. In addition, the plasma treatment significantly increases the stabilized water flux through the membranes, from ~ 5 to $\sim 18 \text{ Lm}^{-2}\text{h}^{-1}\text{psi}^{-1}$ for PC-TE (Figure 4.8.a.), and from ~ 6 to $\sim 11 \text{ Lm}^{-2}\text{h}^{-1}\text{psi}^{-1}$ for PET-TE (Figure 4.8.b.). Also shown in Figure 4.8.a. are results acquired with PC-TE membranes treated with PVP as a wetting agent. Note that the water flux results for these materials are virtually identical to those obtained for our plasma-treated membranes, suggesting the plasma treatment affords the same wettability advantage of PVP without the accompanying disadvantages of high waste volume and loss of functionality with washing. These water flux results, combined with the SEM results indicating no changes to pore dimensions, clearly indicate our standard plasma treatment does not cause structural damage to the membrane.

4.3. Discussion

4.3.1. Effectiveness and permanence of polar surface functionality. As noted in the introduction, PC-TE and PET-TE membranes are used in many applications where their availability in a wide range of very consistent pore sizes makes them highly desirable, but their hydrophobic surfaces diminish their usefulness in many aqueous-based systems. Thus, methods for permanently altering the surface properties while maintaining the robust nature of the polymer, including the pore size and structure, are extremely desirable. Here, we have demonstrated that our oxidizing H_2O vapor plasma treatments can permanently alter the surface chemistry of track-etched membranes via a chemical change to the surface, without morphological changes.

Our wCA data clearly demonstrate that our H₂O plasma treatment improves wettability on both sides of PC-TE and PET-TE membranes. Additionally, extending our wCA studies to samples aged for up to one month clearly demonstrates the polar surface modifications have a high degree of stability and permanence. Indeed, modified PC-TE experiences only slight hydrophobic recovery whereas modified PET-TE appears completely stable. These findings suggest the formation of volatile LMWOM is minimized during H₂O plasma modification or that formation and loss during the aging period has minimal impact on observed membrane wettability. This is further supported by the water flux measurements wherein we observe reproducible behavior that is significantly higher and remains higher than the untreated membranes over the course of the flux experiment. Had our treatment generated significant quantities of LMWOM, greater irreproducibility and decay of the flux closer to that of the untreated membranes would have been observed. Indeed, the flux behavior of our treated PC-TE membranes is nearly identical to the commercially available hydrophilic PVP-coated membranes, indicating our plasma treatment would be a viable alternative to PVP wetting agents.

One possible explanation for the decreased wCA with plasma modification is that surface etching results in changes in surface roughness compared to the untreated materials. Our SEM results, however, clearly show that changes in surface morphology were not responsible for improved wettability when the standard treatment conditions were used. Although significant changes in pore size and roughness are possible at longer treatment times or with higher *P*, changes in morphology can be ruled out as the cause of improved wettability on samples modified using the more conservative treatment conditions employed here. Thus, the changes

we observe must be primarily the result of chemical changes to the materials, as revealed by XPS data.

4.3.2. Mechanism for surface modification. Here, we propose the mechanism by which oxygen functionalities are implanted into both PC-TE and PET-TE membranes is similar to that proposed previously for H₂O plasma modifications to PSf and PES membranes.^{16, 17, 28} Effectively, we hypothesize that plasma electrons and OH radicals (\bullet OH) are the primary actors in the H₂O plasma surface modification. Initially, plasma activation generates relatively high energy electrons that can produce \bullet OH from the parent H₂O source gas. With both materials, it is generally accepted that in environments where \bullet OH are abundant, -OH groups can be readily implanted at several different locations. For PC, the most likely place for this to occur is the methyl groups, Figure 4.9.a.,²⁹ where the C-H and C-C bond energies are relatively low. For PET, it has been suggested that ring-opening is a viable pathway for oxidation in the presence of H₂O,³⁰ Figure 4.9.b., which is also a plausible process for the PC materials. Note that this mechanism shows initial oxidation occurring via \bullet OH attack at the aromatic carbons. Given the observed decrease in intensity of the π - π^* shakeup satellite band in XPS spectra of both treated membranes, Figures 4.5.c. and 4.5.d., we believe ring opening is occurring to some extent during our treatments. Subsequent oxidation of implanted groups could lead to carboxylic acid groups, consistent with the XPS findings. Continued plasma exposure eventually leads to conversion of these oxidized groups to CO₂ or other volatile species as demonstrated by the etching/surface roughening we observe with long plasma treatment times.

It is also likely that radical oxygen also participates in the modification process via a ring-opening mechanism, Figure 4.10., as proposed by Hicks and coworkers for thermoplastic materials such as PSf.³¹ In this mechanism, atomic oxygen (O \bullet) attacks the aromatic ring

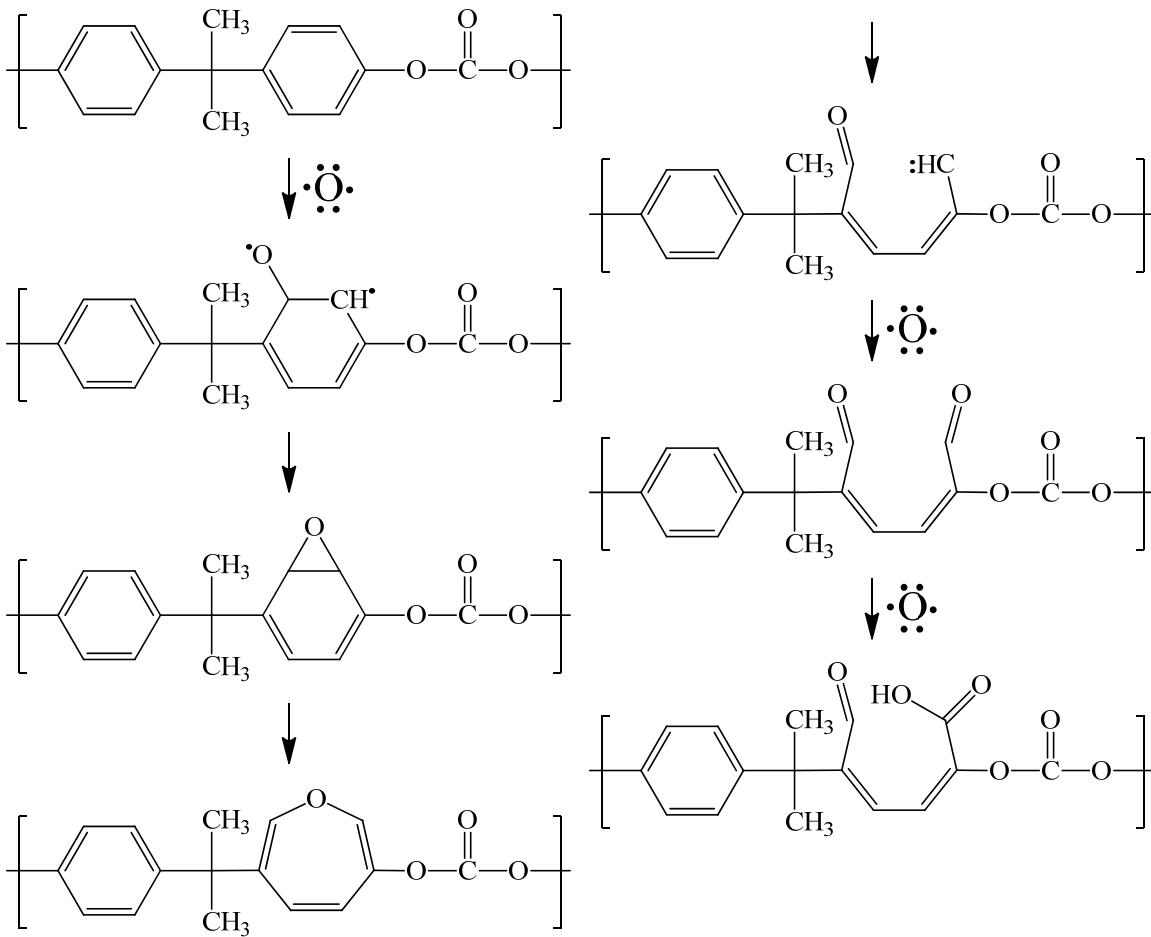


Figure 4.10. Ring opening and functionalization of PC by oxygen radicals.

directly, forms an epoxide, ultimately opening the ring and forming aldehyde groups. Further oxidation leads to formation of carboxylic acid groups and subsequent hydrolysis/alcoholysis would again result in the loss of CO₂. Note that further reactions with the remaining double bonds (i.e. by either electron impact or O•) could cause chain scission and additional oxidation or cross-linking of the polymer. Notably, if the modification process was dominated by reactions with O•, we would anticipate substantial etching of the polymer, but poor functionalization with respect to permanence of treatment.

Additional support for these mechanisms comes from our TR-OES measurements, Figure 4.7. Specifically, significant CO production occurs when a membrane is present in the plasma, with substantial CO* signal on both the upstream and downstream sides of the membrane as well, Figure 4.7.b. In addition, O* is clearly consumed during membrane modification, as we observe ~80% decrease in signal when a PC-TE membrane is placed in the reactor, regardless of the sampling location (i.e. upstream or downstream). Notably there is also a significant, albeit less dramatic, drop in the OH* signal when the membrane is present. These results suggest that indeed both •OH and •O are likely contributing the incorporation of oxygen functionality during H₂O plasma treatment.

4.3.3. Modification of pore surfaces. Assuming the above mechanisms prevail in the H₂O vapor plasma modification of PC-TE and PET-TE membranes, it is also instructive to consider the extent to which reactive plasma species react with pore walls during plasma modification. Our stacked membranes experiments, Figure 4.6., revealed that membranes in the interior of the stack are effectively modified. This suggests reactive species diffuse through the pore structure, thereby exposing the pore walls to the same reactive species as are created in the plasma. Although there is a limit to the distance reactive species can travel in the membrane

stack, the first five membranes have significantly lower wCAs after treatment. The final membrane in the stacks of 10 and 15 also show significantly lower wCAs after treatment, but these changes do not likely result from plasma species penetrating the entire stack, but rather are likely from plasma species that interact with the exposed membrane face at the end of the membrane stack.

Several studies have explored the ability of various plasmas to penetrate through porous media,^{16, 32-35} including previous work in our laboratory with H₂O and NH₃/O₂ plasmas.^{15, 17, 36} In general, it is believed that the plasma itself is not sustained within the pore structures, regardless of the geometry, but rather it is the reactive species that traverse the pores, modifying the interior of the membrane structure. Notably, using a stacked membrane experiment similar to that used here, Johansson and Masuoka³⁵ determined that polymerizing species in their butane plasmas penetrated the entire cross section of PC-TE membranes, but did not completely modify the cross section of polyvinylidene fluoride (PVDF) and nylon membranes. These differences were attributed to differences in pore geometry, namely that the PC-TE membranes did not have a tortuous pore structure whereas the other two membranes did. In contrast, recent work by Intranuovo et al. demonstrated that C₂H₄/N₂ plasmas effectively modified the entire cross section of poly(D,L-lactic acid) scaffolds, suggesting polymerizing species easily traversed the tortuous pore structure of these materials.³³ Note that the pore sizes in the latter case were ~250 μm in diameter (4 mm thick), whereas the PC-TE membranes had 0.2 μm pores and were only 10 μm thick. Using similar polycaprolactone scaffolds, Jacobs et al. also found that plasma species formed in atmospheric dry air plasmas easily modified the entire pore structure, resulting in completely wettable surfaces after a 2 min treatment.³⁴

All of these studies compare favorably with the previous results from our laboratory as well as those presented here and suggest our mechanisms for modification that include $\bullet\text{OH}$ and $\bullet\text{O}$ radicals are plausible. Additional direct evidence for the ability of $\bullet\text{OH}$ to traverse the membrane cross section within a pore comes from our imaging of radicals interacting with surfaces (IRIS) studies which examine the surface reactivity of plasma species during surface modification. We found that $\sim 50\%$ of the $\bullet\text{OH}$ scattered from the surface of PSf, PE, PES, and PTFE membranes, regardless of membrane type or pore geometry.²⁸ As IRIS experiments do not follow individual species, but rather measure the collective contributions of multiple reactions, it is plausible that reactions such as hydrogen abstraction by surface interactions of $\bullet\text{O}$, recombination of adsorbed OH and H, and/or dissociative adsorption of H_2O , followed by desorption of OH, and recombination of adsorbed OH and H atoms, could all contribute to the observed OH scatter. Regardless of the specific molecular-level reaction occurring, all of this suggests that reactive species could easily propagate through the pores of the membranes.

4.3.4. Membrane performance. The water flux data shown in Figure 4.6. suggest H_2O plasma treatments enhance water flux through track-etched membranes. As has been discussed in the literature, permeate flux increases can be correlated to a range of physical and chemical changes in the membrane surface, including surface charge, hydrophilicity, roughness, and pore size.³⁷⁻³⁹ The SEM results in Figure 4.3., however, clearly show little to no change in pore dimensions or surface roughness under standard treatment conditions. Thus, it is likely the increased hydrophilicity imparted by implanted oxygen functionality that is the underlying cause of the increased water flux. Interestingly, Kim et al. attribute increases in pure water flux for their NH_3 plasma-modified thin-film composite membranes to increased hydrophilicity.³⁷ wCAs for their membranes decreased by 36-79%, with the largest changes occurring at longer treatment

times (10 min) and high powers (90 W). They suggested that increased hydrogen bonding between water and the surface of the modified pore walls increases permeability of water through the membrane via both dissolution and diffusion. Interestingly, the highest flux performance did not directly correlate with the most wettable membranes. They found flux declined at higher treatment powers and attributed this to increased cross-linking at the membrane surface. Because the amount of plasma-induced cross-linking varies between different polymers, membrane material is an important factor in overall performance of plasma treated membranes.

Here, we found that robust polar surface modification of both PC-TE and PET-TE membranes is possible using our H₂O plasma treatments. There are, however, notable differences in the way each polymer responds to the modification. These modifications appear to result from the difference between the carbonate and ester functionalities of the polymers, and not the physical structure of the membranes, as the latter is largely the same for the two membranes. As noted above, PC is especially susceptible to hydrolysis in aqueous environments and hydrolysis produces CO₂.^{20, 23, 29, 31} The TR-OES data in Figure 4.7. clearly demonstrate carbon-containing gases are formed via the interaction of the H₂O plasma with PC-TE membranes, most likely including CO₂, although this is not explicitly monitored with OES. Moreover, the concentration and type of oxygen-containing moieties in the polymers, both before and after treatment are likely contributing factors. Specifically, XPS elemental composition data shows ~15% and ~27% oxygen in the native materials. Upon plasma treatment, those numbers each rise by ~10%, suggesting similar treatments for the two materials. Examination of the high resolution C_{1s} data, however, shows that ~31% of the carbon in native PET is bound to at least one oxygen, whereas only ~24% of the carbon in native PC is in an

oxygenated environment. Upon H₂O plasma treatment, the oxygenated carbon content of both membranes increases, but that for PC only increases by ~10%, whereas that for PET increases by more than 30%. Moreover, the carbon in the treated PET-TE membranes appears to be in a much more oxidized environment, potentially thereby resisting additional changes in polymer structure upon aging.

4.4. Summary

Overall, the results reported here are consistent with our past studies of H₂O vapor plasma treatments of PES and PSf. Wettability is greatly improved with very little change to surface morphology and limited hydrophobic recovery is observed upon aging. The increased wettability can be attributed to an increase in the oxygen content of the surface of the membranes, and not to changes in the surface morphology. Water flux studies showed that the standard treatment conditions did not result in negative changes to pore structure, whereas the stacked membrane studies demonstrated the entire surface area of the membrane, including pore walls was effectively modified by our treatment. Thus, observed increases in water flux are attributable to the chemical changes made to the membrane surfaces and pore walls. Further support for this hypothesis comes from the penetration depth study, which demonstrated that the plasma penetrates from both the upstream and downstream directions indicating that the plasma treats the entire cross section of the pores. Collectively, the results presented here demonstrate that H₂O plasmas are extremely effective at permanently modifying a range of polymer structures, most likely via implantation of oxygen functionalities initiated by electron impact, •OH insertion and/or •O oxidation accompanied by ring-opening in the polymer backbone.

REFERENCES

1. Tompkins, B. D.; Dennison, J. M.; Fisher, E. R., H₂O plasma modification of track-etched polymer membranes for increased wettability and improved performance. *J. Membr. Sci.* **2013**, 428, 576-588.
2. Chang, S., Application of submerged hollow fiber membrane in membrane bioreactors: Filtration principles, operation, and membrane fouling. *Desalination* **2011**, 283, 31-39.
3. De Bartolo, L.; Morelli, S.; Bader, A.; Drioli, E., Evaluation of cell behaviour related to physico-chemical properties of polymeric membranes to be used in bioartificial organs. *Biomaterials* **2002**, 23, (12), 2485-2497.
4. Li, J.; Chase, H. A., Applications of membrane techniques for purification of natural products. *Biotechnol. Lett* **2010**, 32, (5), 601-608.
5. Shi, X.; Field, R.; Hankins, N., Review of fouling by mixed feeds in membrane filtration applied to water purification. *Desalin. Water Treat.* **2011**, 35, (1-3), 68-81.
6. Zhang, M. M.; Li, C.; Benjamin, M. M.; Chang, Y. J., Fouling and natural organic matter removal in adsorben/membrane systems for drinking water treatment. *Environ. Sci. Technol.* **2003**, 37, (8), 1663-1669.
7. Ahmad, A. L.; Majid, M. A.; Ooi, B. S., Functionalized PSf/SiO₂ nanocomposite membrane for oil-in-water emulsion separation. *Desalination* **2011**, 268, (1-3), 266-269.
8. Koo, C. H.; Mohammad, A. W.; Suja, F.; Talib, M. Z. M., Review of the effect of selected physicochemical factors on membrane fouling propensity based on fouling indices. *Desalination* **2012**, 287, 167-177.
9. Pandey, S. R.; Jegatheesan, V.; Baskaran, K.; Shu, L., Fouling in reverse osmosis (RO) membrane in water recovery from secondary effluent: a review. *Rev. Environ. Sci. Biotechnol.* **2012**, 11, (2), 125-145.
10. Xu, W. D.; Chellam, S., Initial stages of bacterial fouling during dead-end microfiltration. *Environ. Sci. Technol.* **2005**, 39, (17), 6470-6476.
11. Choi, K. Y. J.; Dempsey, B. A., In-line coagulation with low-pressure membrane filtration. *Water Res.* **2004**, 38, (19), 4271-4281.
12. Qin, J. J.; Cao, Y. M.; Oo, M. H., Preparation of poly(ether sulfone) hollow fiber UF membrane for removal of NOM. *J. Appl. Polym. Sci.* **2006**, 99, (1), 430-435.
13. Shi, Q.; Su, Y. L.; Zhu, S. P.; Li, C.; Zhao, Y. Y.; Jiang, Z. Y., A facile method for synthesis of pegylated polyethersulfone and its application in fabrication of antifouling ultrafiltration membrane. *J. Membr. Sci.* **2007**, 303, (1-2), 204-212.

14. Sotto, A.; Boromand, A.; Zhang, R.; Luis, P.; Arsuaga, J. M.; Kim, J.; Van der Bruggen, B., Effect of nanoparticle aggregation at low concentrations of TiO₂ on the hydrophilicity, morphology, and fouling resistance of PES-TiO₂ membranes. *J. Colloid Interface Sci.* **2011**, 363, (2), 540-550.
15. Kull, K. R.; Steen, M. L.; Fisher, E. R., Surface modification with nitrogen-containing plasmas to produce hydrophilic, low-fouling membranes. *J. Membr. Sci.* **2005**, 246, (2), 203-215.
16. Steen, M. L.; Hymas, L.; Havey, E. D.; Capps, N. E.; Castner, D. G.; Fisher, E. R., Low temperature plasma treatment of asymmetric polysulfone membranes for permanent hydrophilic surface modification. *J. Membr. Sci.* **2001**, 188, (1), 97-114.
17. Steen, M. L.; Jordan, A. C.; Fisher, E. R., Hydrophilic modification of polymeric membranes by low temperature H₂O plasma treatment. *J. Membr. Sci.* **2002**, 204, (1-2), 341-357.
18. Baytekin, H. T.; Wirth, T.; Gross, T.; Treu, D.; Sahre, M.; Theisen, J.; Schmidt, M.; Unger, W. E. S., Determination of wettability of surface-modified hot-embossed polycarbonate wafers used in microfluidic device fabrication via XPS and ToF-SIMS. *Surf. Interface Anal.* **2008**, 40, (3-4), 358-363.
19. Grace, J. M.; Gerenser, L. J., Plasma treatment of polymers. *J. Dispersion Sci. Technol.* **2003**, 24, (3-4), 305-341.
20. Kitova, S.; Minchev, M.; Danev, G., RF plasma treatment of polycarbonate substrates. *J. Optoelectron. Adv. Mater.* **2005**, 7, (5), 2607-2612.
21. Lazea, A.; Kravets, L. I.; Albu, B.; Ghica, C.; Dinescu, G., Modification of polyester track membranes by plasma treatments. *Surf. Coat. Technol.* **2005**, 200, (1-4), 529-533.
22. Li, N. C.; Yu, S. F.; Harrell, C. C.; Martin, C. R., Conical nanopore membranes. Preparation and transport properties. *Anal. Chem.* **2004**, 76, (7), 2025-2030.
23. Muir, B. W.; McArthur, S. L.; Thissen, H.; Simon, G. P.; Griesser, H. J.; Castner, D. G., Effects of oxygen plasma treatment on the surface of bisphenol A polycarbonate: a study using SIMS, principal component analysis, ellipsometry, XPS and AFM nanoindentation. *Surf. Interface Anal.* **2006**, 38, (8), 1186-1197.
24. Orhan, M.; Kut, D.; Gunesoglu, C., Improving the antibacterial property of polyethylene terephthalate by cold plasma treatment. *Plasma Chem. Plasma Process.* **2012**, 32, (2), 293-304.
25. Sartowska, B.; Buczkowski, M.; Starosta, W., SEM observations of particle track membrane surfaces modified using plasma treatment. *Mater. Chem. Phys.* **2003**, 81, (2-3), 352-355.

26. Toufik, M.; Mas, A.; Shkinev, V.; Nechaev, A.; Elharfi, A.; Schue, F., Improvement of performances of PET track membranes by plasma treatment. *Eur. Polym. J.* **2002**, 38, (2), 203-209.
27. Kang, M. S.; Chun, B.; Kim, S. S., Surface modification of polypropylene membrane by low-temperature plasma treatment. *J. Appl. Polym. Sci.* **2001**, 81, (6), 1555-1566.
28. Steen, M. L.; Butoi, C. I.; Fisher, E. R., Identification of gas-phase reactive species and chemical mechanisms occurring at plasma-polymer surface interfaces. *Langmuir* **2001**, 17, (26), 8156-8166.
29. Jang, B. N.; Wilkie, C. A., The thermal degradation of bisphenol A polycarbonate in air. *Thermochim. Acta* **2005**, 426, (1-2), 73-84.
30. Rodriguez-Santiago, V.; Bujanda, A. A.; Stein, B. E.; Pappas, D. D., Atmospheric plasma processing of polymers in helium-water vapor dielectric barrier discharges. *Plasma Processes Polym.* **2011**, 8, (7), 631-639.
31. Gonzalez, E., II; Barankin, M. D.; Guschl, P. C.; Hicks, R. F., Ring opening of aromatic polymers by remote atmospheric-pressure plasma. *IEEE Trans. Plasma Sci.* **2009**, 37, (6), 823-831.
32. Bergemann, C.; Quade, A.; Kunz, F.; Ofe, S.; Klinkenberg, E.-D.; Laue, M.; Schroeder, K.; Weissmann, V.; Hansmann, H.; Weltmann, K.-D.; Nebe, B., Ammonia plasma functionalized polycarbonate surfaces improve cell migration inside an artificial 3D cell culture module. *Plasma Processes Polym.* **2012**, 9, (3), 261-272.
33. Intranuovo, F.; Howard, D.; White, L. J.; Johal, R. K.; Ghaemmaghami, A. M.; Favia, P.; Howdle, S. M.; Shakesheff, K. M.; Alexander, M. R., Uniform cell colonization of porous 3-D scaffolds achieved using radial control of surface chemistry. *Acta Biomater.* **2011**, 7, (9), 3336-3344.
34. Jacobs, T.; Morent, R.; De Geyter, N.; Desmet, T.; Dubruel, P.; Leys, C., Visualization of the penetration depth of plasma in three-dimensional porous PCL scaffolds. *IEEE Trans. Plasma Sci.* **2011**, 39, (11), 2792-2793.
35. Johansson, J.; Masuoka, T., Penetration of pores in membranes by plasma polymer forming species. *Macromol. Rapid Commun.* **1999**, 20, (1), 12-15.
36. Steen, M. L.; Flory, W. C.; Capps, N. E.; Fisher, E. R., Plasma modification of porous structures for formation of composite materials. *Chem. Mater.* **2001**, 13, (9), 2749-2752.
37. Kim, E.-S.; Yu, Q.; Deng, B., Plasma surface modification of nanofiltration (NF) thin-film composite (TFC) membranes to improve anti organic fouling. *Appl. Surf. Sci.* **2011**, 257, (23), 9863-9871.
38. Tang, C. Y.; Kwon, Y.-N.; Leckie, J. O., Effect of membrane chemistry and coating layer on physiochemical properties of thin film composite polyamide RO and NF membranes I.

FTIR and XPS characterization of polyamide and coating layer chemistry. *Desalination* **2009**, 242, (1-3), 149-167.

39. Tang, C. Y.; Kwon, Y.-N.; Leckie, J. O., Effect of membrane chemistry and coating layer on physiochemical properties of thin film composite polyamide RO and NF membranes II. Membrane physiochemical properties and their dependence on polyamide and coating layers. *Desalination* **2009**, 242, (1-3), 168-182.

CHAPTER 5

ETCHING AND POST-TREATMENT SURFACE STABILITY OF TRACK-ETCHED POLYCARBONATE MEMBRANES BY PLASMA PROCESSING USING VARIOUS RELATED OXIDIZING PLASMA SYSTEMS

This chapter is based on manuscript, written by Brendan D. Tompkins, Jordan M. Dennison, and Ellen R. Fisher, that has been accepted for publication by the journal *Plasma Processes and Polymers*.¹ The text, figures, and tables from this publication are reproduced here with permission from John Wiley & Sons (License Number: 3415481125283, June 24th, 2014). The research contained in this chapter builds on the work described in Chapter 4. Etching of polycarbonate materials during plasma processing is investigated by comparing treatments on track-etched polycarbonate membranes using four related oxidizing plasma systems, namely O₂, CO₂, H₂O vapor, and HCOOH vapor. Surface analysis methods are used to examine treatment effectiveness and stability of the modified material. Pore size measurements are correlated with gas-phase diagnostics to identify the species that contribute to etching in each of the related plasma systems. Funding for this research was provided by the National Science Foundation (CHE-1152963).

5.1. Introduction

Polycarbonate (PC) is an important thermoplastic material that finds many uses, including in optical,^{2,3} biomedical,^{4,5} patterned microarray assay,⁶ and microfluidic devices.⁷⁻⁹ PC is generally rigid, optically clear, and has good chemical and thermal stability. The surface properties of PC, however, are less desirable for many of these applications. Its low surface

energy often prevents wetting and interferes with adhesion to PC. Surface modification using reactive plasmas has become a popular method for solving these issues. Indeed, low-temperature plasmas are known for their ability to modify the surface of a material without influencing the bulk properties. For example, plasma modification has been used to alter the surface properties of PC for improved blood compatibility,¹⁰ increased adhesion,¹¹⁻¹⁴ decreased surface wear,¹⁵ and increased wettability.¹⁶

The use of O₂ plasma to modify PC has received the most attention owing to its ability to simultaneously implant new polar functionality and etch PC surfaces. The desirability of this dual role depends on the goal of the plasma processing. A number of researchers have used O₂ plasma etching to change the dimensions of PC membranes¹⁷ or develop textures on solid PC substrates.^{18, 19} Indeed, O₂ plasma is very effective in this role. The use of O₂ plasma to implant new functionalities on PC surfaces can, however, lead to undesirable complications. Many researchers have noted that O₂ plasma-modified PC surfaces are unstable, exhibiting significant hydrophobic recovery after treatment.²⁰⁻²² Muir, et al. attributed this to chain scission and the formation of low molecular weight fragments.²³ A similar study reported by Greenwood et al. found that those loosely bound fragments are easily washed away,²⁴ exacerbating the loss of treatment effectiveness when modified PC materials are used in aqueous environments. Larsson and Dérand found that PC surfaces treated in high intensity O₂ plasmas (applied rf power (P) = 400-600 W) remained hydrophilic after rinsing, but significant surface roughening accompanied the treatment.²¹ Clearly, the surface modification of PC materials requires a more subtle approach. Balancing surface modification against unwanted etching requires a greater understanding of the processes taking place at the PC surface.

Previous work in our laboratory demonstrated that OH radicals generated in H₂O and NH₃/O₂ plasmas contribute to the implantation of new polar functionalities onto polymer surfaces modified using those plasma systems.²⁵⁻²⁷ Indeed, polyethersulfone (PES) and polysulfone (PSf) membranes modified in these plasma systems were rendered completely wetting and the surface modification was permanent (lasting from months to years). These plasma systems also had the capacity to damage the PES and PSf, especially with higher *P*.¹⁷ At that time it was reasoned that higher *P* results in more energetic gas-phase species, resulting in enough energy to efficiently break the bonds holding the polymer chain together (scission), leading to damage by way of etching the polymer. Higher *P* generally leads to both increased internal energy of gas phase species and more fragmentation of the precursor gas.²⁸ Certainly, the internal energy of gas-phase species in the plasma is an important factor in polymer etch rate and damage. Not all reactive species follow the same reaction pathway, however; therefore, the densities of different gas-phase species are also relevant to this discussion.

More recent work in our laboratory investigated the effects of H₂O plasma on track-etched PC membranes (PC-TE).¹⁶ Similar to our earlier studies on PSf and PES, we found that a short treatment (i.e. 2 min) using a low *P* H₂O plasma gave a significant net increase in the wettability of PC-TE, and only moderate hydrophobic recovery was observed over a one month aging period. We also found, however, that the same plasma conditions (specifically *P* and pressure) etched the PC material when longer treatment times were used. We hypothesized that the atomic oxygen generated in these oxidizing plasma systems was capable of inserting itself into the phenyl groups, leading to ring opening and, ultimately, polymer chain scission. This hypothesis is supported by a similar study performed on PES,²⁹ a NEXAFS study of PC exposed to a DC O₂ plasma,³⁰ and other literature accounts of O₂ plasma etching of PC.^{17, 19} Moreover, a

high degree of PC chain scission would explain the instability of the PC surface following O₂ plasma processing. Thus, we further hypothesize that manipulating the gas-phase density of atomic oxygen may yield better surface modification outcomes.

Here, we compare O₂, CO₂, H₂O, and formic acid (HCOOH) plasma systems for PC surface modification using one of our home-built inductively coupled rf plasma reactors. PC-TE is the model PC material used in this study. The primary goal is to relate the etch rate and surface functionalization of PC to the gas-phase chemistry in each plasma system. Etch rate is determined using scanning electron microscopy (SEM) to measure the change in pore radius of PC-TE, taking advantage of the narrow pore size distribution of PC-TE. The implantation of functional groups is verified using x-ray photoelectron spectroscopy (XPS) to measure the composition of the surface and water contact angle (wCA) to measure changes in surface wettability. These results are compared to the identity and relative density of key radical species from optical emission spectroscopy (OES) data to elucidate which species are primarily responsible for etching and surface modification.

5.2. Results

5.2.1. Plasma etching of PC-TE and etch rate measurements. Untreated PC-TE generally has smooth outer surfaces with regular, cylindrical pores. SEM images from untreated PC-TE show that *Side A* is slightly more pitted with a clear grain/directionality, Figure 5.1.a., compared to the expected morphology exhibited by *Side B*, Figure 5.1.b. We suspect this sidedness starts at some point during the fabrication process and results in some variation between lots. Indeed, the rough morphology of *Side A* corresponds to a dull appearance compared to *Side B*, a distinction noted by the manufacturer. The pitting on *Side A* overlaps with many of the pore

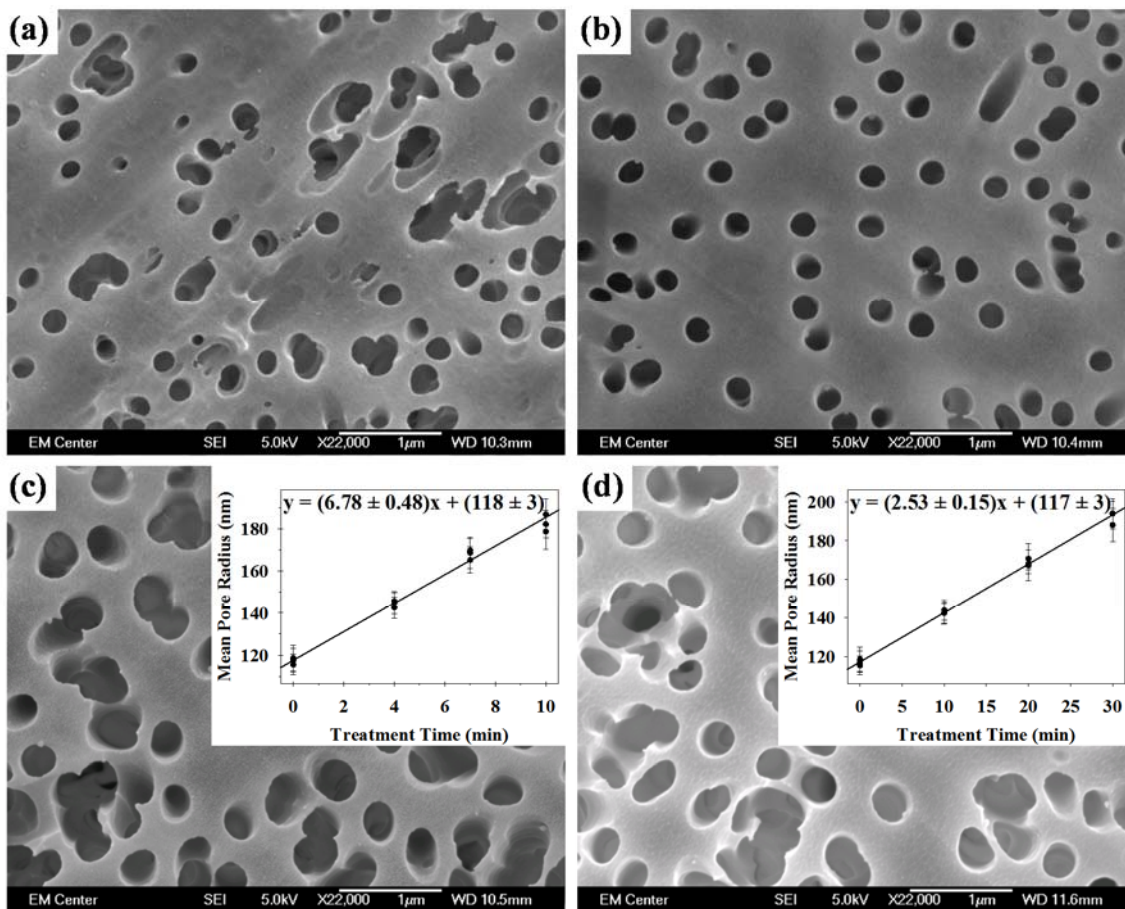


Figure 5.1. SEM images of (a) untreated PC-TE *Side A*, and (b) untreated PC-TE *Side B*, as well as the (c) upstream and (d) downstream sides of PC-TE following 10 and 30 min of O₂ plasma processing, respectively. Linear regression analyses of pore radius as a function of O₂ plasma treatment time are also shown (insets).

openings, an issue further exacerbated by plasma processing, making it difficult to identify the regular cylindrical pores needed for the pore measurement technique used here. *Side B*, however, exhibits the smooth surface and regular cylindrical pores expected with PC-TE and noted in our previous study of these materials.¹⁶ Pore measurements made using the series of SEM images from *Side B* show the weighted mean radius of as-received membranes is 117 ± 1 nm. This result is consistent with pore measurements made on the lot reported in our previous study and with the manufacturer's specification. Given the well-defined pores on *Side B*, we restricted the rest of our PC-TE morphology and etch rate investigations to *Side B*.

Oxidizing plasmas such as those studied here (e.g. O₂, CO₂, H₂O, and HCOOH) etch PC materials under certain plasma processing conditions. Notable among these systems is a 100% O₂ plasma, known to be effective for etching^{17-19, 23} and modifying PC.^{8, 14, 18, 20-23, 31} Although polymer etching and surface modification using O₂ plasmas have been thoroughly examined within the literature, select results obtained using our reactor system will be presented here for comparison. Figure 5.1.c. and Figure 5.1.d. shows representative images from upstream and downstream sides of PC-TE following O₂ plasma exposure. Measurements reveal that the pore openings at the surface of the upstream facing side grow successively larger as the treatment time is increased and this growth is linear with respect to treatment time, Figure 5.1.c. (inset). Over a 4-10 min time range including the untreated pore radius as $t = 0$, the etch rate was calculated to be 6.78 ± 0.48 nm/min. Lower etch rates are observed when *Side B* is the downstream facing side (2.53 ± 0.15 nm/min). Despite these substantial etch rates, there is still very little change in surface texture on the scale of our SEM analysis for either side of the membrane.

Processing of PC-TE using H₂O, CO₂, or HCOOH plasmas results in similar changes to the surface and pore structure, Figure 5.2. As with the O₂ system, there are minimal changes to morphology on the upstream and downstream sides following shorter treatment times (<30 min). The upstream sides of samples modified using H₂O or HCOOH plasmas for 30 min, however, develop a texture comprising raised nodules, Figures 5.2.c. and 5.2.e., which become more pronounced with treatment times > 30 min. For each of these plasma systems, the pores appear to grow in a linear fashion, but calculated etch rates are significantly slower than those in the O₂ system, Figure 5.2. (insets). Notably, H₂O and CO₂ have similar, moderate etch rates on the upstream side (3.10 ± 0.20 and 2.90 ± 0.23 nm, respectively) and, like the O₂ plasma system, etching on the downstream side is significantly slower. The HCOOH plasma system has the slowest etch rate on both upstream and downstream sides of PC-TE (1.74 ± 0.16 and 0.47 ± 0.10 nm, respectively). This is a somewhat surprising result, given the texture formation observed with HCOOH plasma modification, and is discussed further in Section 5.3.3.

5.2.2. Etched PC-TE surface analysis. Etching is but one of the changes that occurs at the polymer plasma interface during plasma processing. Oxidizing plasmas, such as those examined in this study, are known to implant new functionality on polymer surfaces. Here, changes in elemental composition (e.g. increased oxygen content) and the introduction of new functionalities are identified using XPS. In our previous study, we found that oxygen content increases by >10% following H₂O plasma processing, Table 5.1.¹⁶ This can be attributed to reactions with H₂O_(g) and oxygen containing species generated from H₂O in the plasma. XPS measurements of PC-TE freshly treated using O₂, CO₂, and HCOOH plasma reveal similar increases in oxygen content. As might be expected, the largest measured increase occurs with samples treated using O₂ plasmas, where O/C increases from 0.171 ± 0.001 to 0.462 ± 0.003 and

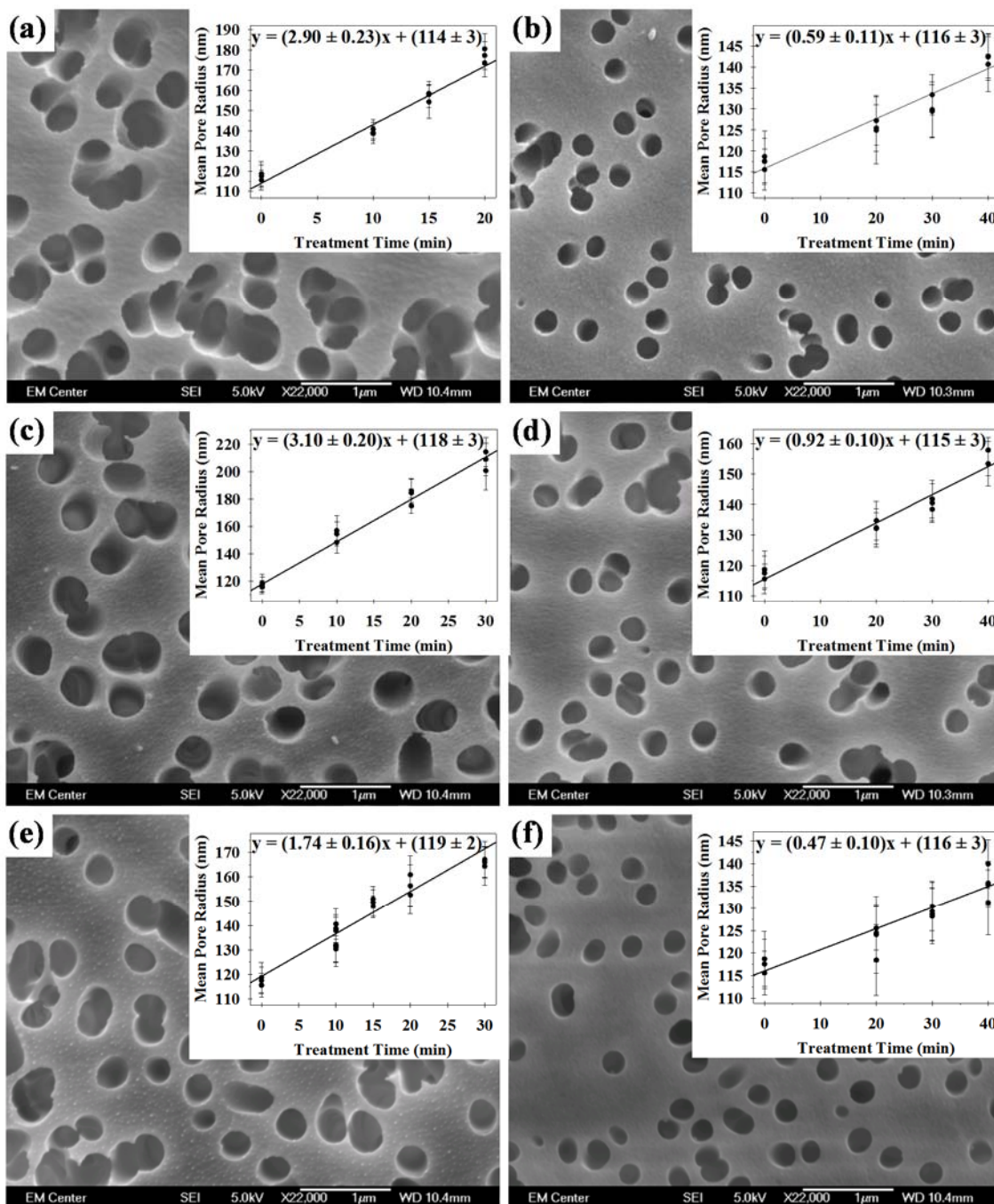


Figure 5.2. SEM images of upstream (left) and downstream (right) sides of PC-TE after (a-b) CO₂, (c-d) H₂O, and (e-f) HCOOH plasma processing (30 min, $P = 25$ W, 50 mTorr, 9 cm downstream). Linear regression analyses of pore radius as a function of treatment time are also shown (insets).

Table 5.1. wCA and surface atomic composition of PC-TE following plasma processing.

Precursor	Orientation	wCA (°)	Atomic Concentration (%) ^a		
			Carbon	Oxygen	O/C
Untreated ^b	--	97 ± 3	85.0 ± 0.1	14.6 ± 0.1	0.171 ± 0.001
O ₂	Upstream ^c	39 ± 2	68.1 ± 0.2	31.4 ± 0.2	0.462 ± 0.003
	Downstream	38 ± 2	68.0 ± 0.1	32.0 ± 0.1	0.471 ± 0.002
CO ₂	Upstream	36 ± 2	72.0 ± 0.3	28.0 ± 0.3	0.389 ± 0.005
	Downstream	30 ± 2	70.0 ± 0.3	30.0 ± 0.3	0.429 ± 0.005
H ₂ O ^b	Upstream	38 ± 2	74.3 ± 1.8	25.7 ± 1.8	0.357 ± 0.033
	Downstream	35 ± 3	73.9 ± 0.8	26.1 ± 0.8	0.354 ± 0.014
HCOOH	Upstream	31 ± 2	71.9 ± 0.3	28.1 ± 0.3	0.391 ± 0.006
	Downstream	30 ± 1	72.6 ± 0.1	27.5 ± 0.1	0.378 ± 0.002

^aReported error is one standard deviation unless stated otherwise. ^bResults reported previously.¹⁶

^cTrace nitrogen was also detected (<1%).

0.471 ± 0.002 on the upstream and downstream sides, respectively. Plasma processing using CO₂ and HCOOH results in more modest gains, similar to H₂O plasma processing, as each of these plasma systems has the capacity to generate a similar cross-section of oxygen containing species.

A closer examination of the XPS C_{1s} region allows examination of the precise environment in which this oxygen is located. The fitting techniques used here are the same as that described in Chapter 4. We observe a similar C_{1s} profile regardless of the plasma system used, Figure 5.3. The surface of untreated PC-TE consists of C-C/C-H (aliphatic/aromatic), C-O, and O=C(-O)₂ functionalities, consistent with virgin polycarbonate. Following plasma processing, C=O and O=C-O binding environments are also observed. Indeed, the areas of all CO_x environments except O=C(-O)₂ increase following O₂ plasma processing, Table 5.2. These increases are also observed following plasma processing using H₂O. In comparison to the H₂O plasma treated PC-TE, O₂ plasma treatment yields the highest concentration of each CO_x binding environment, CO₂ plasma treatment implants more C-O and O-C=O on the downstream side, and HCOOH plasma treatment yields the highest O-C=O concentration relative to the area of other CO_x binding environments. In each case, the change in CO_x moiety area is consistent with changes in elemental composition.

Plasma processing of hydrophobic polymer surfaces using oxygen-containing plasmas typically results in a marked increase in wettability. Previously, we demonstrated that surface modification via H₂O plasma dramatically improves the wettability of a PC-TE membrane surface, where standard treatment conditions reduced wCAs from 97 ± 3° to 38 ± 2° on the upstream facing side of a freshly treated sample, Table 5.1.¹⁶ Each of the other plasma systems studied here give similar improvements in wettability. The lowest wCA we observe on the

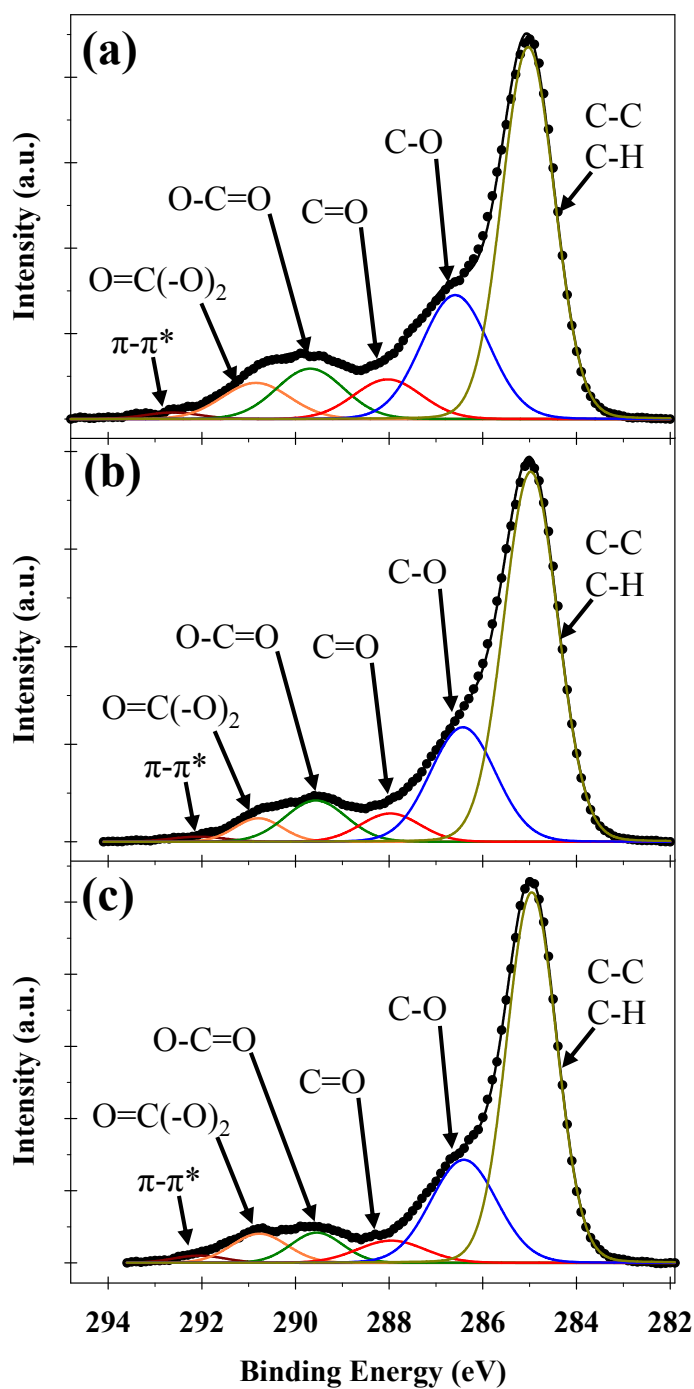


Figure 5.3. High resolution C_{1s} XPS spectra from (a) O_2 , (b) CO_2 , and (c) $HCOOH$ plasma treated $0.2 \mu m$ PC-TE. Standard treatment conditions were used.

Table 5.2. High resolution XPS C_{1s} moieties on PC-TE following plasma processing.

Precursor	Orientation	High resolution C _{1s} moieties (%) ^a				
		C-C/C-H	C-O	C=O	O=C-O	O=C(-O) ₂
Untreated ^b	--	75.6 ± 1.1	16.9 ± 0.9	--	--	7.6 ± 0.2
O ₂	Upstream	53.3 ± 0.3	23.1 ± 0.3	7.3 ± 0.5	9.6 ± 0.4	6.7 ± 0.1 ^c
	Downstream	53.4 ± 0.3	24.0 ± 0.6	5.7 ± 0.5	11.8 ± 1.1	5.2 ± 1.0
CO ₂	Upstream	60.7 ± 0.8	23.3 ± 0.5	5.1 ± 0.1	5.3 ± 0.2	5.5 ± 0.1
	Downstream	57.7 ± 0.2	24.3 ± 0.5	6.1 ± 0.7	7.9 ± 0.6	4.0 ± 0.6
H ₂ O ^b	Upstream	66.7 ± 1.2	20.4 ± 0.8	3.9 ± 0.4	5.6 ± 0.3	3.4 ± 0.3
	Downstream	64.0 ± 1.4	21.1 ± 0.6	5.6 ± 0.4	6.7 ± 0.4	2.6 ± 0.1
HCOOH	Upstream	59.3 ± 1.3	24.1 ± 1.1	4.9 ± 0.3	8.2 ± 0.4	3.5 ± 0.1
	Downstream	59.8 ± 0.9	24.5 ± 0.5	5.8 ± 0.3	7.5 ± 0.4	2.5 ± 0.2

^aReported error is one standard deviation unless stated otherwise. ^bResults reported previously.¹⁶
^cError is two standard deviations.

upstream side is measured on HCOOH plasma treated PC-TE ($31 \pm 2^\circ$) and the highest upstream wCA is measured on O₂ plasma treated PC-TE ($39 \pm 2^\circ$). These results are somewhat unexpected given that XPS analysis shows O₂ plasma modification yields the most oxygen incorporation. When the PC-TE surface is isolated from the plasma glow by facing downstream, both CO₂ and HCOOH plasmas yield similarly low wCAs ($30 \pm 2^\circ$ and $30 \pm 1^\circ$, respectively).

Many polymers are known to exhibit hydrophobic recovery following plasma surface modification and PC is no exception. As discussed in Section 1, PC modification by O₂ plasma has been studied extensively, and the wetting behavior follows a fairly predictable pattern.²⁰⁻²² Initially, O₂ plasma exposure renders the PC surface hydrophilic. As the treated polycarbonate ages, the wCA rebounds slightly before stabilizing. The degree of hydrophobic recovery seems to depend on the treatment conditions. However, the aged PC surface is typically more hydrophilic than virgin PC. Previously, we found that wCAs recover by ~17% over 4 weeks following H₂O plasma treatments carried out using standard treatment conditions.¹⁶ This wCA aging study was repeated on PC-TE following plasma processing using CO₂ and HCOOH, Figure 5.4. Both plasma treatments result in a much lower wCA on freshly treated PC-TE. Over one month of aging, the upstream facing side of CO₂ plasma modified PC-TE only exhibits ~10% recovery and the downstream facing side has no measureable hydrophobic recovery. This aging behavior is unique; PC-TE surfaces modified using the other plasma systems typically exhibit some hydrophobic recovery regardless of orientation. For example, the wCAs on PC-TE recover by ~16% following HCOOH plasma treatment, a behavior that closely resembles that on PC-TE following H₂O plasma treatment. After one month, however, the surfaces of CO₂ and HCOOH plasma modified PC-TE are more wettable than those modified using H₂O plasma.

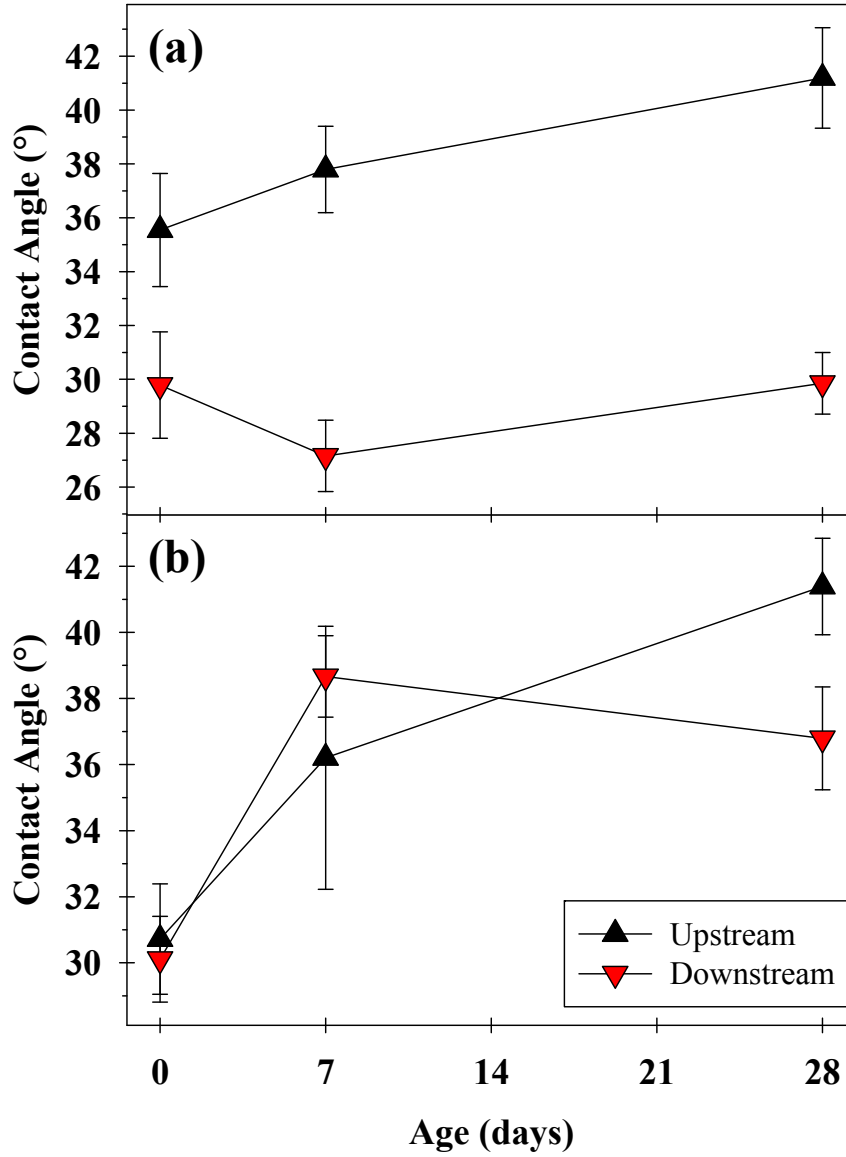


Figure 5.4. wCA as a function of time after treatment for 0.2 μm PC-TE samples modified using (a) CO₂ plasma and (b) HCOOH plasma. Standard treatment conditions were used and samples were aged under ambient laboratory conditions.

5.2.3. *Actinometric optical emission spectroscopy.* To unravel the processes that lead to etching and surface modification of PC-TE, OES was used to examine the excited state gas-phase species present in each plasma system, Figure 5.5. Each of the plasma systems examined here are related by their oxidizing nature and their ability to form oxidizing species. The emission spectrum from the O₂ plasma reveals only the presence of O*, Figure 5.5.a. The remaining plasma systems each form a more diverse set of excited state species. The carbon atom in CO₂ and the hydrogen atoms in H₂O lead to a range of emissions from CO* in the CO₂ plasma and OH* in the H₂O plasma, Figures 5.5.b. and 5.5.c. The HCOOH plasma, however, is best described as an amalgamation of the CO₂ and H₂O plasmas, as the emission spectrum contains significant signals from both CO* and OH*. Various peaks from Ar* are also observed in each spectrum, resulting from the small amount of Ar added for actinometry purposes. Previous work suggested that certain gas-phase species contribute to polymer etching (e.g. atomic oxygen),¹⁶ whereas other gas-phase species are more likely to follow reaction pathways that lead to surface modification (e.g. OH).²⁷ Stacked spectra of the spectral regions containing the OH* and O* emission signals from each plasma system are shown in Figure 5.6. Indeed, the two plasma systems with the fastest etching rates, O₂ and CO₂, have no emission from OH*, Figure 5.6.a., and give the most intense emission from O*, Figure 5.6.b. Meanwhile, the O* emission signal is the weakest in the HCOOH plasma compared to the other plasma systems.

To further examine the differences in O* and OH* relative gas-phase density, actinometry was used to correct for differences in plasma energetics between the four plasma systems, Figure 5.7.a. As expected, the O₂ plasma system has the highest O* density, where atomic oxygen can form from the dissociation of O₂. O* density is successively lower in the CO₂, H₂O, and HCOOH plasma systems. In each case, these differences likely result from

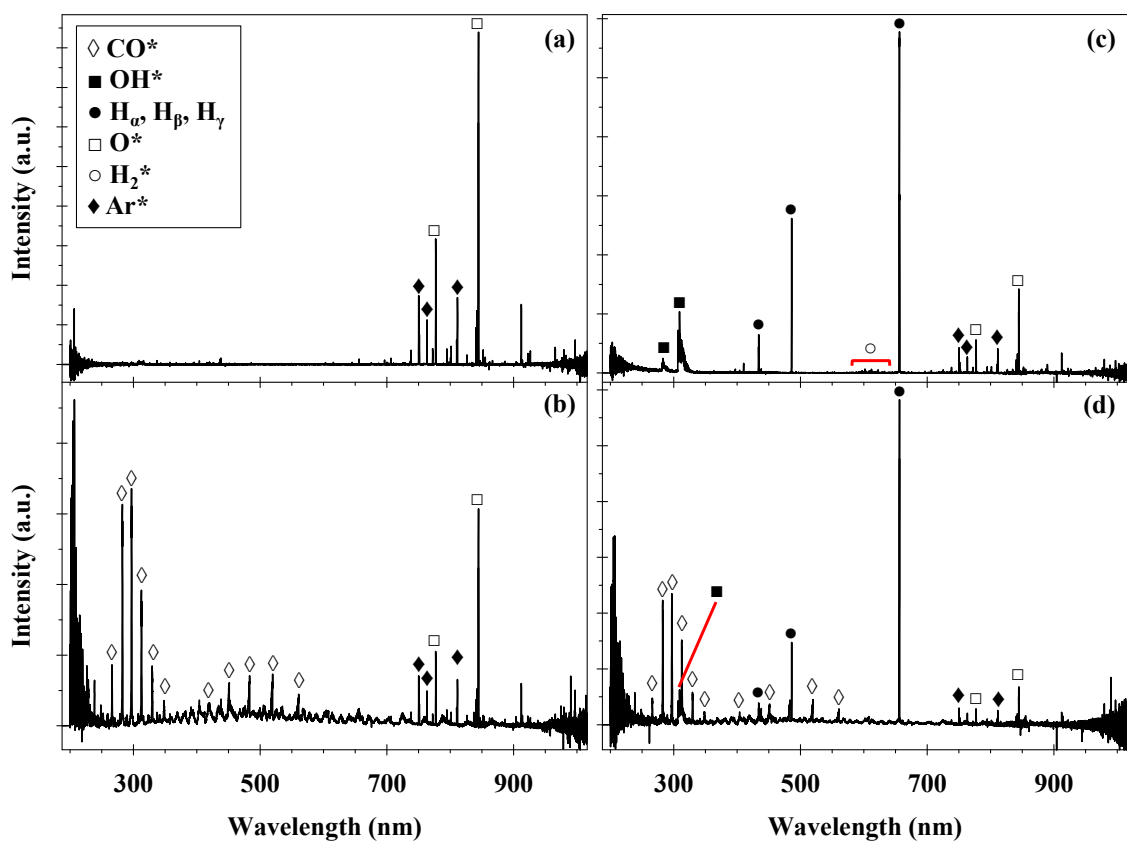


Figure 5.5. OES spectra from (a) O $_2$, (b) CO $_2$, (c) H $_2$ O, and (d) HCOOH plasmas operating under standard treatment conditions collected in irradiance mode. Plasma emission was collected 9 cm downstream from the coil region.

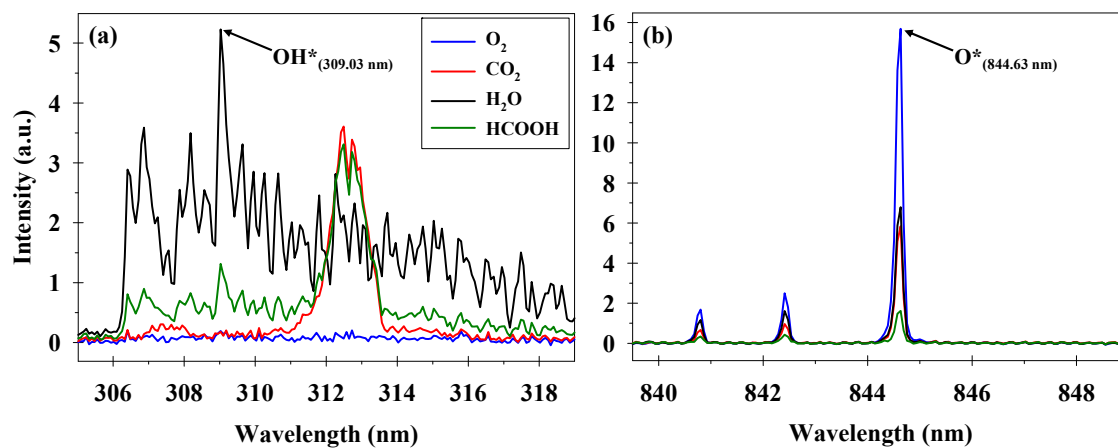


Figure 5.6. Stacked OES spectra from O₂, CO₂, H₂O, and HCOOH plasmas showing the regions containing the (a) OH* (309 nm) and (b) O* (844 nm) emission used to calculate relative gas-phase density.

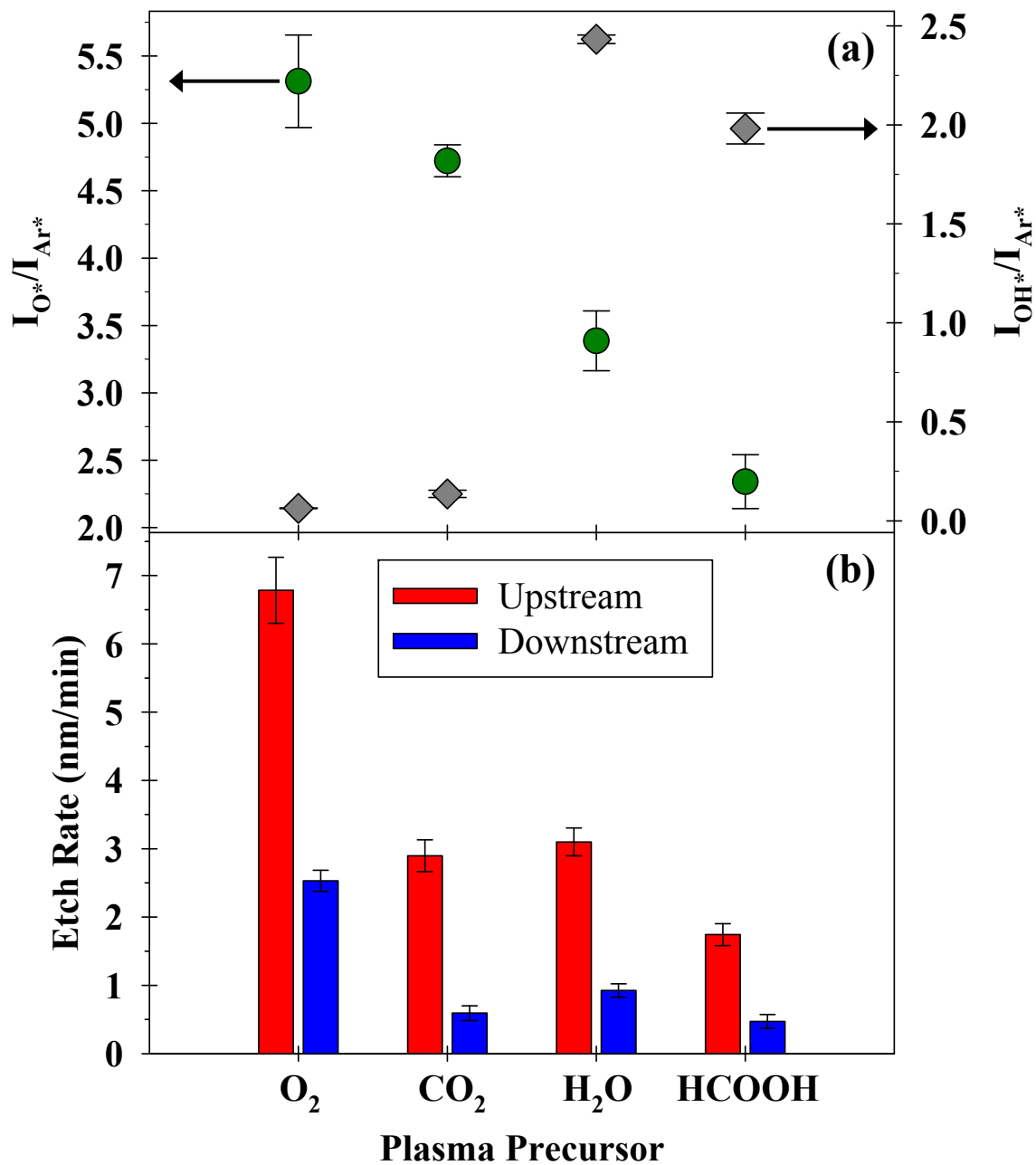


Figure 5.7. (a) AOES measurements of relative gas-phase density of O* (left axis) and OH* (right axis); (b) summary of measured etch rates on the upstream and downstream sides during O₂, CO₂, H₂O, and HCOOH plasma processing of PC-TE.

comparatively more complicated reaction pathways leading to O^* and the availability of recombination pathways that consume O^* . The relative OH^* density, however, is only significant in the H_2O and $HCOOH$ plasma systems. The most direct pathway for OH radical formation is dissociation in the H_2O and $HCOOH$ plasma systems, but recombination pathways likely contribute to the observed gas-phase density as well. Although the radical species present in the O_2 and CO_2 plasma systems would be capable of combining with hydrogen to form OH , the absence of any source of hydrogen in these plasmas means that OH formation is impossible.

5.3. Discussion

In a previous study,¹⁶ we found that plasma surface modification using mild treatment conditions rendered the surface of PC-TE wettable and did not cause any observable changes in the pore structure or membrane morphology. We also explored extremes of the treatment parameter space, finding that increasing treatment times and applied plasma powers increased the pore radius and, in some cases, textured the membrane surface. The present study further elucidates the underlying mechanisms of this etching by comparing four similar oxidizing plasma systems, namely O_2 , CO_2 , H_2O , and $HCOOH$, and extending the treatment time so as to reveal the extent of the PC-TE etching in each system. We begin here by considering the relevance of certain gas-phase species to PC etching in light of the observed etch rates and extend the discussion to the impact of PC etching on material stability and modification efficacy.

5.3.1. Gas-phase processes leading to PC etching. Polymer etching occurs for several reasons during plasma processing, which can be largely grouped into either chemical or physical processes. Although many plasma systems are capable of physical etching of polymers (sputtering), the design of the inductively coupled rf plasmas, relatively remote substrate

placement, and relatively low P systems used in this study are not conducive to sputtering. Thus, the observed etching is dominated by chemical processes, which entail chemical reactions between reactive gas-phase species and the surface to form volatile products. Consequently, efforts to control chemical etching must focus on production and control of these reactive gas-phase species.

Among the related oxidizing plasma systems studied here, the O_2 plasma induces the highest PC-TE etch rate. Indeed, this system was included primarily as a high etch rate control case, based on the many literature reports of O_2 plasma etching of PC.^{17-19, 23} Many researchers have identified atomic oxygen as being responsible for etching polymer materials when exposed to O_2 discharges. For example, Hofrichter et al.¹¹ examined etching and changes in the surface structure of spin coated and commercially available PC during H_2 , N_2 , and O_2 plasma processing. They found that etch rate generally increased as a function of P , proportional to the density of atomic oxygen. PC etch rates during O_2 plasma processing in their reactor systems were 0.6-1.7 $nm\ s^{-1}$. Mozetič and coworkers³² examined the etching of polyethylene terephthalate (PET) during direct exposure to an rf O_2 plasma and measured an etch rate of 4.7 $nm\ s^{-1}$. They attributed the observed etching to reactions of the PET with atomic oxygen to form volatile products. They rule out etching contributions from oxygen ions on the grounds that their gas-phase density is too low to account for the mass of carbon removed from the surface.³² We suspect this reasoning is flawed and ignores the work by Coburn and Winters,³³ and others³⁴ that clearly demonstrate the synergistic behavior of neutral species and ions acting on a surface concomitantly. Our recent work demonstrated that the surface reaction probabilities of some plasma species are strongly influenced by ions impinging on the surface.³⁵ The extent to which oxygen ions influence the surface reaction probability of neutral oxygen on PC is, however,

currently unknown. The downstream substrate placement used during experiments reported here, however, limits the density of ions and other highly energetic particles at the plasma-polymer interface. Moreover, variables that are likely to influence the density of ions near the surface, namely substrate placement, P , and pressure, were kept constant. Differences in the observed etch rate will, therefore, be dictated primarily by changes in the density of atomic oxygen or other neutral species, and the influence of oxygen ions is beyond the scope of this work. Mozetič and coworkers³⁶ also measured significant etching (0.5 nm min^{-1}) on PET in the afterglow of an O_2 discharge, conditions where ground state atomic oxygen is effectively the only reactive species present. This suggests atomic oxygen is primarily responsible for the etching observed during O_2 plasma processing of PC-TE reported here as well.

By comparison, CO_2 and H_2O plasmas yield more moderate etch rates during the plasma processing of PC-TE. Actinometric OES experiments reveal the trend in relative O^* gas-phase density is $\text{O}_2 > \text{CO}_2 > \text{H}_2\text{O}$, Figure 5.7.a. Assuming the only source of O^* is excitation via electron impact of ground state atomic oxygen, the relative gas-phase density of atomic oxygen should be proportional to the relative gas-phase density of O^* . Under certain circumstances, however, this assumption is known to be false. Notably, the dissociative excitation of ground state O_2 can make significant contributions to O^* in a pure O_2 plasma,³⁷ an effect exacerbated at low operating pressures (1-10 mTorr).^{38, 39} Dissociative excitation of O_2 also makes a more substantial contribution to the 777 nm O^* emission line, compared to the 844 nm line used for O^* actinometry here.³⁹ Although the dissociative excitation of ground state O_2 likely makes a minor contribution to $I_{\text{O}^*}/I_{\text{Ar}^*}$ measured in the pure O_2 plasma, this pathway can be ignored in the CO_2 and H_2O plasma systems. Bousquet et al.⁴⁰ investigated the atomic oxygen excitation kinetics in O_2 , CO_2 , and H_2O plasmas. They found that production of O^* via dissociative

excitation of O₂, CO₂, CO, H₂O, or OH in CO₂ and H₂O plasma systems was negligible. They concluded that O* is formed via electron impact excitation of ground state oxygen and that O* actinometry is a robust method for measuring atomic oxygen density in these systems. The etch rates observed during O₂, CO₂, and H₂O plasma processing are, therefore, proportional to the atomic oxygen density in each system. This is consistent with our hypothesis that atomic oxygen is primarily responsible for the etching observed in these oxidizing plasma systems.

In each system studied here, the etch rate is much higher on the upstream side than on the downstream side, providing further evidence of a connection between etch rate and atomic oxygen density. The configuration of our experiments place PC-TE perpendicular to the long axis of the reactor such that the membrane occupies almost the entire internal diameter of the reactor.²⁵ This arrangement protects the downstream facing side while exposing the upstream facing side to the plasma glow. Recalling the work by Mozetič and coworkers, O₂ plasmas etch PET quickly upon direct exposure,⁴¹ but atomic oxygen is long lived enough to continue etching far into the afterglow.³⁶ Recombination of atomic oxygen to form molecular oxygen requires a ternary mechanism, making the reaction kinetically very slow.³⁶ Therefore, in an O₂ plasma a significant amount of this long lived atomic oxygen is likely to reach the downstream side of PC-TE. A greater diversity of gas-phase species in the other systems (i.e. H in the H₂O and HCOOH plasmas; CO in the CO₂ and HCOOH plasmas) means there are more pathways available to consume atomic oxygen. This explains the lower ratios of downstream to upstream etching in the CO₂, H₂O, and HCOOH plasmas.

Interestingly, although the O* density is measurably lower in the H₂O plasma system compared to the CO₂ plasma system, the etch rate on the upstream facing side of the membrane is the same within error. Besides atomic oxygen, the most abundant neutral fragments detected

are CO* in the CO₂ plasma and OH* in the H₂O plasma. Despite the lower atomic oxygen density in the H₂O plasma, OH radicals also contribute to the observed etching, resulting in a higher etch rate than would be expected solely from atomic oxygen. Hall et al.⁴² examined the plasma induced modification and etching of PC using O₂, H₂O, N₂, Ar, and a range of alcohols as precursor gases. They observed significant etching using each of the precursor alcohols with the highest etch rate during H₂O plasma processing. Based on the detection of OH* in each of these plasma systems using OES, they hypothesized that OH radicals were responsible for etching PC. This hypothesis, however, ignores contributions from other species, notably atomic oxygen, which must be present in their H₂O plasma, for example. Unfortunately, evaluating the veracity of their claim is precluded because their OES measurements cover only a limited range (300-430 nm), making it impossible to identify or quantify other radical species.

To our knowledge, there are no published accounts of 100% HCOOH plasmas or the use of HCOOH plasmas to modify polymer surfaces. The HCOOH plasma emission spectrum reveals the plasma comprises the species found in the CO₂ and H₂O plasmas. Overall, however, the HCOOH plasma does not behave as though it is an average of the H₂O and CO₂ plasma systems. Indeed, it yields the slowest PC-TE etch rate, most likely as a result of the remarkably low density of atomic oxygen produced in the HCOOH plasma. This lack of atomic oxygen is not intuitive, given that HCOOH contains the same stoichiometric amount of oxygen compared to O₂ and CO₂. The difference lies with the more complicated reaction pathways leading to atomic oxygen production in the HCOOH system, as well as the observation that the recombination pathways that consume atomic oxygen are more plentiful.

5.3.2. Implications of etching on PC surface modification and stability. Along with etching, there is concomitant implantation of polar functional groups and a corresponding

increase in the surface tension and energy on the plasma processed PC-TE surface. This makes plasma modified PC surfaces susceptible to aging phenomena, processes that act on the higher energy activated surface to achieve a more stable lower energy state. Our previous work revealed that wCAs on H₂O plasma modified PC-TE recovered by ~17% one month after treatment.¹⁶ By comparison, O₂ plasma modified surfaces recover by as much as ~55% over the same time period.²⁰ Many processes cause aging or hydrophobic recovery on modified polymer surfaces, including adsorption of non-polar contaminants from the environment, short-range rearrangement of polymer chains to bury polar functional groups, and long-range rearrangement of polymer chains exposing unmodified polymer chains at the surface.^{41, 43} Contamination can be mitigated by appropriate storage. The energetics of short-range rearrangements are likely intrinsic to polymer composition and structure, meaning they will be difficult or impossible to control for a given polymer. Long-range rearrangement of the polymer surface results from disrupting the long polymer chains that contribute to the stability of the polymer surface. Regardless of the mechanism by which it occurs, aging causes loss of implanted functionality at the surface and hydrophobic recovery on PC.²² The mitigation of aging on PC, induced by damage from plasma processing, is of great interest.

Chain scission events that occur at the surface of a polymer remove the high energy barrier that prevents rearrangement of the surface. Jang et al. examined the thermal break down of PC, showing that the lowest bond dissociation energies in the PC backbone are found in the aliphatic region.⁴⁴ These plasmas contain many reactive species capable of etching PC that are also able to follow reaction pathways that would otherwise be unfavorable. Previously, we concluded that atomic oxygen attack in the aromatic regions of PC is likely to lead to complete chain scission, providing an easy pathway to etching.¹⁶ Another possible pathway is scission at

the carbonate functional group, ultimately yielding stable and volatile CO₂, and unbound bisphenol A fragments.^{45, 46} The bond dissociation energies in and around the aromatic and carbonate functional groups are higher than those of the aliphatic carbons, meaning the overall activation energy of these pathways are higher. Regardless, we believe these pathways are contributing to etching based on the observed increases in CO, C=O, and O-C=O groups, and decreases in carbonate functionality following treatment. These chain scission mechanisms result in the breaking of polymer chains at the PC surface, resulting in formation of short PC oligomers and a surface composed of PC chain ends.

When CO_x functionalities are implanted in conjunction with the chain scission processes discussed above, the result is a surface composed of low molecular weight oxidized material (LMWOM). Although this oxidized material initially contributes to the increased wettability observed on the plasma treated PC surface, the fragments are loosely bound and more mobile than the unmodified polymer chains. LMWOM can diffuse into the PC and can be washed off in an aqueous environment.^{22, 23} Because etching of the PC surface is the final outcome of many chain scission events, the plasma system with the slowest etch rate will have the slowest chain scission rate and should yield the most stable surface modification. Indeed, the HCOOH plasma has the slowest etch rate on the upstream facing side of the PC-TE, and it remains relatively stable after one month of aging, showing only minimal hydrophobic recovery.

Although the upstream facing side of PC-TE exhibits some degree of hydrophobic recovery regardless of plasma precursor, remarkably, the downstream side of the CO₂ plasma modified PC-TE exhibits no hydrophobic recovery over a 4 week aging period. This stability could result if the CO₂ plasma were inducing cross-linking at the PC surface. Muir et al.²³ demonstrated, however, that oxidizing plasmas operating under similar conditions to those

studied here were not effective for cross-linking the surface of PC. Likewise, Hofrichter et al.¹¹ showed that high purity PC films resist cross-linking during plasma processing. Thus, we find it more likely that a gas-phase species is responsible for eliminating the etchant, which protects the PC surface from etching. Of the species present in the CO₂ plasma, CO is the most likely candidate. Figure 5.5.b. shows that a large quantity of CO is generated in the CO₂ plasma, and CO is known to react with atomic oxygen and other radicals. The remarkable stability on the downstream facing side of CO₂ plasma processed PC-TE results from two circumstances: the downstream facing side is protected from high energy species in the plasma glow and CO consumes reactive radicals that would otherwise disrupt the surface. Additional experiments are required to examine the gas-phase on the downstream facing side of PC-TE during processing.

5.3.3. PC-TE morphology with oxidizing plasma treatment. In considering the “best” plasma system to use for processing PC materials, the impact on surface morphology and topography must be considered. SEM images of CO₂ and O₂ plasma processed PC-TE reveal a flat surface free of significant defects, similar to unmodified PC-TE. A number of researchers have used atomic force microscopy (AFM) measurements to characterize more subtle changes in roughness on PC with plasma treatment. Larsson and Dérand²¹ found that treatment using high intensity O₂ plasma increased the root-mean-square (RMS) roughness of PC to 9.0 nm, compared to 0.55 nm on untreated samples. Hofrichter et al.¹¹ found that RMS roughness increased from 1.42 nm to 1.55 nm on microwave O₂ plasma modified Lexan® samples. Greenwood et al.²⁴ used an inductively coupled rf O₂ plasma operating at $P = 20$ W, similar to that used here, and observed very little change in roughness on treated PC samples. Although etching is certainly happening in each of these cases, the etching rate during O₂ plasma processing is consistent across the PC surface, yielding a generally flat morphology.

In contrast, the PC-TE surface is textured with tiny nodules after H₂O and HCOOH plasma processing, especially following long treatment times. These findings are interesting in comparison to those reported by d'Agostino and coworkers^{18, 19} on the nano-texturing of PC by plasma etching to alter the wetting and reflective properties. They found that a capacitively-coupled O₂ plasma raised a texture on a PC surface in as little as 5 min at $P = 100$ W. This is not a counter-example to the studies mentioned above. Instead, they found that re-deposition of metal from the electrodes was responsible for a masking effect, causing inconsistent etch rates across the surface. There is no evidence that such a mechanism is responsible for the texturing of H₂O and HCOOH plasma modified PC-TE reported here. Indeed, our reactor systems have no metal parts in the glass envelope where the plasma is generated, and XPS analysis does not reveal any metal contamination. In light of this, our results that show H₂O and HCOOH plasmas have the capacity to texture PC reveals something unique. Volatile inorganic oxygen and oxidized carbon do not contribute to film formation during plasma processing. The large amounts of atomic hydrogen in the H₂O and HCOOH plasmas could be participating in recombination reactions and the formation of hydrocarbon film deposition precursors (i.e. CH radicals). Such a film could be directly responsible for texture formation, or generate a masking effect similar to that observed by d'Agostino and coworkers. Additional studies to ascertain the presence of film formation precursors in the gas-phase, their specific molecule-surface interactions, and their contributions to film formation are currently underway.

5.4. Summary

The study described in this chapter explores the differences between O₂, CO₂, H₂O, and HCOOH plasma treatments on PC-TE. Although each system ultimately results in etching of the

PC-TE, each system exhibits slightly different morphology outcomes. The O₂ and CO₂ plasma treatments do not result in any large scale roughness, visible using SEM, over any of the treatment times studied here. In contrast, the H₂O and HCOOH plasmas yield a surface consisting of small nodules that develop as the treatment progresses. The texture likely arises from re-deposition of hydrocarbon material or a similar process. Regardless, the textured surface of the H₂O and HCOOH plasma treated PC-TE does not limit its wettability. Indeed, all plasma treatments render the freshly treated samples wettable, owing to the implantation of similar polar functional groups. Compared to our previous study, however, the HCOOH treatments give the lowest wCA on freshly treated samples and CO₂ treatments yield the most stable PC surface, with little or no hydrophobic recovery.

Each of these plasma systems also exhibit different etch rates for PC-TE membranes. For perspective, the time required to completely etch through the PC-TE material can be calculated based on the 10 μm thickness reported by the manufacturer and the etch rates measured here, assuming the etch rate remains linear over the process time. Complete etching of the PC-TE would take place in 17.9 hours using the O₂ plasma system operating under the conditions used in this study. By comparison, the CO₂, H₂O, and HCOOH plasma systems would take 47.8, 41.5, and 75.4 hours, respectively. Total process time for PC etch is certainly minimized using the O₂ plasma system under these conditions. The slower etch rates achieved using the CO₂, H₂O, and HCOOH systems may, however, provide additional control over a PC etch process.

Our results clearly demonstrate PC-TE etch rates correlate directly to the relative gas-phase density of atomic oxygen and, to a lesser extent, OH radicals in the plasma systems. The O₂ plasma system produces the largest amount of atomic oxygen and has the highest etch rate. Although high concentrations of atomic oxygen are also found in the CO₂ plasma system, CO is

believed to act as an oxygen scavenger to limit surface interactions. The H₂O plasma system generates less atomic oxygen but has a similar etch rate to the CO₂ plasma. OH radicals, another oxidizing species, are also produced in the H₂O plasma and contribute to etching. The gas-phase composition of the HCOOH plasma resembles the CO₂ and H₂O systems in certain respects. Owing to the remarkably small amount of atomic oxygen generated, the slowest etch rate is achieved during HCOOH plasma modification of PC-TE.

REFERENCES

1. Tompkins, B. D.; Dennison, J. M.; Fisher, E. R., Etching and Post-Treatment Surface Stability of Track-Etched Polycarbonate Membranes by Plasma Processing Using Various Related Oxidizing Plasma Systems. *Plasma Processes Polym.* **2014**, Accepted, 10.1002/ppap.201400044.
2. Chen, J. G.; Zhang, T.; Zhu, J. S.; Zhang, X. Y.; Zhou, J. L.; Fan, J. F.; Hu, G. H., Low-loss planar optical waveguides fabricated from polycarbonate. *Polym. Eng. Sci.* **2009**, 49, (10), 2015-2019.
3. Languy, F.; Habraken, S., Performance comparison of four kinds of flat nonimaging Fresnel lenses made of polycarbonates and polymethyl methacrylate for concentrated photovoltaics. *Opt. Lett.* **2011**, 36, (14), 2743-2745.
4. Vani, K.; Thomas, S.; Prabhawathi, V.; Boobalan, T.; Sawant, S. N.; Doble, M., In vitro biocompatibility of modified polycarbonate as a biomaterial. *Colloids Surf., B* **2013**, 108, (0), 191-198.
5. Wang, Q.; Webster, T. J., Nanostructured selenium for preventing biofilm formation on polycarbonate medical devices. *J. Biomed. Mater. Res., Part A* **2012**, 100A, (12), 3205-3210.
6. Tamarit-López, J.; Morais, S.; Puchades, R.; Maquieira, Á., Oxygen plasma treated interactive polycarbonate DNA microarraying platform. *Bioconjugate Chem.* **2011**, 22, (12), 2573-2580.
7. Jankowski, P.; Ogończyk, D.; Derzsi, L.; Lisowski, W.; Garstecki, P., Hydrophilic polycarbonate chips for generation of oil-in-water (O/W) and water-in-oil-in-water (W/O/W) emulsions. *Microfluid. Nanofluid.* **2013**, 14, (5), 767-774.
8. Baytekin, H. T.; Wirth, T.; Gross, T.; Treu, D.; Sahre, M.; Theisen, J.; Schmidt, M.; Unger, W. E. S., Determination of wettability of surface-modified hot-embossed polycarbonate wafers used in microfluidic device fabrication via XPS and ToF-SIMS. *Surf. Interface Anal.* **2008**, 40, (3-4), 358-363.
9. Sheng, Y.; Bowser, M. T., Isolating single stranded DNA using a microfluidic dialysis device. *Analyst* **2014**, 139, (1), 215-224.
10. Gomathi, N.; Neogi, S., Investigation on argon–oxygen plasma induced blood compatibility of polycarbonate and polypropylene. *J. Adhes. Sci. Technol.* **2009**, 23, (13/14), 1811-1826.
11. Hofrichter, A.; Bulkin, P.; Drévilion, B., Plasma treatment of polycarbonate for improved adhesion. *J. Vac. Sci. Technol., A* **2002**, 20, (1), 245-250.

12. Latella, B. A.; Triani, G.; Zhang, Z.; Short, K. T.; Bartlett, J. R.; Ignat, M., Enhanced adhesion of atomic layer deposited titania on polycarbonate substrates. *Thin Solid Films* **2007**, 515, (5), 3138-3145.
13. Ong, H. C.; Chang, R. P. H.; Baker, N.; Oliver, W. C., Improvement of mechanical properties of amorphous carbon films deposited on polycarbonate plastics. *Surf. Coat. Technol.* **1997**, 89, (1-2), 38-46.
14. Kitova, S.; Minchev, M.; Danev, G., RF plasma treatment of polycarbonate substrates. *J. Optoelectron. Adv. Mater.* **2005**, 7, (5), 2607-2612.
15. Slawomir, Z.; Rakowski, W. A.; Jonas, S., Anti-wear properties of amorphous a-C:H and a-C:N:H carbon coatings deposited on polycarbonate. *Surf. Interface Anal.* **2012**, 44, (8), 1229-1232.
16. Tompkins, B. D.; Dennison, J. M.; Fisher, E. R., H₂O plasma modification of track-etched polymer membranes for increased wettability and improved performance. *J. Membr. Sci.* **2013**, 428, 576-588.
17. Li, N. C.; Yu, S. F.; Harrell, C. C.; Martin, C. R., Conical nanopore membranes. Preparation and transport properties. *Anal. Chem.* **2004**, 76, (7), 2025-2030.
18. Palumbo, F.; Di Mundo, R.; Cappelluti, D.; d'Agostino, R., Superhydrophobic and superhydrophilic polycarbonate by tailoring chemistry and nano-texture with plasma processing. *Plasma Processes Polym.* **2011**, 8, (2), 118-126.
19. Di Mundo, R.; Troia, M.; Palumbo, F.; Trotta, M.; d'Agostino, R., Nano-texturing of transparent polymers with plasma etching: tailoring topography for a low reflectivity. *Plasma Processes Polym.* **2012**, 9, (10), 947-954.
20. Jokinen, V.; Suvanto, P.; Franssila, S., Oxygen and nitrogen plasma hydrophilization and hydrophobic recovery of polymers. *Biomicrofluidics* **2012**, 6, (1), 016501-10.
21. Larsson, A.; Dérand, H., Stability of polycarbonate and polystyrene surfaces after hydrophilization with high intensity oxygen RF plasma. *J. Colloid Interface Sci.* **2002**, 246, (1), 214-221.
22. Morra, M.; Occhiello, E.; Garbassi, F., Hydrophobic recovery and misting behavior of plasma treated PS and PC surfaces. *Angew. Makromol. Chem.* **1991**, 189, 125-136.
23. Muir, B. W.; McArthur, S. L.; Thissen, H.; Simon, G. P.; Griesser, H. J.; Castner, D. G., Effects of oxygen plasma treatment on the surface of bisphenol A polycarbonate: a study using SIMS, principal component analysis, ellipsometry, XPS and AFM nanoindentation. *Surf. Interface Anal.* **2006**, 38, (8), 1186-1197.
24. Greenwood, O. D.; Hopkins, J.; Badyal, J. P. S., Non-isothermal O₂ plasma treatment of phenyl-containing polymers. *Macromolecules* **1997**, 30, (4), 1091-1098.

25. Steen, M. L.; Hymas, L.; Havey, E. D.; Capps, N. E.; Castner, D. G.; Fisher, E. R., Low temperature plasma treatment of asymmetric polysulfone membranes for permanent hydrophilic surface modification. *J. Membr. Sci.* **2001**, 188, (1), 97-114.
26. Kull, K. R.; Steen, M. L.; Fisher, E. R., Surface modification with nitrogen-containing plasmas to produce hydrophilic, low-fouling membranes. *J. Membr. Sci.* **2005**, 246, (2), 203-215.
27. Steen, M. L.; Butoi, C. I.; Fisher, E. R., Identification of gas-phase reactive species and chemical mechanisms occurring at plasma–polymer surface interfaces. *Langmuir* **2001**, 17, (26), 8156-8166.
28. Grill, A., *Cold Plasma Materials Fabrication: From Fundamentals to Applications*. IEEE Press: Piscataway, NJ, 1994.
29. Gonzalez, E., II; Barankin, M. D.; Guschl, P. C.; Hicks, R. F., Ring opening of aromatic polymers by remote atmospheric-pressure plasma. *IEEE Trans. Plasma Sci.* **2009**, 37, (6), 823-831.
30. Koprinarov, I.; Lippitz, A.; Friedrich, J. F.; Unger, W. E. S.; Wöll, C., Oxygen plasma induced degradation of the surface of poly(styrene), poly(bisphenol-A-carbonate) and poly(ethylene terephthalate) as observed by soft X-ray absorption spectroscopy (NEXAFS). *Polymer* **1998**, 39, (14), 3001-3009.
31. Hofrichter, A.; Bulkin, P.; Drevillon, B., An interfacial study of a hydrogenated carbon interlayer for adhesion enhancement of plasma deposited silica thin films on polycarbonate. *J. Adhes. Sci. Technol.* **2002**, 16, (4), 395-407.
32. Doliška, A.; Vesel, A.; Kolar, M.; Stana-Kleinschek, K.; Mozetič, M., Interaction between model poly(ethylene terephthalate) thin films and weakly ionised oxygen plasma. *Surf. Interface Anal.* **2012**, 44, (1), 56-61.
33. Coburn, J. W.; Winters, H. F., Ion- and electron-assisted gas-surface chemistry—An important effect in plasma etching. *J. Appl. Phys.* **1979**, 50, (5), 3189-3196.
34. Gogolides, E.; Vauvert, P.; Kokkoris, G.; Turban, G.; Boudouvis, A. G., Etching of SiO₂ and Si in fluorocarbon plasmas: A detailed surface model accounting for etching and deposition. *J. Appl. Phys.* **2000**, 88, (10), 5570-5584.
35. Cuddy, M. F.; Blechle, J. M.; Fisher, E. R., Ion contributions to gas-surface interactions in inductively-coupled fluorocarbon plasmas. *Int. J. Mass spectrom.* **2012**, 330, 46-57.
36. Vesel, A.; Kolar, M.; Doliška, A.; Stana-Kleinschek, K.; Mozetič, M., Etching of polyethylene terephthalate thin films by neutral oxygen atoms in the late flowing afterglow of oxygen plasma. *Surf. Interface Anal.* **2012**, 44, (13), 1565-1571.
37. Hancock, G.; Toogood, M. J., Laser-induced fluorescence of oxygen atoms in a plasma reactor. *Appl. Phys. Lett.* **1992**, 60, (1), 35-37.

38. Granier, A.; Nicolazo, F.; Vallée, C.; Gouillet, A.; Turban, G.; Grolleau, B., Diagnostics in O₂ helicon plasmas for SiO₂ deposition. *Plasma Sources Sci. Technol.* **1997**, 6, (2), 147-156.
39. Katsch, H. M.; Tewes, A.; Quandt, E.; Goehlich, A.; Kawetzki, T.; Döbele, H. F., Detection of atomic oxygen: Improvement of actinometry and comparison with laser spectroscopy. *J. Appl. Phys.* **2000**, 88, (11), 6232-6238.
40. Bousquet, A.; Cartry, G.; Granier, A., Investigation of O-atom kinetics in O₂, CO₂, H₂O and O₂/HMDSO low pressure radiofrequency pulsed plasmas by time-resolved optical emission spectroscopy. *Plasma Sources Sci. Technol.* **2007**, 16, (3), 597.
41. Pascual, M.; Balart, R.; Sánchez, L.; Fenollar, O.; Calvo, O., Study of the aging process of corona discharge plasma effects on low density polyethylene film surface. *J. Mater. Sci.* **2008**, 43, (14), 4901-4909.
42. Hall, C.; Murphy, P.; Griesser, H., Etching and deposition mechanism of an alcohol plasma on polycarbonate and poly(methyl methacrylate): an adhesion promotion mechanism for plasma deposited a:SiO_xC_yH_z Coating. *Plasma Processes Polym.* **2012**, 9, (9), 855-865.
43. Truica-Marasescu, F.; Jedrzejowski, P.; Wertheimer, M. R., Hydrophobic recovery of vacuum ultraviolet irradiated polyolefin surfaces. *Plasma Processes Polym.* **2004**, 1, (2), 153-163.
44. Jang, B. N.; Wilkie, C. A., The thermal degradation of bisphenol A polycarbonate in air. *Thermochim. Acta* **2005**, 426, (1-2), 73-84.
45. Grace, J. M.; Gerenser, L. J., Plasma treatment of polymers. *J. Dispersion Sci. Technol.* **2003**, 24, (3-4), 305-341.
46. Gerenser, L. J., XPS studies of in-situ plasma-modified polymer surfaces. *J. Adhes. Sci. Technol.* **1993**, 7, (10), 1019-1040.

CHAPTER 6

ACETIC ACID PLASMA POLYMER COATINGS ON POLYCARBONATE FOR IMPROVED COATING INTEGRITY AND STRUCTURE RETENTION IN OPTICAL AND BIOMEDICAL APPLICATIONS

This chapter is based on a manuscript written by Brendan D. Tompkins, Jordan M. Dennison, and Ellen R. Fisher and will be submitted to the journal *ACS Applied Materials & Interfaces*. This work describes a unique PECVD system based on an acetic acid plasma for the deposition of self-limiting thin hydrocarbon film coatings on polycarbonate. Track-etched polycarbonate membranes are used as the model substrate and the films are studied in terms of their surface properties and deposition characteristics. These films are believed to be a good candidate for adhesion inter-layers on polycarbonate for a variety of technologies. Funding for this research was provided by the National Science Foundation (CHE-1152963).

6.1. Introduction

Patterned, nano-textured, and 3-dimensional polycarbonate (PC) structures have numerous applications, including cell culture substrates,^{1,2} biomimetic materials,^{3,4} antireflective optical materials,^{5,6} and scratch resistant materials.⁷ Control over surface properties, such as surface energy, chemical functionality, and abrasion resistance, is critical for each of these applications. Surface modification of PC, however, can be uniquely challenging. Non-depositing plasma surface functionalization, when used alone, often leads to PC chain scission, the formation of loosely bound low molecular weight oligomers, and an unstable surface subject to hydrophobic recovery.⁸ Alternatively, deposition of thin films using plasma enhanced

chemical vapor deposition (PECVD) can surface modify a polymer with negligible impact on the underlying polymer. Despite the formation of a stable layer of functional material, adhesive failure at the PC-PECVD film interface often occurs. The challenges of applying robust adherent coatings to PC while limiting damage to textures and patterns are hindering their use in a wide range of applications. Development of new minimally invasive coating technologies is critical to the further advancement of PC as a 21st century material.

Researchers have had mixed success in their attempts to use plasma surface modification for improved thin film adhesion on PC materials. Gururaj, et al. found that surface activation using atmospheric pressure air plasmas improved the adhesion of sol-gel coatings on PC.⁹ Panwar, et al. found that extended exposure to a low pressure air plasma resulted in a more stable PC surface and reduced hydrophobic recovery.¹⁰ Muir, et al. noted, however, that prolonged exposure to O₂ plasma reduced the adhesion of plasma deposited a-SiC_xO_yH_z from tetramethyldisiloxane on PC as samples aged for ~1 month.¹¹ Subsequently, Muir, et al. demonstrated loosely bound low molecular weight material forms during plasma surface activation,⁸ an observation corroborated by other researchers.¹² Using slightly different strategies, others have shown that the application of a hydrocarbon or similar interlayer greatly improves adhesion of subsequent film layers on PC. Hofrichter, et al. found that a 10 nm *a*-CH interlayer on PC, applied using CH₄ plasmas following O₂ plasma surface activation, greatly improved SiO₂ coating adhesion.¹³ More recently, Hall, et al. found that butanol plasma from a 5.4 kW microwave plasma reactor improved the adhesion of plasma deposited a-SiC_xO_yH_z layers.¹⁴ Regardless, polymer etching, commonly associated with each of these plasma systems, presents further complications. Indeed, O₂ plasma readily etches polycarbonate,^{15, 16} and the

process conditions of other plasmas (e.g. those used by Hall) are enough to induce significant etching in PC.¹⁴

Here, we present our work using acetic acid vapor (CH_3COOH) as a film deposition precursor to modify the surface of PC materials. Polycarbonate track-etched membranes (PC-TE), a simple 3-D polymer structure, are used as model substrates to examine the impact that CH_3COOH plasma processing has on PC. There are very few reports that examine any type of surface modification using CH_3COOH plasmas;¹⁷ to our knowledge, this is the first report wherein films deposited from CH_3COOH plasmas are examined. Our results for PC-TE were compared to those from CH_3COOH plasma processing of Si wafers to elucidate the differences between polymer and non-polymer surfaces. Our materials were characterized using x-ray photoelectron spectroscopy (XPS), water contact angle (wCA), scanning electron microscopy (SEM), and variable angle spectroscopic ellipsometry (VASE). Optical emission spectroscopy (OES) was used to identify the presence of specific radical species in the CH_3COOH plasma, suggesting mechanisms for gas phase species influencing the chemistry of modified surfaces. Our results indicate that CH_3COOH plasma treatments lead to the formation of a self-limiting $\text{C}_x\text{O}_y\text{H}_z$ film on PC, having only a negligible impact on material dimensions.

6.2. Results and Discussion

6.2.1. CH_3COOH PECVD films on PC-TE. The composition of the PC-TE surface was measured using XPS to explore the effect of CH_3COOH plasma exposure. From previous studies,¹⁸ we know that untreated PC-TE comprises C-C/C-H, C-O, and $\text{O}=\text{C}(\text{-O})_2$ binding environments, with an $\text{O}/\text{C} = 0.171$, Tables 6.1. and 6.2. Following a short CH_3COOH plasma exposure (2 min), the spectrum for the PC-TE shows a slight increase in oxygen, corresponding

Table 6.1. wCA and XPS atomic concentrations (%) for PC-TE and Si substrates.

Substrate	Orientation	Treatment Time (min)	wCA (°) ^a	Atomic Concentration (%) ^a			
				Carbon	Oxygen	Silicon	O/C
PC-TE ^b	--	Untreated	97 ± 3	85.0 ± 0.1	14.6 ± 0.1	--	0.171 ± 0.001
PC-TE	Upstream	2	85 ± 5	83.4 ± 0.3	16.6 ± 0.3	--	0.200 ± 0.004
	Downstream	2	95 ± 5	84.4 ± 0.3	15.6 ± 0.3	--	0.185 ± 0.004
PC-TE	Upstream	40	90 ± 3	86.0 ± 0.3	14.0 ± 0.3	--	0.163 ± 0.004
	Downstream	40	95 ± 3	87.4 ± 0.2	12.6 ± 0.2	--	0.145 ± 0.002
Si Wafer	--	40	56 ± 1	74.9 ± 0.2	24.4 ± 0.3	--	0.325 ± 0.004
	Downstream ^c	40	66 ± 5	22.7 ± 0.4	47.1 ± 0.2	28.9 ± 0.5	2.07 ± 0.03

^aError represents one standard deviation of the mean of several measurements.

^bResults reported previously.¹⁸

^cSi wafer was placed immediately downstream from a PC-TE membrane 9 cm downstream.

Table 6.2. High resolution XPS C_{1s} Binding Environments for PC-TE and Si substrates.

Substrate	Orientation	Treatment Time (min)	High resolution C _{1s} moieties (%) ^a				
			C-C/C-H	C-O	C=O	O=C-O	O=C(-O) ₂
PC-TE ^b	Untreated	0	75.6 ± 1.1	16.9 ± 0.9	--	--	7.6 ± 0.2
PC-TE	Upstream	2	76.5 ± 0.2	17.4 ± 0.4	4.00 ± 0.3	1.2 ± 0.3	1.0 ± 0.3
	Downstream	2	76.0 ± 0.3	18.7 ± 0.3	0.4 ± 0.1	--	4.9 ± 0.1
PC-TE	Upstream	40	77.4 ± 0.6	17.1 ± 0.3	3.3 ± 0.1	2.2 ± 0.2	--
	Downstream	40	81.9 ± 0.3	14.9 ± 0.8	1.6 ± 0.6	--	1.7 ± 0.2
Si Wafer	--	40	62.4 ± 0.3	23.1 ± 0.5	9.4 ± 0.7	5.1 ± 0.6	--
	Downstream ^c	40	77.8 ± 0.6	13.9 ± 0.7	6.2 ± 0.7	2.1 ± 0.3	--

^aError represents one standard deviation of the mean of several measurements.

^bResults reported previously.¹⁸

^cSi wafer was placed immediately downstream from a PC-TE membrane, 9 cm downstream from the coil region.

to the appearance of C=O and O-C=O binding environments, although these changes are less pronounced on the downstream side of the membrane. The initial increase in oxygen concentration reverses with extended CH₃COOH plasma exposure, with the O/C ratios on the upstream and downstream sides being slightly less than that for the untreated PC-TE. Concomitantly, we observe the complete disappearance of the O=C(-O)₂ environment, though the distribution of the other CO_x environments remains similar, Figure 6.1.a. Indeed, by 40 min it appears that PC is buried beyond the sampling depth of the XPS experiment. High resolution C_{1s} spectra from the downstream side of the 40 min treatment, still look mostly like PC, Figure 6.1.b. Overall, these results indicate that some film deposition or deep surface modification occurs on the upstream side while the downstream side remains relatively unchanged.

wCAs were measured to determine if the oxygen functionalities being implanted were at the surface or incorporated into the CH₃COOH film. In previous studies, the implantation of polar functional groups increased the wettability of polymer membrane materials.¹⁹⁻²¹ This is also true for water plasma-treated PC-TE which displayed a significant decrease in wCA from 97 ± 3° on the untreated membrane to 38 ± 2° on the treated membrane (upstream facing side).¹⁸ Interestingly, CH₃COOH plasma exposure had little impact on the wCA of PC-TE, Table 6.1. Only short treatment times on the upstream side of PC-TE resulted in any significant change in wCA (85 ± 5°). Indeed, all other wCA measurements on CH₃COOH plasma modified PC-TE are identical to the untreated PC-TE, within experimental error, and these wCA remain stable as sample films age for one month, Figure 6.2. Although coincidental, it appears that the CH₃COOH modified PC-TE and unmodified PC-TE have similar surface energies. Moreover, the oxygen functionalities detected in our XPS experiments are not localized on the surface; they are likely distributed throughout the film.

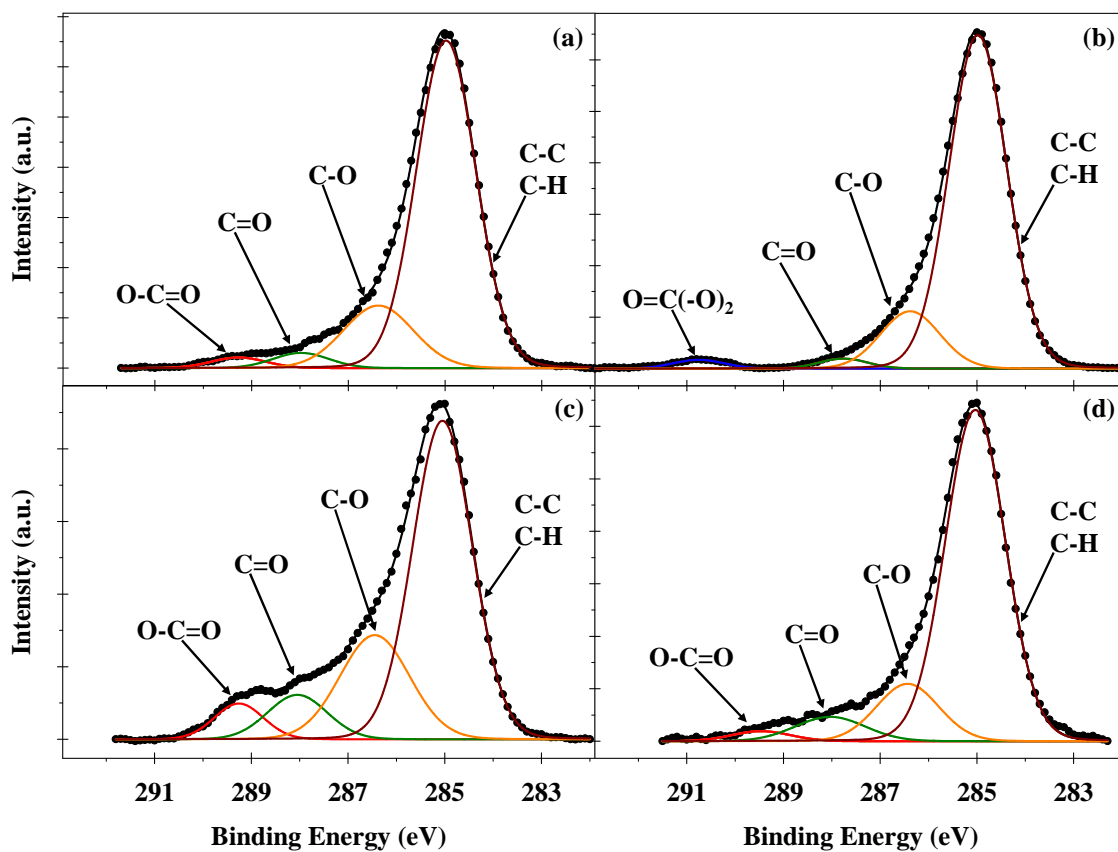


Figure 6.1. High resolution C_{1s} XPS spectra of representative CH_3COOH plasma modified samples ($P = 25$ W, 50 mTorr, 40 min). Spectra shown are for (a) PC-TE upstream side, (b) PC-TE downstream side, (c) Si wafer only, and (d) Si wafer placed downstream of PC-TE membrane.

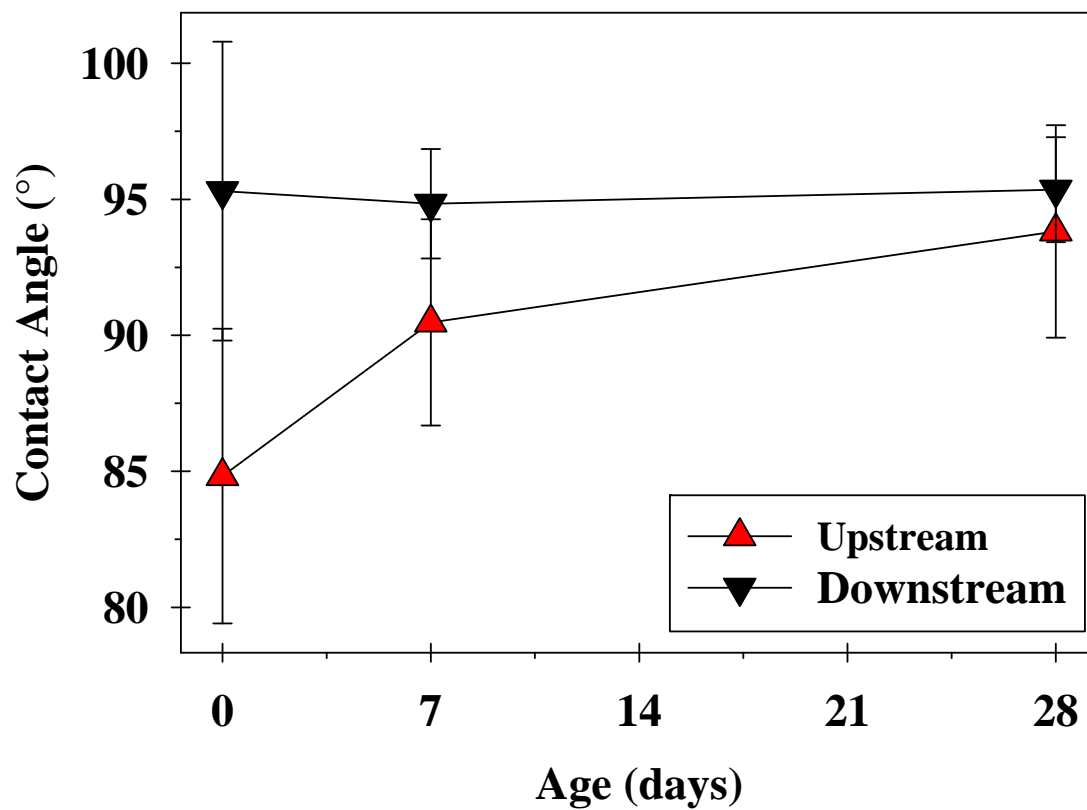


Figure 6.2. wCA measurements on the upstream (red triangles) and downstream (black triangles) sides of CH_3COOH PECVD films on PC-TE as a function of sample age.

Representative SEM images from the shiny side of untreated and CH₃COOH plasma treated PC-TE membranes are shown in Figure 6.3. The untreated membranes are flat with circular or slightly elliptical pore openings, consistent with the manufacturer's specifications, Figure 6.3.a. Following CH₃COOH plasma exposure, the SEM shows the upstream sides of treated PC-TE membranes are nearly indistinguishable from untreated samples. Indeed, samples still have approximately the same pore size with no visible damage after 40 min of CH₃COOH plasma exposure, Figure 6.3.b. Previous work in our laboratories demonstrated that long treatment times (≥ 30 min) using H₂O vapor plasma under similar conditions resulted in significant expansion of the pore openings on PC-TE.¹⁸

To help reconcile our XPS and SEM results, pore radii were measured from SEM images to track changes in the coating thickness as a function of CH₃COOH plasma exposure time, Figure 6.4. Given that film deposition from inductively coupled rf plasmas operating at these conditions is expected to be non-line-of-sight (i.e. it should not exhibit anisotropic behavior),²² the film deposition rate should be equal on the surface as well as the pore walls. Therefore, the pore radius should give us an approximate measure of the deposited film thickness. Linear regression analysis revealed the pore radius decreases at a rate of -0.17 ± 0.12 nm/min on the upstream side of PC-TE, Figure 6.4.a. Interestingly, when the untreated pore radius is not included in this analysis, the decrease in pore radius with increasing exposure time becomes insignificant (-0.08 ± 0.32 nm/min). For comparison, the rates of change in pore radius on the downstream side of PC-TE with and without the untreated pore radius included in the analysis are -0.15 ± 0.09 and -0.06 ± 0.16 nm/min, respectively, Figure 6.4.b. These observations suggest that the film remains quite thin on both upstream and downstream sides. This was expected on

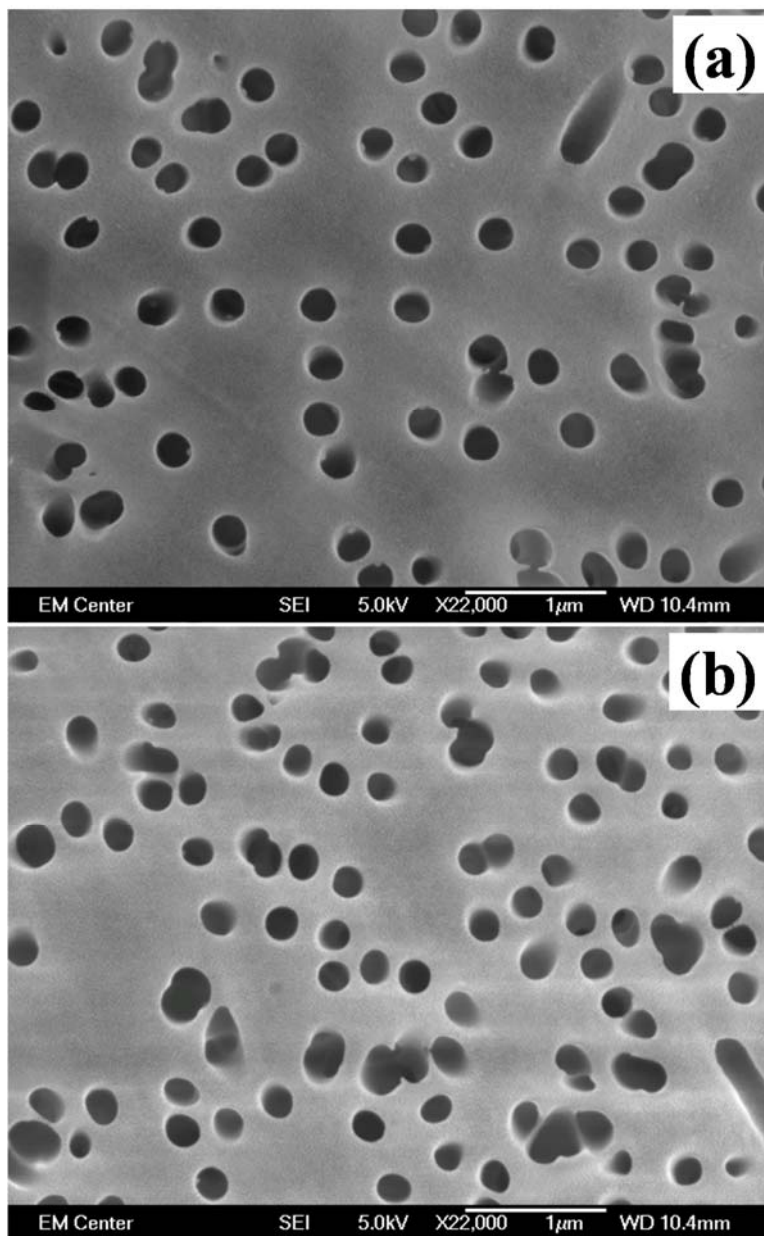


Figure 6.3. SEM images of (a) untreated PC-TE and (b) CH_3COOH plasma modified PC-TE ($P = 25 \text{ W}$, 50 mTorr , 40 min).

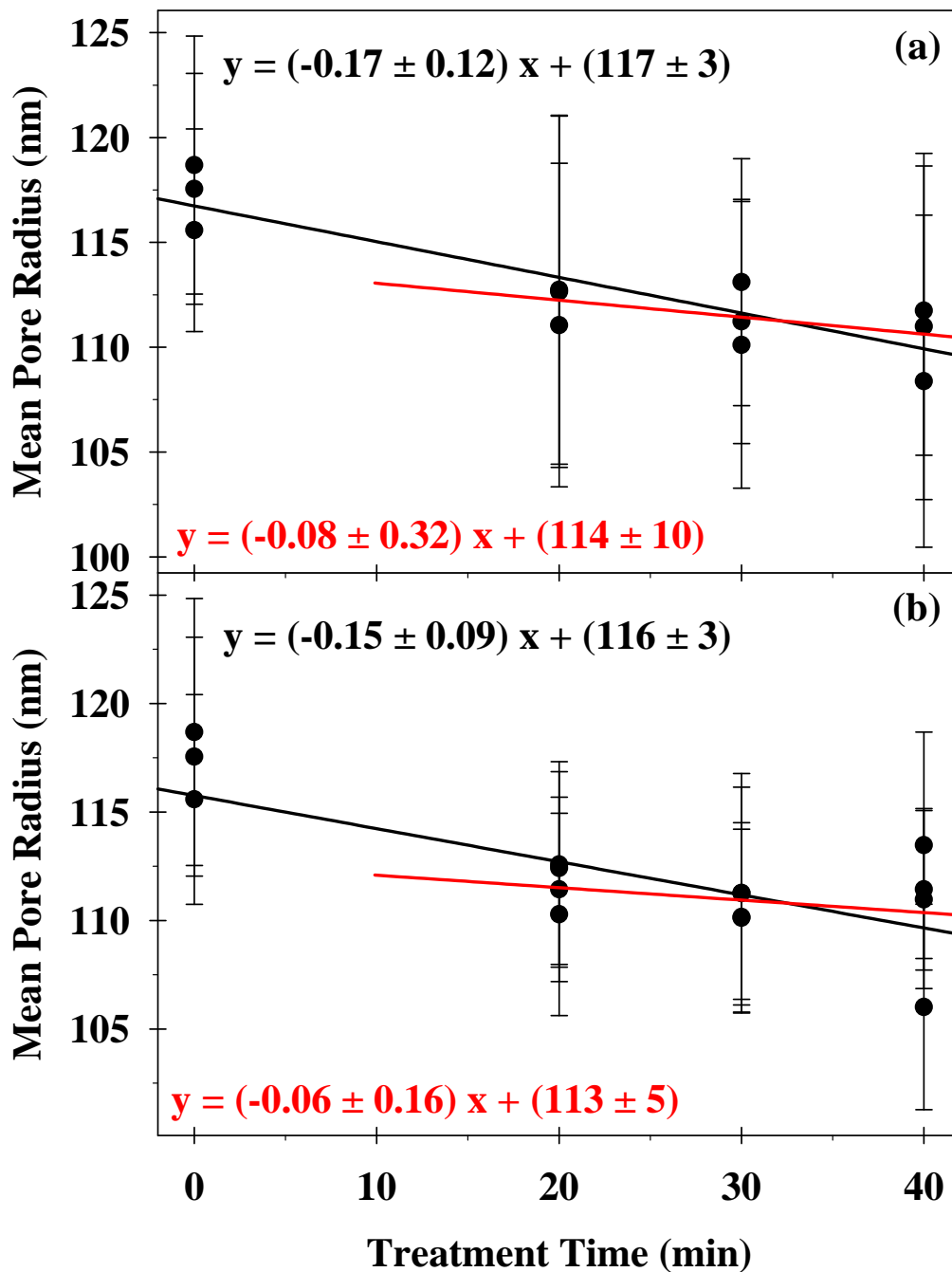


Figure 6.4. (a) Mean pore radius measurements from upstream-facing side of PC-TE membrane and (b) mean pore radius measurements from downstream-facing side of PC-TE membrane. Linear regression analysis was used to determine the deposition rate including the untreated PC-TE as t=0 (black line) and based just the 20-40 min samples time points (red line).

the downstream side where the O=C(-O)₂ environment is persistent. Angle resolved-XPS (AR-XPS) data were collected to potentially identify signals from the underlying PC material on the upstream side of PC-TE following a 40 min CH₃COOH plasma treatment; high resolution spectra collected at 85° were nearly identical to those collected at 45° (Figure 6.1.a) and lacked any trace of the carbonate functional group indicative of PC. The AR-XPS data shows that the CH₃COOH film on the upstream side is of significant thickness although the pore dimensions of PC-TE are unaffected.

6.2.2. CH₃COOH PECVD films on silicon. To further investigate the nature of these CH₃COOH films, we modified Si wafers in CH₃COOH plasmas to perform XPS and ellipsometry experiments without interference from the underlying PC material. Optimization of the Cauchy model for the VASE data from O₂ plasma-cleaned Si wafers treated for 40 min in an CH₃COOH plasma gave a refractive index (n) of 1.51, consistent with the predominantly hydrocarbon film found on the PC-TE using XPS (Figure 6.1.c) and the deposition rate was found to be 0.93 ± 0.08 nm/min, Figure 6.5. Unlike PC membranes, not only is there definitive evidence of film deposition on the Si wafers, but the film deposition rate appears completely linear over the range of times tested. For comparison, were CH₃COOH to deposit at the same rate on PC-TE, we would expect the pore radius to be ~80 nm after 40 min of exposure. Regardless, our AR-XPS results show that this is more than negligible deposition on the upstream PC-TE surface. Ellipsometry measurements on a Si wafer placed immediately downstream from a PC-TE membrane show only negligible film growth (<1 nm), and XPS analysis reveals significant signal from the underlying Si substrate, consistent with the measured film thickness. Based on analysis of the high resolution C1s region, however, we found that the film has a similar composition to the material deposited on the membrane and the unimpeded Si

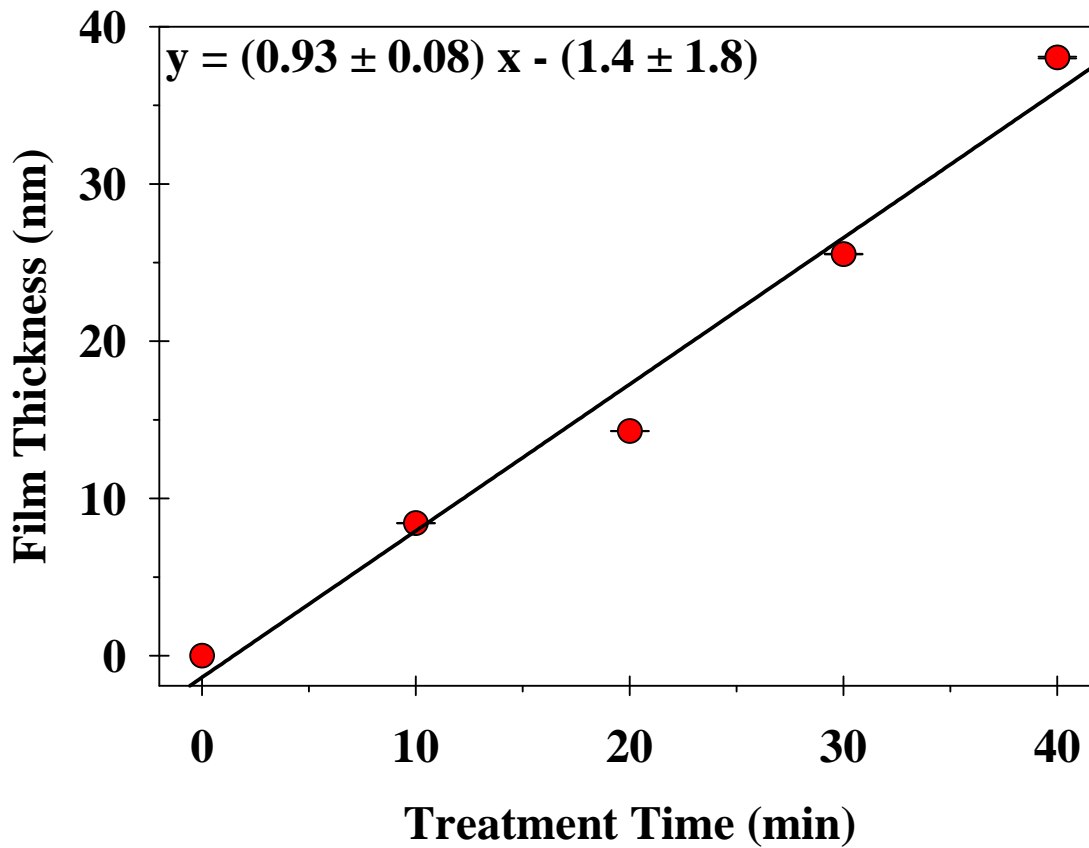


Figure 6.5. CH₃COOH plasma polymer film thickness on Si wafers following CH₃COOH plasma modification as a function of deposition time. Linear regression analysis was used to determine the deposition rate.

wafer, Figure 6.1.d., albeit with different oxygen content. There appears to be little difference in how CH₃COOH plasmas interact with the downstream side of PC-TE and Si wafers when they are isolated from the plasma glow.

6.2.3. CH₃COOH plasma diagnostics. To gain a deeper understanding of how these polycarbonate surface modifications occur, we collected OES spectra 9 cm downstream from the coil region of the plasma reactor, the substrate location used throughout this study, Figure 6.6. The most significant species detected included CO*, OH*, H α , and C₂* (swan band), which have all been observed previously in other plasma systems in our laboratory.^{23,24} Notably, we did not detect any signal from CH*. CH radicals have a high surface reaction probability²⁵ and CH radical density is proportional to deposition rate.²⁶ The lack of signal arising from CH* means that deposition likely follows some type of surface radical initiation mechanism; film formation takes place when the parent CH₃COOH or large dissociation fragments react with radical sites. For example, Coclite and Gleason found that the deposition of organosilicon polymer is initiated at surface radical sites.²⁷ The deposition rate that we observe in our CH₃COOH system is much slower because there is no surface radical propagation mechanism possible to promote deposition. The final material is thus the result of this deposition tempered by competitive etching.

OES also gives us insight into potential etching mechanisms during CH₃COOH plasma processing. In previous studies, we hypothesized that O* was the dominant etchant when present during plasma surface modification of polymers.^{18,28} Interestingly, there is no significant signal from O* under the CH₃COOH plasma conditions studied here. We suspect that atomic oxygen is indeed formed in the CH₃COOH plasma system, but that it is quickly consumed by recombination with carbon containing species to form CO or CO₂. These more stable

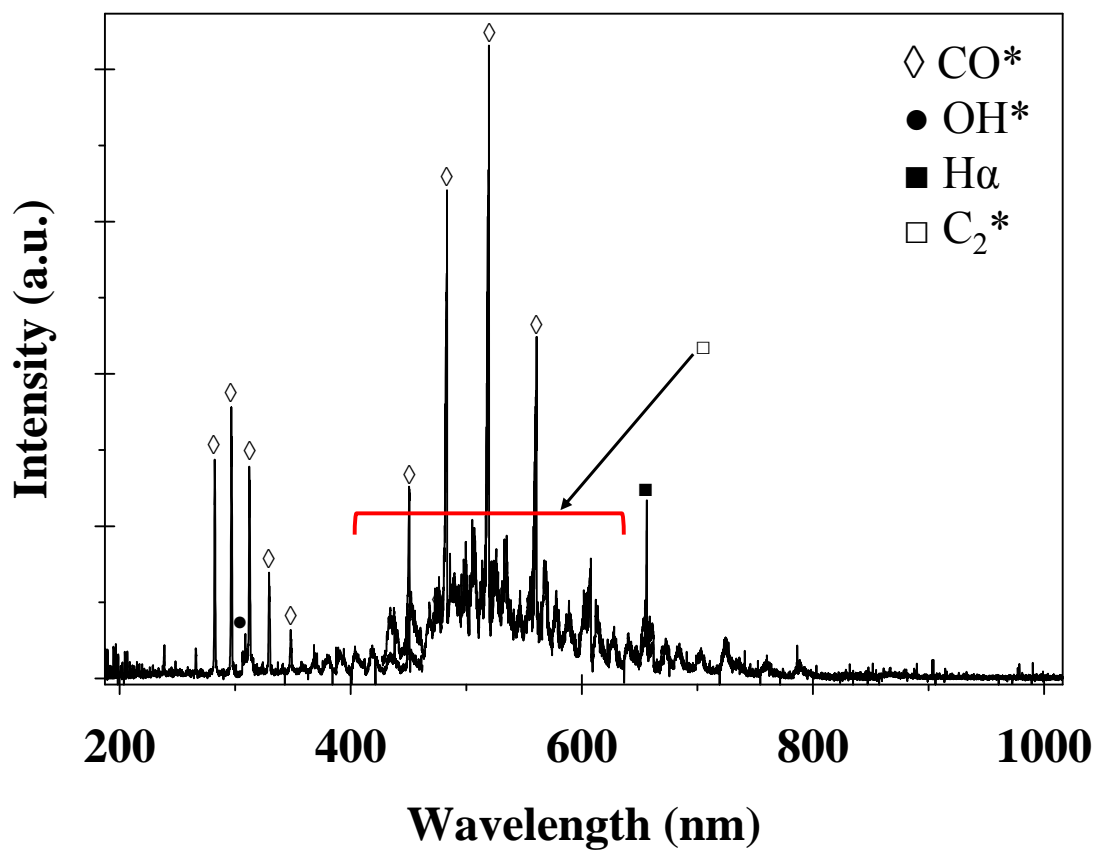


Figure 6.6. Optical emission spectrum of CH₃COOH plasma emission, collected 9 cm downstream from the induction coil region ($P = 25$ W, 50 mTorr).

recombination products are less reactive and do not contribute to ring opening and chain scission mechanisms like atomic oxygen does.¹⁸ By keeping the atomic oxygen density low, etching in this competitive etching/deposition system is suppressed.

Another contributing factor to consider was presented by Coclite and Gleason in their recent work on initiated PECVD for the deposition of organosilicon polymers.²⁷ They found that adsorption of unreacted monomer inhibited film formation, slowing deposition rates below a substrate temperature threshold that depended on monomer flow rate. Based on the pressure and flow behavior of CH₃COOH in our reactor systems, we suspect a large quantity of CH₃COOH condenses on the PC-TE and reactor walls. This thin film of CH₃COOH is displaced somewhat when higher energy species from the plasma impact the surface, allowing slow film formation but preventing significant damage (etching). This same mechanism provides a larger degree of protection to the downstream facing side and helps explain why only negligible deposition was observed on downstream PC-TE and Si wafer experiments. The density of high energy species is insufficient to displace the adsorbed CH₃COOH film and film formation is prevented.

6.3. Summary

Our goal with this work was to present a new method for introducing a carbon based interlayer coating onto the surface of a structured/patterned/3-D PC materials using CH₃COOH plasma surface modification without significantly altering the dimensions of that material. We were able to modify the surface of our model PC-TE material, yielding a film composed of C-C/C-H, C=O and O-C=O binding environments and a surface energy comparable to the original PC surface. A careful study of deposition rate on the PC-TE revealed that only a negligible change in pore radius accompanies film deposition. Our comparison to CH₃COOH plasma

polymer films on Si wafers shows that the CH₃COOH plasma system has unique behavior with respect to PC materials, thereby providing a relatively straightforward method for modifying PC materials without disrupting micro- or nano-structured surfaces. Continuing studies in our laboratory will seek to test abrasion resistance and adhesion strength of a model coating system commonly used for optical and biomedical applications (i.e. plasma deposited *a*-C_xO_yH_z) on CH₃COOH plasma modified polycarbonate.

REFERENCES

1. Nuutinen, T.; Silvennoinen, M.; Päiväsaari, K.; Vahimaa, P., Control of cultured human cells with femtosecond laser ablated patterns on steel and plastic surfaces. *Biomed. Microdevices* **2013**, *15*, 279-288.
2. Reynolds, P. M.; Pedersen, R. H.; Riehle, M. O.; Gadegaard, N., A dual gradient assay for the parametric analysis of cell-surface interactions. *Small* **2012**, *8*, (16), 2541-2547.
3. Spohr, R.; Sharma, G.; Forsberg, P.; Karlsson, M.; Hallén, A., Stroke asymmetry of tilted superhydrophobic ion track textures. *Langmuir* **2010**, *26*, (9), 6790-6796.
4. Palumbo, F.; Di Mundo, R.; Cappelluti, D.; d'Agostino, R., Superhydrophobic and superhydrophilic polycarbonate by tailoring chemistry and nano-texture with plasma processing. *Plasma Processes Polym.* **2011**, *8*, (2), 118-126.
5. Saarikoski, I.; Suvanto, M.; Pakkanen, T., Modification of polycarbonate surface properties by nano-, micro-, and hierarchical micro–nanostructuring. *Appl. Surf. Sci.* **2009**, *255*, (22), 9000-9005.
6. Di Mundo, R.; Troia, M.; Palumbo, F.; Trotta, M.; d'Agostino, R., Nano-texturing of transparent polymers with plasma etching: tailoring topography for a low reflectivity. *Plasma Processes Polym.* **2012**, *9*, (10), 947-954.
7. Chivatanasontorn, V.; Tsukise, S.; Kotaki, M., Surface texture effect on scratch behavior of injection molded plastics. *Polym. Eng. Sci.* **2012**, *52*, (9), 1862-1867.
8. Muir, W.; Arthur, S.; Thissen, H.; Simon, G.; Griesser, H.; Castner, D., Effects of oxygen plasma treatment on the surface of bisphenol A polycarbonate: a study using SIMS, principal component analysis, ellipsometry, XPS and AFM nanoindentation. *Surf. Interface Anal.* **2006**, *38*, (8), 1186-1197.
9. Gururaj, T.; Subasri, R.; Raju, K. R. C. S.; Padmanabham, G.; Raju, K., Effect of plasma pretreatment on adhesion and mechanical properties of UV-curable coatings on plastics. *Appl. Surf. Sci.* **2011**, *257*, (9), 4360-4364.
10. Panwar, A.; Barthwal, S.; Ray, S., Aging and annealing behavior of polycarbonate surfaces modified by direct-current glow discharge in air. *J. Appl. Polym. Sci.* **2009**, *112*, (2), 700-708.
11. Muir, B.; Thissen, H.; Simon, G.; Murphy, P.; Griesser, H., Factors affecting the adhesion of microwave plasma deposited siloxane films on polycarbonate. *Thin Solid Films* **2006**, *500*, (1-2), 34-40.
12. Baytekin, H. T.; Wirth, T.; Gross, T.; Treu, D.; Sahre, M.; Theisen, J.; Schmidt, M.; Unger, W. E. S., Determination of wettability of surface-modified hot-embossed

- polycarbonate wafers used in microfluidic device fabrication via XPS and ToF-SIMS. *Surf. Interface Anal.* **2008**, 40, (3-4), 358-363.
13. Hofrichter, A.; Bulkin, P.; Drevillon, B., An interfacial study of a hydrogenated carbon interlayer for adhesion enhancement of plasma deposited silica thin films on polycarbonate. *J. Adhes. Sci. Technol.* **2002**, 16, (4), 395-407.
 14. Hall, C.; Murphy, P.; Griesser, H., Etching and deposition mechanism of an alcohol plasma on polycarbonate and poly(methyl methacrylate): an adhesion promotion mechanism for plasma deposited a:SiO_xC_yH_z Coating. *Plasma Processes Polym.* **2012**, 9, (9), 855-865.
 15. Tompkins, B. D.; Dennison, J. M.; Fisher, E. R., Etching and post-treatment surface stability of track-etched polycarbonate membranes by plasma processing using various related oxidizing plasma systems. *Plasma Processes Polym.* Submitted.
 16. Li, N.; Yu, S.; Harrell, C.; Martin, C., Conical nanopore membranes. Preparation and transport properties. *Anal. Chem.* **2004**, 76, (7), 2025-2030.
 17. Anzawa, E.; Kral, M.; Ogino, A.; Nagatsu, M., Improvement of hydrophilicity of polymer surface by surface-wave excited Ar plasma with acetic acid. *Electr. Eng. Jpn.* **2011**, 176, (4), 1-6.
 18. Tompkins, B. D.; Dennison, J. M.; Fisher, E. R., H₂O plasma modification of track-etched polymer membranes for increased wettability and improved performance. *J. Membr. Sci.* **2013**, 428, 576-588.
 19. Kull, K. R.; Steen, M. L.; Fisher, E. R., Surface modification with nitrogen-containing plasmas to produce hydrophilic, low-fouling membranes. *J. Membr. Sci.* **2005**, 246, (2), 203-215.
 20. Steen, M. L.; Hymas, L.; Havey, E. D.; Capps, N. E.; Castner, D. G.; Fisher, E. R., Low temperature plasma treatment of asymmetric polysulfone membranes for permanent hydrophilic surface modification. *J. Membr. Sci.* **2001**, 188, (1), 97-114.
 21. Wavhal, D. S.; Fisher, E. R., Hydrophilic modification of polyethersulfone membranes by low temperature plasma-induced graft polymerization. *J. Membr. Sci.* **2002**, 209, (1), 255-269.
 22. Takenaka, K.; Shiratani, M.; Takeshita, M.; Kita, M.; Koga, K.; Watanabe, Y., Control of deposition profile of copper for large-scale integration (LSI) interconnects by plasma chemical vapor deposition. *Pure Appl. Chem.* **2005**, 77, (2), 391-398.
 23. Liu, D. P.; Zhou, J.; Fisher, E. R., Correlation of gas-phase composition with film properties in the plasma-enhanced chemical vapor deposition of hydrogenated amorphous carbon nitride films. *J. Appl. Phys.* **2007**, 101, (2), 023304.

24. Steen, M. L.; Jordan, A. C.; Fisher, E. R., Hydrophilic modification of polymeric membranes by low temperature H₂O plasma treatment. *J. Membr. Sci.* **2002**, 204, (1–2), 341-357.
25. Liu, D. P.; Cuddy, M. F.; Fisher, E. R., Comparison of CH, C₃, CHF, and CF₂ surface reactivities during plasma-enhanced chemical vapor deposition of fluorocarbon films. *ACS Appl. Mater. Interfaces* **2009**, 1, (4), 934-943.
26. Pastol, A.; Catherine, Y., Optical emission spectroscopy for diagnostic and monitoring of CH₄ plasmas used for a-C:H deposition. *J. Phys. D: Appl. Phys.* **1990**, 23, 799-805.
27. Coclite, A. M.; Gleason, K. K., Initiated PECVD of organosilicon coatings: a new strategy to enhance monomer structure retention. *Plasma Processes Polym.* **2012**, 9, (4), 425-434.
28. Steen, M. L.; Butoi, C. I.; Fisher, E. R., Identification of gas-phase reactive species and chemical mechanisms occurring at plasma–polymer surface interfaces. *Langmuir* **2001**, 17, (26), 8156-8166.

CHAPTER 7

PLASMA SYNTHESIS OF HYDROCARBON/FLUOROCARBON THIN FILMS WITH COMPOSITIONAL GRADIENTS

This chapter is based on work published under the same title in *Plasma Processes and Polymers*, written by Brendan D. Tompkins and Ellen R. Fisher.¹ The text, figures, and tables from this publication are reproduced here with permission from John Wiley & Sons (License Number: 3207910564427, August 14th, 2013). The original publication and this chapter describe how PECVD was used to synthesize hydrocarbon/fluorocarbon thin films with compositional gradients by continuously changing the ratio of gases in a C₃F₈/H₂ plasma. Surface and bulk film analysis techniques were used to elucidate the deposition mechanism and develop a model that accurately predicts film thickness. Funding for this work was provided by the National Science Foundation (CHE-0911248).

7.1. Introduction

Graded or gradient materials, structures designed with a stepwise or continuous change in composition or structure in one or more dimensions, have become the subject of intense research interest for a number of applications, including biomedical devices,² biomimetic materials,^{3,4} release coatings,⁵ adhesion interlayers,^{6,7} and optical materials.⁸ Having a gradient composition or structure can significantly reduce internal stress and improve material compatibility at the interface between two materials or direct the interactions of another substance on a gradient surface. Polymer scaffolds with functional gradients also show promise in controlling the transport properties critical for successful tissue growth.⁹ Although gradient structures and

surfaces can be achieved using different methods, they all address some important issues in modern materials fabrication. Here, we review some of the key results for gradient films from the literature to set the stage for the current studies.

Fabrication of bulk materials and thin films with a gradient composition has the potential to produce highly tailorable materials. Most studies of compositional materials have focused on gradient materials wherein some property gradually changes laterally across a surface. For example, Albert et al.¹⁰ explored vapor deposition of various silane precursors to form lateral composition and surface energy gradients on silicon with cm length scales. In contrast, there are far fewer reports of gradients formed with respect to depth in a bulk material or film. Karabanova et al.¹¹ studied gradients formed in semi-interpenetrating networks of polyurethane and poly(2-hydroxyethyl methacrylate) (pHEMA) and found the gradients consisted of nano-domains of one polymer or the other, depending on their location within the inter-penetrating layer. Although these gradient polymer materials showed some unique and promising properties, the nature of the inter-penetrating gradient layer depends on the thermodynamics of mixing between the two polymers and will, therefore, be limited in terms of tunability. Gleason and coworkers¹² prepared gradient films from HEMA and pentafluorophenylmethacrylate (PFM) using photo initiated chemical vapor deposition (piCVD) by introducing a constant flow of PFM during the final stage of pHEMA film formation. In this work, the authors suggest that the fabrication of arbitrary structures is possible using their technique but they stop short of a demonstration.

Plasma-enhanced chemical vapor deposition (PECVD) is widely used for producing thin films with a wide range of chemistries. Fluorocarbon (FC) thin films have become one of the most popular materials produced via PECVD as they are used in a variety of material surface

modifications, including low-k dielectric layers,¹³ corrosion inhibiting barrier films,^{7, 14, 15} and durable low friction coatings.¹⁶ Notably, the precise conditions used during FC film deposition can have a large impact on the final properties of the material. Indeed, factors such as monomer choice, plasma power, and reactor pressure can result in radically different properties, allowing the film to be “tuned” to the specific application. Typical films are thin, conformal, and defect free, along with being relatively inert and having a low surface energy. Despite the high tunability of plasma processes, few studies have explored formation of graded structures within PECVD films. Peri et al.¹⁷ examined variations in cross-linking density with depth in plasma polymerized octafluorocyclobutane films using x-ray and neutron reflectivity. They found that a region of gradient chemical composition and cross-link density always forms at the substrate-film interface. Changing applied power and monomer inlet location also resulted in a region of gradient cross-link density at the film-air interface.

Another study of plasma modification of glycidyl ether of bisphenol A polymer (SU-8) using CF₄ and CF₄/H₂ plasmas focused on decreasing optical losses in SU-8 optical waveguides for telecommunications.⁸ Angle resolved XPS revealed plasma modification resulted in the implantation of a concentration gradient of atomic fluorine. By extrapolating these results, the fluorinated layer was estimated to be 504 Å thick. Overall, they found that by incorporating a fluorine gradient into the SU-8 surface using CF₄/H₂ plasmas, optical losses could be reduced by up to 60% compared with the unmodified polymer. This modification technique is, however, limited by the ability of reactive species to penetrate or diffuse into an existing polymer network. Further improvements might be realized by fabricating the gradient material such that composition and structure can be tuned at will to form arbitrary structures. Indeed, there have been very few reports that examine this approach to thin film fabrication.

Two additional studies are worth noting here as they explored the deposition of mixed hydrocarbon (HC)/FC films. First, Srividya et al.⁷ studied the deposition of various mixtures of C₂F₆, hexafluoroacetone, and acetylene, to be used as barrier coatings on 301 stainless steel. To limit film incompatibility and promote adhesion, they deposited polysilicon and amorphous HC layers to act as adhesion interlayers for the FC film. They found that higher FC content in the monomer feed led to higher fluorine content in the film and ultimately better corrosion resistance. Second, Tanaka and Kogoma⁵ reported the preparation of release coatings on polyethylene terephthalate consisting of a graded plasma-copolymer film prepared using an atmospheric pressure dielectric barrier discharge reactor. Fabricating films by stepwise deposition of various mixtures of hexafluoropropylene and ethylene, they found that starting at a high proportion of HC and ending with a high proportion of FC resulted in materials with high integrity.

The primary goal of the present study was to demonstrate that by continuously changing the ratio of gases in C₃F₈/H₂ plasmas we could fabricate gradient films. Previous work in our laboratories demonstrated that PECVD performed with CF₄/H₂ and C₂F₆/H₂ mixtures resulted in films with different compositions depending on the ratio used.¹⁸ Generally, higher ratios of FC monomer resulted in a plasma polymer with higher fluorine content and higher ratios of H₂ resulted in a more HC-like plasma polymer. Here, we extend this to C₃F₈/H₂ plasmas and investigate how film properties change with precursor gas ratio. We have designed a proof-of-concept system capable of depositing continuous gradient mixed films composed of amorphous HC and FC from C₃F₈/H₂ plasmas. Through the use of a home-built control system, we can prepare nearly any film composition using a pre-determined deposition program. Film chemistry and morphology were characterized by FTIR, XPS, water contact angle (wCA) and SEM, and

the gas phase composition of the plasma was explored using time-resolved optical emission spectroscopy (TR-OES). These analyses have elucidated film deposition mechanisms and a model to predict the overall deposition thickness.

7.2. Results

7.2.1. Analysis of homogeneous films from a static C₃F₈/H₂ PE-CVD system. The aim of this study was to demonstrate the fabrication of graded plasma polymer films with a continuously varying composition of amorphous fluorocarbon (*a*-CF) and amorphous hydrocarbon (*a*-CH). Understanding how regions of specific functionality are confined within a growing plasma polymer film presents a complex materials analysis problem. Although many techniques allow examination of bulk film properties (i.e. FTIR) or the film surface (i.e. wCA and XPS), analysis of specific layers within a graded composition film using those same techniques is more problematic. To address this, we initially studied a series of homogeneous plasma polymerized films prepared from various static C₃F₈/H₂ mixtures. Results from these experiments could then be used to predict the composition of films deposited from a system wherein the C₃F₈/H₂ ratio is changing over the course of the deposition.

Figure 7.1. shows FTIR spectra from a series of homogeneous films deposited on freshly pressed KBr pellets from various static C₃F₈/H₂ mixtures. These data allow identification of signals from *a*-CH or *a*-CF materials and evaluation of whether a film is more HC or FC-like. Although each sample was prepared from a mixture of C₃F₈ and H₂, for clarity, they will be referred to by the % C₃F₈ used during deposition. IR absorption peak identifications were made based on a study of similar films reported previously.¹⁸ The film deposited using 80% C₃F₈ is dominated by a broad peak at $\nu = 1224 \text{ cm}^{-1}$, consistent with the asymmetric stretching of CF₂

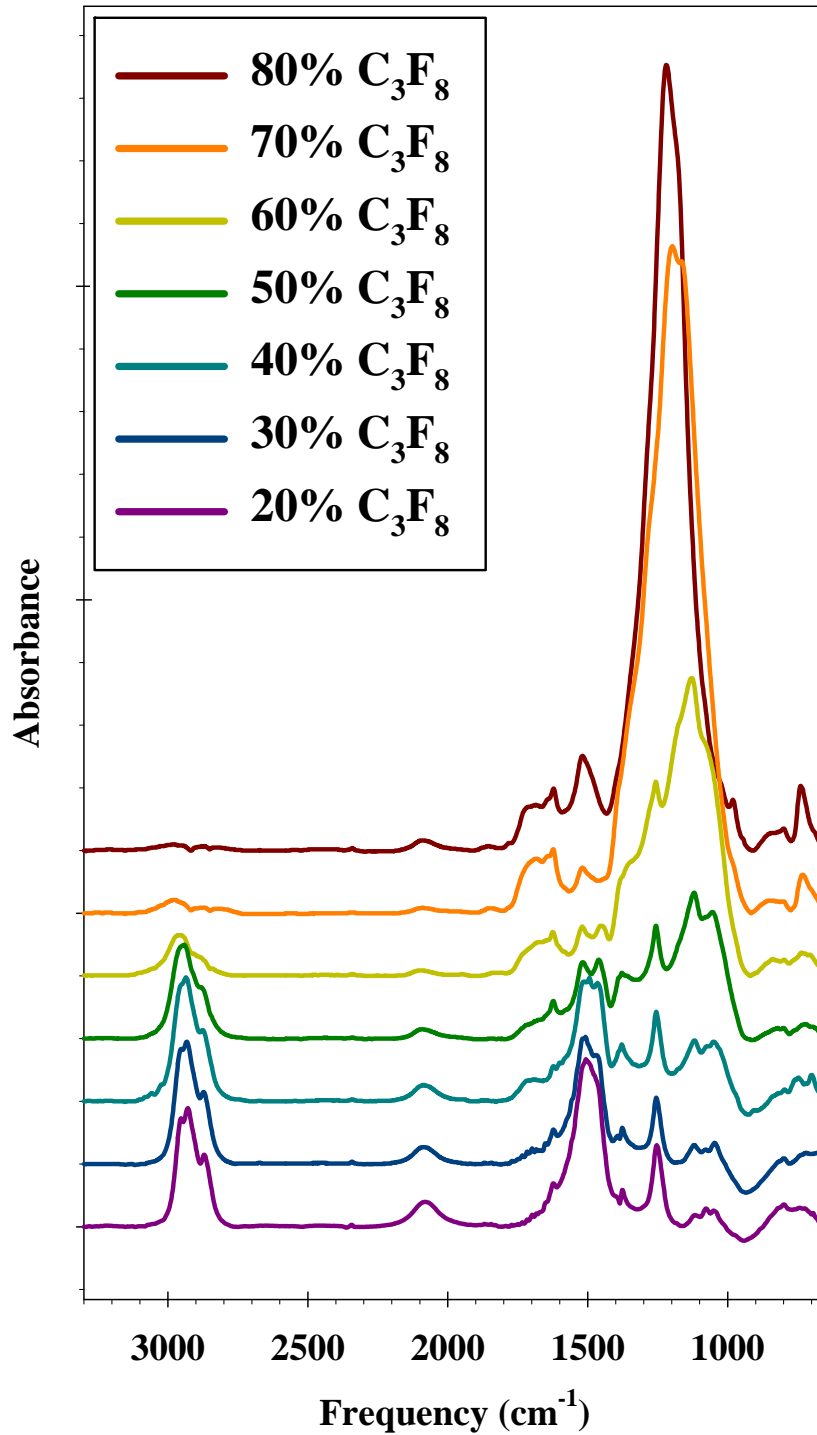


Figure 7.1. Transmission FTIR spectra from homogeneous HC/FC films deposited from static C_3F_8/H_2 ratios. All films were deposited with a 20 min deposition time.

groups. The shape of this peak is typical for plasma polymerized films where the random construction of the amorphous polymer film causes CF₂ moieties to exist in a wide variety of chemical environments, leading to a broad CF₂ stretching band. In contrast, only a faint peak exists at $\nu = 3000\text{-}2800\text{ cm}^{-1}$, the region where signals from CH stretching in HC moieties would be observed. Spectra from films deposited using lower concentrations of C₃F₈ have a progressively less intense CF₂ stretching absorption and the CH stretch peaks become far more prominent. Indeed, the film deposited using 20% C₃F₈ has very little CF₂ signal. These results show a wide range of film compositions, consisting of varying amounts of CH- and CF-type functionalities depending on the C₃F₈/H₂ mixture used.

Figure 7.2. contains elemental composition data as well as wCAs for films deposited using a static ratio of feed gases. Overall, elemental composition measurements, Figure 7.2.a., are consistent with FTIR spectra shown in Figure 7.1. The atomic concentration of carbon far exceeds that of fluorine ($84.1 \pm 0.3\%$ C and $8.0 \pm 0.3\%$ F) in surfaces of films deposited using 20% C₃F₈, indicating a predominantly *a*-CH material is deposited. Incremental increases in FC in the feed result in corresponding increases in fluorine content in the deposited films. Films deposited using 80% C₃F₈ comprise $42.7 \pm 0.1\%$ C and $57.3 \pm 0.1\%$ F, consistent with a predominantly *a*-CF material. For comparison, a film prepared using 100% C₃F₈ comprises $38.4 \pm 0.1\%$ C and $61.6 \pm 0.1\%$ F. Although XPS does not probe hydrogen incorporation directly, we believe that more fluorine atoms in these films are replaced by hydrogen as the % H₂ in the feed increases. This hypothesis is supported by our FTIR results. Note that at high H₂ content in the feed, we observe the incorporation of oxygen and nitrogen in the films, likely as a result of reactions that occur upon exposure to atmosphere. Although we passivate our films after

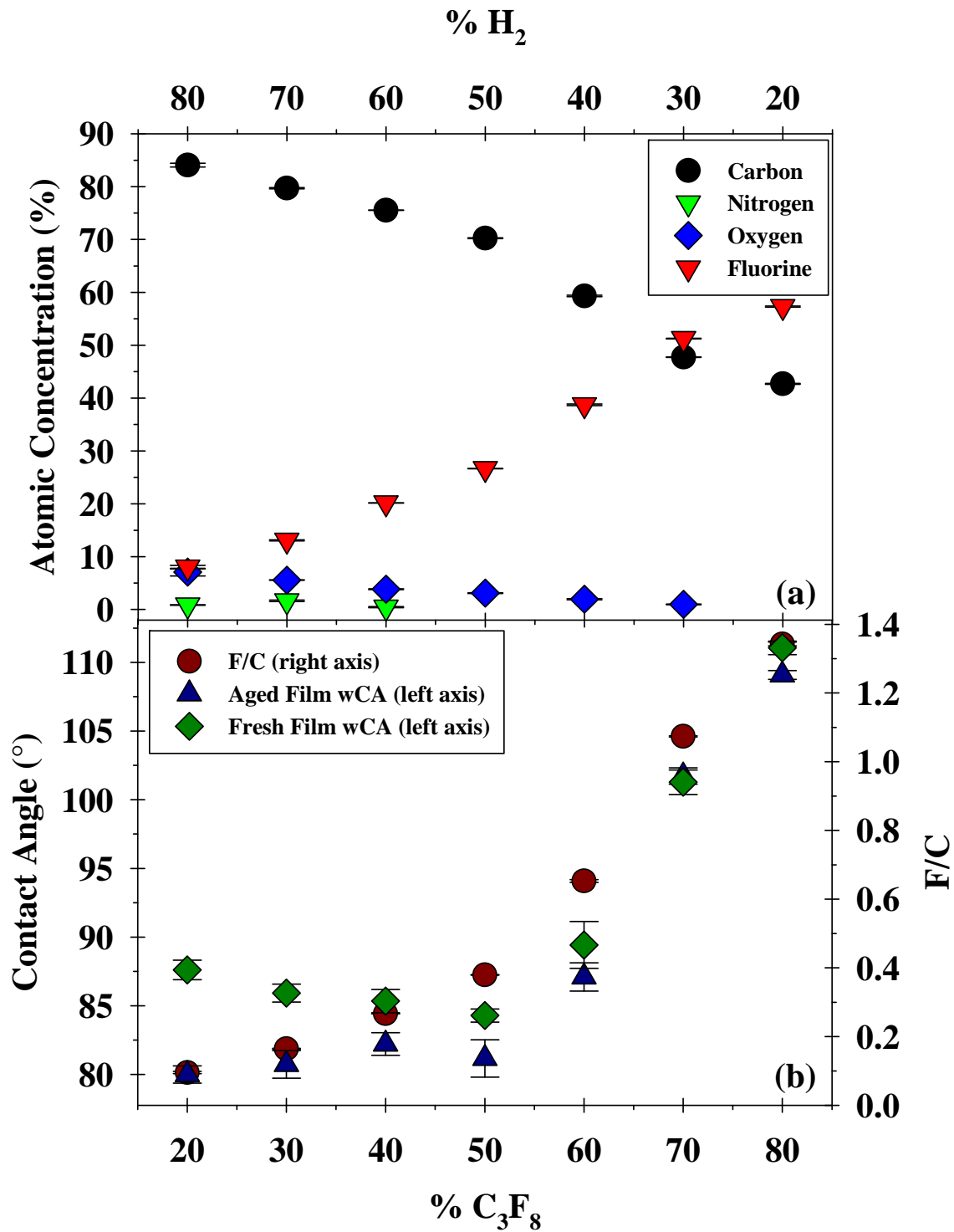


Figure 7.2. (a) Elemental composition and (b) wCA and F/C ratio of homogeneous HC/FC films as a function of % C_3F_8 in the gas feed. Samples were deposited on silicon [100] wafers using a 10 min deposition time from plasmas containing constant ratios of C_3F_8 and H_2 .

deposition by leaving them in the feed gas for 5 min with no plasma, this approach becomes less effective as the *a*-CH content in the film increases.

wCA measurements examine how the outermost surface of a film behaves as a function of the feed gas composition. As the fluorine content of a polymer film increases, there is generally a concomitant increase in the wCA. Indeed, this is what we find for films deposited over a range of C₃F₈/H₂ compositions, Figure 7.2.b. For freshly deposited films, the wCAs are 88° and 111° using 20% and 80% C₃F₈, respectively. For comparison, the wCA of films deposited in the same reactor system using 100% C₃F₈ is 115°. Figure 7.2.b. also includes the F/C calculated from the XPS elemental composition results, which tracks nearly directly with the wCA changes. Interestingly, although the lowest F/C ratio occurs at 20% C₃F₈, the minimum wCA is measured on films deposited using 50% C₃F₈. This is likely due to subtle differences in the packing efficiency of reactive species as they attach to the growing plasma polymer film.¹⁹

To further investigate the stability of these films, wCAs were measured on a separate set of samples that were aged for two weeks, Figure 7.2.b. The wCAs of films deposited using 80% C₃F₈ are nearly identical to their freshly deposited counterparts, whereas aged films deposited from 20% C₃F₈ show a significantly lower wCA (80°). The error was less than ±1.8° for all wCA measurements reported in this chapter. Although surface rearrangements could cause this decrease with the latter samples, samples prepared from 50% C₃F₈ also exhibit a lower wCA with aging, despite the fresh film having the lowest surface energy of all the films. It is far more likely that atmospheric gases are responsible for oxidizing the surface as supported by elemental composition measured using XPS. Films prepared from low C₃F₈ feed gas ratios have a more reactive surface, leading to incorporation of polar functional groups during aging, and ultimately resulting in lower wCA for aged samples.

The high resolution C_{1s} spectra were fit to determine the relative contribution of various carbon binding environments [CF_3 , CF_2 , $O=C-O$, $CF-CF$, $CF-C$, $C=O$, $C-CF$, $C-O$, $C-C(C-H)$] based on our previous work¹⁹⁻²¹ and other literature sources²². Although $CF-CF$, $CF-C$, and $C-CF$ may exist as a continuum and could be fit in a number of ways, we fit each as a separate binding environment to better characterize the distribution amongst these binding environments. Optimization was performed using a number of constraints. The peak full width at half maximum (FWHM) values were limited to ≤ 1.8 eV and a 94/6 Gaussian/Lorentzian peak shape was used. Initially, the relative peak positions were fixed but this gave poor fitting results. Thus, peak positions were allowed to shift while fitting the first spectrum from a given sample. The final peak positions were then verified by using those relative positions to fit the other C_{1s} spectra collected from different spots on the same sample. Each fit spectrum was shifted so that the binding energy (BE) of the aliphatic carbon component was 285.0 eV.

Figure 7.3. shows high resolution C_{1s} XPS spectra from select films prepared using static H_2/C_3F_8 ratios, along with the deconstructed fits to the spectra. When there is only 20% C_3F_8 in the feed gas, the film surface is dominated by aliphatic carbon ($C-C/C-H$) binding environments with a relatively small contribution from fluorinated and oxidized carbon binding environments, Figure 7.3.a. Here, it is difficult to tell exactly how fluorine and oxygen are incorporated because of the severe overlap of their binding energies. The fluorinated carbon binding environments become more prominent in films deposited from an equal mixture of C_3F_8 and H_2 , Figure 7.3.b. This spectrum was fit using six different chemical environments corresponding to carbon with various degrees of fluorination. Although this film still has a large contribution from the hydrocarbon ($C-C/C-H$) binding environment, there are also strong contributions from CF_2 and CF_3 . This is consistent with a mixed film composition wherein both *a*-CF and *a*-CH

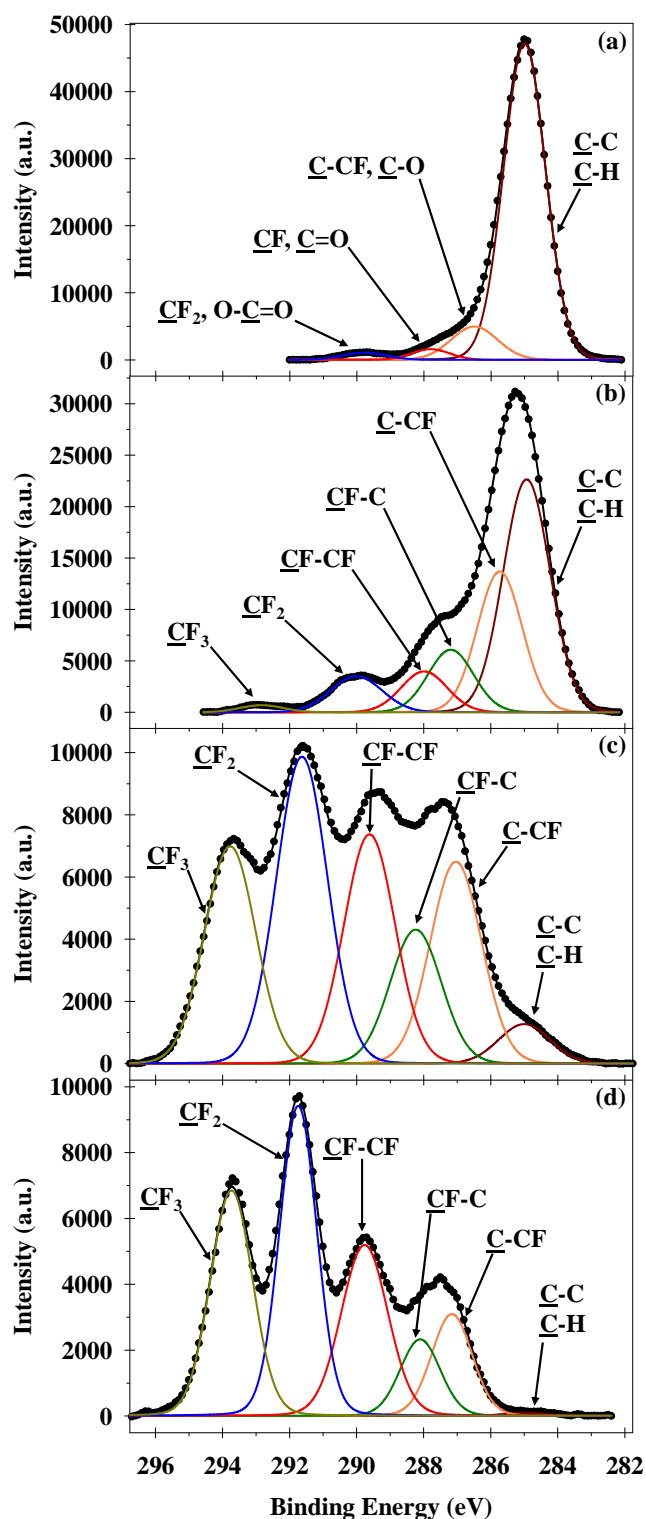


Figure 7.3. High resolution XPS C_{1s} spectra of homogeneous HC/FC films deposited using (a) 20/80, (b) 50/50, and (c) 80/20 C_3F_8/H_2 gas ratios, along with deconstructed fits showing the relative contribution of the various C_{1s} binding environments. Samples were prepared on silicon [100] wafers using a 10 min deposition time.

moieties are present. The trace amount of oxygen in this sample was not considered in the fitting because of the minor impact it would have on the overall spectrum.

Films deposited from 80% C₃F₈ are almost entirely *a*-CF in nature, Figure 7.3.c. The composition is dominated by fluorinated binding environments, primarily CF₂ and CF₃, with only a small contribution from C-C/C-H. We suspect that lower order fluorocarbon environments arise from cross-linking in the film. The high resolution C_{1s} spectrum of a film prepared from 100% C₃F₈ demonstrates this point, Figure 7.3.d. Less cross-linking causes a significant decrease in the contribution from lower order fluorocarbon binding environments. There is also a concomitant decrease in the CF₂ and CF₃ FWHM that comes from a more consistent local chemical environment. A more detailed analysis of the relative contributions from high resolution C_{1s} moieties can be found in Table 7.1.

One interesting aspect of our analysis of high resolution XPS spectra is the impact that changing film composition has on the BE of specific FC binding environments. Figure 7.4. contains overlaid high resolution C_{1s} spectra from a series of films wherein the gas composition was incrementally changed from 20% to 80% C₃F₈. The effect of increasing fluorine content is clearly seen in the BE of the CF₂ and CF₃ film components. Films prepared using 20% C₃F₈ have a small contribution from CF₂ at 289.7 eV. This is an exceptionally low BE given that a film composed entirely of CF₂ units (i.e. Teflon®) is expected to have a CF₂ BE of 292.0 eV. Films prepared from 80% C₃F₈ have a CF₂ BE of 291.6 eV, consistent with the *a*-CF material formed under these conditions. For comparison, a film prepared using 100% C₃F₈ in the same reactor system has a CF₂ BE of 291.7 eV. These differences in BE will be considered further in section 7.3.1.

Table 7.1. XPS surface composition of homogeneous films deposited from different static C₃F₈/H₂ mixtures and pure C₃F₈.

C ₃ F ₈ :H ₂	High Resolution C _{1s} Moieties [%] ^{a)}					
	C-C/C-H	<u>C</u> -CF/C-O	CF/C=O	<u>CF</u> -CF	CF ₂ /O- <u>C</u> =O	CF ₃
20:80 ^{b)}	85.0 ± 0.5	10.4 ± 0.5	2.4 ± 0.3	–	2.1 ± 0.3	–
30:70 ^{b)}	78.1 ± 0.5	12.7 ± 0.2	3.9 ± 0.1	–	3.2 ± 0.1	–
40:60	61.5 ± 1.7	18.1 ± 2.0	10.9 ± 0.5	3.7 ± 0.2	5.4 ± 0.1	0.5 ± 0.1
50:50	47.9 ± 2.9	23.8 ± 2.4	11.7 ± 0.5	7.6 ± 0.3	7.6 ± 0.2	1.3 ± 0.1
60:40	18.5 ± 0.9	34.8 ± 0.9	15.4 ± 0.2	13.2 ± 0.3	14.2 ± 0.1	3.9 ± 0.1 ^{c)}
70:30	5.7 ± 0.1	24.0 ± 0.2	15.3 ± 0.1	20.8 ± 0.1	22.2 ± 0.2	12.0 ± 0.2
80:20	3.5 ± 0.1	19.0 ± 1.4	10.2 ± 2.4	21.4 ± 1.6	26.9 ± 0.6	19.0 ± 0.3
100:0	0.3 ± 0.1	11.3 ± 0.2	8.8 ± 0.5	21.6 ± 0.3	32.0 ± 0.3	26.0 ± 0.2

^{a)}Unless otherwise indicated, reported error represents one standard deviation of the mean;

^{b)}Samples have significant contributions from carbon oxygen binding environments based on elemental composition; ^{c)}Error is two standard deviations of the mean.

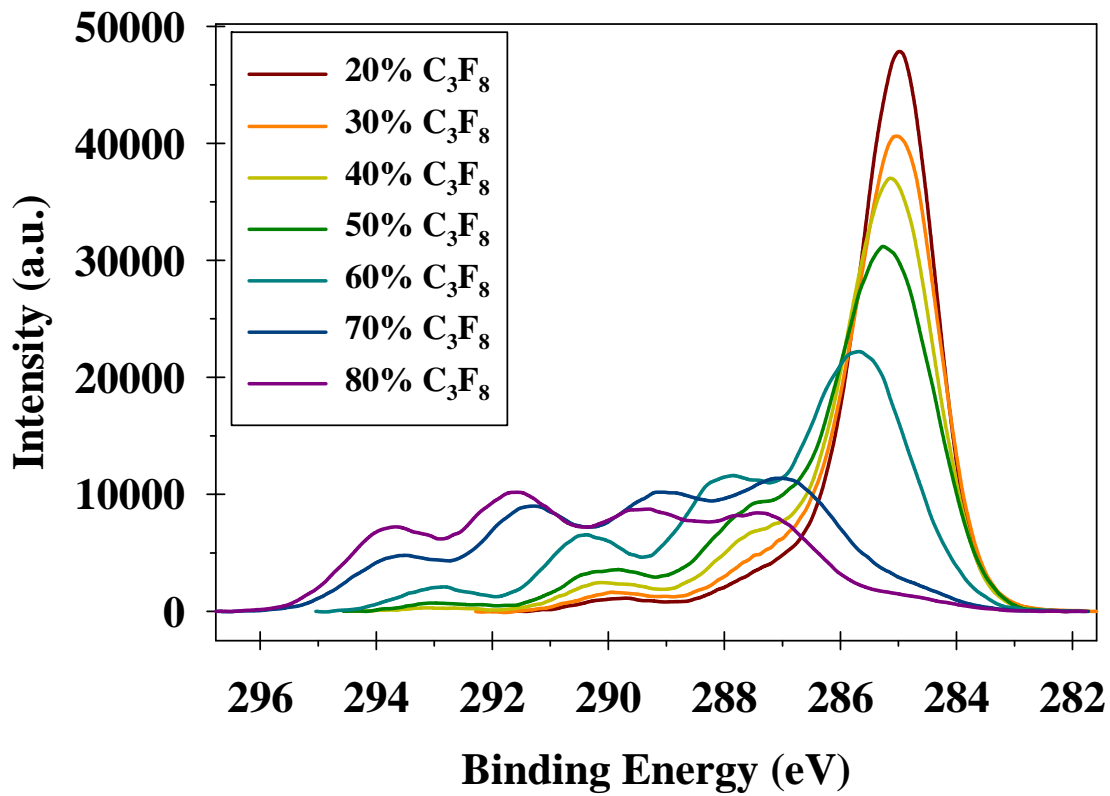


Figure 7.4. Stacked high resolution XPS C_{1s} spectra of homogeneous HC/FC films deposited from constant ratios of C_3F_8 and H_2 . Samples were prepared as described for Figure 3.

7.2.2. *Dynamic C₃F₈/H₂ PECVD system.* As noted in Section 7.1., we have developed a system capable of changing the plasma feed gas composition in real time during film deposition. Our first goal in validating this technique was to show that the dynamic feed gas composition and plasma composition occurred on a similar time-scale, allowing for the fabrication of gradient films. TR-OES, a technique commonly applied to real-time analysis of plasma conditions during semiconductor processing, was chosen to investigate the time dependent behavior of the plasma. The complete emission spectrum was collected every 5 s by averaging 30 spectra using a 150 ms integration time. Emission line intensities from species of interest [CF₂* (251.7 nm), CF* (202.5 nm), H α (656.2 nm), CH* (431.0 nm), CHF* (578.5 nm)] were normalized against the Ar* emission line (750.3 nm). The normalized emission intensities were plotted as a function of time to investigate changes in gas phase density with changing feed gas composition. Figure 7.5. demonstrates the TR-OES technique in the following dynamic C₃F₈/H₂ model system: the feed gas mixture was cycled between 20/80 and 80/20 C₃F₈/H₂ at a rate of 0.2 %/s. The full cycle was repeated three times while running the plasma continuously. As expected, changes in the gas phase density of fluorine and hydrogen-containing species are proportional to changes in their respective feed gases. Moreover, the gas phase density of each species appears the same from cycle to cycle. Indeed, the plasma composition is consistent with overall atomic make-up of the feed gas at any given time.

Given that changes in feed gas composition lead to proportional changes in the plasma, our next goal was to examine the surface properties of films deposited under dynamic conditions. Figure 7.6. shows the wCAs from a series of freshly deposited gradient films compared to the wCA results from freshly deposited homogeneous films shown in Figure 7.2.b. These films were prepared using a similar gradient deposition program to that used in Figure 7.5. The

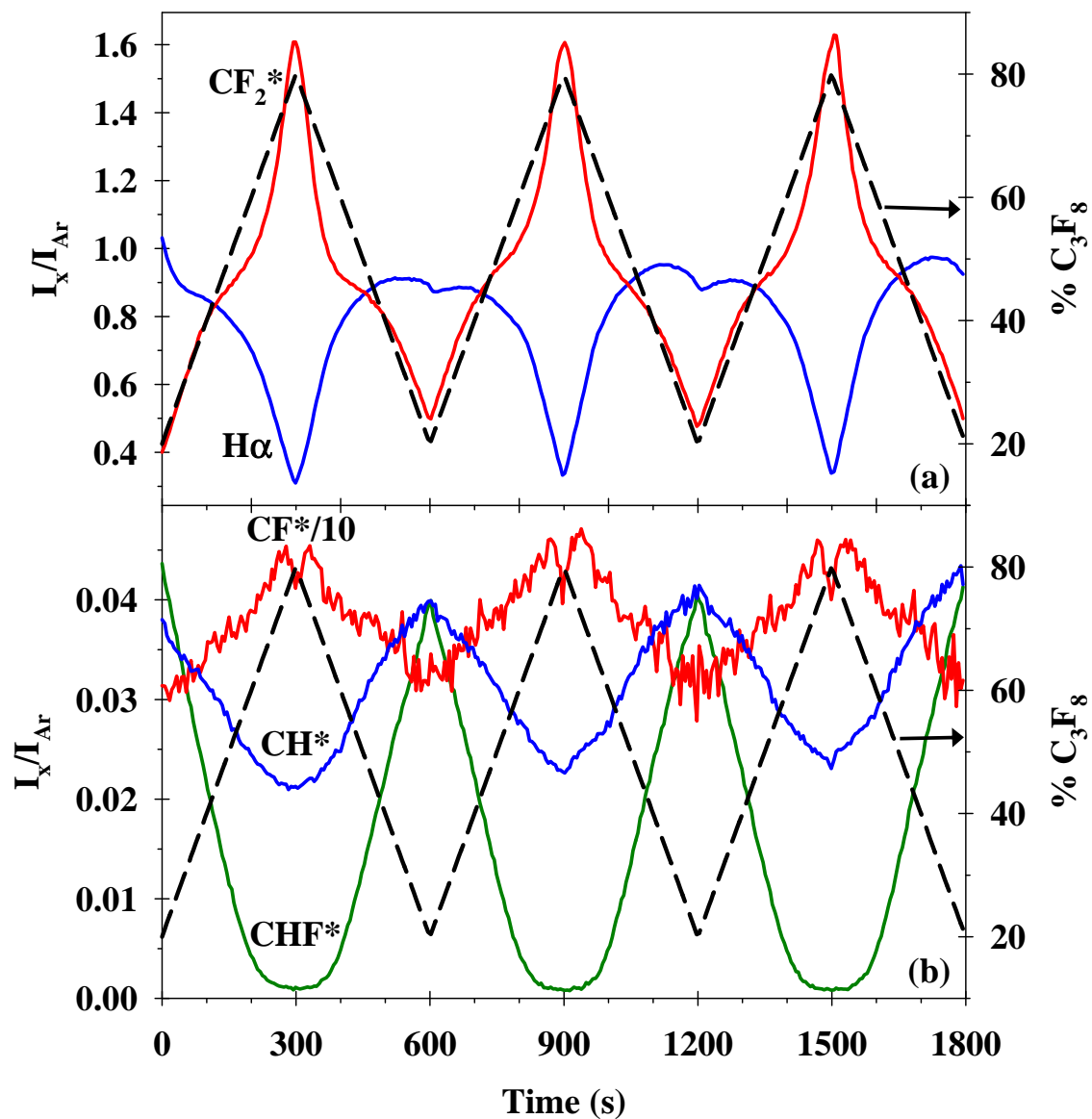


Figure 7.5. TR-OES of plasma emission during multiple cycles of a HC/FC film deposition program. The gas composition (dashed line – right axis) was varied from 20-80%. The emission from (a) CF_2^* and $\text{H}\alpha$, as well as (b) CH^* , CF^* , and CHF^* show how the gas phase composition changes with changing feed gas ratios.

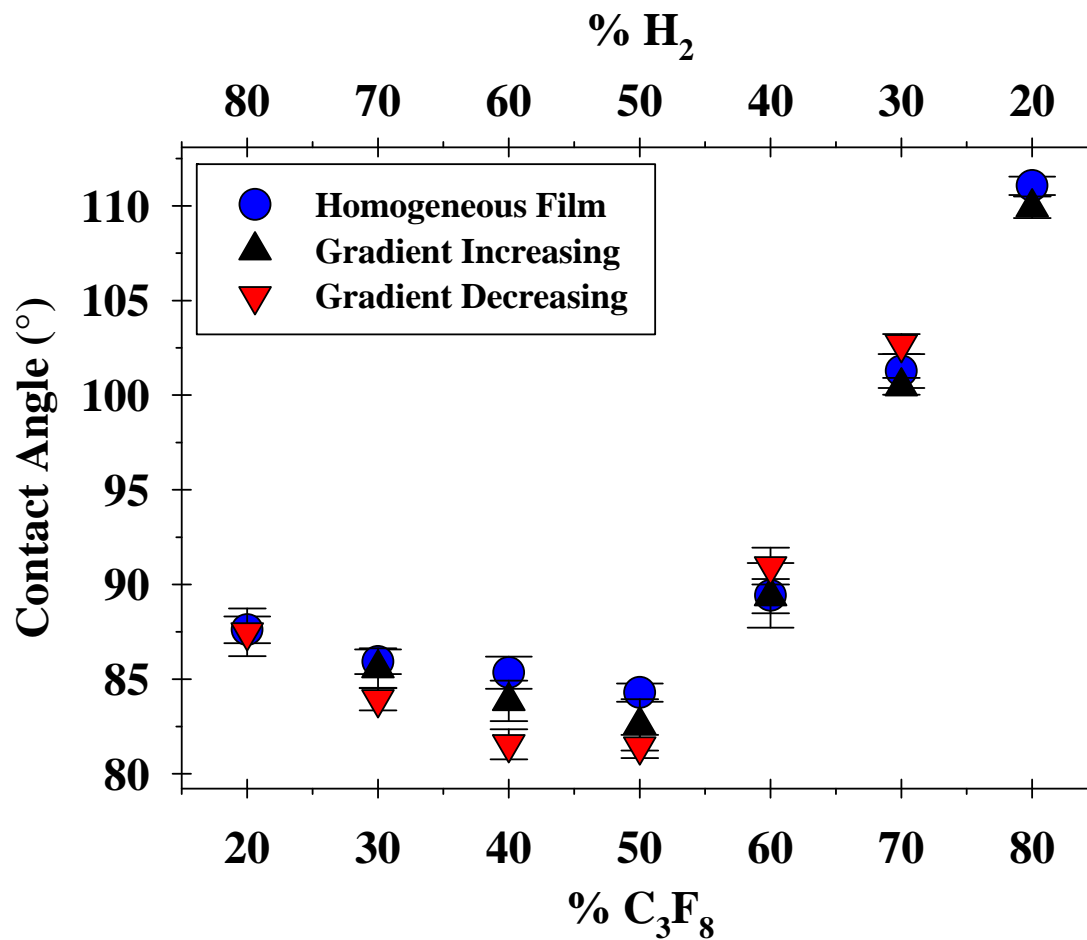


Figure 7.6. Comparison of wCA measurements from homogeneous HC/FC films (circles) and gradient HC/FC films deposited from an increasing ratio (triangles) or decreasing ratio (down triangles) of C₃F₈/H₂.

specified surface composition was achieved by stopping the deposition at 10% increments during the second cycle of the program to match the C₃F₈/H₂ mixtures used to prepare the homogeneous films. The wCAs of the gradient film surfaces compare well with the corresponding homogeneous films, suggesting that gradient deposition programs yield a film surface with similar composition and structure. Moreover, this holds regardless of whether the feed gas ratio is increasing or decreasing, yielding an underlying composition that is more *a*-CF-like or more *a*-CH-like.

Figure 7.7. shows FTIR spectra from model gradient films created to examine the bulk plasma polymer formed under dynamic plasma conditions. Gradient films were deposited on freshly pressed KBr pellets using the respective deposition programs in Figure 7.7. (inset). Interestingly, the spectra of these gradient film samples appear to be a composite of the spectra from the homogeneous films deposited using 20% C₃F₈ and 80% C₃F₈. Both gradient films have prominent CH stretch absorption ($\nu = 3000\text{-}2800\text{ cm}^{-1}$), which is consistent with *a*-CH type film composition. Whereas the homogenous films with significant CH stretch signals only contained a weak CF₂ absorption peak, these gradient films have a strong CF₂ absorption peak, similar to that seen in homogeneous films consisting primarily of *a*-CF type material. Overall, the spectral profiles of these gradient films are very similar, despite different gradient slopes and deposition times. The general shape of the CF₂ absorption peak in Figure 7.7.a. is similar to homogeneous films deposited using >70% C₃F₈ and the absorption maximum occurs at $\nu = 1208.6 \pm 0.4\text{ cm}^{-1}$. Figure 7.7.b. shows a similar result where $\nu = 1206.0 \pm 1.7\text{ cm}^{-1}$. There is a detailed discussion of peak position and the implications for film structure in section 7.3.3.

As one additional characterization of our gradient film deposition process, we measured film thicknesses and calculated film deposition rates. Figure 7.8. shows the calculated deposition

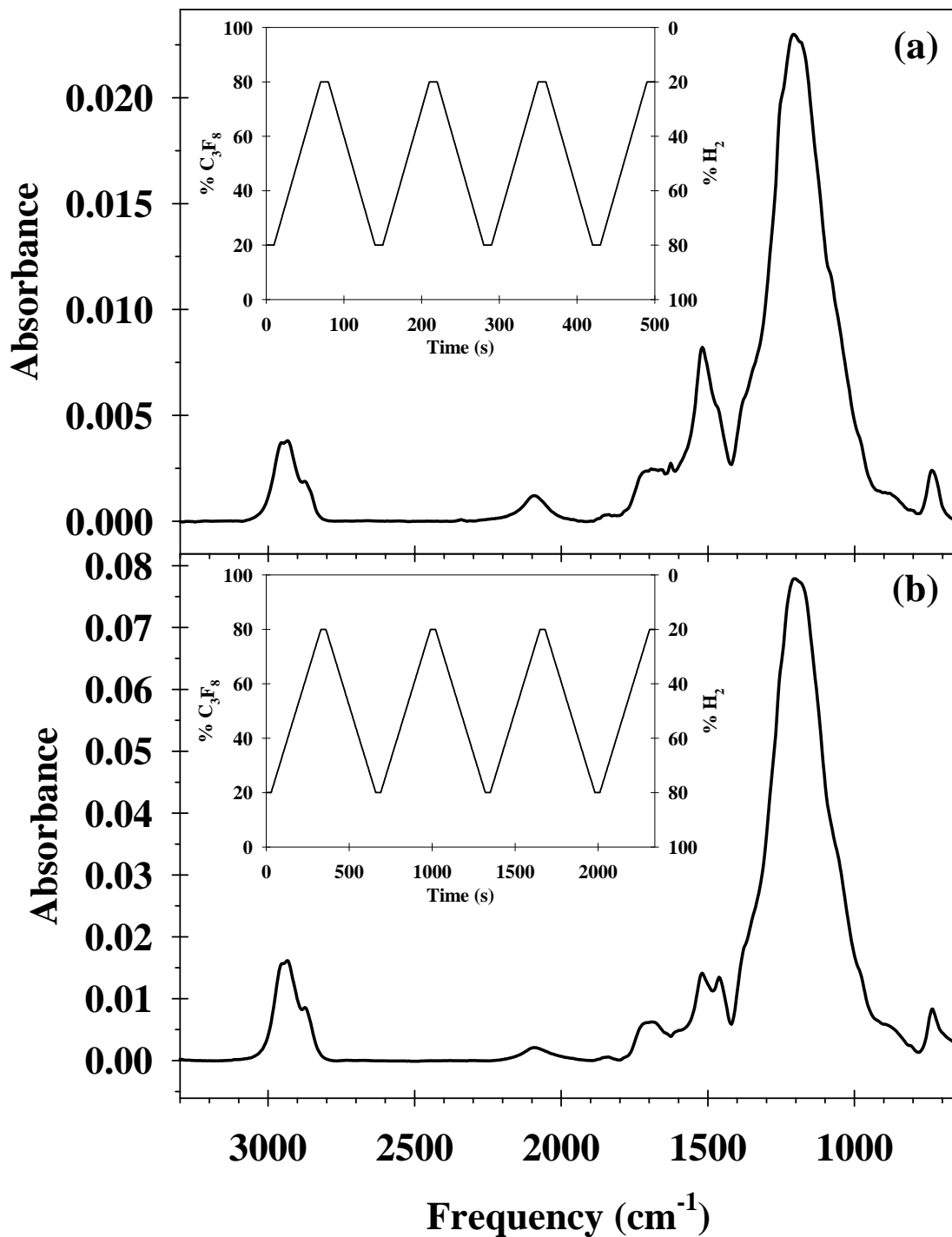


Figure 7.7. Transmission FTIR spectra from gradient HC/FC films deposited on KBr from different dynamic $\text{C}_3\text{F}_8/\text{H}_2$ PECVD deposition programs of (a) 20-80% (1%/s) and (b) 20-80% (0.2%/s). Insets show the respective deposition programs used to prepare each sample.

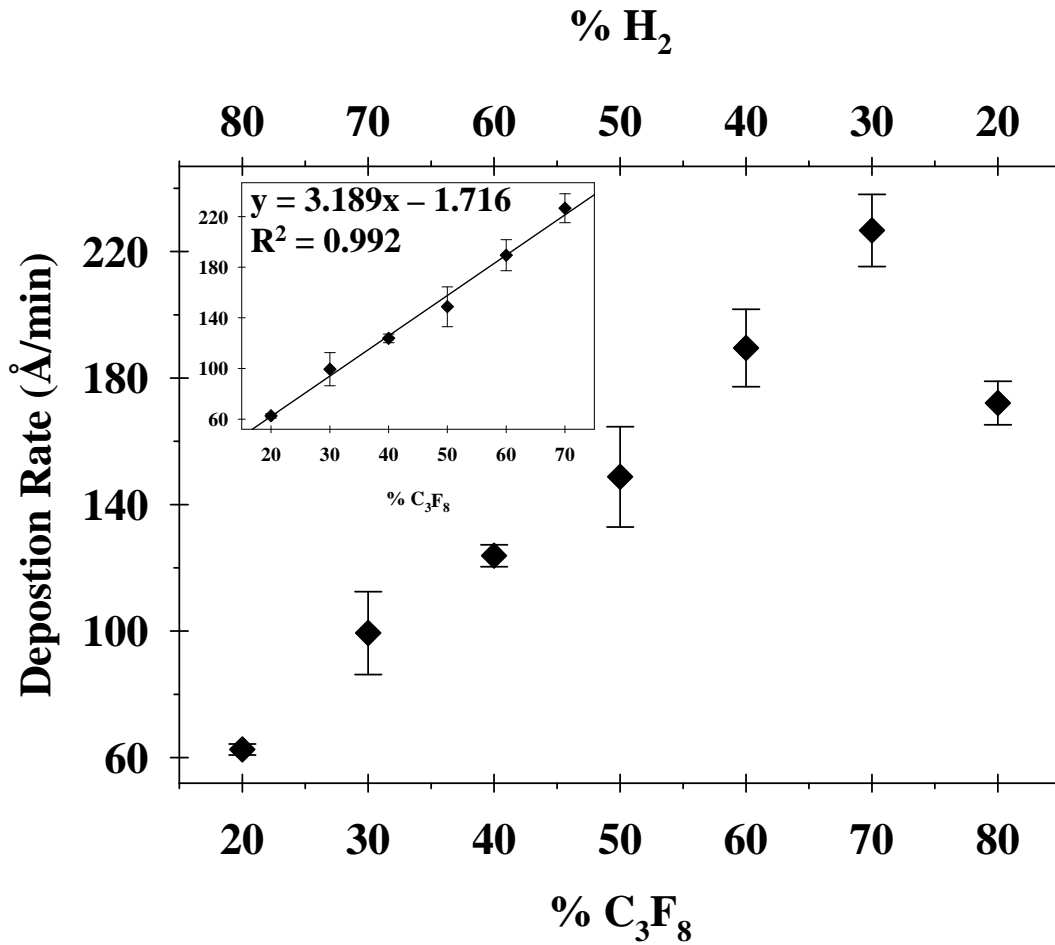


Figure 7.8. Deposition rate of homogeneous HC/FC films deposited from constant ratios of C₃F₈ and H₂. Samples were prepared on silicon [100] wafers using a 10 min deposition time. Linear least squares fit of deposition rate (inset) was used to predict the total film thickness from a dynamic C₃F₈/H₂ PECVD system over a 20-70% C₃F₈ range.

rates from a series of homogeneous films measured using VASE. The lowest deposition rate is observed at 20% C₃F₈, whereas the highest deposition rate is observed at 70% C₃F₈. Over this range, the deposition rate appears to depend strongly on the mass of C₃F₈ entering the reactor, Figure 7.9. Here, we define the ratio of deposition rate to % C₃F₈ as the deposition efficiency. This is expected given that C₃F₈ is the only source of carbon containing moieties responsible for the growing plasma polymer film. Indeed, over the 20-70% C₃F₈ range the deposition efficiency is constant within error. Only when C₃F₈ exceeds 70% does the deposition efficiency begin to decrease. H₂ is known to facilitate deposition of FC films under certain conditions through the production of H radicals which are known to react with atomic fluorine and produce HF.²³ Indeed, the concentration of fluorine radicals is so low over the range of C₃F₈/H₂ ratios studied that it was not detected in our TR-OES experiments. Overall, these results suggest that the minimum threshold required to maximize the deposition rate is 30% H₂, above which the additional H₂ only serves to replace F in the growing polymer film.

To examine differences in deposition rate between the static and dynamic C₃F₈/H₂ plasma systems, we developed a model for the deposition rate using linear regression over the 20-70% C₃F₈ range, Figure 7.8. (inset). The first integral of the resulting linear equation was used to solve for the total film thickness from a test deposition program. When applied to a deposition program that operated over 20-70% C₃F₈ at a rate of 0.17%/s through 2 full cycles, the model predicts a total film thickness of 284 nm. We attempted to visualize the film structure and verify the total film thickness by performing SEM on the cross-section of a sample prepared using that deposition program, Figure 7.10. From VASE data, we found that the permittivity (ϵ) of the static films ranged from 2.3 for 20% C₃F₈ to 1.8 for 80% C₃F₈, Figure 7.11.b. Despite this measureable range in ϵ , we could not detect any contrast difference in the film layers that would

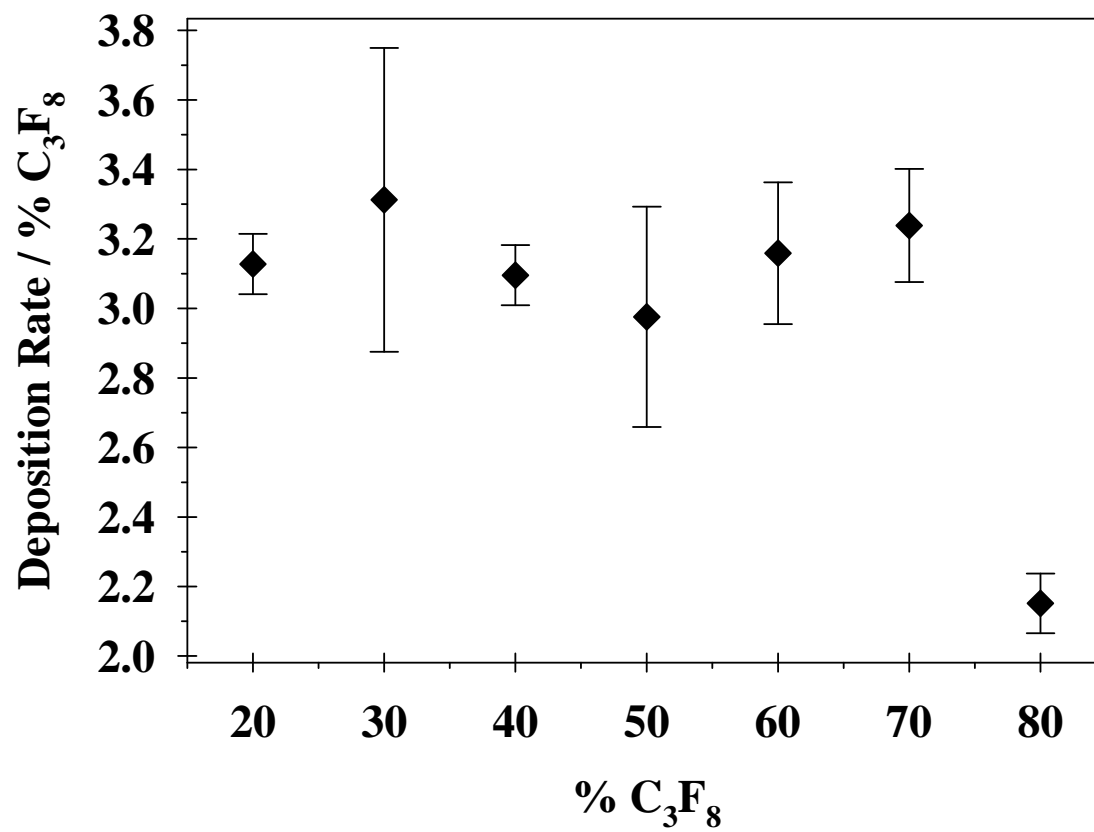


Figure 7.9. Deposition rate dependence on C₃F₈/H₂ mixture when % C₃F₈ is taken into account.

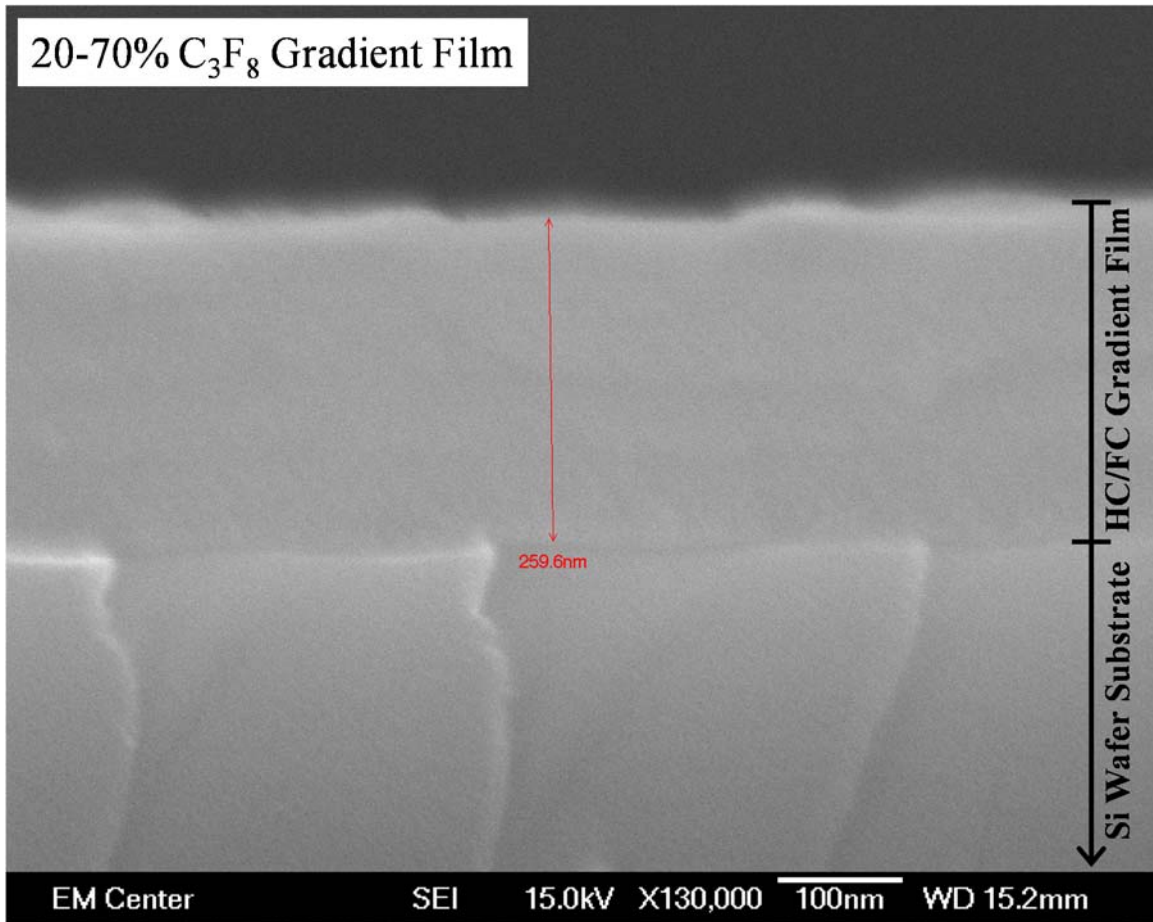


Figure 7.10. SEM image of the cross section of a gradient HC/FC film prepared using a dynamic deposition program operating over a 20-70% C₃F₈ range for two cycles.

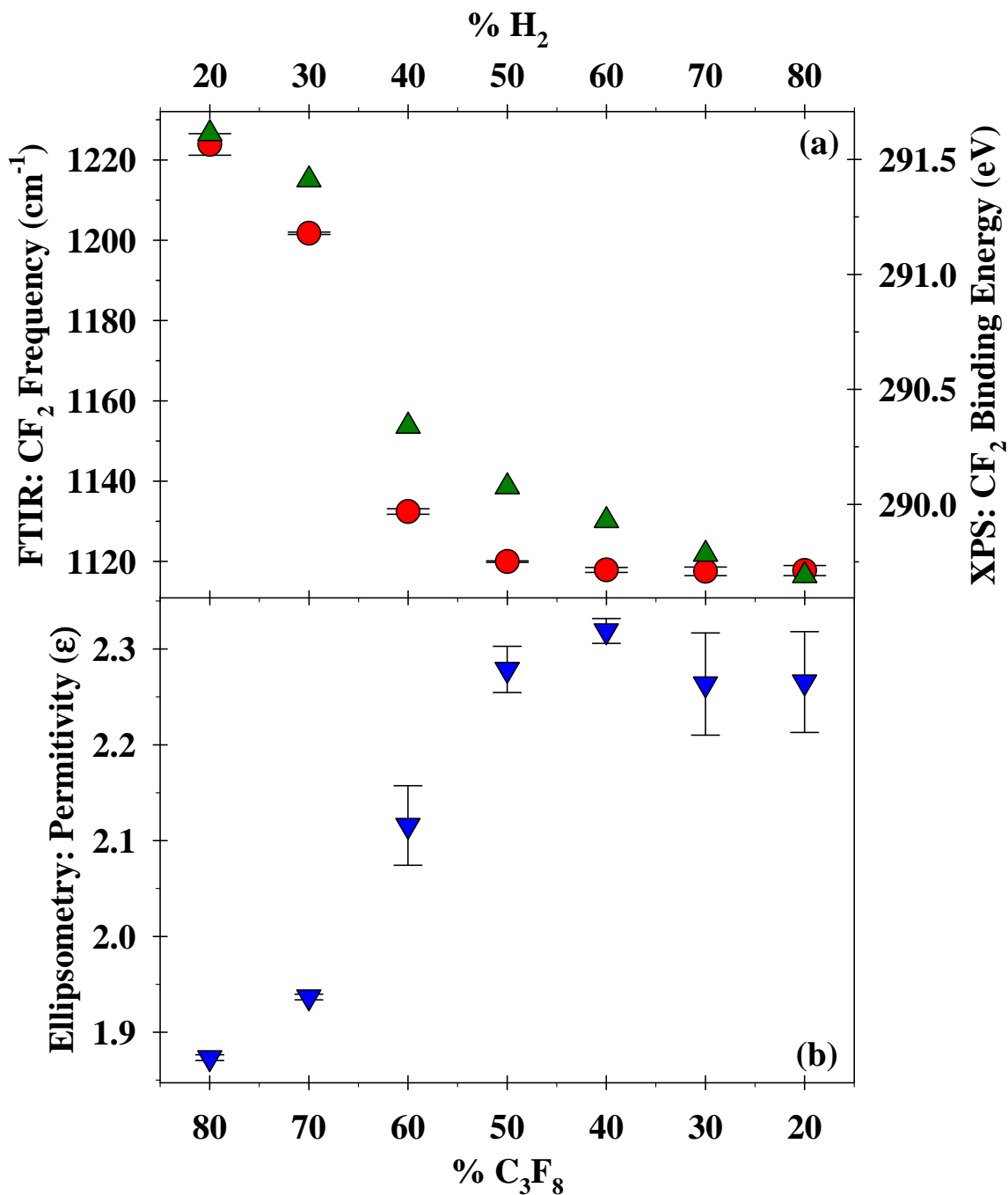


Figure 7.11. (a) CF₂ frequency from FTIR and CF₂ binding energy from high resolution C1s XPS from homogeneous C₃F₈/H₂ plasma polymerized films as a function of feed gas composition. (b) Permittivity (ε) from ellipsometry as a function of feed gas composition.

have allowed us to visualize these layers individually. Moreover, there was some difficulty in obtaining this SEM image to measure the total film thickness because the electron beam was found to deform the film on the outer edge where charging was most severe, possibly leading to an underestimate in total film thickness. Replicate measurements on this image show that the film thickness was 272 ± 8 nm, which has a 4.2% error compared to the theoretical film thickness we calculated. Although this result should be treated as preliminary, we consider it support for our hypothesis that the static C_3F_8/H_2 system deposition rate results can be used to predict the deposition rate for the dynamic C_3F_8/H_2 system.

7.3. Discussion

The overall goal of this study was to investigate gradient film deposition using a PECVD system comprising C_3F_8/H_2 mixtures. Many of the central issues associated with this lie with verifying the effect of dynamic changes in gas mixture on the growing film, rather than with engineering a plasma system that is capable of changing the gas mixture in real time. Here, we have not only achieved control over film composition, we also have garnered insight into the underlying process for creating gradient films using PECVD.

7.3.1. Variable film composition from a single PECVD system. Our FTIR and XPS data clearly show that a wide range of films, composed of *a*-CH and *a*-CF type moieties, are achieved over the range of static C_3F_8/H_2 mixtures tested. Increased fluorine incorporation is observed as the % C_3F_8 is increased, as demonstrated by increased intensity of *a*-CF related signals in FTIR and XPS; closer examination of these signals gives further insight into the film formation mechanism. The effect of increasing *a*-CF content is clearly seen by the increasing XPS BE of the CF_2 and CF_3 moieties. The BE of these C_{1s} environments increases with the probability that

they lie near other fluorine-containing groups. Indeed, the observed BE ranges from 289.7 eV up to 291.6 eV, which is approaching 292 eV, the expected C_{1s} BE of a polymer composed entirely of CF₂ units (i.e. Teflon®). This dramatic shift in BE occurs because of the powerful electron withdrawing nature of fluorine, which easily takes electron density away from neighboring carbon atoms. The practical effect of this is that the electron shell around the carbon atom contracts and the BE of core shell electrons increases. Figure 7.11.a. shows the continuous shift in BE we observed for CF₂ moieties as the film composition is altered. This trend indicates that these films are well mixed or homogeneous as opposed to consisting of discrete domains of *a*-CF or *a*-CH-type material. If the latter were true, we would expect to see constant BEs in each film, regardless of the bulk composition. This phenomenon is not without precedent. Visser et al.²⁴ studied the fabrication of multilayer FC/HC films deposited from various mixtures of hexafluoroacetone and acetylene using a capacitively coupled rf discharge plasma reactor. Although not explicitly discussed by Visser et al., an examination of their published high resolution C_{1s} XPS spectra reveals that the difference between the CF₂ BE and C-C BE decreases by as much as 2 eV when the amount of hexafluoroacetone in the feed is decreased from 90% to 50%. For comparison, the difference between the CF₂ BE and C-C BE decreases by 1.5 eV as the amount of C₃F₈ is decreased from 80% to 50% in our C₃F₈/H₂ plasma system.

Although our films are composed of *a*-CF and *a*-CH material building blocks, our wCA results suggest that there are more than two distinct surfaces formed. Films deposited from FC-rich mixtures (i.e. 80% C₃F₈) generally have a high surface tension; whereas films deposited using lower proportions of FC gas (i.e. 20% C₃F₈) have a relatively low surface tension. Interestingly, the lowest wCAs are observed on films deposited using 50% C₃F₈. This suggests there is an optimum mixture of *a*-CF and *a*-CH moieties that leads to a lower overall surface

tension. We have observed this phenomenon during previous studies of plasma polymer deposition from pure perfluorinated precursors (e.g. CF_4 , C_2F_6 , C_3F_8 , and C_3F_6).¹⁹ Those films were studied by preparing Zisman plots to determine the critical surface tension. The critical surface tension increased along with the F/C of those films. It was reasoned that this is not intrinsic to the presence or concentration of CF_x units at the film surface, but rather results from the high molar volume of CF_x units which leads to less efficient packing and increased surface tension. The low wCA for surfaces prepared using 50% C_3F_8 suggests that these films have an optimum ratio of FC and HC building blocks that leads to more efficient packing at the film surface despite the presence of CF_x units and the higher concentration of fluorine measured using XPS. Overall, these measurements show that three distinct surfaces form depending on the $\text{C}_3\text{F}_8/\text{H}_2$ mixture used, namely: a predominately *a*-CH surface, a predominately *a*-CF surface, and a mixed surface with unique surface tension characteristics. Moreover, these interesting surface tension properties further expand the number of tunable properties from this mixed plasma system.

wCA measurements also give insight into the stability of films deposited from the $\text{C}_3\text{F}_8/\text{H}_2$ plasma system. Homogeneous films that were tested two weeks after deposition show different degrees of aging behavior; films with higher *a*-CH content have lower wCA compared to the as deposited film. These findings are reasonable given our XPS results that show significant O and N incorporation in those same samples. We believe this is the result of a larger number of reactive sites that remain on the more *a*-CH-like surfaces post deposition. Seth and Babu²⁵ found that “*a*-C:H, F” films deposited from various mixtures on 1,3-butadiene and CF_4 were more susceptible to etching by O_2 plasma when the CF_4 fraction in the plasma exceeded 40%. They attributed this to the presence of dangling bonds and a defective open structure

observed when the CF_4 fraction exceeds some threshold. Interestingly, we observe the opposite trend in stability as our mixed $\text{C}_3\text{F}_8/\text{H}_2$ films are exposed to ambient atmosphere; film stability increases along with F incorporation. It is possible that film stability is related to the degree to which the depositing monomer is fragmented in the gas phase or substituted at the surface during growth. Although the higher α -CH content films investigated here are susceptible to oxidation upon exposure to atmosphere, this could be mitigated by depositing a thin overlayer of α -CF material to passivate the surface.

The TR-OES experiment sheds light on film formation mechanisms in $\text{C}_3\text{F}_8/\text{H}_2$ plasmas. By tracking the relative density of key gas phase radical species as the gas phase mixture changes with respect to time we can gain some understanding of how the specific elemental composition, measured using XPS, comes about. During FC deficient phases of the deposition program we find elevated densities of hydrogen-containing excited state radical species (e.g. $\text{H}\alpha$, CH^* , CHF^*). Previous work measured CH surface scatter coefficients (S) in $\text{CH}_2\text{F}_2/\text{C}_3\text{F}_8$ plasmas with different gas ratios and generally found $S(\text{CH}) < 0.1$ regardless of plasma conditions.²⁰ This shows that impinging CH radicals have a very high surface reaction probability (>0.9) and suggests one possible route for hydrogen incorporation for the formation of α -CH-like film chemistries. In contrast, $S(\text{CHF})$ values ranged from 1.00 to 1.65, consistent with the surface production of CHF radicals. The production and loss of CHF radicals from the growing plasma polymer surface explains why fluorine incorporation is so low in films prepared from 20% C_3F_8 .

As expected, the densities of excited state fluorine containing radicals (e.g. CF^* and CF_2^*) are highest during the FC-rich phase of a deposition program. More recent work in our group has examined the surface production of CF and CF_2 radicals during ion-rich and ion-

limiting conditions and it was found that surface production of both radicals are enhanced when ions are allowed to interact with the growing film surface.²⁶ The TR-OES experiments presented here were performed co-axial to the long axis of the reactor and include both the intense plasma glow from the coil region and dim plasma glow in the downstream region. It is likely that a large portion of the observed CF* and CF₂* signals originate from radical production on the reactor walls in the coil region where ion densities and energies are the highest. Given the downstream deposition position, ion bombardment probably plays a less significant role in F abstraction via CF and CF₂ loss. Overall, different C₃F₈/H₂ mixtures lead to different gas phase densities of depositing and non-depositing radical species, resulting in the variety of possible film chemistries we observe.

7.3.2. Depositing film composition is independent of underlying film. Until now our discussion has focused on mechanisms in static plasma systems where a constant C₃F₈/H₂ mixture is used to deposit a film whose composition is constant with respect to depth. Analysis of films from a dynamic plasma system is not as straightforward. If we only consider the characteristics of the topmost layer of a gradient film, two possible scenarios can explain the observed composition and structure: the plasma is largely responsible for the film surface or the film surface varies based on differences in the underlying film layers. If the latter scenario were to prevail, then predictions about the surface properties of the gradient films would break down and we would expect different properties from a given film if the preceding surface was more *a*-CF or *a*-CH-like.

We extended our wCA studies to gradient films prepared using a dynamic plasma system to examine if differences in underlying structure have any effect on the behavior of the topmost layer of deposited film, Figure 7.6. The wCA on each gradient film was nearly identical to the

corresponding homogeneous film. This is indeed an important result because it shows that the structure and composition of material deposited at the surface of the gradient film is similar to the corresponding homogeneous film surface. Moreover, it suggests that the film chemistry evolves with the changing plasma composition leading to an outer film chemistry that is not sufficiently different to have an impact on the composition and structure of subsequent layers. It is also possible that monomers largely retain their structure during the film growth process. Downstream PECVD of hexafluoropropylene oxide (HFPO), reported previously, is an example of such a plasma system.²⁷ The resulting plasma polymer was composed of CF₂ and CF₃ units with very little cross-linking. Limited ion exposure results in fewer FC backbone rearrangements due to the remote substrate placement. In a more recent report, Gleason and coworkers²⁸ investigated initiated PECVD of 1,3,5-trivinyl-1,1,3,5,5-pentamethyltrisiloxane using tert-butyl peroxide as the initiator. They used a low power microwave plasma ($P = 50$ W) to activate the initiator leading to polymerization via a radical mechanism taking place at the surface. In this case, the applied power was enough to initiate radical polymerization but insufficient to fragment and rearrange the monomer in the gas phase or at the surface. These reports show that it is possible to maintain the film structure with continued plasma exposure during plasma polymer film growth.

7.3.3. Composition of sub-surface layers remain fixed. As stated previously, two possible scenarios could be played out during deposition in this dynamic plasma system, each having unique implications for underlying layers in a gradient film. In the first scenario, underlying layers are not fixed and film species are able to rearrange or migrate during continued plasma exposure as subsequent layers are deposited. If this scenario prevails, the dynamic plasma conditions required to fabricate a continuous gradient will prevent precise control of the film

structure. In the second scenario, deposition proceeds in a layer-by-layer fashion wherein the composition of the top most layer is based only on the plasma conditions at that moment; once a layer is covered by a subsequent layer, it becomes fixed and continued plasma exposure has no effect on structure or composition.

During the collection of FTIR spectra on our homogeneous film series we observed the absorption frequency of the CF₂ peak experienced a similar shifting phenomenon as the BE of CF₂ environments in the XPS spectra, Figure 7.11.a. In section 7.3.1., we discussed the effect that electron withdrawing group concentration has on the BE of carbon atom core shell electrons in a CF₂ moiety. The same concepts apply to the absorption frequency of the CF₂ peak of our FTIR spectra. As the number of nearby fluorine containing groups increase, more electron density is removed from a carbon atom. In this case, the bond length between a carbon atom and the attached fluorine becomes shorter and the vibrational frequency increases. The end result is that we can use the CF₂ peak position to probe the relative local concentration of fluorine vs. hydrogen atoms in the amorphous polymer network. If the CF₂ peak position is consistent with high fluorine content but the CH stretching signal is also strong, the regions of the film giving rise to those signals are likely segregated into different layers within the film. Indeed, the CF₂ absorption peak in Figures 7.7.a. and 7.7.b. occurs at $\nu = 1208.6 \pm 0.4 \text{ cm}^{-1}$ and $\nu = 1206.0 \pm 1.7 \text{ cm}^{-1}$, respectively. Both peak maxima are consistent with the CF₂ absorption frequencies of homogeneous films deposited using >70% C₃F₈. These results show that, although a gradient program was used to fabricate the overall film structure, the *a*-CF layers are consistent with the homogeneous films prepared using constant plasma conditions. This demonstrates the gradient film structure is retained with continued plasma exposure under these conditions.

It is still possible that reactive ions can penetrate into the growing polymer film to some extent and that the growth rate of the film would mask any evidence that the film layers are mixing. Although it is impossible to eliminate this possibility with the techniques used here, we extended our FTIR analysis to samples deposited with a higher gradient slope in an attempt to address this question, Figure 7.7.b. Given that the layers separating predominately *a*-CF and predominantly *a*-CH regions of the film are comparatively thin in this sample, one would expect layer mixing to be exacerbated. Yet, the position of the CF₂ absorption peak remains at a position consistent with homogeneous films deposited at 70-80% C₃F₈. This is consistent with the work of Standaert et al.²⁹ who studied the effect of the passivating film thickness on etch rate during FC plasma (e.g. CF₄, CHF₃, and c-C₄F₈) processing of various dielectric films and semiconductor materials. Their findings showed that, under etching conditions, etching was most effective when the FC passivating film thickness was <1 nm and that etch rates began to approach 0 nm/min when the passivating film thickness was >3.5 nm. The experiments reported by Standaert et al. were performed under relatively extreme conditions using plasmas with *P* = 1400 W and substrates biased specifically to induce etching. Thus, these values should be taken as an upper bound of the film thickness through which reactive FC plasma species can penetrate, far greater than the penetration thicknesses under the conditions used to prepare the gradient films in our study. Using this analysis, the composition and structure of layers within our gradient films should not change once they are buried beneath the surface of the growing film because the penetration depth of reactive plasma species will be so shallow under the conditions used in our experiments.

As a final note, it is useful to consider the potential utilization of this gradient film fabrication technique. We anticipate that factors such as substrate identity or overall film

thickness will not limit the application of our films or the technique. Indeed, similar *a*-CH and *a*-CF film chemistries have been shown to adhere or improve adhesion to a wide variety of substrates, including stainless steel,^{30, 31} polymer,^{5, 16} semiconductor,³² and metal oxide surfaces.³³ Although some of these surfaces require additional preparation steps prior to thin film growth, the surfaces generally lend themselves well to coating, yielding robust and strongly adherent films. Similar film chemistries have reportedly delaminated from a range of surfaces,^{18, 25} which can be an issue with any thin film deposition system. Even though we did not explicitly examine delamination and adhesion in this study, neither freshly treated or aged samples demonstrated any type of mechanical failure, consistent with the observation that graded film structures are often used as adhesion interlayers because they are less prone to delamination.

7.4. Summary

Using various static mixtures from our C₃F₈/H₂ plasma system, we have verified that a wide range of films are possible from these gas mixtures, broadly described by three categories based on wCA and structure, specifically intermediate wCA *a*-CH, low wCA homogeneous *a*-CH/*a*-CF, and high wCA *a*-CF. Using the same C₃F₈/H₂ plasma system operating in a dynamic mode, we fabricated continuously graded polymer films. FTIR spectra revealed that layers within a gradient film retained the structure of films prepared using static conditions, and both static and dynamic plasmas resulted in films with similar wCA values. We also tested the deposition rate over a range of static conditions to develop a model that predicted the deposition rate under dynamic conditions and preliminary tests showed that the actual film thickness was reasonably close to the prediction. Collectively, these results show that continuous gradient film

structures can be fabricated according to an arbitrary design and demonstrate a new level of tailorability for plasma polymerization systems.

Central to this control is the dependence of film structure and composition on plasma conditions and the stability of the film during continued plasma processing. Our wCA measurements on graded films showed that the composition and structure of a depositing film are independent of differences in the underlying film layer. Instead, film composition and structure correlated with the plasma species present at the moment of film formation in a dynamic plasma system, measured using TR-OES. Moreover, composition and structure were consistent with the presence of specific gas-phase species as well as with previous investigations of the surface reactivity of those radicals. The resulting films were stable as they were subsumed in the growing plasma polymer during continued plasma processing.

REFERENCES

1. Tompkins, B. D.; Fisher, E. R., Plasma synthesis of hydrocarbon/fluorocarbon thin films with compositional gradients. *Plasma Processes Polym.* **2013**, 10, (9), 779-791.
2. Hansen, A.; Zhang, R.; Bradley, M., Fabrication of arrays of polymer gradients using inkjet printing. *Macromol. Rapid Commun.* **2012**, 33, (13), 1114-1118.
3. Cai, L.; Lu, J.; Sheen, V.; Wang, S. F., Lubricated biodegradable polymer networks for regulating nerve cell behavior and fabricating nerve conduits with a compositional gradient. *Biomacromolecules* **2012**, 13, (2), 358-368.
4. Claussen, K. U.; Giesa, R.; Scheibel, T.; Schmidt, H. W., Learning from nature: synthesis and characterization of longitudinal polymer gradient materials inspired by mussel byssus threads. *Macromol. Rapid Commun.* **2012**, 33, (3), 206-211.
5. Tanaka, K.; Kogoma, M., Deposition of ethylene-hexafluoropropene gradient plasma-copolymer using dielectric barrier discharge reactor at atmospheric pressure: Application to release coatings on pressure-sensitive tape. *Plasmas Polym.* **2003**, 8, (3), 199-208.
6. Hedgemann, D.; Brunner, H.; Oehr, C. In *Improving the adhesion of siloxane-based plasma coatings on polymers with defined wetting properties*, Society of Vacuum Coaters: 45th Annual Technical Conference Proceedings, Buena Vista, FL, 2002; Buena Vista, FL, 2002; p 174.
7. Srividya, C.; Babu, S. V.; Visser, S. A., Surface and corrosion characteristics of a-C : H/fluorocarbon films. *J. Adhes.* **1998**, 67, (1-4), 81-95.
8. Airoudj, A.; Debarnot, D.; Beche, B.; Boulard, B.; Poncin-Epaillard, F., Improvement of the optical transmission of polymer planar waveguides by plasma treatment. *Plasma Processes Polym.* **2008**, 5, (3), 275-288.
9. Leong, K. F.; Chua, C. K.; Sudarmadji, N.; Yeong, W. Y., Engineering functionally graded tissue engineering scaffolds. *J. Mech. Behav. Biomed. Mater.* **2008**, 1, (2), 140-152.
10. Albert, J. N. L.; Kim, J. D.; Stafford, C. M.; Epps, T. H., Controlled vapor deposition approach to generating substrate surface energy/chemistry gradients. *Rev. Sci. Instrum.* **2011**, 82, (6).
11. Karabanova, L. V.; Mikhalovsky, S. V.; Lloyd, A. W., Gradient semi-interpenetrating polymer networks based on polyurethane and poly(2-hydroxyethyl methacrylate) for biomedical applications. *J. Mater. Chem.* **2012**, 22, (16), 7919-7928.
12. Montero, L.; Baxamusa, S. H.; Borros, S.; Gleason, K. K., Thin hydrogel films with nanoconfined surface reactivity by photoinitiated chemical vapor deposition. *Chem. Mater.* **2009**, 21, (2), 399-403.

13. Endo, K.; Shinoda, K.; Tatsumi, T., Plasma deposition of low-dielectric-constant fluorinated amorphous carbon. *J. Appl. Phys.* **1999**, 86, (5), 2739-2745.
14. Delimi, A.; Galopin, E.; Coffinier, Y.; Pisarek, M.; Boukherroub, R.; Talhi, B.; Szunerits, S., Investigation of the corrosion behavior of carbon steel coated with fluoropolymer thin films. *Surf. Coat. Technol.* **2011**, 205, (16), 4011-4017.
15. Lewis, F. o.; Cloutier, M.; Chevallier, P.; Turgeon, S. p.; Pireaux, J.-J.; Tatoulian, M.; Mantovani, D., Influence of the 316 L stainless steel interface on the stability and barrier properties of plasma fluorocarbon films. *ACS Appl. Mater. Interfaces* **2011**, 3, (7), 2323-2331.
16. Cheng, Q.; Komvopoulos, K., Nanoscale mechanical and tribological properties of fluorocarbon films grafted onto plasma-treated low-density polyethylene surfaces. *J. Phys. D: Appl. Phys.* **2012**, 45, (9), 095401.
17. Peri, S. R.; Akgun, B.; Satija, S. K.; Jiang, H.; Enlow, J.; Bunning, T. J.; Foster, M. D., Control of interface nanoscale structure created by plasma-enhanced chemical vapor deposition. *ACS Appl. Mater. Interfaces* **2011**, 3, (9), 3375-3383.
18. Mackie, N. M.; Dalleska, N. F.; Castner, D. G.; Fisher, E. R., Comparison of pulsed and continuous-wave deposition of thin films from saturated fluorocarbon/H-2 inductively coupled rf plasmas. *Chem. Mater.* **1997**, 9, (1), 349-362.
19. Cuddy, M. F.; Fisher, E. R., Contributions of CF and CF₂ species to fluorocarbon film composition and properties for C_xF_y plasma-enhanced chemical vapor deposition. *ACS Appl. Mater. Interfaces* **2012**, 4, (3), 1733-1741.
20. Liu, D. P.; Cuddy, M. F.; Fisher, E. R., Comparison of CH, C₃, CHF, and CF₂ surface reactivities during plasma-enhanced chemical vapor deposition of fluorocarbon films. *ACS Appl. Mater. Interfaces* **2009**, 1, (4), 934-943.
21. Martin, I. T.; Malkov, G. S.; Butoi, C. I.; Fisher, E. R., Comparison of pulsed and downstream deposition of fluorocarbon materials from C₃F₈ and c-C₄F₈ plasmas. *J. Vac. Sci. Technol., A* **2004**, 22, (2), 227-235.
22. Sandrin, L.; Silverstein, M. S.; Sacher, E., Fluorine incorporation in plasma-polymerized octofluorocyclobutane, hexafluoropropylene and trifluoroethylene. *Polymer* **2001**, 42, (8), 3761-3769.
23. d'Agostino, R.; Cramarossa, F.; Illuzzi, F., Mechanisms of deposition and etching of thin-films of plasma-deposited fluorinated monomers in radiofrequency discharges fed with C₂F₆-H₂ and C₂F₆-O₂ mixtures. *J. Appl. Phys.* **1987**, 61, (8), 2754-2762.
24. Visser, S. A.; Hewitt, C. E.; Fornalik, J.; Braunstein, G.; Srividya, C.; Babu, S. V., Compositions and surface energies of plasma-deposited multilayer fluorocarbon thin films. *Surf. Coat. Technol.* **1997**, 96, (2-3), 210-222.

25. Seth, J.; Babu, S. V., Fluorohydrogenated amorphous-carbon (a-C-H,F) films prepared by the plasma decomposition of 1,3-butadiene and carbon tetrafluoride. *Thin Solid Films* **1993**, 230, (2), 90-94.
26. Cuddy, M. F.; Blechle, J. M.; Fisher, E. R., Ion contributions to gas-surface interactions in inductively-coupled fluorocarbon plasmas. *Int. J. Mass spectrom.* **2012**, 330, 46-57.
27. Butoi, C. I.; Mackie, N. M.; Barnd, J. L.; Fisher, E. R.; Gamble, L. J.; Castner, D. G., Control of surface film composition and orientation with downstream PECVD of hexafluoropropylene oxide. *Chem. Mater.* **1999**, 11, (4), 862-+.
28. Coclite, A. M.; Gleason, K. K., Initiated PECVD of organosilicon coatings: a new strategy to enhance monomer structure retention. *Plasma Processes Polym.* **2012**, 9, (4), 425-434.
29. Standaert, T.; Hedlund, C.; Joseph, E. A.; Oehrlein, G. S.; Dalton, T. J., Role of fluorocarbon film formation in the etching of silicon, silicon dioxide, silicon nitride, and amorphous hydrogenated silicon carbide. *J. Vac. Sci. Technol., A* **2004**, 22, (1), 53-60.
30. Hasebe, T.; Murakami, K.; Nagashima, S.; Yoshimoto, Y.; Ihara, A.; Otake, M.; Kasai, R.; Kasuya, S.; Kitamura, N.; Kamijo, A.; Terada, H.; Hotta, A.; Takahashi, K.; Suzuki, T., Design for improved adhesion of fluorine-incorporated hydrogenated amorphous carbon on metallic stent: Three-layered structure with controlled surface free energy. *Diamond Relat. Mater.* **2011**, 20, (7), 902-906.
31. Lewis, F.; Turgeon, S.; Chevallier, P.; Pireaux, J. J.; Tatouliau, M.; Mantovani, D., On the growth of fluorocarbon thin films deposited on plasma-etched 316L stainless steel. *Plasma Processes Polym.* **2010**, 7, (3-4), 309-317.
32. Endo, K.; Tatsumi, T.; Matsubara, Y.; Horiuchi, T., Application of fluorinated amorphous carbon thin films for low dielectric constant interlayer dielectrics. *Jpn. J. Appl. Phys.* **1998**, 37, (4A), 1809-1814.
33. Ji, H.; Côté, A.; Koshel, D.; Terreault, B.; Abel, G.; Ducharme, P.; Ross, G.; Savoie, S.; Gagne, M., Hydrophobic fluorinated carbon coatings on silicate glaze and aluminum. *Thin Solid Films* **2002**, 405, (1-2), 104-108.

CHAPTER 8

SUMMARY OF RESEARCH AND PERSPECTIVES

This chapter summarizes the research contained in this dissertation. The global themes and specific impact of the work described in the preceding chapters are discussed, and future research directions arising from this work are considered.

8.1. Research Summary

Techniques for the plasma processing of polymeric materials were first described in the 1960s, and the development of these techniques has continued unabated to this day. This results in part because of the complicated nature of both plasmas and polymer surfaces, requiring that plasma modification schemes for polymers be developed on a case by case basis. Regardless of this apparent piecemeal approach, (1) new plasma chemistries for polymer modification and (2) new techniques for characterizing the structure of polymer surfaces are critical for improving the performance of polymers for a wide variety of technologies and industries. This dissertation makes substantial and original contributions to both areas of research.

The work described in this dissertation highlights our progress towards understanding non-depositing oxidizing plasmas, including those based on O₂, H₂O, CO₂, and formic acid (HCOOH), for polymer surface modification. In particular, we expanded our previous H₂O plasma polymer modification research^{1,2} to include a wider range of polymeric materials (Chapter 3), finding that H₂O plasma modifications are broadly applicable and initially give improved wettability on those polymers included in the study. During aging, however, the H₂O plasma modified polymers each exhibited hydrophobic recovery, the extent of which was similar

to O₂ plasma modified polymers described in the literature. H₂O plasmas were also effective for improving wettability and aqueous performance of track-etched polycarbonate (PC-TE) membranes (Chapter 4). In the course of that work we proposed a number of reaction schemes to explain the processes taking place at the H₂O plasma-polymer interface. Those reactions were further investigated by comparing the H₂O plasma system to the closely related O₂, H₂O, and CO₂ plasma systems (Chapter 5). In this context, a robust method was developed to determine the etch rate of PC by measuring the pore size of treated PC-TE. By comparing the relative gas-phase density of radicals in each plasma system with the etch rate, we demonstrated that atomic oxygen and, to a lesser extent, OH radicals both contribute to the etching of PC materials.

Significant progress has also been made in the development of plasma enhanced chemical vapor deposition (PECVD) techniques for the fabrication of composite polymer structures to alter the surface properties of polymers and other materials. The use of acetic acid (CH₃COOH) as a precursor for PECVD was investigated for the fabrication of composite polymer structures for biomedical and optical applications (Chapter 6). The CH₃COOH PECVD system was used to deposit a thin *a*-C_xH_yO_z film on PC-TE and silicon wafers. Although the deposition rate on silicon was constant, the pore measurement technique developed in Chapter 5 revealed that the deposition on PC-TE was self-limiting. A dynamic PECVD technique was also developed for the fabrication of more complex composite materials (Chapter 7). LabVIEW® was used to create an interface (Appendix A) for controlling the ratio of precursor gases in a C₃F₈/H₂ plasma system in real time, making it possible to deposit films with a gradient composition profile. A range of surface and bulk analysis techniques were used to characterize homogeneous and gradient depositions to show that composition and structure are retained during the growth of arbitrary complex films.

Another theme that emerged throughout the course of this research is the need for non-destructive techniques that reveal the structure of plasma modified surfaces and composite polymer materials. High resolution C_{1s} XPS fitting models for hydrocarbon/fluorocarbon materials were refined to the point that changes in the CF_2 moiety binding energy (BE) could be used to assess the homogeneity and distribution of fluorine in mixed PECVD films (Chapter 7). Shifts in CF_2 BE, combined with spectroscopic evidence from Fourier transform infrared spectroscopy (FTIR) and variable angle spectroscopic ellipsometry (VASE), were used to elucidate the internal structure of a gradient film and the deposition process used to fabricate it. The theory developed to explain the variability of CF_2 BEs was applied to high resolution C_{1s} XPS spectra from H_2O plasma treated polymers to confirm structural reorganization during aging. These intricate XPS fitting techniques, used here to probe the internal structure of thin films and the evolution of polymer surfaces, represent a deeper exploration of the plasma polymerized thin films and are a tangible contribution to the wider scientific research community.

8.2. Future Directions

Collectively, the work to identify plasma modification systems capable of stable surface treatments on polymers presented in this dissertation and the many literature accounts of polymer surface aging should impress upon the reader that this problem has yet to be fully understood by the scientific community. Although it is the author's belief that there is no perfect plasma modification scheme for polymers and modified polymer surfaces will always exhibit some aging, there are still benefits to expanding our understanding of plasma-polymer interaction

leading to surface modification. Below, we present some preliminary results wherefrom we can proceed toward this goal of greater understanding.

The research in Chapter 5 was inspired by the hypothesis that certain plasma species (e.g. atomic oxygen) were primarily responsible for etching and damage of polymers and that managing the gas-phase density of these species would yield better plasma modification outcomes. Our investigations into the acetic acid (CH_3COOH) plasma system, presented in Chapter 6, were undertaken for this reason. As it turned out, a 100% CH_3COOH plasma deposits a thin $a\text{-C}_x\text{H}_y\text{O}_z$ films under the conditions used in this study. It is well known, however, that etching and deposition occur simultaneously in many plasma systems.³ If one were to balance the etching and deposition processes to achieve an equilibrium, the result would be a plasma system capable implanting functionality on a polymer surface without etching away the underlying polymer material. To this end, we have undertaken preliminary experiments using plasmas from various mixtures of CH_3COOH and H_2O vapor in an attempt to find this equilibrium point. Using track-etched polycarbonate (PC-TE) membranes as substrates, precursors were mixed to achieve 100 mTorr reactor pressure based in individual partial pressures, and plasma modifications were carried out at $P = 100$ W for 2 min. The treatment efficacy was assessed by measuring water contact angles (wCA) immediately after treatment, Figure 8.1. These results suggest that a 75/25 $\text{CH}_3\text{COOH}/\text{H}_2\text{O}$ mixture yields a wCA similar to that obtained from 100% H_2O plasma treated PC-TE. This is a very promising result. It remains unclear, however, whether the presence of the H_2O oxidant contributes to competitive etching on the PC surface or the H_2O prevents deposition precursors from forming in the first place. Further experiments are needed to understand this fascinating mixed plasma system.

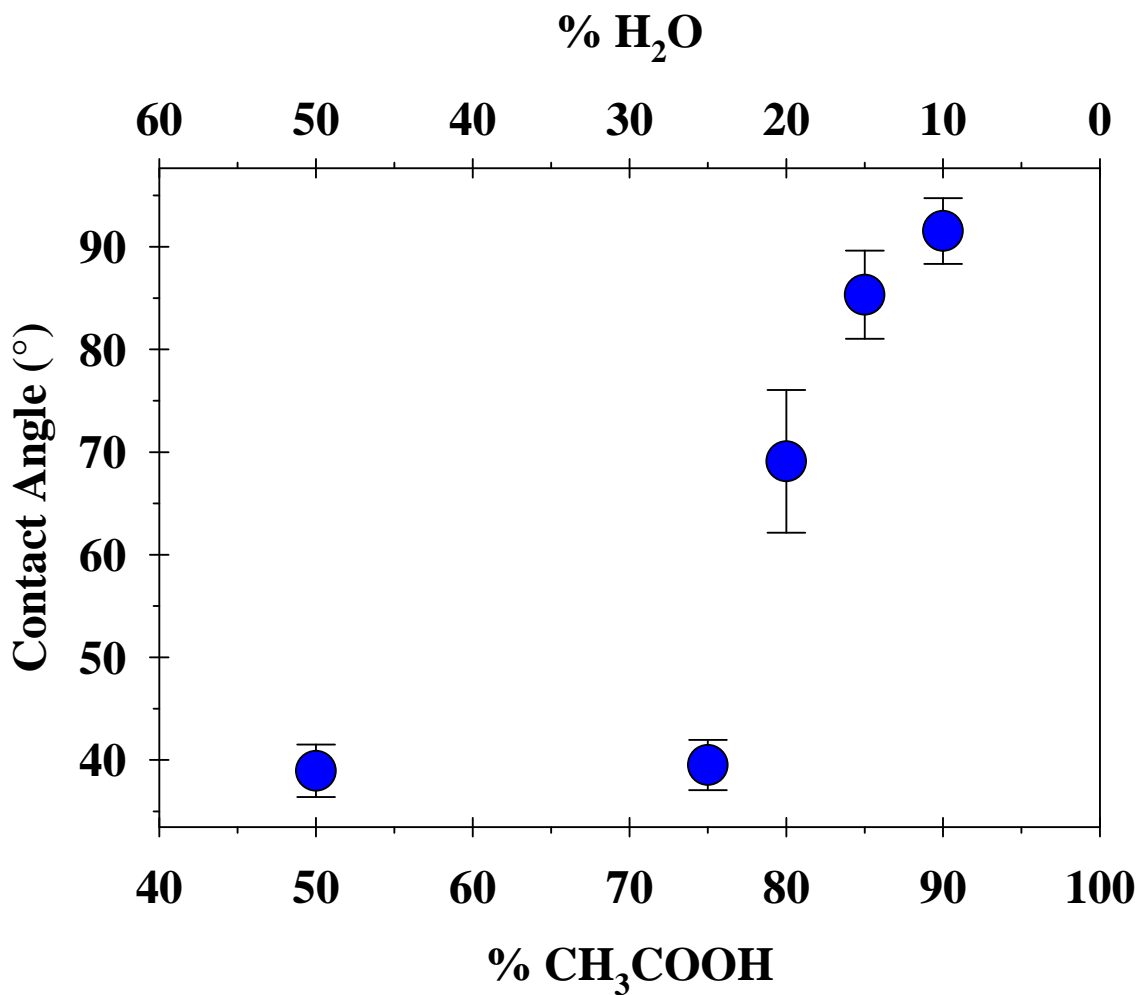


Figure 8.1. wCA measurements on the upstream side of PC-TE following treatment using various CH₃COOH/H₂O mixtures ($P = 100$ W, 100 mTorr, 2 min treatment time, 9 cm downstream sample placement). Error bars represent one standard deviation.

Chapter 5 describes the first use of a pure formic acid (HCOOH) plasma for polymer modification and shows that the HCOOH plasma system is a promising candidate for surface modifications. Although our work shows that the HCOOH plasma is comparable to other oxidizing plasmas, such as O₂, H₂O, and CO₂, very little is understood about the gas-phase dynamics within the HCOOH plasma system and how these processes influence polymer surface modification outcomes. To further investigate the HCOOH plasma system, we have performed preliminary experiments using various mixtures of H₂ and CO₂. PC-TE samples were treated for 2 min using 200 mTorr total pressure and $P = 25$ W. wCAs were measured on the upstream and downstream sides immediately after treatment to determine effectiveness, Figure 8.2. The 100% H₂ plasma yields a surface with the same wCA as the untreated PC-TE, and the wCA of PC-TE treated using the 100% CO₂ plasma is consistent with the CO₂ plasma results described in Chapter 5. When the mixture is adjusted to give the same stoichiometry as the HCOOH plasma system (50/50 CO₂/H₂), the treatment outcome differs dramatically from that achieved using the HCOOH plasma. Moreover, unlike the HCOOH, the intermediate CO₂/H₂ mixtures give different wCAs on the upstream and downstream sides, respectively. This demonstrates the HCOOH treatment is not simply a result of the elemental composition of the HCOOH plasma; the underlying causes of this observation remain to be discovered. These experiments may also help answer questions related to the texturing of PC surfaces (Chapter 5). The SEM images of HCOOH and H₂O plasma treated PC-TE samples depicted in Figure 5.2. reveal a unique surface texture that develops with long treatment times. We hypothesize that deposition precursors form when hydrogen is present and this material is responsible for the observed texture. Further experiments using the CO₂/H₂ system may reveal how such features form and how the presence of hydrogen alters polymer surfaces with CO₂/H₂, H₂O, and HCOOH plasma modification.

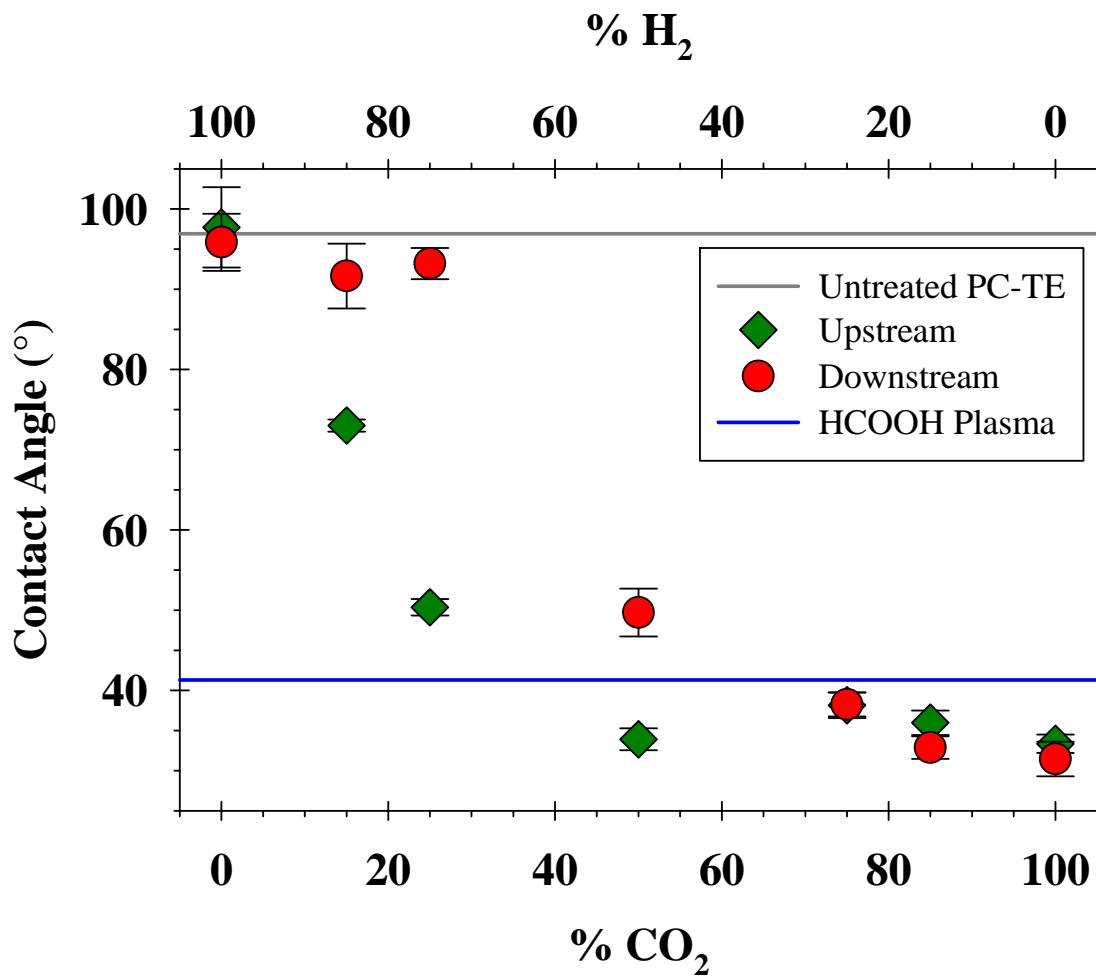


Figure 8.2. wCA measurements on the upstream and downstream sides of PC-TE following treatment using various CO₂/H₂ mixtures ($P = 25$ W, 200 mTorr, 2 min treatment time, 9 cm downstream sample placement). The wCA of untreated and HCOOH plasma treated PC-TE are shown for comparison. Error bars represent one standard deviation.

REFERENCES

1. Steen, M. L.; Jordan, A. C.; Fisher, E. R., Hydrophilic modification of polymeric membranes by low temperature H₂O plasma treatment. *J. Membr. Sci.* **2002**, 204, (1–2), 341-357.
2. Steen, M. L.; Hymas, L.; Havey, E. D.; Capps, N. E.; Castner, D. G.; Fisher, E. R., Low temperature plasma treatment of asymmetric polysulfone membranes for permanent hydrophilic surface modification. *J. Membr. Sci.* **2001**, 188, (1), 97-114.
3. Grill, A., *Cold Plasma Materials Fabrication: From Fundamentals to Applications*. IEEE Press: Piscataway, NJ, 1994.

APPENDIX A

PROGRAMMING AND CONTROL INTERFACE FOR AUTOMATION OF DATA COLLECTION AND EXTERNAL CONTROL OF MASS FLOW CONTROLLERS

This appendix describes the instrument control program and interface designed to manipulate the mass flow controller (MFC) set points in real time for the fabrication of the arbitrary film structures described in Chapter 7.

A.1. National Instruments DAQ to MKS 247D Hardware Interface

The mass flow rates of gases used for the research reported in this dissertation were controlled using MFCs (MKS Instruments, Inc.; 1179, 1479, and M100 Series). These controllers are operated using a model 247D four-channel readout, also from MKS Instruments, Inc. The 247D unit operates up to 4 MFCs using a 0-5 V analog signal corresponding to the full scale range of the MFC. Typically this analog signal is adjusted with the controls on the front of the readout based on constant flow rate set by the user. The 247D unit is also equipped with analog inputs for external control. These were used to interface the 247D unit with a computer via a National Instruments PCI-6024E DAQ and NI-BNC-2120 I/O interface unit so that flow set points could be adjusted automatically and in real-time based on a pre-set program. The NI-BNC-2120 is equipped with 8 analog inputs and 2 analog outputs in the form of BNC terminals. The interface between the 247D and the NI-BNC-2120 was made by manually soldering BNC connectors onto the appropriate leads of a parallel style cable (DB-25) connected to the back of the 247D unit based on the pin out pattern described in the 247D instrument manual.¹ The BNC connectors were attached to the NI-BNC-2120 to adjust the set point and read the transducer and

scaled outputs from two separate MFCs. The NI-BNC-2120 was also connected to the analog output of the PDR2000 Dual Capacitance Manometer display (MKS Instruments, Inc.) to log the reactor pressure.²

A.2. LabVIEW® Mass Flow Controller Data Acquisition and Control Program

The instrument control program created to control the 247D unit externally, entitled “MKS 247D Control vX.vi,” where X refers to the version number of the program, was programmed using LabVIEW® v8.5. Versions 1-6 are versions created during the iterative development of the program. “MKS 247D Control v7.vi” was the first fully functional version and was used for most of the research described in Chapter 7 of this dissertation. Version 7 was designed to run a gas flow program with up to 6 steps. Subsequent work required the ability to deposit films with more layers. “MKS 247D Control v8.vi” was created to address this problem and can accommodate a gas flow program of up to 18 steps. The programming structure of versions 7 and 8 are fundamentally identical, and the description in this Section applies to both versions.

The user interface exists on the front panel of the program, Figures A.1.-A.4. The upper left corner contains the input controls that define the physical hardware addresses corresponding to the connectors on the NI-BNC-2120 unit, Figure A.1. The remainder of the top of the front panel consists of chart recorder objects for monitoring the MFC and pressure readouts during program operation, Figures A.1.-A.2. The lower portion of the front panel consists of input controls that define a line-by-line flow program based on step time, initial flow rate, final flow rate, initial % Channel 2, final % Channel 2, and function type, Figures A.3.-A.4. To clarify the

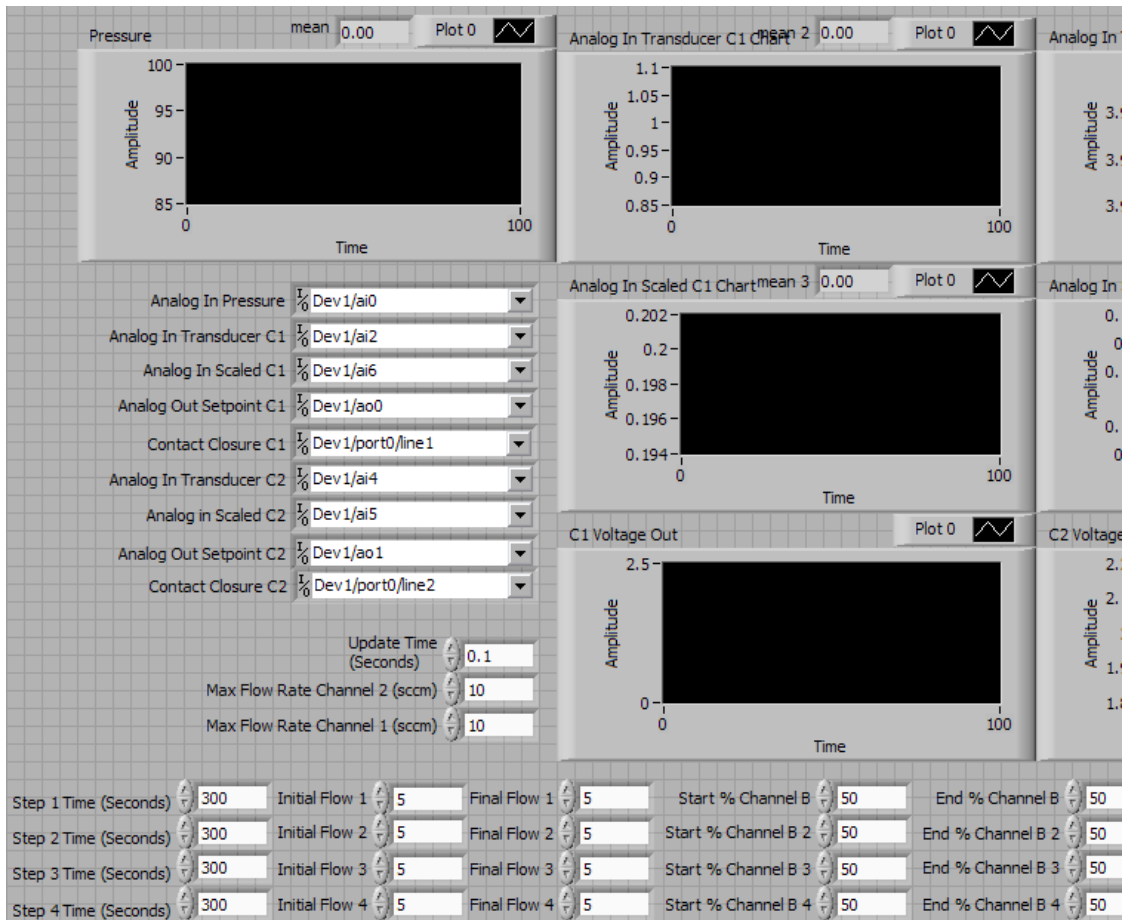


Figure A.1. LabView® “MKS 247D Control v8.vi” front panel, upper left quadrant.

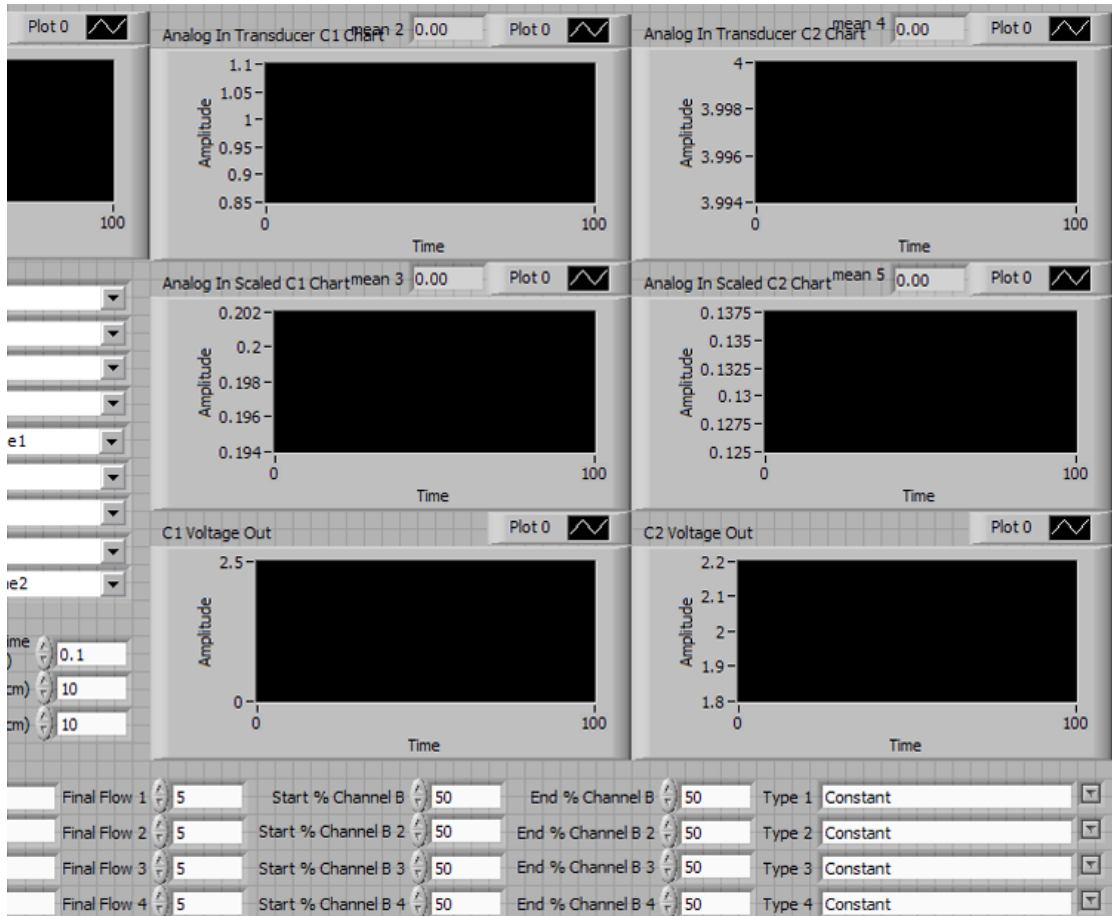


Figure A.2. LabView® “MKS 247D Control v8.vi” front panel, upper right quadrant.

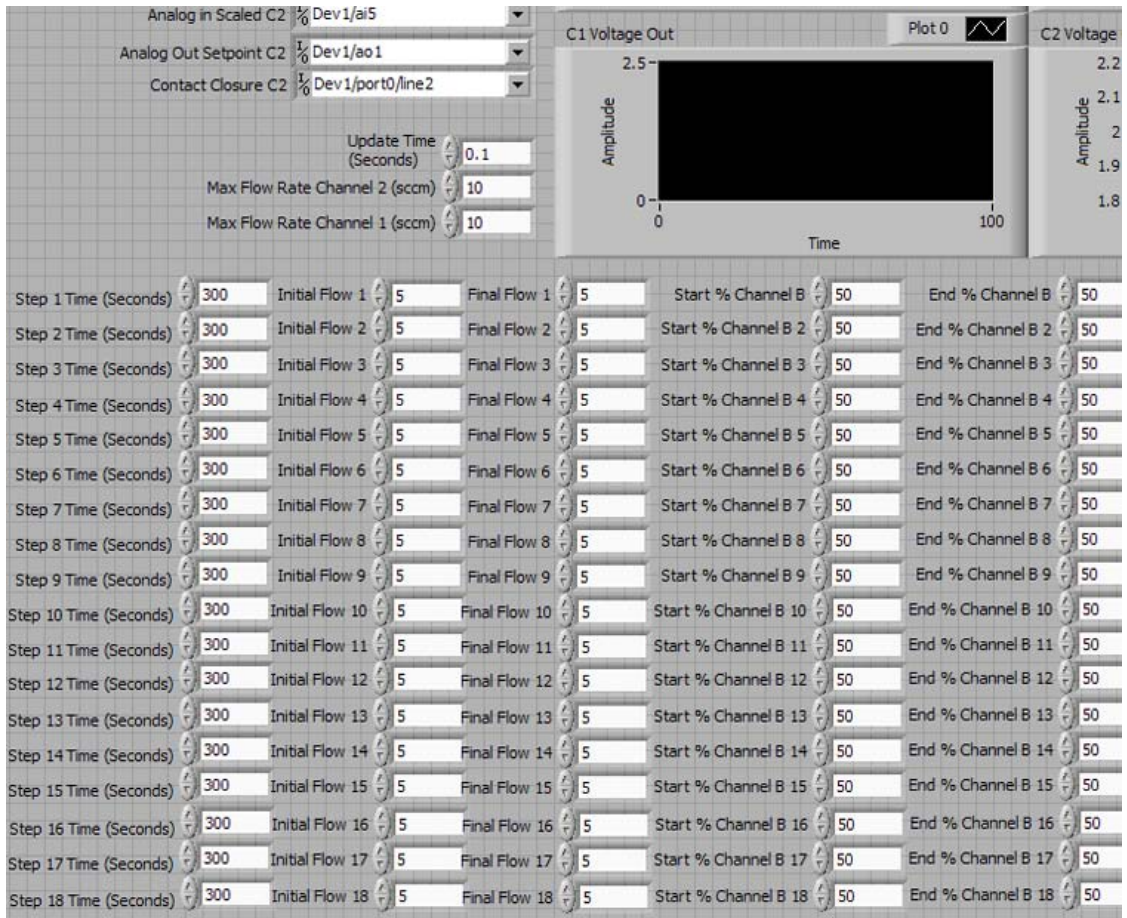


Figure A.3. LabView® “MKS 247D Control v8.vi” front panel, lower left quadrant.

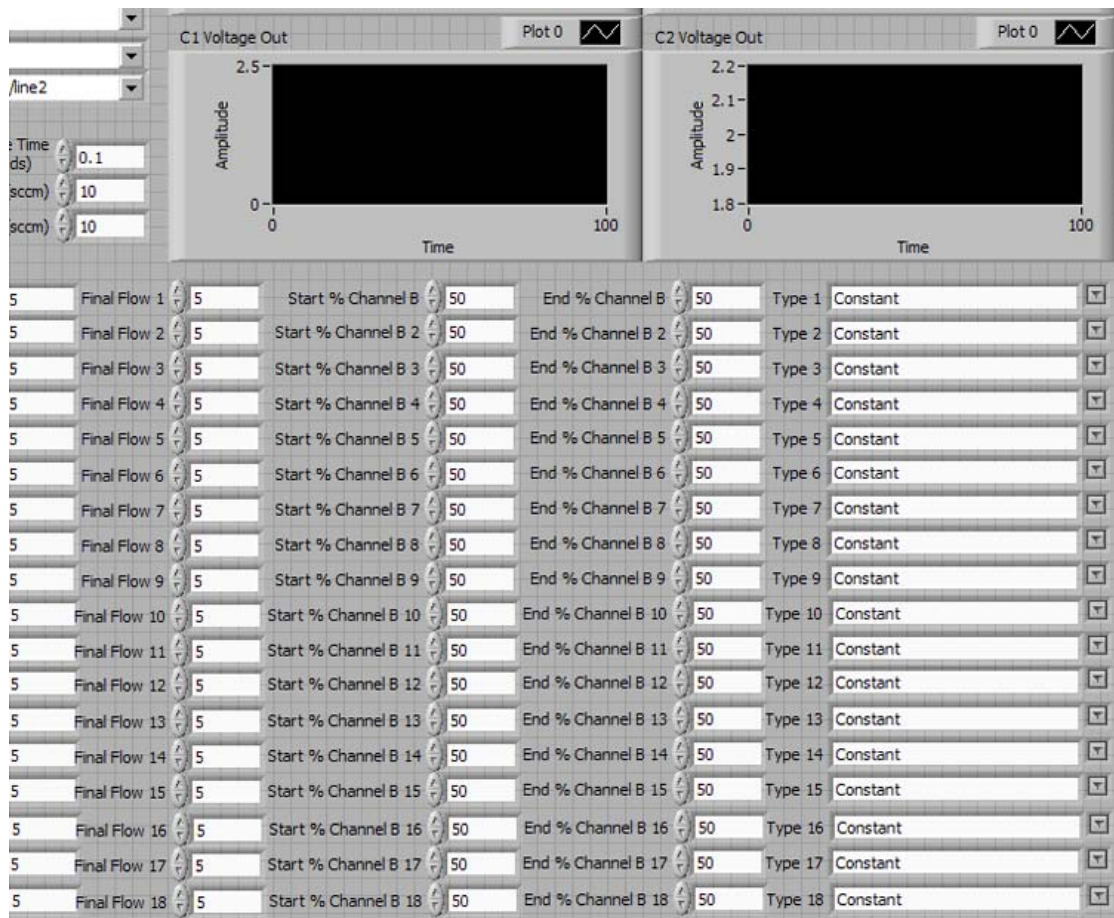


Figure A.4. LabView® “MKS 247D Control v8.vi” front panel, lower right quadrant.

channel labeling, Channel B is equivalent to Channel 2. For consistency, the numerical channel designations will be used in the remainder of this appendix.

The overall program is based on a stacked sequence structure that dictates the order that specific sets of instructions are executed when the program is run. For clarity, these sets of instructions or “Frames” will be described based on the order they appear in the program. Frame 0 contains instructions for deleting all residual data from the chart recorder objects on the front panel, Figure A.5. This is done by setting the history property node for each recorder object equal to a null array.

The purpose of Frame 1 is to create an array for each MFC channel containing the flow rate voltage set points based on the line-by-line flow program set by the user on the front panel. A separate array is generated for each line in the flow program using the inputs for that line, Figures A.6.-A.9. All inputs except the step time are double precision so that fractional numbers can be used. The step time is used to define the length of array for each step and is therefore forced to be a 32 bit integer. Each input is fed into a case structure based on the flow profile type set on the front panel. The case structure was designed so that different mathematical functions could be used to yield the desired voltage profile. Figure A.6. shows the “logarithmic” case. A ramp pattern operator is set to generate a logarithmic pattern based on equation A.1.³ for $i = 1, 2, 3, \dots, (n-1)$ using the initial and final flow values as start and end points.

$$x_i = e^{[\ln(x_o) + i\Delta x]} \quad (\text{A.1.})$$

The Channel 1 to Channel 2 ratio is set using a linear ramp pattern operator based on equation A.2.³

$$x_i = x_o + i\Delta x \quad (\text{A.2.})$$

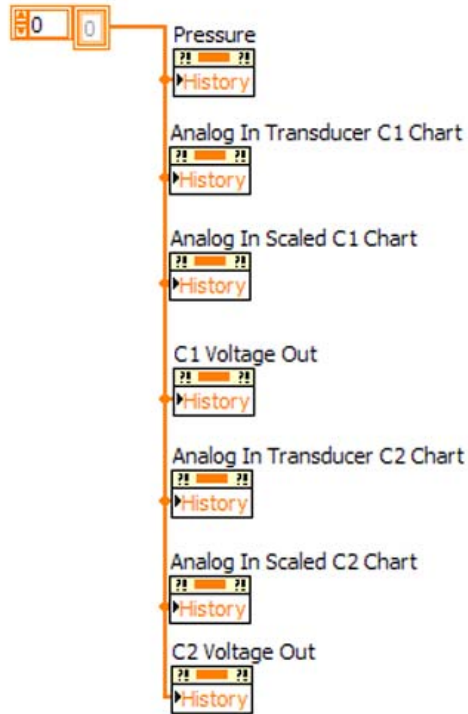


Figure A.5. LabView® “MKS 247D Control v8.vi” block diagram, Frame 0. These programming instructions force the chart recorders on the front panel to clear any leftover data.

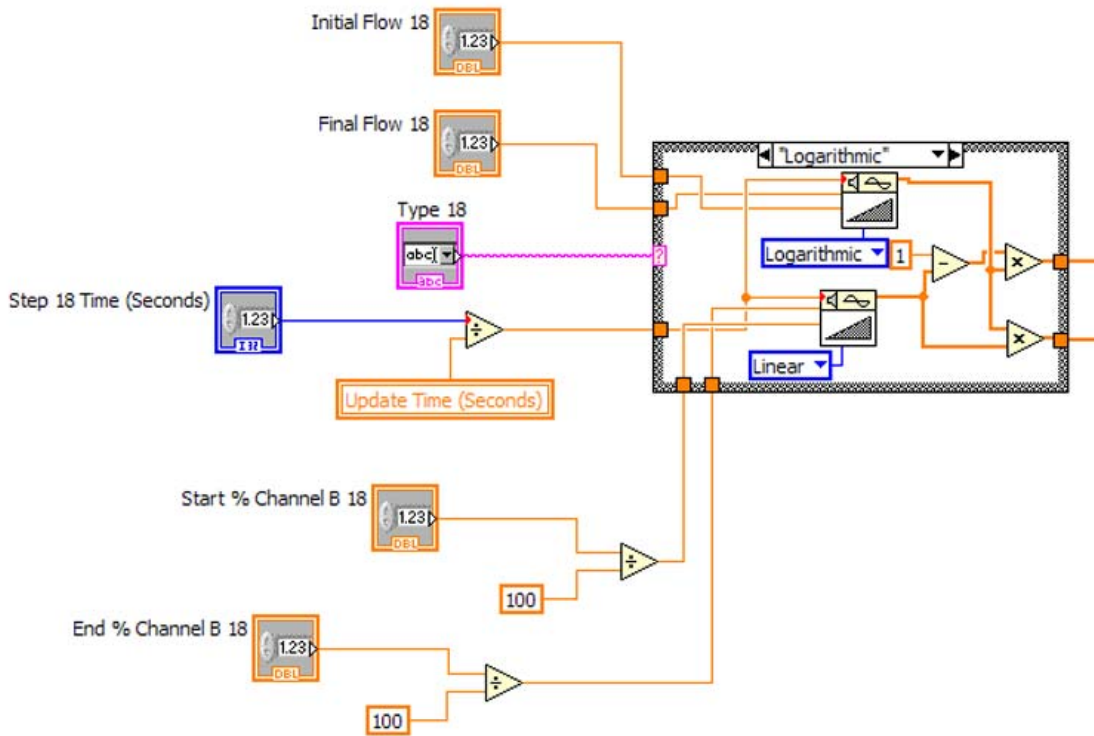


Figure A.6. LabView® “MKS 247D Control v8.vi” block diagram, Frame 1. These programming instructions define an array based on the line-by-line flow instructions set on the front panel. The case dependent frame shown populates the array to achieve a logarithmic change in flow rate.

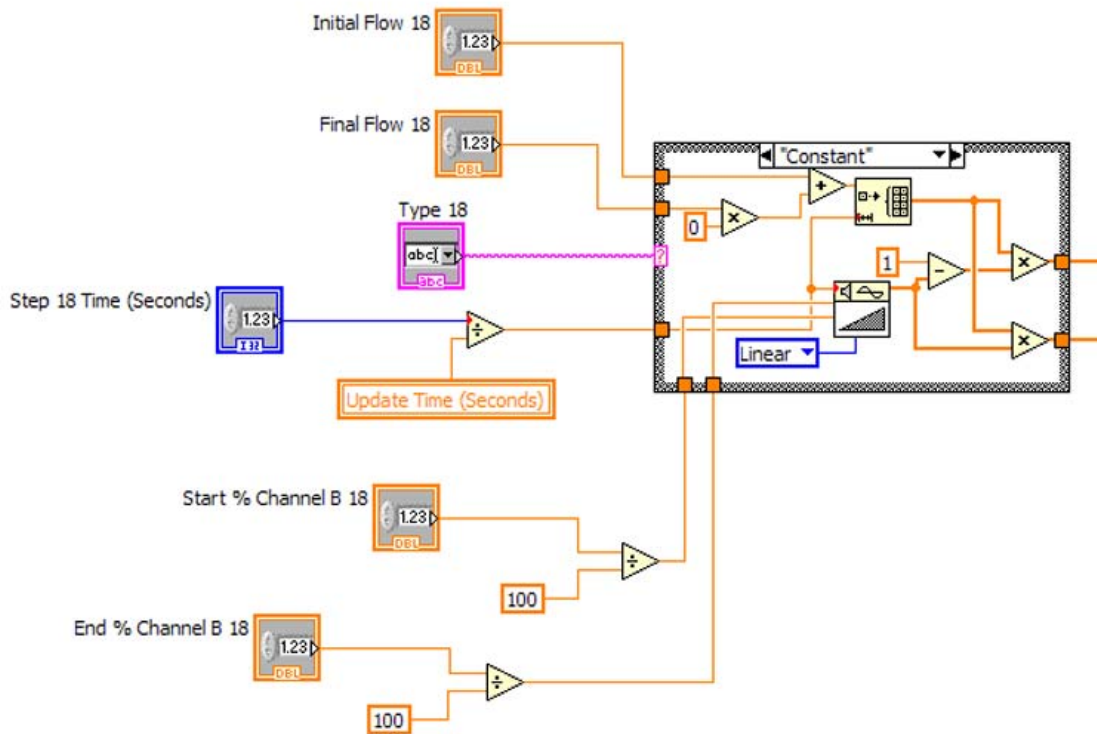


Figure A.7. LabView® “MKS 247D Control v8.vi” block diagram, Frame 1. These programming instructions define an array based on the line-by-line flow instructions set on the front panel. The case dependent frame shown populates the array so that the flow rate is held constant.

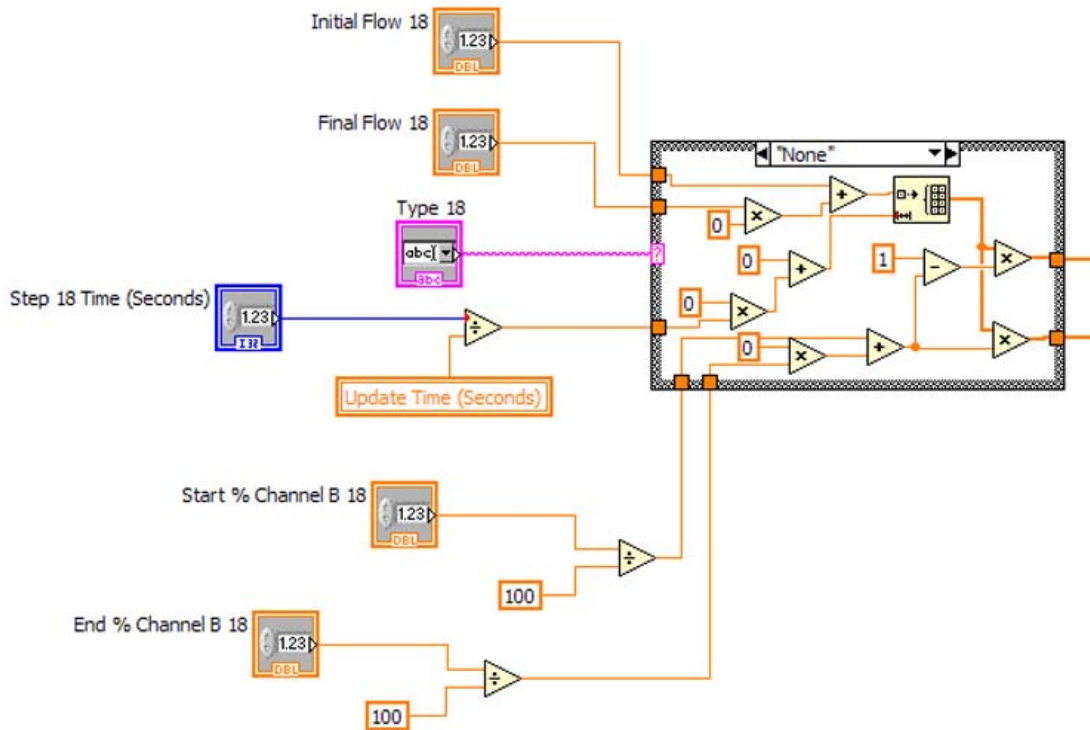


Figure A.8. LabView® “MKS 247D Control v8.vi” block diagram, Frame 1. These programming instructions define an array based on the line-by-line flow instructions set on the front panel. The case dependent frame shown generates an empty array allowing the user to turn off lines in the flow instructions.

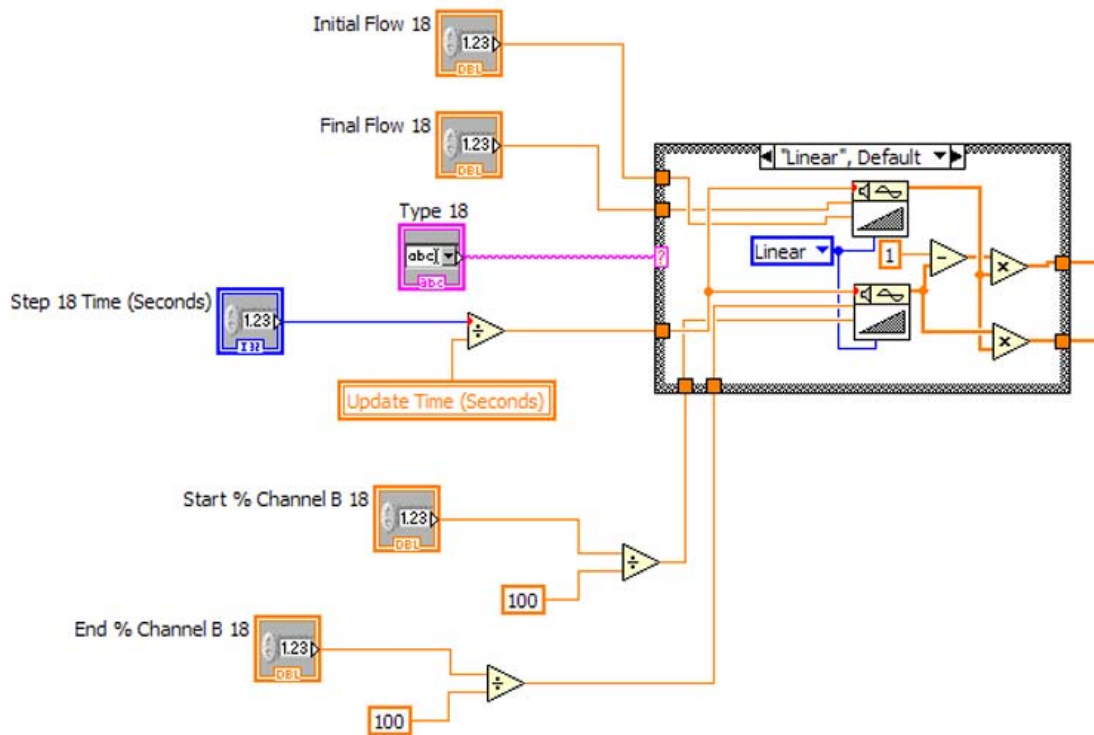


Figure A.9. LabView® “MKS 247D Control v8.vi” block diagram, Frame 1. These programming instructions define an array based on the line-by-line flow instructions set on the front panel. The case dependent frame shown populates the array to achieve a linear change in flow rate.

Figure A.7. shows the “constant” case. This case is designed to ignore the final flow rate so that the step runs at a constant rate based on the initial flow rate. Figure A.8. shows the “none” case. This case was designed to negate all inputs from a given flow program line to avoid errors when fewer than 18 program lines are being used. Figure A.9. shows the “linear” case. This case was designed so that both flow rate and the Channel 1 to Channel 2 ratio would be defined by a linear ramp pattern operator. The linear case was used to prepare all samples reported in Chapter 7. Once the Channel 1 and Channel 2 arrays for each flow program line are generated, they are concatenated using the build array function and used to calculate the array of voltage set points needed to alter the set points on each MFC, Figure A.10.

The purpose of Frame 2 is to control the timing by which analog signals are sent to and received from the 247D unit. This is accomplished using a timed loop structure operating at a 1 kHz base clock frequency and a loop frequency set by the update time input on the front panel, Figure A.11. The update time controls the time resolution of analog signals sent to and from the 247D unit. It was found during testing that update times <0.1 s overwhelmed the available computer memory, causing stability issues. The 0.1 s update time was used for all work reported in Chapter 7. Within the timed loop, the physical I/O hardware addresses are input into a function that creates an analog input or analog output virtual channel. This virtual channel is then directed to write the analog voltage from the set point array to the 247D unit or read the analog voltage from the 247D and PDR2000 units. Finally, the virtual channel is cleared so as not to overwhelm the memory during subsequent loop iterations. The received analog voltages are converted to meaningful data and output to chart recorder objects on the front panel for monitoring and diagnostic purposes, Figure A.12. The received analog voltage signals are also converted into a text string, concatenated into an array, and combined with a machine time stamp

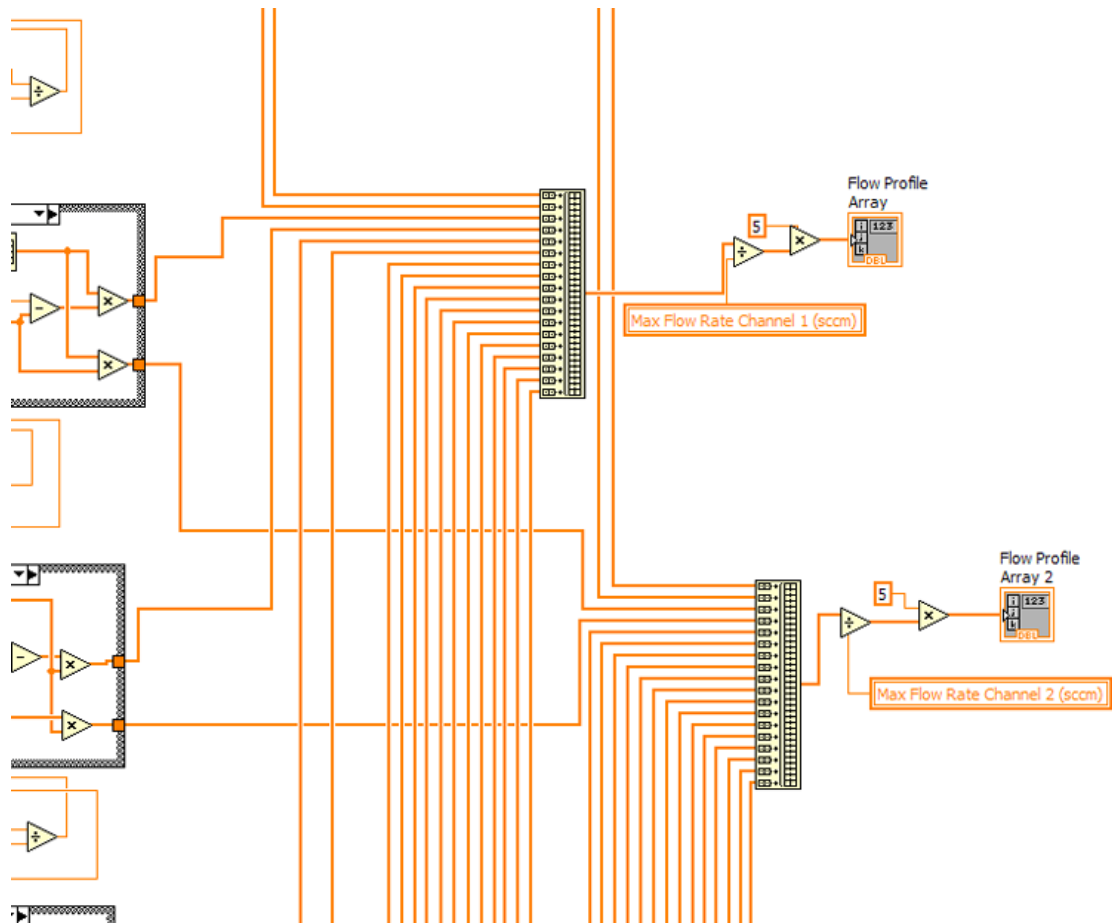


Figure A.10. LabView® “MKS 247D Control v8.vi” block diagram, Frame 1. These programming instructions concatenate the arrays from each flow instruction line into two arrays that define the overall flow profile for each MFC channel.

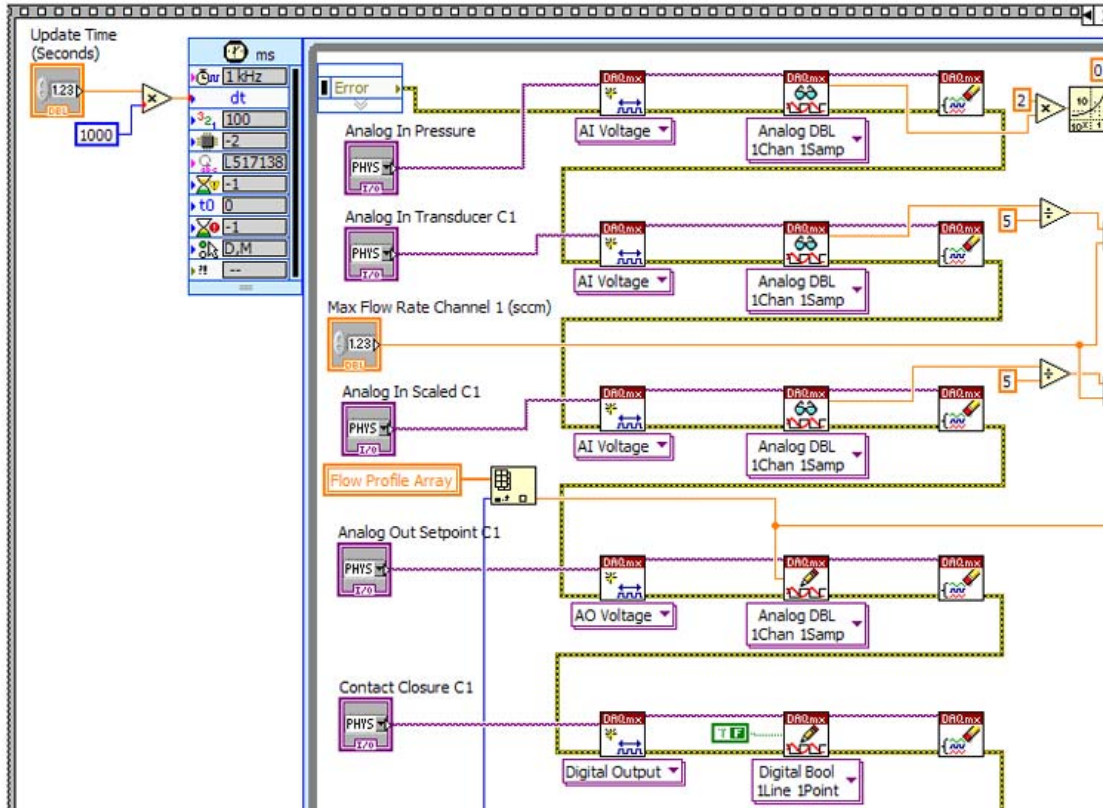


Figure A.11. LabView® “MKS 247D Control v8.vi” block diagram, Frame 2. These programming instructions show the left side of the timed loop responsible for sending and receiving DC voltage signals to and from the data acquisition and control unit.

so that data can be reconstructed following program operation, Figure A.13. The loop is controlled by comparing the loop iteration count to the MFC channel set point array for Channel 2, created in Frame 1, Figure A.14. The array element used in any given loop iteration is based on the iteration count of the loop and the loop is set to stop with the final array element.

Frame 3 contains vestigial programming that was originally intended to turn off the 247D unit following completion of the flow program, Figure A.15. This was accomplished using a similar strategy to that used in Frame 2. A digital output write command is set to send the correct voltage state to the 247D directing the channel to power down. However, testing showed that more stable operation was achieved by allowing the channels to equilibrate before and after operating the program. Therefore, this feature was never used for any of the study procedures.

The purpose of Frame 4 is to convert the array of output values generated in Frame 2 into a form that can be used outside of the LabVIEW® program, Figure A.16. The text string array is converted into a tab delimited spreadsheet string array and written to a file based on an open file dialog. The resulting file can be opened using Microsoft Excel® or similar text editing program.

A.3. System Test Results

Testing of the 247D hardware interface and the “MKS 247D Control v7.vi” program was conducted to verify the ability to continuously ramp the gas flow rates. The same reactor system used for preparing the gradient films described in Chapter 7 was used for this testing. Channel 1 was attached to H₂ (Airgas, Inc.; 99.9%) and Channel 2 was attached to C₃F₈ (Airgas, Inc.; VSLI Grade, 99.96%). The MFCs used for this experiment were rated for a maximum flow rate of 20 sccm. The flow rate program used for this test began by turning on the flow at the maximum flow rate and holding for 180 s. The flow was then decreased to 0 sccm over 600 s based on a

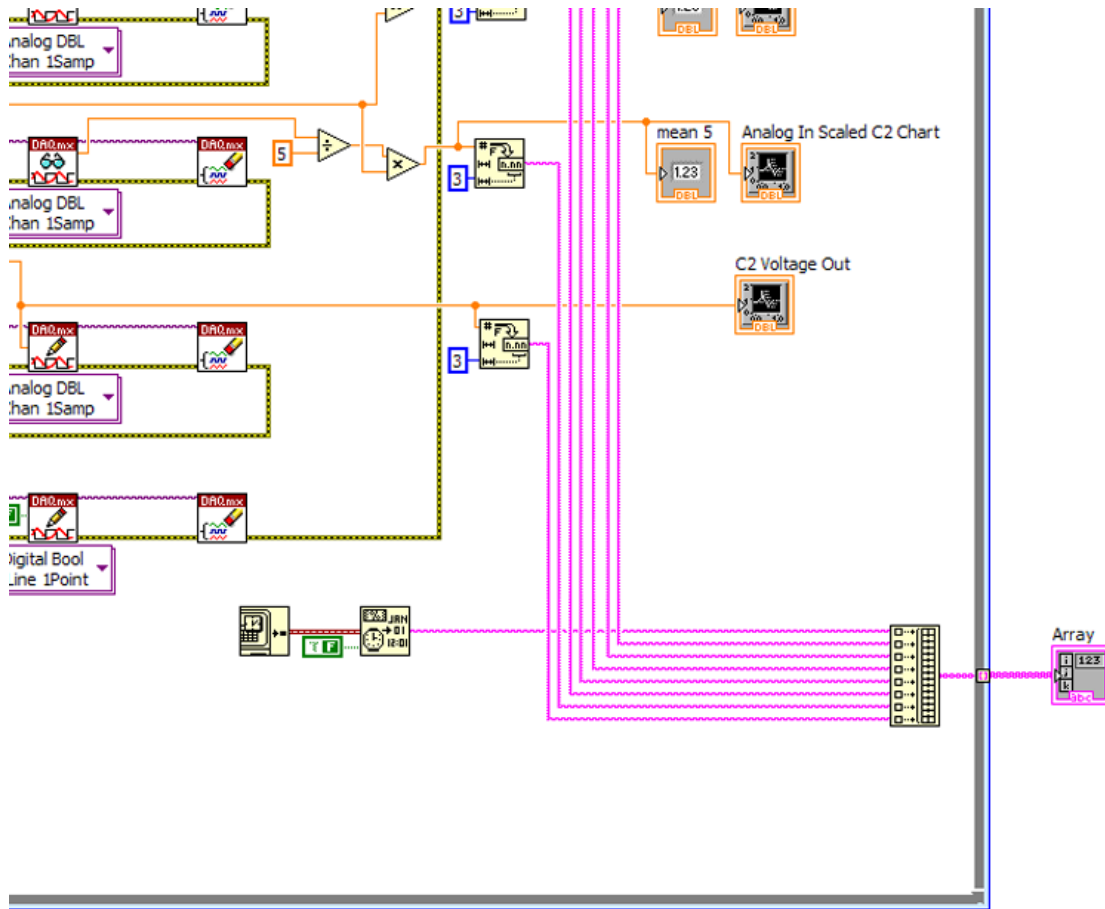


Figure A.13. LabView® “MKS 247D Control v8.vi” block diagram, Frame 2. These programming instructions specify the line in the flow profile array to be executed and stops the timed loop when all array elements have been executed.

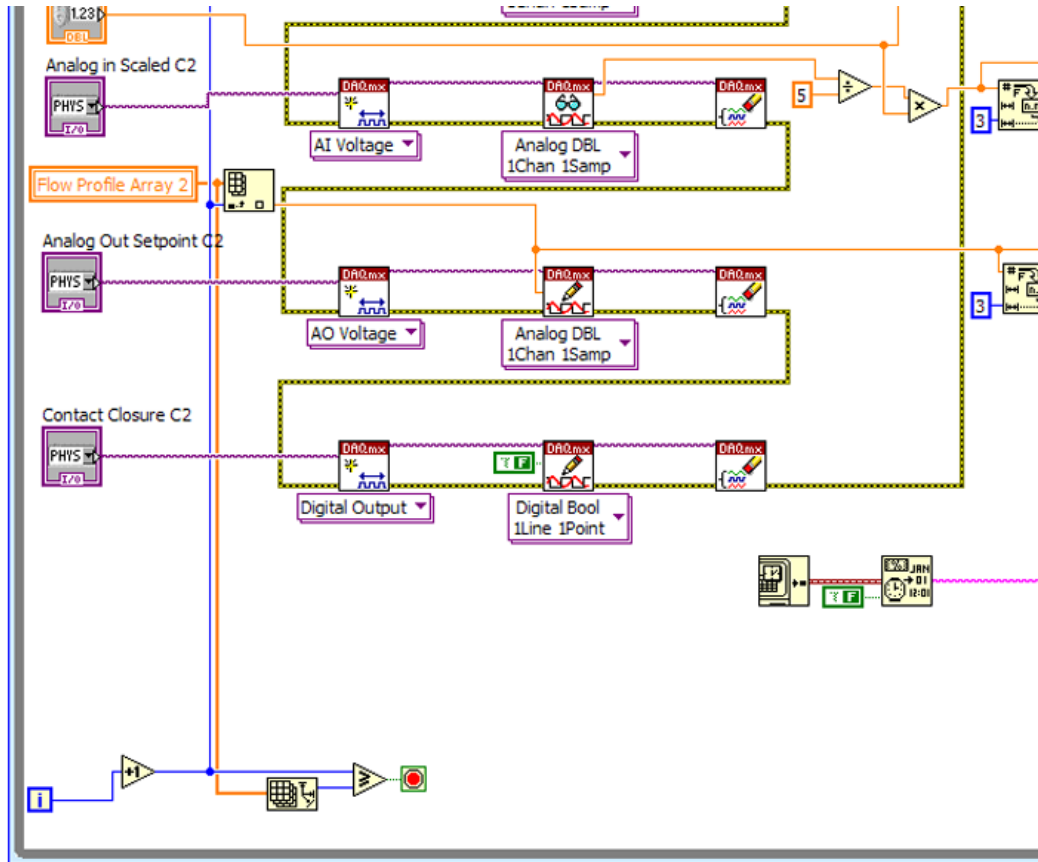


Figure A.14. LabView® “MKS 247D Control v8.vi” block diagram, Frame 2. These programming instructions compile an array from each analog output channel at the completion of each loop iteration.

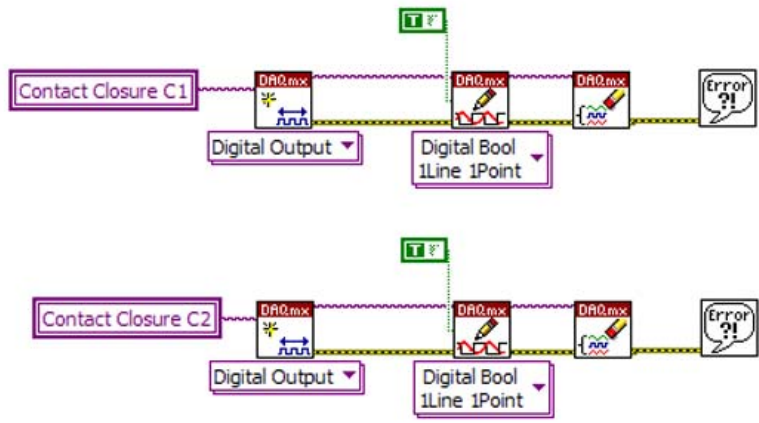


Figure A.15. LabView® “MKS 247D Control v8.vi” block diagram, Frame 3. These programming instructions force the contacts to close following the completion of timed loop in Frame 2. This is a vestigial structure in the program as the contacts were not used during normal operation by this version of the program.

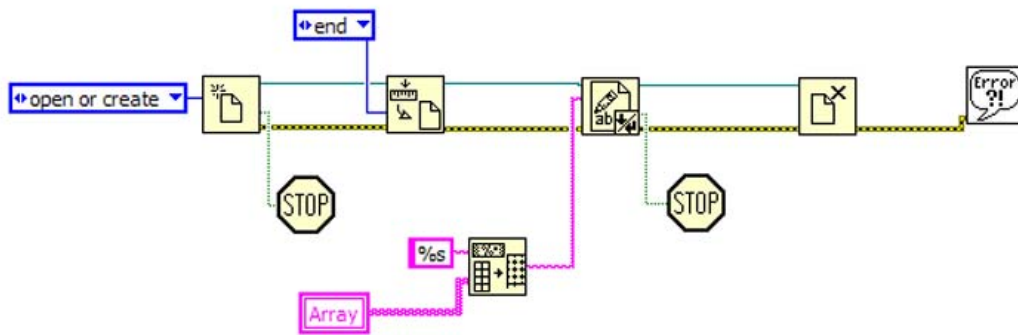


Figure A.16. LabView® “MKS 247D Control v8.vi” block diagram, Frame 4. These programming instructions convert the array containing all analog output readings into a text file for diagnostic and data recording purposes.

linear function. Finally, the flow was held at 0 sccm for 180 s. Each channel was tested independently, and the reactor pressure was monitored to characterize the pumping response. The results of testing Channel 1 are shown in Figure A.17. A comparison of the flow rate set point and the actual flow demonstrates that the flow measured by the MFC is nearly identical to the set point over the entire range of the test, Figure A.17.a. The pressure response logged from the PDR2000 corresponds well to this change in flow rate, Figure A.17.b. Indeed, when the flow rate set point and actual flow rate reach 0 sccm at 780 s, the pressure is nearly at base pressure. The absence of lag time between flow set point and pressure show the reactor pumping system is well suited for this application. Tests on Channel 2 yielded similar results, Figure A.18.

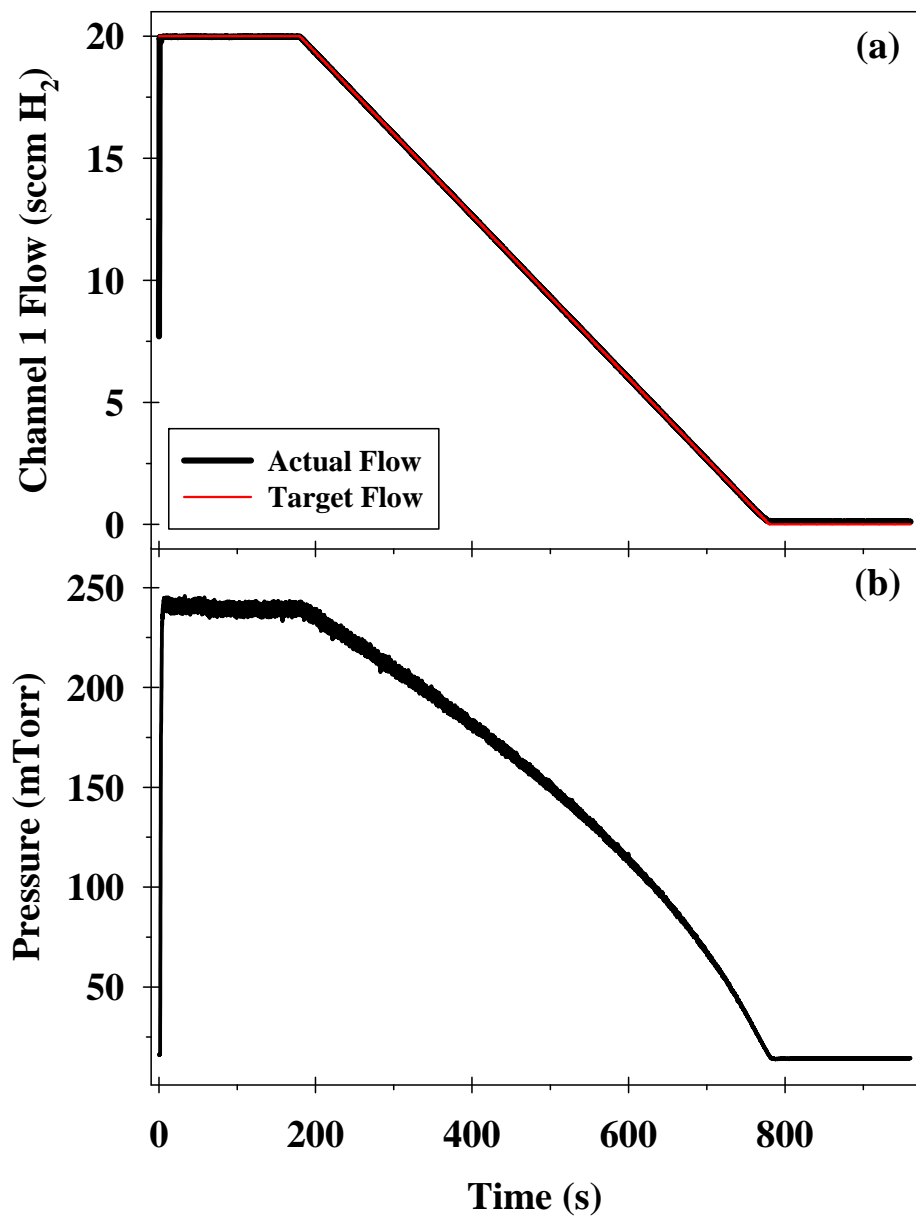


Figure A.17. MFC Channel 1 flow rate control results. (a) Target and actual flow rate of H₂ using a linear ramp from 20 to 0 sccm, and (b) the reactor pressure response over that same range.

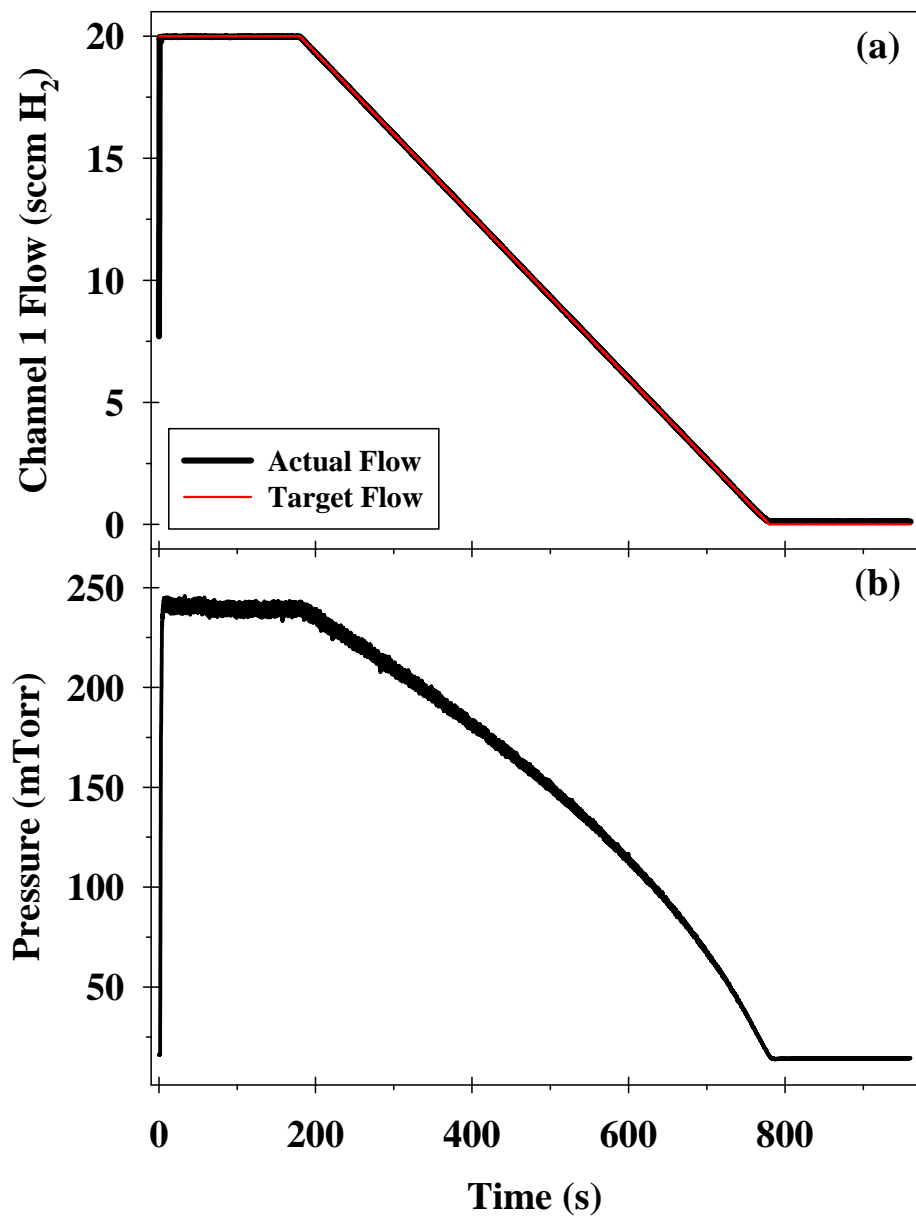


Figure A.18. MFC Channel 2 flow rate control results. (a) Target and actual flow rate of C_3F_8 using a linear ramp from 20 to 0 sccm, and (b) the reactor pressure response over that same range.

REFERENCES

1. MKS Instruments Inc., *MKS Type 247D Four-Channel Readout Instrument Manual*. Andover, MA, 1997.
2. MKS Instruments Inc., *MKS Type PDR 2000 Dual Capacitance Diaphragm Gauge Controller Instruction Manual*. Andover, MA, 2001.
3. *LabVIEW®*, v8.5; National Instruments Inc.: Austin, TX, 2007.

APPENDIX B

AN INVESTIGATION OF THE MECHANISMS AND FILM STRUCTURE THAT CONTROL HYDROPHILIC/OLEOPHOBIC BEHAVIOR ON COATINGS AND MATERIALS WITH SWITCHABLE AFFINITY

This appendix is adapted from the independent research proposal written for the Colorado State University Department of Chemistry PhD program proposal writing requirement. A brief description of the contents of this appendix follows.

Oleophobic or superoleophobic coatings that are also hydrophilic or superhydrophilic have recently become the subject of a great deal of research owing to their potential use for anti-fog coatings, bio-fouling resistant coatings, and coatings for separation media. Despite recent success in making such coatings, very little is understood about the mechanism that controls their environmental responsiveness. As a result, it is unclear how to best structure such films or fabricate devices to give optimum performance. This proposal outlines a multi-pronged approach to fabricate novel oleophobic/hydrophilic films using a combination of initiated chemical vapor deposition, plasma enhanced chemical vapor deposition, and self-assembled monolayer deposition based on azide/alkyne “click” chemistry. These deposition techniques will be designed so that film thickness and cross-linking can be tuned. By carefully tailoring these film properties, we hope to relate film structure to oleophobic/hydrophilic performance. Taking advantage of recent advances in contact angle measurements on polymer surfaces, contact angle goniometer hysteresis experiments will be performed to further elucidate the surface mechanisms related to film performance. Different surface processes, such as diffusion of non-polar probe liquids into the film or polymer chain reorganization induced by contact with a probe liquid, will

result in different contact angle hysteresis values based how the film is structured. Finally, the most promising film systems from the basic research portion of this proposal will be developed into separation media by applying the films to reentrant mesh materials. Performance of these materials will be tested using model mixtures based on the probe liquids used for contact angle goniometer hysteresis experiments to expand our understanding of how these remarkable surfaces perform.

B.1. Statement of Motivation and Previous Research

Oleophobic (OPB) or superoleophobic (SOPB) coatings that are also hydrophilic (HPL) or superhydrophilic (SHPL) have recently become the subject of a notable communication¹ and one recent review.² This is due in part to their potential for use in anti-fog optical coatings,^{3,4} as the next generation of bio-fouling resistant surfaces,^{5,6} and in high performance materials for oil spill remediation.^{1,7,8} To date, SOPB/SHPL coating technologies have been achieved by applying some type of fluorosurfactant to a HPL coating on a textured material using traditional solution based coating techniques^{1,9,10} or by spray casting a pre-fabricated nano-composite.^{11,12} Although the resulting films exhibit SOPB/HPL behavior, they require costly fluorosurfactant,¹³ are time consuming to prepare, and it is difficult to achieve a robust, defect-free film.¹⁴ There is a critical need to explore new fabrication techniques to solve these problems with the current technology.

Ongoing debate in the literature revolves around how SOPB/HPL materials achieve their “switchable” affinity. It was originally thought that when a surface is presented with a non-polar liquid, the thin fluorocarbon coating swells or uncoils to repel the non-polar liquid; when the surface is presented with a polar liquid, the fluorocarbon coating retracts to expose underlying

HPL polymer, Figure B.1.¹⁵ Thus, the surface achieves two distinct surface tensions based on environmental conditions. A recent report by Li, et al. contradicts this assumption.¹⁶ They attribute the different behavior of polar and non-polar substances on these surfaces to a difference in diffusion kinetics between the various test liquids as they penetrate the thin fluorocarbon coating. As a small molecule, H₂O diffuses through the OPB layer very fast compared to large nonpolar molecules, such as *n*-hexadecane (C₁₆H₃₄). The diffusion rate of a probe liquid into a fluoropolymer surface varies depending on differences in structure.¹⁷ Based on these reports, we would expect SOPB/HPL materials to exhibit some irreversible fouling with extended exposure of the HPL under-layer to non-polar contaminants. Yet, at least one recent study has demonstrated that this is not an issue by repeatedly cycling their SOPB/HPL material between polar and non-polar conditions.¹ At this point, it remains unclear how the ideal SOPB/HPL surface is structured on the molecular level and further investigations are required to inform this debate.

B.2. Novel Research and Proposed Techniques

The primary goal of this proposed research will be to investigate the origin of the responsive surface tension that is believed to give OPB/HPL materials a switchable affinity and thereby inform the controversy discussed in Section B.1. To this end, we will design new OPB/HPL film deposition/fabrication techniques that allow for uniquely tunable properties within the OPB and HPL layers, respectively. A combination of surface analysis techniques, including contact angle goniometry (CAG) and variable angle spectroscopic ellipsometry (VASE), will then be used to determine the extent to which diffusion and/or chain reorganization contribute to OPB/HPL behavior and switchable affinity. In conjunction with this basic

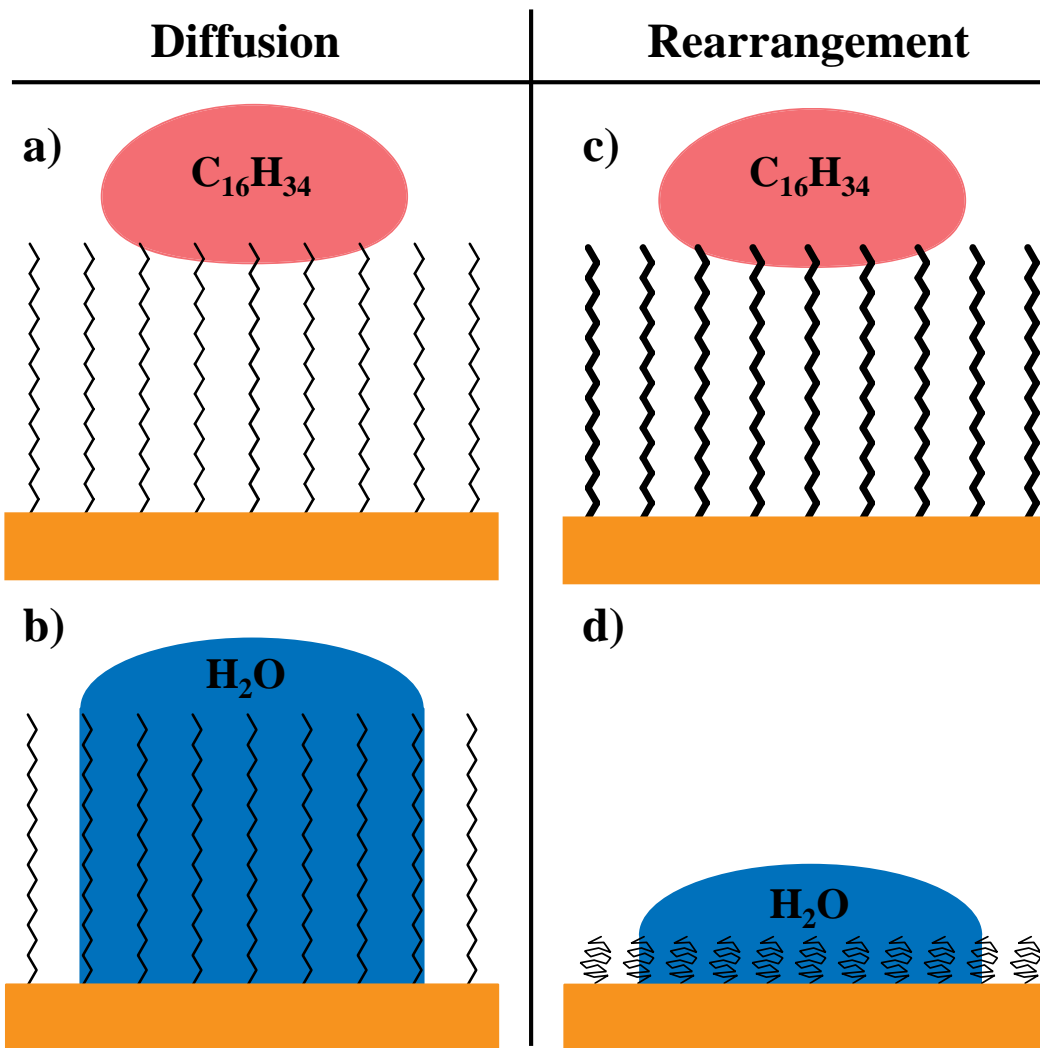


Figure B.1. Diffusion (a-b) and rearrangement (c-d) mechanisms for switchable affinity upon exposure to non-polar and polar liquids.

research, we will further develop these OPB/HPL films for separation applications. The OPB/HPL film systems will be applied to a range of reentrant mesh materials, thereby creating SOPB/SHPL media for separation applications. The separation capabilities of these SOPB/SHPL devices will be examined using model and “real world” oil-in-water emulsions. Beyond developing a commercially viable separation technologically, we expect that this pilot separation study will validate our findings with respect to the underlying origins of OPB/HPL behavior.

Central to our goal of understanding OPB/HPL mechanisms will be the ability to tailor the properties of thin film systems to gain an understanding of the parameters that limit OPB/HPL behavior. To our knowledge, OPB/HPL coating technologies that allow this level of control have not been described in the literature. We will develop films that either limit diffusion to the underlying HPL layer or limit reorganization of the OPB layer. Diffusion through the OPB layer to the underlying polymer material is easily controlled by changing the thickness of the hydrophobic OPB coating. We expect that the extent of switching behavior will increase and switching response time will decrease with decreasing coating thickness until the OPB layer no longer acts as a low surface tension coating, Figure B.2.a-c. However, a dependence on coating thickness does not rule out the possibility that the OPB layer is reorganizing. The OPB coating will, therefore, be designed such that a small degree of cross-linking can be introduced at a desired depth within the film. This cross-linked region should begin to limit film reorganization depending on the density and distribution of cross-linking incorporated into the OPB layer, Figure B.2.d-f. Our ability to fabricate these films with a constant coating density will also be of interest as the ability of the contacting liquid to make contact with the HPL layer is likely critical to OPB/HPL behavior, as well.

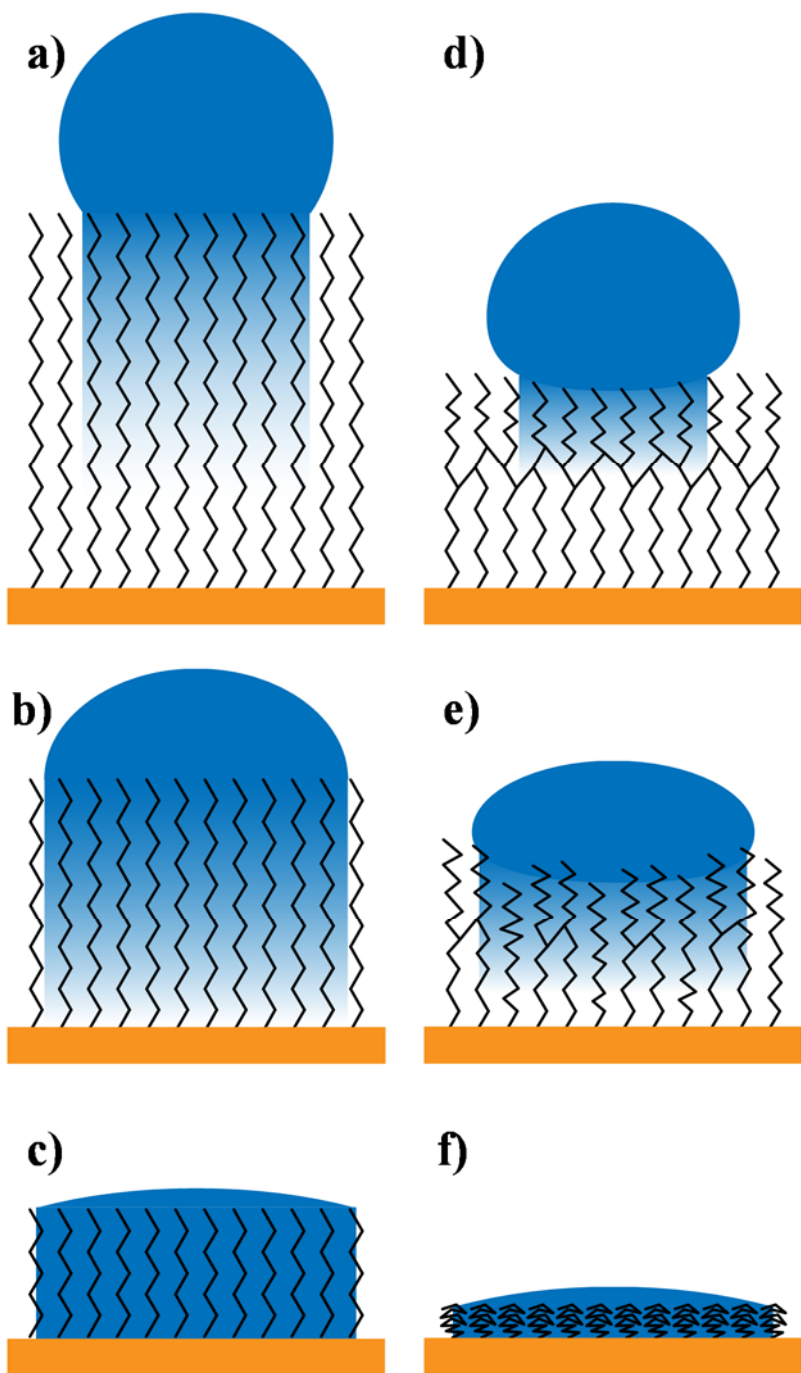


Figure B.2. Predicted aqueous contact angle as a function of (a-c) thickness and (d-f) cross-link density for diffusion controlled and reorganization controlled OPB/HPL phenomena, respectively.

B.2.1. Fabrication of OPB/HPL Films. Design of these OPB/HPL thin-film systems will be separated into two phases: fabrication of the HPL base-layer and fabrication of the OPB top-layer. Kota, et al.¹ found great success using cross-linked poly(ethylene glycol) diacrylate (x-PEGDA) blended with fluorodecyl polyhedral oligomeric silsesquioxane (F-POSS) to achieve SOPB/SHPL surface using a dip coating method. The blended F-POSS/x-PEGDA material had excellent performance but no attempt was made to control the surface structure or understand how the surface structure gave SOPB/SHPL characteristics. We intend to use vapor deposited poly(hydroxyethyl methacrylate) (pHEMA) films for our HPL polymer base-layer. Our approach will be based on the reports of initiated chemical vapor deposition (iCVD) of hydroxyethyl methacrylate (HEMA) by Gleason and coworkers.¹⁸⁻²¹ pHEMA is similar in many ways to the polyethylene glycol based polymers such as x-PEGDA. It is already relatively hydrophilic as synthesized, for example. However, pHEMA and the pHEMA deposition process have distinct advantages in this application. The deposition of pHEMA on 3D porous materials using the iCVD process has already been demonstrated.¹⁸ The coatings designed for the basic research portion of this proposal can be further developed into proof of concept SOPB/SHPL materials developed on reentrant substrates and structures. The cross-linking density of pHEMA prepared using iCVD can be controlled, leading to tunable reversible swelling behavior within the pHEMA film.²⁰ This will make it possible to measure solvent diffusion through the OPB top-layer by measuring pHEMA swelling using variable angle spectroscopic ellipsometry (VASE). Furthermore, we can design control experiments to verify diffusion measurements through the outer OPB coating by changing the cross-link density within the pHEMA film. Finally, the surface is populated by hydroxyl groups that can be used in the attachment of the OPB top-layer, Figure B.3.

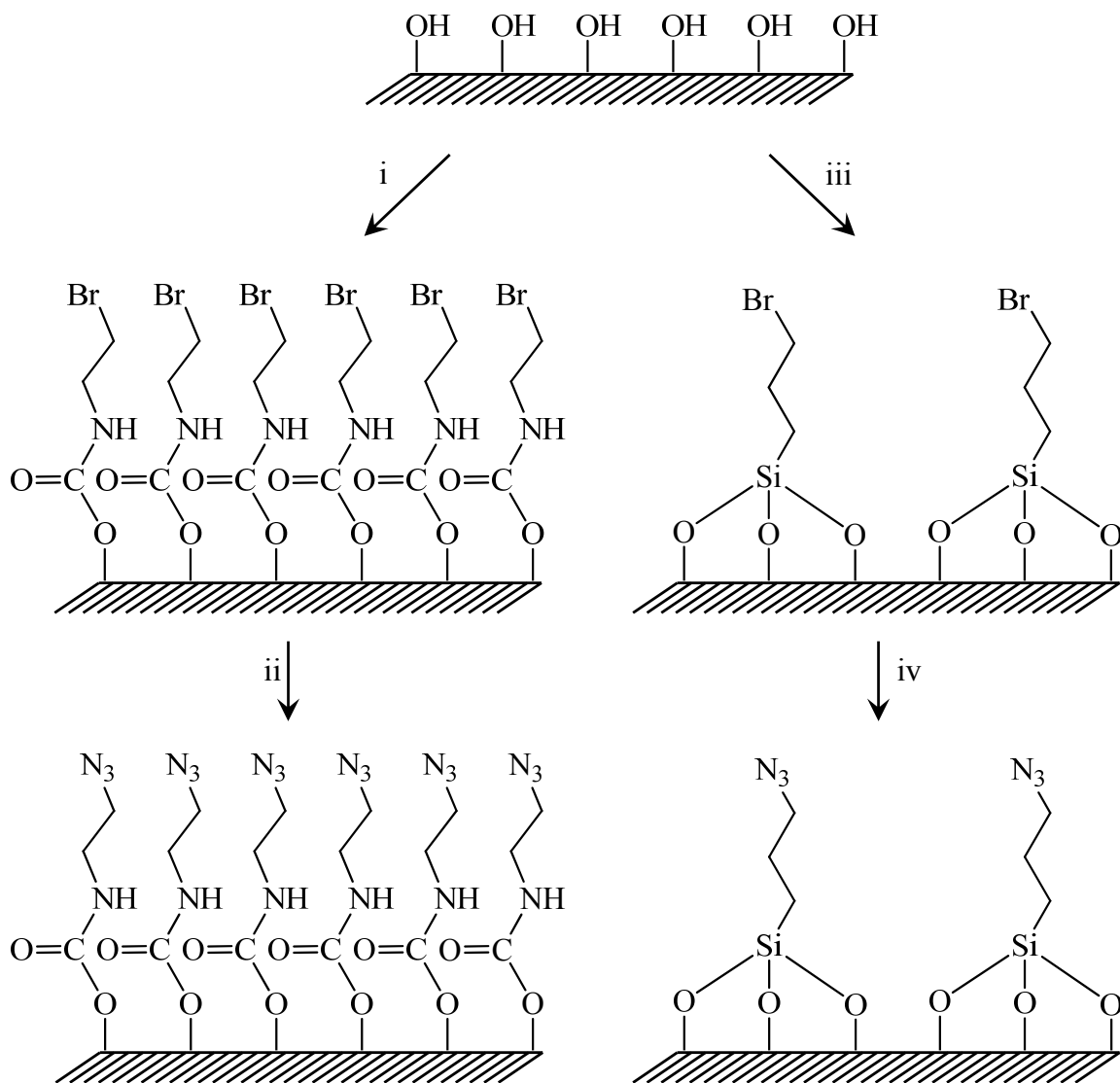


Figure B.3. Incorporation of azide surface functionality using isocyanate or triethoxysilane chemistry. Conditions: (i) 2-bromoethyl isocyanate, dibutyl tin dilaurate, THF; (ii) NaN₃, H₂O; (iii) (3-bromopropyl) triethoxysilane, CH₂Cl₂; and (iv) NaN₃, H₂O.

Given the complexity and the number of confounding factors associated with studying OPB/HPL phenomena, we propose two possible routes for the controlled fabrication of the OPB top-layer. The first proposed method is based on a version of “Click” chemistry first discovered by Huisgen²² and later popularized by Sharpless and coworkers.²³ The goal is to incorporate cross-linkable alkyne chemistry into a partially fluorinated self-assembled monolayer. Starting with a pHEMA surface, (3-bromopropyl)isocyanate will be reacted with the existing surface hydroxyl groups using dibutyltin dilaurate as a catalyst, based on the work by Ratner and coworkers, Figure B.3.^{24, 25} An alternative to the isocyanate chemistry would be to use (3-bromopropyl) trimethoxysilane in place of (3-bromopropyl) isocyanate. Silanes are known to cross-link with one another at a surface which would be undesirable given that we wish to study diffusion beyond this layer.²⁶ However, the coating density of (3-bromopropyl) trimethoxysilane will likely be different, giving us some flexibility in that respect. The alkyl bromide groups will then be converted into azide groups using an aqueous solution of sodium azide. A range of partially fluorinated mono- and dialkynes will be synthesized based on the on the reaction outlined in Figure B.4. using the starting materials listed in Table B.1. Briefly, a partially fluorinated primary alcohol will be converted into an aldehyde using the Swern reaction followed by conversion to an alkyne anion by the Corey-Fuchs reaction. A range of primary halide functionalized alkynes or water will be added to yield the desired mono- and dialkyne. This terminal alkyne will be attached to the azide-functionalized surface using the CuBr catalyzed alkyne-azide “Click” reaction, Figure B.5.²⁷ Finally the surface will be irradiated with ultra-violet light to induce cross-linking in the alkyne-rich layer of the film. The end result will be a fluorocarbon terminated monolayer with a cross-linked hydrocarbon underneath. Following proof of concept, we plan to use mixtures of the partially fluorinated mono- and dialkynes so that

Table B.1. Proposed precursors for alkyne and dialkyne synthesis.

1° Alcohol	1° Bromoalkyne	Product
1H,1H-perfluorononan-1-ol	5-bromopent-1-yne	1H,3H,3H,4H,4H,5H,5H-perfluoropentadec-1,6-diyne
1H,1H,2H,2H-perfluorodecan-1-ol	4-bromobut-1-yne	1H,3H,3H,4H,4H,7H,7H-perfluoropentadec-1,5-diyne
1H,1H,2H,2H,3H,3H-perfluoroundecan-1-ol	3-bromoprop-1-yne	1H,3H,3H,6H,6H,7H,7H-perfluoropentadec-1,4-diyne
1H,1H,2H,2H,3H,3H,4H,4H,5H,5H,6H,6H-perfluorotetradecan-1-ol	H ₂ O	1H,3H,3H,4H,4H,5H,5H,6H,6H,7H,7H-perfluoropentadec-1-yne

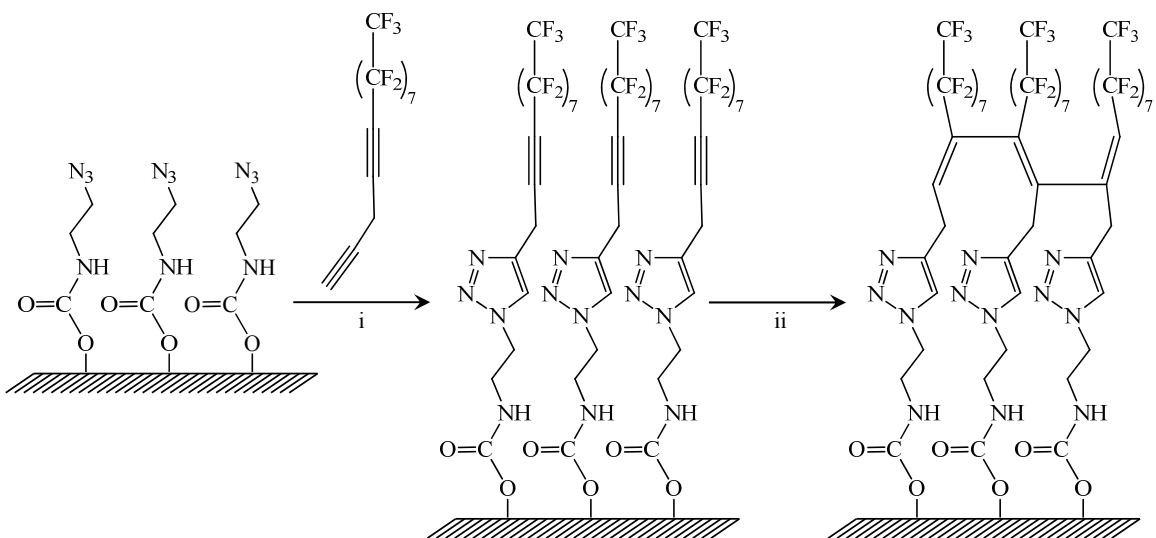


Figure B.5. Azide/alkyne "Click" chemistry for cross-linked fluorinated self-assembled monolayer films. Conditions: (i) CuBr; (ii) UV.

cross-link density can be tuned. This will be accomplished using three possible routes: 1) di-yne mixtures will be made to achieve a tunable mismatch in the –yne functional group position to limit cross-link density, 2) mono- and dialkynes will be mixed so that cross-linking can be limited by the di-yne concentration, and (3) UV irradiation intensity will be tuned to control the extent of cross-linking in a homogenous di-yne film.

The second proposed coating method for OPB layer formation will be plasma enhanced-chemical vapor deposition (PECVD). PECVD allows for unprecedented control over film deposition parameters and makes for uniquely tunable films (i.e. composition, functionality, and structure). This approach is not without precedent; some of the earliest reports of OPB/HPL surfaces used PECVD to deposit a hydrophilic polymer layer prior to fluorosurfactant film deposition.^{28, 29} More recently, Kumar and coworkers⁶ achieved good results by co-depositing 1H,1H,2H,2H-perfluorodecyl acrylate and diethyleneglycol dimethyl ether using PECVD. Similar to the coating studies mentioned in Section 1, no attempt was made to structure the material in any specific way. However, these studies show that the stepwise fabrication of an OPB/HPL material is possible using a completely PECVD-based approach. The ease by which a film can be subtly altered via changing deposition parameters means PECVD will make a good platform for investigating OPB/HPL behavior. Moreover, PECVD does not require the same time consuming synthesis required to make solution-phase deposition precursors. Our initial goal will be to use PECVD of a fluorocarbon precursor (i.e. perfluoroethane (C_2F_6), perfluoropropane (C_3F_8), hexafluoropropylene (C_3F_6), octafluorocyclobutane (*c*- C_4F_8), or hexafluoropropylene oxide (HFPO) to form a fluoropolymer on pHEMA that exhibits OPB/HPL behavior. Following proof of concept we will adjust film thickness and cross-linking. Film thickness is easily adjusted by changing the deposition time. Tuning cross-link density of

PECVD films is conceptually more complicated, though practically just as easy. Several research groups have demonstrated that PECVD techniques can yield films with different degrees of cross-linking. Foster and coworkers^{30, 31} showed that higher applied plasma powers can be used to enhance cross-linking during *c*-C₄F₈ deposition. Fisher and coworkers³² demonstrated that films deposited from a continuous wave *c*-C₄F₈ plasma operating at 5-50 W have cross-linking that varies from 10.7-61.2%, respectively. In a similar study,^{33, 34} they found that cross-linking could be varied in pulsed HFPO plasmas by changing the duty cycle, yielding a range of amorphous to highly ordered Teflon®-like materials. Moreover, NEXAFS measurements demonstrated that low duty cycles result in highly ordered films where (CF₂)_n chains are oriented perpendicular to the surface, similar to those depicted in Figure B.2.a-c. These studies demonstrate that cross-linking is easily controlled by adjusting the plasma parameters. We intend to take advantage of this to localize a region of higher cross-link density within a film by adjusting the plasma parameters in real time during deposition, thus limiting chain reorganization within the OPB/HPL test film. We propose a new technique wherein the pulse frequency and duty cycle of a pulsed HFPO or *c*-C₄F₈ plasma are modulated using an arbitrary function generator. By increasing the pulse frequency and duty cycle at the desired point during deposition, we can place a layer of higher cross-link density at a pre-determined depth within the film, Figure B.6. From this, it should be possible to fabricate a range of films where we can control chain reorganization while keeping the surface energy constant. An alternative method would be to modulate applied power to adjust cross-linking density. However, increasing the energy in the system may extend the cross-linked layer into the already deposited fluoropolymer material or damage the underlying pHEMA layer.

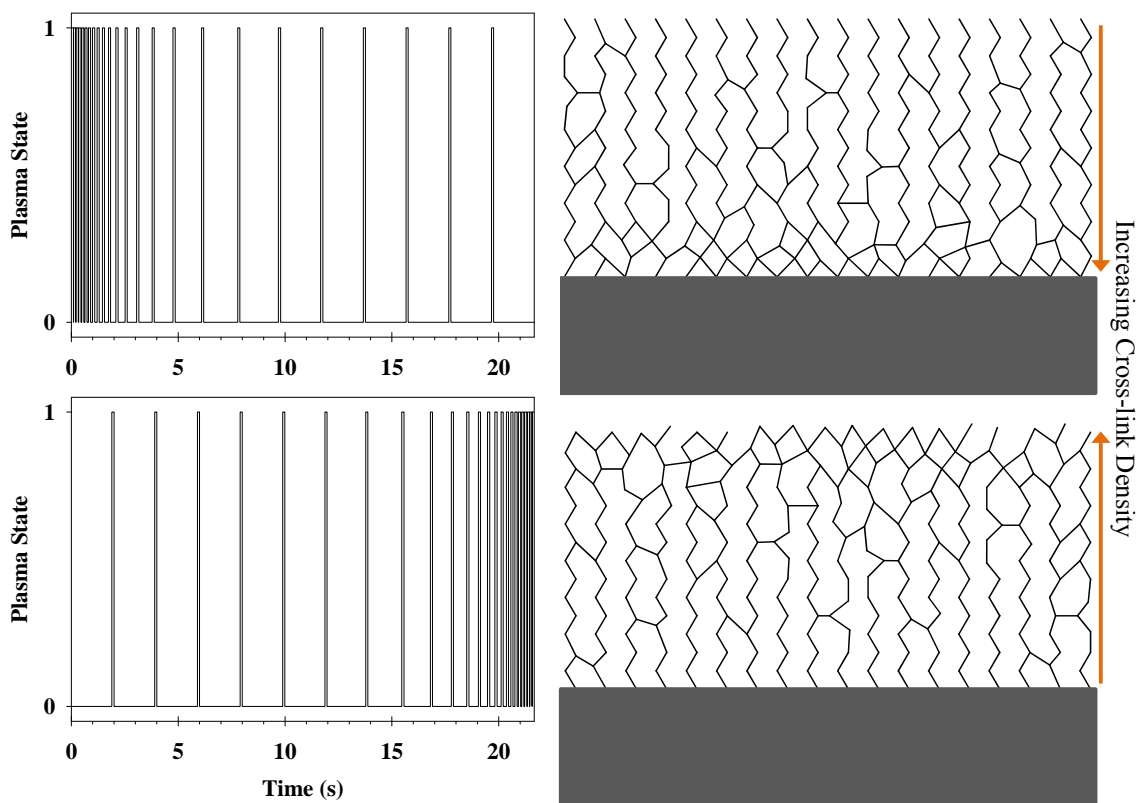


Figure B.6. Pulse modulation for controlled cross-linking in *pp*-HFPO or *pp-c*-C₄F₈ films.

B.2.2. OPB/HPL Film Characterization and Study of Switchable Affinity. All OPB/HPL film system prototypes will be tested and characterized to eliminate versions that fail to exhibit OPB/HPL characteristics so that we can begin to understand the structural properties of films with switchable affinity. This will be accomplished by measuring film surface tensions (γ) with CAG using *n*-hexadecane ($C_{16}H_{34}$) and H_2O as probe liquids. Young's equation shows that the contact angle (θ) made at the three phase point should decrease as the probe liquid surface tension decreases for a stable surface, Equation 1.³⁵

$$\gamma_{LV} \cos \theta = \gamma_{SV} - \gamma_{SL} \quad (B.1.)$$

On an ideal surface (a perfectly flat, homogeneous, and stable surface), the contributions from the solid surface to the surface tension components are constant. However, we are interested in surfaces that violates this trend; the goal of this research is to achieve a surface where $\theta(C_{16}H_{34}) > \theta(H_2O)$, the nominal threshold where a film is considered to have OPB/HPL properties. After identifying such films, the basic structure of each will be determined using a combination of attenuated total reflection-Fourier transform infrared spectroscopy (ATR-FTIR), x-ray photoelectron spectroscopy (XPS), and ToF-SIMS. ATR-FTIR and XPS will be used to verify the composition of the OPB layers fabricated using either the SAM or pulsed plasma polymerization approach. ToF-SIMS will be used to gain additional information about thickness of each film layer, structural information, and the extent to which the OPB and HPL film layers interpenetrate. The extent of interpenetration is of particular interest in the case of the pulsed plasma polymerization method as energetic processes that take place in the plasma may yield a poorly defined OPB/HPL interface.

Reorganization and diffusion phenomena in the OPB top-layer will be examined using CAG, primarily. As mentioned above, the solid-liquid, solid-vapor, and liquid-vapor surface

tension components of an ideal system are constant. Advancing and receding CAG measurements made on an ideal system should be identical based on Young's equation.¹⁷ However, some degree of non-ideal behavior is observed on all surfaces, and, in certain cases, results from a change in the contribution from the solid surface to the surface tension components when the three-phase point is advancing or receding, yielding the hysteresis parameter (θ_{hyst}), Equation B.2.

$$\theta_{adv} - \theta_{rec} = \theta_{hyst} \quad (B.2.)$$

In the case of the surfaces outlined in Section 2 and the film systems proposed here, it is hypothesized that the OPB/HPL behavior arises from changes in solid surface tension under influence of the contacting/sorbed liquids. To expand our understanding of these unique films we intend to explore the reorganization of the OPB/HPL surface or the sorption process, as the case may be. Tavana, et al.¹⁷ examined contact angle hysteresis on fluoropolymer surfaces using a series of *n*-alkane probe liquids such that molecular size, surface tension, and chemical functionality were systematically varied. They found that the time dependent θ_{rec} behavior and the magnitude of θ_{hyst} could be related to a number of different phenomena taking place at and within the fluoropolymer film surface in contact with the probe liquid. They found that a θ_{rec} slope dependence on probe liquid molecular size was consistent with absorption of the probe liquid into the fluoropolymer surface. They also verified that the magnitude of θ_{hyst} was proportional to the sorption of the probe liquid onto the surface based on the relative θ_{hyst} values from a series of halogen substituted naphthalene probe liquids.

Based on these reports, we will perform similar experiments to understand the liquid surface interactions on OPB/HPL materials. OPB/HPL films will be tested as fabricated or, aged under aqueous/polar or *n*-hexadecane/non-polar conditions. An *n*-alkane series will be used to

obtain the θ_{hyst} and the slope of the θ_{rec} phase of an advancing/receding CAG experiment. A comparison of the θ_{hyst} values for the *n*-alkane series will tell us the tendency of the polymer chains to reorganize under non-polar/low surface tension conditions. A comparison of θ_{rec} slopes will tell us the rate that non-polar/low surface tension molecules penetrate into the surface of the OPB top-layer. We will also attempt to use a series of short chain polyethylene glycol (PEG) oligomers as probe liquids to garner similar information under polar/higher surface tension conditions in an effort to gain understanding of the penetration of polar molecules through the OPB top-layer and interactions with the HPL base-layer. Finally, we will perform advancing/receding CAG experiments using H₂O as a probe liquid to obtain θ_{rec} slopes. By relating OPB/HPL performance to the θ_{rec} slope we hope to support or disprove the hypothesis that water diffusion through the OPB layer is responsible for OPB/HPL properties.

Additional experiments using VASE will be performed to verify CAG experiments. Under appropriate conditions, VASE has the ability to measure the film thickness of individual layers in a multi-layer film system with high accuracy. Moreover, the J. A. Woollam M-2000 spectroscopic ellipsometer can be equipped with a liquid cell, making it possible to study the swelling of OPB/HPL layers *in situ*. The ability of H₂O to diffuse past the OPB layer is of particular interest. A pHEMA film with a reasonable degree of cross-linking will swell when in contact with H₂O.²⁰ Swelling will be determined as a function of time for samples in contact with H₂O. Swelling and CAG θ_{hyst} results will be compared to determine if reorganization accompanies swelling and if either are necessary conditions for overall OPB/HPL performance.

B.2.3. Preparation of SOPB/SHPL Materials and Pilot Separation Experiments. In parallel with the basic research outlined above, we will also develop the most promising film systems into proof-of-concept separation media. This will be done both to attempt to develop a

practical material for separations as well as to verify our conclusions about the structural requirements for the best OPB/HPL film system. We will begin by applying the most successful OPB/HPL film system to mesh or screen material. A screen material with the correct geometry and mesh size will behave as a reentrant structure without any complicated fabrication steps, such as those required to fabricate reentrant surfaces on solid substrates,^{36,37} Figure B.7. Furthermore, the vapor phase deposition processes used for making OPB/HPL films on flat substrates will lend themselves well to making defect free films on more complicated 3D materials such as screens. Depending on our success in developing the plasma polymer OPB-layer fabrication technique, we may be able prepare all film layers using a single piece of deposition equipment with little or no waste.

We will fabricate a simple bench scale separation experiment based on the designs by Kota, et al.,¹ Figure B.5. Kota used their device to study the separation of aqueous rapeseed oil and hexadecane emulsions and found that F-POSS/x-PEGDA polymer blends coated onto mesh material could achieve separation efficiencies >99%, even after the addition of surfactants to stabilize the emulsion. Such mixtures are of industrial and commercial importance, but they provide limited information with respect to the more complicated mixtures these materials might encounter. Environmental disasters, such as the sinking of the Deepwater Horizon demonstrate the need for materials capable of separating complex mixtures, indeed.³⁸ However, of the studies referenced in this proposal, no studies address the separation of crude oil from an aqueous matrix or the separation efficiency of individual components of such a complex matrix. We would like to extend our studies to include model and real world oil-in-water mixtures. By testing the separation of a model mixture of hydrocarbons based on the n-alkane series used during our CAG experiments, we can begin to ascertain the limits of this technology. We will quantify the

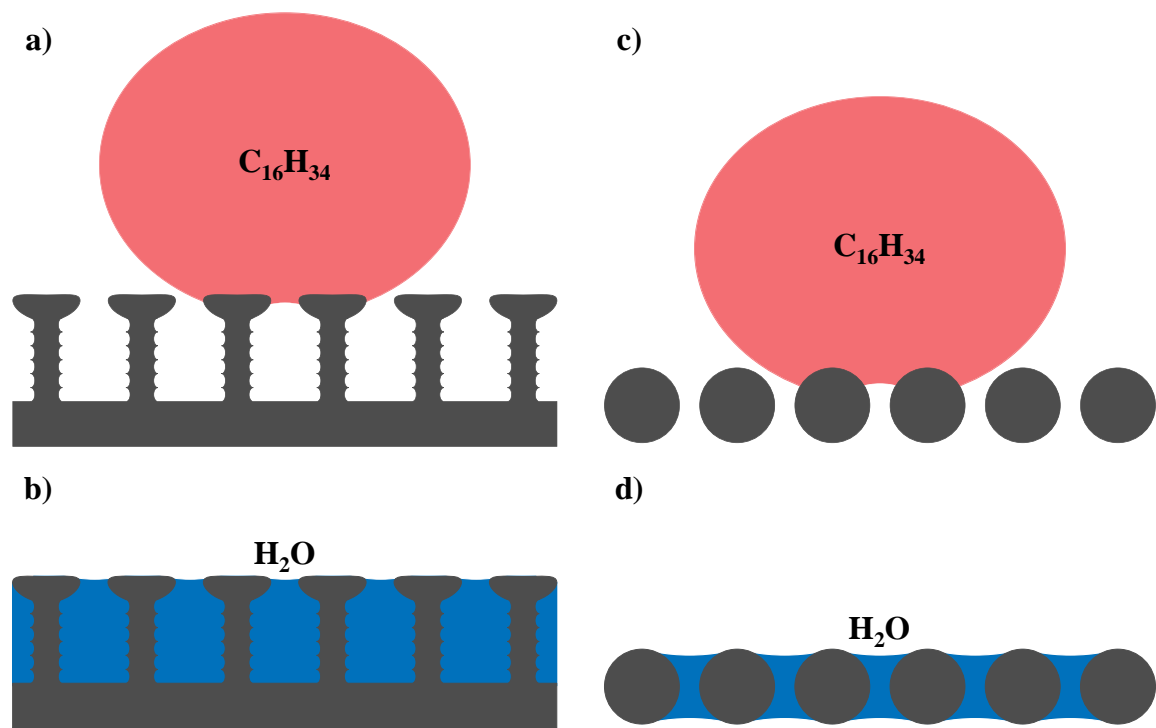


Figure B.7. Desired SOPB/SHPL behavior on a substrate with reentrant feature (a-b) and a reentrant mesh (c-d) upon exposure to non-polar and polar liquids.

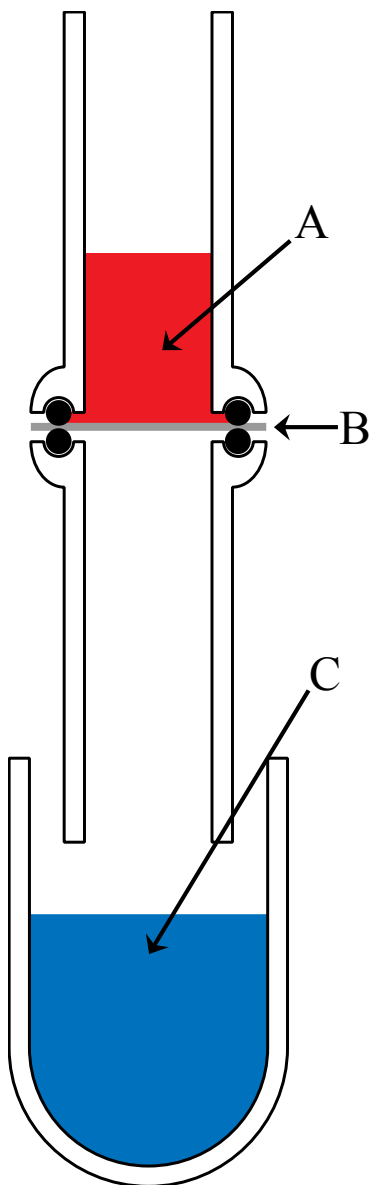


Figure B.8. Apparatus for oil-in-water separation experiments. (A) retentate, (B) SOPB/SHPL reentrant separation media, (C) eluent.

individual components in the eluent by extraction using liquid/liquid separation and testing the given extract using GC-MS or LC-MS, as appropriate. By correlating the CAG results with separation efficiency profile of the individual components, we can begin to understand how such a complex emulsion interacts with the responsive SOPB/SHPL surface.

B.3. Summary and Research Perspectives

The OPB/HPL film fabrication techniques described herein will be a viable platform from which we can begin to understand the mechanism by which surfaces can violate Young's equation. We hope that by studying these remarkable surfaces we can discover the attributes that govern their behavior and propose new methods by which we can improve their performance. Finally, as a consequence of the work proposed here, we expect to develop a viable OPB/HPL technology that does not require the use of the costly and dense materials used now, such as F-POSS. This material will be developed into a separation media for testing the hypotheses described in this proposal. However, these film systems also have potential in the fabrication of self-cleaning and anti-fog materials.

REFERENCES

1. Kota, A. K.; Kwon, G.; Choi, W.; Mabry, J. M.; Tuteja, A., Hygro-responsive membranes for effective oil–water separation. *Nat. Commun.* **2012**, 3, 1025.
2. Liu, K.; Tian, Y.; Jiang, L., Bio-inspired superoleophobic and smart materials: Design, fabrication, and application. *Prog. Mater. Sci.* **2013**, 58, (4), 503-564.
3. Howarter, J. A.; Genson, K. L.; Youngblood, J. P., Wetting behavior of oleophobic polymer coatings synthesized from fluorosurfactant-macromers. *ACS Appl. Mater. Interfaces* **2011**, 3, (6), 2022-2030.
4. Howarter, J. A.; Youngblood, J. P., Self-cleaning and next generation anti-fog surfaces and coatings. *Macromol. Rapid Commun.* **2008**, 29, (6), 455-466.
5. Wang, Y.; Finlay, J. A.; Betts, D. E.; Merkel, T. J.; Luft, J. C.; Callow, M. E.; Callow, J. A.; DeSimone, J. M., Amphiphilic co-networks with moisture-induced surface segregation for high-performance nonfouling coatings. *Langmuir* **2011**, 27, (17), 10365-10369.
6. Kumar, V.; Pulpytel, J.; Giudetti, G.; Rauscher, H.; Rossi, F.; Arefi-Khonsari, F., Amphiphilic copolymer coatings via plasma polymerisation process: switching and anti-biofouling characteristics. *Plasma Processes Polym.* **2011**, 8, (5), 373-385.
7. Field, R. W., Surface science: Separation by reconfiguration. *Nature* **2012**, 489, (7414), 41-42.
8. Feng, L.; Zhang, Z.; Mai, Z.; Ma, Y.; Liu, B.; Jiang, L.; Zhu, D., A super-hydrophobic and super-oleophilic coating mesh film for the separation of oil and water. *Angew. Chem. Int. Ed.* **2004**, 43, (15), 2012-2014.
9. Choi, W.; Tuteja, A.; Chhatre, S.; Mabry, J. M.; Cohen, R. E.; McKinley, G. H., Fabrics with tunable oleophobicity. *Adv. Mater.* **2009**, 21, (21), 2190-2195.
10. Howarter, J. A.; Youngblood, J. P., Amphiphile grafted membranes for the separation of oil-in-water dispersions. *J. Colloid Interface Sci.* **2009**, 329, (1), 127-132.
11. Yang, J.; Zhang, Z.; Xu, X.; Zhu, X.; Men, X.; Zhou, X., Superhydrophilic-superoleophobic coatings. *J. Mater. Chem.* **2012**, 22, (7), 2834-2837.
12. Campos, R.; Guenther, A. J.; Meuler, A. J.; Tuteja, A.; Cohen, R. E.; McKinley, G. H.; Haddad, T. S.; Mabry, J. M., Superoleophobic surfaces through control of sprayed-on stochastic topography. *Langmuir* **2012**, 28, (25), 9834-9841.
13. Mabry, J. M.; Vij, A.; Iacono, S. T.; Viers, B. D., Fluorinated polyhedral oligomeric silsesquioxanes (F-POSS). *Angew. Chem. Int. Ed.* **2008**, 47, (22), 4137-4140.
14. Meuler, A. J.; Chhatre, S. S.; Nieves, A. R.; Mabry, J. M.; Cohen, R. E.; McKinley, G. H., Examination of wettability and surface energy in fluorodecyl POSS/polymer blends. *Soft Matter* **2011**, 7, (21), 10122-10134.

15. Howarter, J. A.; Youngblood, J. P., Self-cleaning and anti-fog surfaces via stimuli-responsive polymer brushes. *Adv. Mater.* **2007**, 19, (22), 3838-3843.
16. Li, L.; Wang, Y.; Gallaschun, C.; Risch, T.; Sun, J., Why can a nanometer-thick polymer coated surface be more wettable to water than to oil? *J. Mater. Chem.* **2012**, 22, (33), 16719-16722.
17. Tavana, H.; Jehnichen, D.; Grundke, K.; Hair, M. L.; Neumann, A. W., Contact angle hysteresis on fluoropolymer surfaces. *Adv. Colloid Interface Sci.* **2007**, 134–135, (0), 236-248.
18. Yague, J. L.; Gleason, K. K., Systematic control of mesh size in hydrogels by initiated chemical vapor deposition. *Soft Matter* **2012**, 8, (10), 2890-2894.
19. Baxamusa, S. H.; Montero, L.; Dubach, J. M.; Clark, H. A.; Borros, S.; Gleason, K. K., Protection of sensors for biological applications by photoinitiated chemical vapor deposition of hydrogel thin films. *Biomacromolecules* **2008**, 9, (10), 2857-2862.
20. Chan, K.; Gleason, K. K., Initiated chemical vapor deposition of linear and cross-linked poly(2-hydroxyethyl methacrylate) for use as thin-film hydrogels. *Langmuir* **2005**, 21, (19), 8930-8939.
21. Montero, L.; Baxamusa, S. H.; Borros, S.; Gleason, K. K., Thin hydrogel films with nanoconfined surface reactivity by photoinitiated chemical vapor deposition. *Chem. Mater.* **2009**, 21, (2), 399-403.
22. Huisgen, R., 1,3-dipolar cycloadditions. Past and future. *Angew. Chem. Int. Ed.* **1963**, 2, (10), 565-598.
23. Demko, Z. P.; Sharpless, K. B., A click chemistry approach to tetrazoles by huisgen 1,3-dipolar cycloaddition: synthesis of 5-sulfonyl tetrazoles from azides and sulfonyl cyanides. *Angew. Chem. Int. Ed.* **2002**, 41, (12), 2110-2113.
24. Gonçalves, I. C.; Martins, M. C. L.; Barbosa, M. A.; Ratner, B. D., Protein adsorption and clotting time of pHEMA hydrogels modified with C18 ligands to adsorb albumin selectively and reversibly. *Biomaterials* **2009**, 30, (29), 5541-5551.
25. Kwok, C. S.; Mourad, P. D.; Crum, L. A.; Ratner, B. D., Surface modification of polymers with self-assembled molecular structures: multitechnique surface characterization. *Biomacromolecules* **2000**, 1, (1), 139-148.
26. Tripp, C. P.; Hair, M. L., Direct observation of the surface bonds between self-assembled monolayers of octadecyltrichlorosilane and silica surfaces: a low-frequency IR study at the solid/liquid interface. *Langmuir* **1995**, 11, (4), 1215-1219.
27. Lutz, J.-F., 1,3-dipolar cycloadditions of azides and alkynes: a universal ligation tool in polymer and materials science. *Angew. Chem. Int. Ed.* **2007**, 46, (7), 1018-1025.
28. Hutton, S. J.; Crowther, J. M.; Badyal, J. P. S., Complexation of fluorosurfactants to functionalized solid surfaces: smart behavior. *Chem. Mater.* **2000**, 12, (8), 2282-2286.
29. Lampitt, R. A.; Crowther, J. M.; Badyal, J. P. S., Switching liquid repellent surfaces. *J. Phys. Chem. B* **2000**, 104, (44), 10329-10331.

30. Peri, S. R.; Habersberger, B.; Akgun, B.; Jiang, H.; Enlow, J.; Bunning, T. J.; Majkrzak, C. F.; Foster, M. D., Variations in cross-link density with deposition pressure in ultrathin plasma polymerized benzene and octafluorocyclobutane films. *Polymer* **2010**, 51, (19), 4390-4397.
31. Peri, S. R.; Akgun, B.; Satija, S. K.; Jiang, H.; Enlow, J.; Bunning, T. J.; Foster, M. D., Control of interface nanoscale structure created by plasma-enhanced chemical vapor deposition. *ACS Appl. Mater. Interfaces* **2011**, 3, (9), 3375-3383.
32. Martin, I. T.; Malkov, G. S.; Butoi, C. I.; Fisher, E. R., Comparison of pulsed and downstream deposition of fluorocarbon materials from C₃F₈ and c-C₄F₈ plasmas. *J. Vac. Sci. Technol., A* **2004**, 22, (2), 227-235.
33. Butoi, C. I.; Mackie, N. M.; Barnd, J. L.; Fisher, E. R.; Gamble, L. J.; Castner, D. G., Control of surface film composition and orientation with downstream PECVD of hexafluoropropylene oxide. *Chem. Mater.* **1999**, 11, (4), 862-+.
34. Butoi, C. I.; Mackie, N. M.; Gamble, L. J.; Castner, D. G.; Barnd, J.; Miller, A. M.; Fisher, E. R., Deposition of highly ordered CF₂-rich films using continuous wave and pulsed hexafluoropropylene oxide plasmas. *Chem. Mater.* **2000**, 12, (7), 2014-2024.
35. Young, T., An essay on the cohesion of fluids. *Philos. Trans. R. Soc. London* **1805**, 95, 65-87.
36. Ellinas, K.; Tserepi, A.; Gogolides, E., From superamphiphobic to amphiphilic polymeric surfaces with ordered hierarchical roughness fabricated with colloidal lithography and plasma nanotexturing. *Langmuir* **2011**, 27, (7), 3960-3969.
37. Dufour, R.; Perry, G.; Harnois, M.; Coffinier, Y.; Thomy, V.; Senez, V.; Boukherroub, R., From micro to nano reentrant structures: hysteresis on superomniphobic surfaces. *Colloid. Polym. Sci.* **2013**, 291, (2), 409-415.
38. Ryerson, T. B.; Camilli, R.; Kessler, J. D.; Kujawinski, E. B.; Reddy, C. M.; Valentine, D. L.; Atlas, E.; Blake, D. R.; de Gouw, J.; Meinardi, S.; Parrish, D. D.; Peischl, J.; Seewald, J. S.; Warneke, C., Chemical data quantify Deepwater Horizon hydrocarbon flow rate and environmental distribution. *Proc. Natl. Acad. Sci. U. S. A.* **2012**, 109, (50), 20246-20253.

LIST OF ABBREVIATIONS

θ_{adv}	advancing contact angle
θ_{hyst}	contact angle hysteresis
θ_{rec}	receding contact angle
<i>a</i> -CF	amorphous fluorocarbon
<i>a</i> -CH	amorphous hydrocarbon
<i>a</i> -C _x O _y H _z	amorphous oxidized hydrocarbon
AC	alternating current
AR-XPS	angle resolved x-ray photoelectron spectroscopy
ATR	attenuated total reflection
AWG	American wire gauge
BE	binding energy
BuLi	<i>n</i> -butyllithium
<i>c</i> -C ₄ F ₈	octafluorocyclobutane
CAG	contact angle goniometry
CF _x	fluorinated carbon
CH ₃ COOH	acetic acid, ethanoic acid
C ₁₆ H ₃₄	<i>n</i> -hexadecane
CHCOOH	formic acid, methanoic acid
CO _x	oxidized carbon
CVD	chemical vapor deposition
DAQ	data acquisition card
DMSO	dimethyl sulfoxide

DSC	differential scanning calorimetry
ESCA	electron spectroscopy for chemical analysis
Et ₃ N	triethylamine
F/C	fluorine to carbon ratio
F-POSS	fluorodecyl polyhedral oligomeric silsesquioxane
FC	fluorocarbon
FTIR	Fourier transform infrared spectroscopy
FWHM	full width at half maximum
GC-MS	gas chromatography mass spectrometry
GmbH	Gesellschaft mit beschränkter Haftung
h	hour, hours
HC	hydrocarbon
HDPE	high density polyethylene
HEMA	hydroxyethyl methacrylate
HFPO	hexafluoropropylene oxide
HPL	hydrophilic
iCVD	initiated chemical vapor deposition
i.d.	internal diameter
I/O	input/output
in.	inch, inches
IRIS	imaging of radicals interacting with surfaces
LC-MS	liquid chromatography mass spectrometry
LDPE	low density polyethylene

LMWOM	low molecular weight oxidized material
MFC	mass flow controller
min	minute, minutes
NEXAFS	near edge x-ray absorption fine structure spectroscopy
O/C	oxygen/carbon
OES	optical emission spectroscopy
OPB	oleophobic
<i>P</i>	applied radio frequency power
PC	polycarbonate
PC-TE	polycarbonate track-etched membrane
PDMS	polydimethylsiloxane
PE	polyethylene
PECVD	plasma enhanced chemical vapor deposition
PES	polyethersulfone
PET	polyethylene terephthalate
PET-TE	polyethylene terephthalate track-etched membrane
PFM	pentafluorophenylmethacrylate
pHEMA	polyhydroxyethyl methacrylate or poly(2-hydroxyethyl methacrylate)
PP	polypropylene
PPh ₃	triphenylphosphine
PS	polystyrene
PSf	polysulfone
psi	pounds per square inch

PU	polyurethane
PVP	polyvinylpyrrolidone
rf	radio frequency
RO	reverse osmosis
SAM	self-assembled monolayer
sccm	standard cubic centimeters per minute
SEM	scanning electron microscopy
SHPL	superhydrophilic
SOPB	superoleophobic
T_g	glass transition point, glass transition temperature
T_m	melting point, melting temperature
T_s	substrate temperature
THF	tetrahydrofuran
ToF-SIMS	time of flight-secondary ion mass spectrometry
TR-OES	time-resolved optical emission spectroscopy
UV	ultra-violet
VASE	variable angle spectroscopic ellipsometry
wCA	water contact angle goniometry
x-PEGDA	cross-linked poly(ethylene glycol) diacrylate
XPS	x-ray photoelectron spectroscopy